Improving CEA-Targeted CAR-T cell Therapy for Solid Tumours

A thesis submitted to the University of Manchester for the degree of Doctor of Philosophy in the Faculty of Biology, Medicine and Health

2020

Weiming Zheng

School of Medical Sciences
Division of Cancer Sciences

Table of Contents

Word count: 44,072

List of Figures

List of Tables

Abstract

Chimeric antigen receptor (CAR)-T cell therapy has shown spectacular objective clinical responses in the treatment of haematological malignancies. However, early trials employing CARs specific for solid tumour antigens such as carcinoembryonic antigen (CEA) have been far less successful. Preclinical studies suggest that this is partly due to several immunosuppressive mechanisms within solid tumours. Therefore, the aim of the project is to improve CAR-T cell therapy targeting CEA by increasing the potency of CAR-T cells and superseding the immunosuppressive tumour microenvironment. To achieve this, CAR-T cells which secrete the pro-inflammatory cytokine IL-12 or disrupt TGF-β or PD-1 signalling through the secretion of antagonistic scFvs were developed.

Mouse anti-CEA CAR-T cells were successfully engineered to constitutively or inducibly express IL-12. Compared to non-IL-12-secreting CAR-T cells *in vitro*, IL-12-secreting CAR-T cells significantly improved CEA-specific cytotoxicity and increased IFN-γ production. Whilst *in vivo* results showed that a single dose of anti-CEA CD28-CD3ζ CAR-T cells constitutively secreting IL-12 mediated complete regression of subcutaneous CEA^+ tumour in some mice, this observation needs to be reproduced. Furthermore, anti-CEA CD28-CD3ζ CAR-T cells inducibly secreting IL-12 did not achieve similar results. Combination of CAR-T cells constitutively or inducibly secreting IL-12 with lymphodepletion pre-conditioning via 5Gy total body irradiation (TBI) resulted in lethal toxicity, which was highly associated with IL-12.

Mouse T cells were also effectively transduced to express an anti-CEA CD28-CD3ζ CAR construct and constitutively secrete αTGF-β or αPD-1 scFv with functional binding and blocking capacity. The secretion of scFv did not enhance the CEA-specific cytotoxicity and cytokine production of CAR-T cells upon co-culture *in vitro*. With regards to the *in vivo* function, scFv-secreting CAR-T cells could not efficiently eradicate subcutaneous CEA^+ tumour, although delayed tumour growth was observed in the therapy of CAR-T cells secreting αPD-1 scFv. Given no significant difference in the infiltration of $CD8^+$ T cells in tumour sites between mock T cell therapy and CAR-T cell therapy demonstrated by IHC analysis, the therapeutic effects of anti-CEA CAR-T cells were possibly limited by the level of T cell infiltration or CAR-T cell retention.

Overall, this thesis has shown that immune modulation on anti-CEA CAR-T cells is a feasible immunotherapeutic strategy for solid tumours. The therapy of anti-CEA CAR-T cells constitutively secreting IL-12 appears to be efficacious in tumour regression *in vivo*, whilst it needs to be further validated. More efforts are also required to determine whether the inducible secretion of IL-12 or the constitutive secretion of αTGF-β or αPD-1 scFv results in improved anti-tumour responses of anti-CEA CAR-T cells.

Declaration

No portion of the work referred to in the thesis has been submitted in support of an application for another degree or qualification of this or any other university or other institute of learning.

Copyright statement

Acknowledgements

First and foremost, I would like to express my deep and sincere gratitude to my supervisors Dr Anne Armstrong, Dr Gray Kueberuwa, Dr Eleanor Cheadle, Professor Robert Hawkins, Dr David Gilham, Dr John Bridgeman for giving me the opportunity to undertake this PhD and providing their invaluable guidance and advice throughout the project. In particular, I would like to thank my co-supervisor Dr Gray Kueberuwa for his support and motivation through my highs and lows, his enlightening academic discussions and his patience in dealing with my endless problems. I am extremely grateful for what he has offered me during these four years. I would also like to thank my co-supervisor Dr Eleanor Cheadle for the support with laboratory work and for the assistance and feedback with my thesis.

I would additionally like to thank all of the fantastic members of the Clinical and Experimental Immunotherapy group. It was an excellent experience to work with them. In particular, a heartfelt thank you to Aoife Kilgallon and Adam Milner who are my precious friends for providing invaluable help and inspiration and sharing many memorable moments throughout my time in the lab, to Dr Milena Kalaitsidou for the scientific advice and selfless support. I would like to thank all of the members of the Breast Biology group and the Targeted Therapy group who were always nice and supportive. I would also like to thank all those who provided technical help throughout the project, in particular the biological resource unit at the CRUK MI for their assistance with in vivo experiments.

None of this would have been possible without the endless love and support of my family. I am greatly indebted to my parents for believing in me and supporting me to pursue the PhD. I am extremely grateful to my wife Man Wun for her constant patience, encouragement and devotion throughout.

1 Introduction

1.1 T cell mediated immunity

Protecting the host from infectious agents and minimising the damage they cause is the primary role of the immune system. It has mainly two separate but interacting systems: innate and adaptive immunity [1]. Innate immunity, which can range from external barriers such as skin and mucous membrane to natural killer cells (NK cells), macrophages, complement and innate immune receptors, is the first line of defence against pathogens and provides a rapid non-specific response to invasion. The adaptive immune system provides highly specific responses for a given pathogen and is capable of generating immunological memory to prevent re-infection.

There are two main types of adaptive immunity: cell-mediated (or cellular) immunity and humoral immunity. While humoral immunity is mediated by B lymphocytes and their secreted antibodies, cellular immunity is mediated by T lymphocytes via cytotoxic T cells (CTLs) through targeting cells that express appropriate surface antigens and killing. Both mechanisms are regulated by helper T cells (Th cells), which release cytokines and licence B cells and $CD8^+$ cells.

1.1.1 T cell development

T cells are derived from pluripotent hematopoietic stem cells in the bone marrow but mature in the thymus. The development of T cells is a series of complex processes, which can be reflected by changes in the status of the T cell receptor genes and in the expression of cell surface proteins such as the CD3 complex, CD4, CD8, CD25 and CD44 [2]. These cell surface proteins are of importance to reflect the state of thymocyte maturation and can be used as markers to identify T cells of different stages of differentiation. T cell precursors arriving in the thymus from the bone marrow do not express any of the three cell surface proteins (CD3, CD4 and CD8) and are called double negative thymocytes due to the absence of co-receptors CD4 and CD8 which bind to major histocompatibility complex class II (MHC-II) and class I (MHC-I) respectively. These cells give rise to the majority of αβ T-cell lineage and the minor population of γδ T cells which lack CD8 or CD4 expression even when mature.

In the double negative stage of αβ T-cell lineage, which can be further divided into four stages of development, rearrangement of the T cell receptor β-chain locus occurs by

randomly recombining variable (V) , diversity (D) and joining (J) gene segments and the expression of the adhesion molecule CD44 and CD25 which is the α chain of IL-2 receptor. Eventually, while thymocytes have no expression of CD44 and CD25 and cease to proliferate, those cells express both CD4 and CD8 molecules and therefore become double positive. At this stage, rearrangement of the α-chain locus begins by randomly recombining V and J segments and double positive thymocytes must recognize self-peptide: MHC (p: MHC) ligand and pass positive selection through receipt of growth signalling upon successful recognition. Those cells that are able to recognize self p: MHC ligand can go on to mature and express T cell receptor (TCR) at high density and lose either the CD4 or CD8 protein expression to become single positive cells. Meanwhile, those thymocytes also undergo the negative selection process during and after the double-positive stage, which eliminates the cells that bind to self antigens with high affinity. Those selection processes lead to the maturation of T cells that are both MHC-restricted and self-tolerant, leaving T cells capable of recognizing non-self peptides bound to MHC molecules. Eventually, $CD4^+$ and $CD8^+$ T cells that complete maturation leave the thymus and migrate to the peripheral lymphoid organs such as lymph nodes, spleen, and mucosal lymphoid organs.

1.1.2 T cell activation

Activation of naïve T cells on first exposure to antigenic peptides on the surface of antigen presenting cells (APCs) such as dendritic cells (DCs), B cells or macrophages is called T cell priming (Figure 1.1). The molecule responsible for antigen specific recognition of T cells is the TCR, which is composed of heterodimer (either α and β or γ and δ chains). It is associated with a set of transmembrane spanning proteins called the CD3 complex, which is necessary for T cell activation by transducing antigen recognition signals into T cells. Notably, the TCR can only recognize antigenic peptides bound to MHC molecules. The MHC molecules can be divided into two classes: MHC-I, which are expressed on the surface of nearly all nucleated cells and MHC-II, which are only expressed on APCs [3]. Before binding to MHC molecules, antigen processing is required to degrade the antigen to peptide fragments. While MHC-I molecules bind peptide fragments of 8 - 10 amino acids, MHC-II molecules can accommodate longer peptide fragments of 13 - 24 amino acids as theirs binding groove is more open.

In general, naïve T cells which have CD8 co-receptors on their surface can recognize peptides from the cytosol when it is presented in complex with MHC class I molecules, whereas T cells bearing CD4 receptors recognize peptides from extracellular proteins loaded on MHC class II molecules. Notably, exogenous peptides can also be cross-

presented by DCs to $CD8^+$ T cells [4]. Apart from antigenic signalling, co-stimulatory signals generated from the binding of co-stimulation receptors and their ligands are also needed to fully activate T cells. CD28 is perhaps the most important and well characterized co-stimulatory receptor involved in T cell activation [5]. Ligation of CD28 by the B7 family molecules including B7-1 and B7-2 expressed on the APCs such as DCs, can induce an increase in interleukin-2 (IL-2) secretion and enhance T cell proliferation, differentiation and survival [6]. Notably, DCs can upregulate the expression of B7 family upon activation and maturation through Toll-like receptor (TLR) signalling, providing the cognate co-stimulatory signals in an antigen-specific interaction with T cells [7]. Other co-stimulatory receptors, including CD2, CD5, CD30, the immunoglobulin (Ig) gene superfamily member ICOS, the TNF receptor family members such as 4-1BB (CD137) and OX40 (CD134), are also important to modulate T cell activation status. In contrast, a set of inhibitory co-stimulation receptors such as cytotoxic T lymphocyte protein-4 (CTLA-4), programmed death-1 (PD-1) that are upregulated on activated T cells mediate negative signals to prevent further stimulation and attenuate the immune response [8].

Upon target recognition, naïve T cells begin to proliferate and differentiate to effector T cells and memory cells. Naïve $CD8^+$ T cells are activated and then differentiate into CTLs. CTLs can kill infected target cells either by utilizing pore-forming molecules such as perforins and various components of cytoplasmic granules, or through activating Fas to induce apoptosis [9]. On the other hand, T cells bearing CD4 receptors can differentiate into several distinct subtypes of T cells. Maturation into distinct subtypes is prominently dependent on the cytokines present in the local environment [10]. The major functional subsets are Th1, Th2 and regulatory T cells (Tregs). Th1 cells largely lead to cellular immunity by activating the microbicidal properties of macrophages and inducing CTL proliferation, whereas Th2 cells initiate B cell humoral response. Th1 cells mainly produce IL-2 and IFN-γ while the effector cytokines of Th2 cells are IL-4, IL-5, IL-6, IL-9, IL-10 and IL-13. Treg cells are a heterogeneous group of cells, which maintain peripheral tolerance to self-antigens and prevent autoimmunity. Treg cells produce a number of inhibitory cytokines such as transforming growth factor-β (TGF-β), IL-10 and IL-35 to suppress immune responses and inflammation.

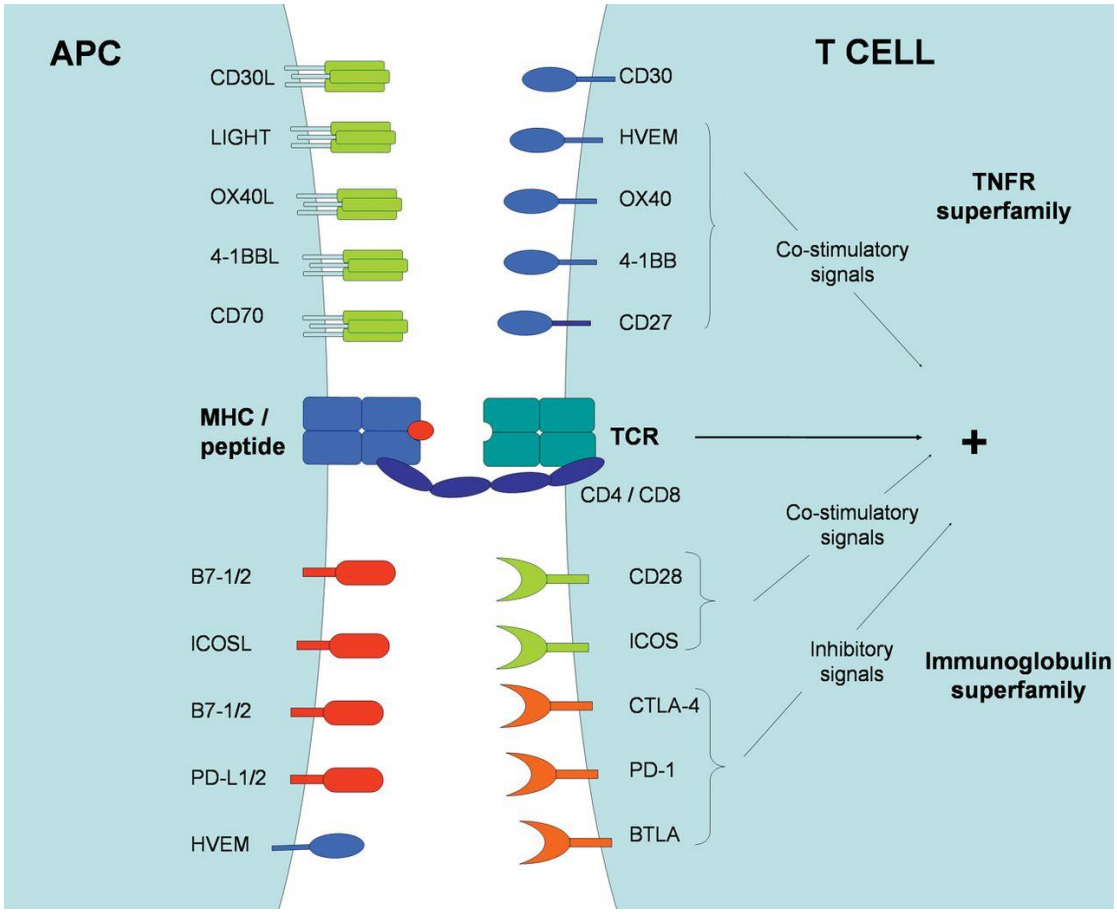

Figure 1.1 Various ligand-receptor interactions between T cells and APCs involved in T cell activation

Upon the antigen recognition of T cells through TCR, some important co-stimulatory molecules, such as CD28, 41BB and ICOS, deliver co-stimulatory signals to fully activate T cells. Inhibitory molecules such as PD-1 and CTLA-4 are commonly upregulated after T cell activation to prevent an excessive response. Adapted from Gray et al., 2006 [11].

1.2 Cancer immunology

Carcinogenesis is a multistep process and reflects genetic alterations that transform normal cells to highly malignant derivatives [12]. From the perspectives of Hanahan and Weinberg [12, 13], most and perhaps all types of tumours share the same set of functional capabilities during their development. And eight broad features have been identified as 'Hallmarks of Cancer', which are self-sufficiency in growth signals, insensitivity to growth-inhibitory (anti-growth) signals, evasion of programmed cell death (apoptosis), limitless replicative potential, sustained angiogenesis, tissue invasion and metastasis, reprogramming of energy metabolism and evading immune destruction. In addition, there are two enabling characteristics crucial to the acquisition of these hallmarks, which are genome instability and mutation and tumour-promoting inflammation.

1.2.1 Tumour microenvironment

The tumour microenvironment (TME) is the cellular environment that surrounds malignant cancer cells in the tumour tissues. The structural constituents of TME can be divided into three categories, the extracellular matrix (ECM), the stromal cells, and the tumour blood and lymphatic vessels.

The onset of angiogenesis is achieved by a plethora of pro-angiogenic factors including vascular endothelial growth factor (VEGF), platelet-derived growth factor (PDGF), basic fibroblast growth factor (bFGF). It can be characterized by aberrant vascular structure, altered endothelial-cell-pericyte interactions, abnormal blood flow, increased permeability and delayed maturation [14]. The ECM contributes to provide cell-adhesion sties and sequester and locally store a wide range of growth factors, such as epidermal growth factor (EGF), FGF and other signalling molecules like TGF-β. ECM constituents including collagens, proteoglycans (PGs) and glycoproteins [15] communicate with epithelial cells, to regulate adhesion, migration, proliferation, apoptosis, survival or differentiation [16]. As for stromal cells, they can be divided into three categories: 1) angiogenic vascular cells, including endothelial cells and pericytes; 2) infiltrating immune cells, including myeloid-derived suppressor cells (MDSCs), tumour infiltrating lymphocytes (TILs), mast cells, neutrophils and inflammatory monocytes; 3) cancer-associated fibroblasts (CAFs) [17]. Stromal cells are of critical importance in promoting tumour development and progression via different mechanisms [18, 19]. Notably, the composition of the TME varies considerably in different tumour types, determined by locations, mutations that led to tumourigenesis, interactions with carcinogens, prior therapy, microbiome and other factors.

The TME has been demonstrated to have critical impacts on both promoting cancer progression and determining the efficacy of cancer therapy, achieved by both direct and indirect interactions with cancer cells. Cancer stroma forms a permissive and supportive environment for tumour progression. It can be described as desmoplasia, which refers to the growth of dense connective tissue and is characterized by activated fibroblasts, specific ECM components, recruited inflammatory and immune cells and angiogenesis [18]. Cancer cells usually secrete a multitude of stroma-modulating growth factors to disrupt normal tissue homeostasis and modulate the TME, such as bFGF, members of the VEGF family, PDGF, epidermal growth factor receptor (EGFR) ligands, interleukins (ILs), colony-stimulating factors (CSFs), TGF-β [18]. These growth factors induce stromal changes, such as angiogenesis and an inflammatory response. In addition, activated by these growth factors, several stromal cell types such as fibroblasts, smooth-muscle cells and adipocytes, secrete additional factors and proteases. Moreover, tumour cells can produce proteases such as matrix matalloproteinases (MMPs), which remodel the ECM and provide a pro-migratory and pro-invasive environment [20].

1.2.2 Cancer immunoediting

The cancer immunoediting hypothesis is used to describe the interactions between the immune system and the tumour, characterised by three phases: elimination, equilibrium and escape (Figure 1.2) [21]. It is a dynamic process that involves host-protective and tumour-sculpting functions of immunity on tumour development.

In the elimination phase, known as immunosurveillance, both the innate and adaptive immunity together detect and destroy nascent tumour cells before they become clinically visible by a variety of mechanisms [22]. For instance, $CD8^+$ T cells may directly mediate cytotoxic responses through the interaction of Fas and TNF-related apoptosis-inducing ligand (TRAIL) receptors on tumour cells or through the release of perforin and granzymes. $CD8^+$ T cells and some types of $CD4^+$ T cells can produce cytokines, such as IFN-γ and tumour necrosis factor (TNF) to enhance immune responses. DCs can enhance cross-presentation of tumour antigens to T cells due to type I IFNs (IFN-α/β) [23]. As for innate immune cells, NK cells can recognize and eliminate tumour cells expressing NKG2D ligands. Macrophages (M1) and granulocytes can also protect against tumour development by secreting tumour necrosis factor-α (TNF-α), IL-1, IL-12 and reactive oxidative species (ROS). Notably, ongoing tumour progression as well as elimination occurs continually during this phase. Sporadic tumour cells that are not eliminated may then enter the equilibrium state in which the immune system prevents tumour progression and tumour

cells enter a functional state of dormancy. The equilibrium phase is maintained by adaptive immunity such as T cells and IL-12 and IFN-γ, whilst innate cells have both pro- and anti-tumour effects [24].

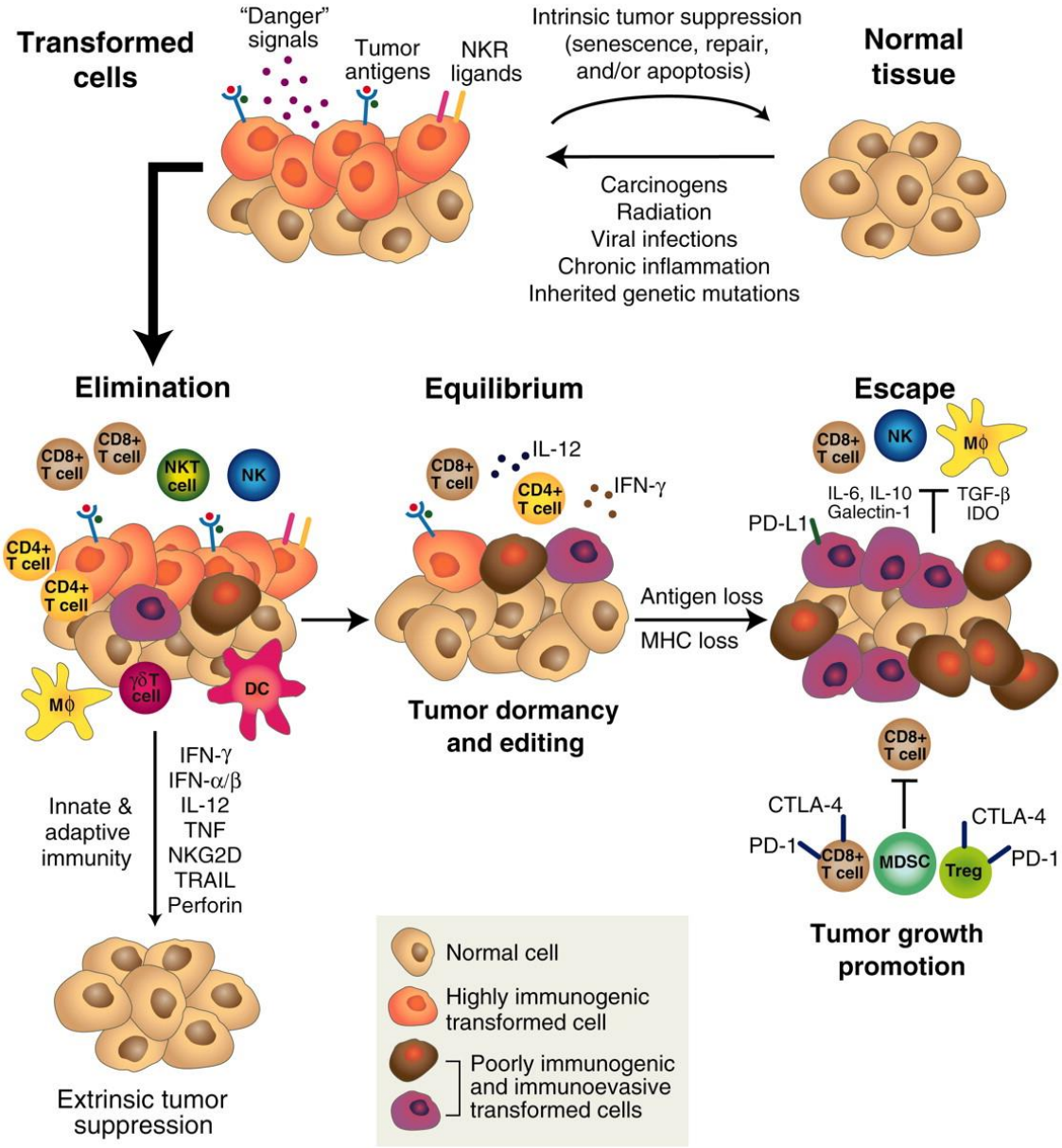

Figure 1.2 Three phases of cancer immunoediting

Cancer immunoediting is an extrinsic tumour suppression process caused by transformed cells escaping instrinsic tumour supppressor mechanisms. It is composed of three phases: elimination, equilibrium and escape. In the elimination phase, cells and molecules of innate and adaptive immunity may recognize and eliminate early tumours. If this process fails to completely eradicate tumour cells, sporadic tumour cells may then enter the equilibrium phase where they may enter a state of functional dormancy and immunogenicity editing by immunity which produces tumour variants with reduced immunogenicity. Eventually, these variants evade the immune system by reducing immune recognition or expressing molecules of cytotoxicity resistance, survival and immunosuppression and then become clinically apparent. Adapted from Schreiber et al., 2011 [25].

1.2.3 Tumour escape from immune surveillance

Despite the fact that the innate and adaptive immunity plays a significant role in eliminating precancerous cells or controlling transformed cells in an equilibrium phase, tumours manage to enter the escape phase, due to the genetic instability of tumour cells and immunological selection pressure which only allows for growth of less immunogenic mutants [26]. Eventually, these tumour cells can acquire the ability to circumvent immune recognition and/or destruction, proliferate progressively and then become clinically apparent. There are a variety of escape mechanisms employed by tumours, many of which operate in parallel.

As well as the loss of tumour antigen expression, tumour cells may downregulate the expression of MHC-I molecules or co-stimulatory molecules such as B7-1 or B7-2 [27] to reduce immune recognition. Besides, tumour cells can increase resistance to the cytotoxic effects of immunity through persistent activation of pro-oncogenic transcription factors such as STAT3 [28] or increased expression of anti-apoptotic effector molecules such as cFLIP [29] and Bcl-xL [30]. It could also include mutations of pro-apoptotic receptors expressed on tumour cells including TRAIL receptor death receptor 5 (DR5) [31] and Fas [32], increased threshold for apoptosis/necroptosis and upregulation of autophagy upon continual stress.

Furthermore, tumour escape can result from the development of an immunosuppressive tumour microenvironment. Tumour cells can upregulate the expression of surface ligands such as PD-L1 or PD-L2 to inhibitory T cell receptors such as PD-1, causing T cell anergy or exhaustion [33]. Tumour cells can also promote immune suppression by producing cytokines such as TGF-β and VEGF and immunoregulatory molecules such as indoleamine 2,3-dioxygenase (IDO) which consumes tryptophan and limits T cell effector functions [34], galectin, CD39 and CD73. Tumour stroma cells play an important immune modulatory role as well [35]; whilst myeloid-derived mesenchymal stem cells block proliferation and function of T effector cells, CAFs can enhance the recruitment and function of immunosuppressive cells and suppress T effector cells through the production of CCL2 and CXCL12 and TGF-β respectively.

Immunosuppressive populations, such as Tregs and myeloid-derived suppressor cells (MDSCs), also play critical roles in inhibiting anti-tumour immunity. Treg cells, which are $CD4^+$ cells expressing CD25 and the transcription factor Foxp3 (forkhead box P3), are recruited to tumours via chemokines such as CCL22 by interaction with CCR4 expressed on Treg cells [36]. Treg cells, after stimulation, inhibit the function of tumour-specific T

cells by secreting TGF-β and IL-10; by expressing the inhibitory co-stimulation molecules CTLA-4 and PD-L1; by consuming IL-2 which is critical for maintaining CTL function; and by inhibiting cytolytic granule release [25, 37].

MDSCs, which arise as the result of the abnormal myelopoiesis in cancer, are a heterogeneous group of myeloid progenitor cells and immature myeloid cells [38]. MDSCs disrupt immunosurveillance via multiple mechanisms [39, 40] such as inhibition of T cell activation and expansion and NK cell cytotoxic activity, disruption of antigen presentation by DCs, M2 macrophage polarization and induction of Treg cell expansion. Those immunosuppressive activities are induced by several factors including TGF-β, ROS, nitric oxide (NO), arginase and IL-10. Interestingly, macrophages exacerbate their M2 polarisation by stimulating MDSCs to secrete additional IL-10.

Solid tumours also pose a physical barrier that prevents attacks by the immune system and T cell penetration. For instance, tumour endothelial cells suppress T cell adhesion (to tumour endothelium) and prevent homing to tumours, partly mediated by VEGF [41] and the endothelin-B receptor (ET_BR) [42]. Furthermore, the hyperpermeability of tumour vessels can lead to excessive fluid loss from the vascular to the extravascular space of the tumour leading to a high pressure system that is not well perfused with oxygen and nutrients from the circulation [43]. This results in hypoxia and formation of a harsh, acidic microenvironment that creates a high stress environment at the tumour core, thus providing a selective pressure for aberrant apoptosis and anaerobic metabolism which promotes tumour progression. Specifically, perfusion reduction can inhibit immune cell entry to the tumour site through the vascular system. Furthermore, hypoxia and low pH in the TME can compromise the killing potential of immune cells and reduce their proliferation rate.

1.2.4 T cell infiltration in cancer prognosis

During the natural development from immune equilibrium to tumour escape, dynamic interactions between host immune responses and tumours modify the immune contexture. The immune contexture refers to the combination of immune parameters associating the type, density, location and functional orientation of immune cell within the TME [44]. The immune parameters consist of the density of $CD3^+$, $CD8^+$ and $CD45RO^+$ T cells and their location at the tumour centre (CT) and invasive margin (IM), in combination with the quality of tertiary lymphoid structures and additional functionality entities such as Th1 cell-related factors (IFN-γ, IL-12, T-bet), immune cytotoxic factors (granzymes, perforin, granulysin), chemokines (CX3CL1, CXCL9, CXCL10, CCL5, CCL2) and adhesion molecules

(MADCAM1, ICAM1, VCAM1). The correlation between a strong lymphocyte infiltration and clinical outcome has been reported in many cancer types, including melanoma [45], ovarian [46], breast [47], colorectal [48], head and neck [49], urothelial [50], bladder [51] and lung cancer [52]. High densities of $CD3^+$ T cells, $CD8^+$ cytotoxic T cells and $CD45RO^+$ memory T cells were associated with a longer disease-free survival (DFS) and/or improved overall survival (OS) [53].

Derived from the immune contexture, a simple and powerful immune scoring system termed the Immunoscore has been utilised to predict the survival and recurrence in patients with CRC [48, 54]. Based on the quantification of $CD3^+$ and $CD8^+$ T cells within the CT and IM, the Immunoscore (I) provides a score ranging from Immunoscore 0 (I0), which has low densities of both cell populations in both regions, to Immunoscore 4 (I4), which has high densities of both cell types in both locations. The five Immunoscore groups were associated with highly significant differences in DFS and OS ($P < 0.0001$) [54]. Currently, the consensus Immunoscore has been validated internationally in colon cancer and acts as a stronger relative prognostic value than AJCC/UICC tumour-node-metastasis (TNM) stage, tumour differentiation and microsatellite instability (MSI) status [55].

According to the level and spatial distribution of $CD3^+$ and $CD8^+$ T cell infiltration, solid tumours can be classified into four main categories, which are hot tumours, altered-immunosuppressed tumours, altered-excluded tumours and cold tumours [56]. These four phenotypes are characterized by high, intermediate and low Immunoscore respectively. Apart from being highly infiltrated, hot tumours present high mutational burden and PD-L1 expression [57]. In contrast, apart from the low degree of T cell infiltration, cold tumours are also characterized by high proliferation with low mutational burden, low expression of MHC-I and absence of PD-L1 expression [57]. The altered-immunosuppressed phenotype displays a low degree of T cell infiltration and presents an immunosuppressive environment that limits T cell recruitment and expansion [58]. In altered-excluded tumours, the infiltration of T cells is low at the tumour centre and high at the invasive margin, reflecting the existence of T cell responses and the ability of tumours to escape such responses by inhibiting T cell infiltration [58].

Based on this immune-based classification of tumours and their characteristics, specific therapeutic strategies can be proposed to achieve maximal efficiency. For example, the increased response to anti-PD-1 or anti-PD-L1 monotherapy was shown in hot tumours which have high levels of PD-L1 expression and infiltration of exhausted or dysfunctional T cells expressing PD-1 [59, 60]. As for cold tumours associated with poor prognosis, the strategies that could overcome the lack of a pre-existing immune responses and turn cold

tumours into hot tumours can be developed. Different therapeutic approaches, such as radiotherapy, cancer vaccines, immune checkpoint inhibitors and adoptive cellular therapy, can be used to boost T cell responses or counteract the immunosuppression of tumours [61]. Notably, it is probable that multiple pro-tumour mechanisms occur in parallel and result in the establishment of cold tumours. This suggests that the combination therapy may be needed to achieve clinical benefit.

1.3 Cancer immunotherapy

Cancer immunotherapy has become an important treatment for cancer, due to the recent developments of immune checkpoint blockade and adoptive cell therapy (ACT) approaches. Two broad strategies are currently applied in cancer immunotherapy. While one strategy is to target the tumour directly, using monoclonal antibodies alone or in combination with radioisotopes or cytotoxic molecules and immunotoxins, another aims at activating immune cells by cancer vaccines, immune checkpoint antagonists, stimulatory agonists and adoptive cellular therapies, which eventually target the tumour.

1.3.1 Immune checkpoint inhibitors

T-cell-mediated immunity is regulated by a balance between co-stimulatory and inhibitory signals (immune checkpoints). Under normal physiological conditions, immune checkpoints are of great importance to prevent autoimmunity, mitigate collateral tissue damage and curtail pathogenic T cell expansion upon systemic or chronic pathogen exposure. There are two immune checkpoint receptors that have been well studied, CTLA-4 and PD-1. CTLA-4 is primarily expressed on activated T cells and Treg cells [62]. The main role of CTLA-4 is to downmodulate the amplitude of T cell activation by outcompeting CD28 in the interactions with B7-1 (CD80) and B7-2 (CD86), partly leading to a delayed time for T cells to eliminate target cells. Conversely, CTLA4 engagement on Treg cells maintains their suppressive function [63]. Blockade of CTLA-4 showed durable anti-tumour immunity *in vivo* by improving the function of effector $CD4^+$ and $CD8^+$ T cells and concomitantly inhibiting the immunosuppressive activity of Treg cells [64]. Ipilimumab, a humanized anti-CTLA-4 antibody monoclonal antibody, was the first immune checkpoint inhibitor approved for the treatment of advanced melanoma.

PD-1 is expressed on all conventional $CD4^+$ and $CD8^+$ T cells upon initial antigen-mediated activation through the TCR and positive costimulatory signals such as CD28. By binding to its PD-1 ligands PD-L1 (B7-H1, CD274) and PD-L2 (B7-DC, CD273), PD-1 plays crucial

roles in fine-tuning T cell differentiation and effector T cell responses, tempering overactivation, limiting immunopathology and developing memory T cell formation and the return to immune homeostasis [65]. The level of PD-1 expression generally decreases on responding T cells when antigen is acutely cleared. However, during cancers in which antigen stimulation persists and PD-L1 and PD-L2 expression is upregulated or maintained by many cytokines such as IFN-γ which is the most potent regulator [65], the PD-1 pathway can lead to T cell anergy and exhaustion. As described in section 1.2.3, the inhibitory PD-1/PD-L1 pathway has been exploited as one of the mechanisms for immune evasion in cancers [33]. A strong correlation between poor diagnosis and high levels of PD-L1 expression on tumour cells or infiltrating APCs has been documented in most human cancers [66]. It has also been demonstrated that PD-1 is highly expressed on TILs in patients with different cancer types and resulted in impaired anti-tumour immune responses [67-70]. Moreover, PD-L1 expression can be further induced by pro-inflammatory cytokine production from TILs, contributing to adaptive immune resistance.

Blockade of PD-1 signalling using monoclonal antibodies to boost anti-tumour immune responses has shown encouraging clinical efficacy on both solid tumours and hematologic malignancies, such as melanoma, non-small cell lung cancer (NSCLC), renal cell carcinoma (RCC), head and neck squamous cell cancer (HNSCC), Hodgkin's lymphoma, diffuse large B cell lymphoma, gastric cancer, small cell lung cancer (SCLC), colorectal cancer, hepatocellular carcinoma (HCC), triple-negative breast cancer (TNBC), urothelial carcinoma (UC) [71]. So far, two PD-1 inhibitors, pembrolizumab and nivolumab, and four PD-L1 inhibitors, atezolizumab, avelumab, durvalumab and cemiplimab, have been approved by the US Food and Drug Administration (FDA) for commercial use.

1.3.2 Adoptive cellular therapy

The concept of adoptive cellular therapy was derived from allogeneic hematopoietic stem cell transplant (HSCT) with or without immune deficiency conditioning for hematologic malignancy treatment such as acute myeloid leukaemia (AML), acute lymphocytic leukaemia (ALL) and chronic myeloid leukaemia (CML). Although a strong graft-versus-leukaemia effect can be produced by allogeneic lymphocytes, it is limited by graft-versus-host disease (GvHD) which can be severe and life-threatening. HSCT for leukaemias showed that T cells have a strong potential to eliminate tumour cells, and if this potential is directed in the correct way, T cells could provide a powerful anti-cancer therapy against a range of cancer types.

To get tumour specific T cells without GvHD, an alternative is to isolate and expand autologous TILs, including T cells, B cells and NK cells, which can be found within tumours in an attempt to control tumour growth. After activation and expansion *ex vivo*, TILs will be reinfused back into patients to initiate tumour cell lysis. Although TIL therapy can mediate durable complete responses in patients with metastatic melanoma [72], it is difficult to apply this approach to other cancers due to the relatively low reactivity of TILs for neoantigens in some cancers and low numbers of TILs in several tumour types. With efforts to broaden ACT for other cancers, T cells derived from peripheral blood have been genetically modified to endow them with anti-tumour activity, using either transgenic TCRs that can elicit robust immune responses to cancers from patients or chimeric antigen receptors (CARs) capable of targeting known tumour antigens [73].

1.4 CAR-T cell therapy

CARs are fusion molecules that link extracellular antigen binding domain to intracellular signalling molecules. T cells engineered with CARs are able to directly bind antigens expressed on the surface of target cells like cancer cells through the antigen-specific binding domain. Notably, unlike TCR technology, this recognition process is not MHC-restricted and thus can overcome one well-documented mechanism of tumour cell evasion, which is achieved by the modulation or down-regulation of MHC expression [74]. However, as it is difficult to find surface antigens that are solely expressed on cancer cells, collateral damage must be tolerable.

1.4.1 CAR design

CARs consist of an extracellular antigen-binding domain, a hinge, a transmembrane domain and an intracellular signalling domain (Figure 1.3).

1.4.1.1 Antigen-binding domain

The specificity of CAR-T cells to recognize tumour cells' surface molecules depends on the target-binding domain. Actually its design can be anything that has high affinity for a given target. It is typically derived from a single chain variable fragment (scFv) from a parental antibody, which combines a light chain and a heavy chain using a flexible linker. A major caveat of scFv-based extracellular recognition domains is that their specificity is restricted to antigens expressed on tumour cells' surface. Therefore, cancer-testis and tumour-specific antigens such as the MAGE family and NY-ESO1 which are intracellular cannot be recognized by CARs [75].

Meanwhile, many other antigen recognition region alternatives are available, such as IL-13 mutein [76], heregulin [77] or T1E peptide [78]. For instance, CAR-T cells expressing IL-13 muteins could recognize and kill IL-13receptor α-2 (IL13Rα2)-positive glioma cells efficiently with abundant production of IL-2 and showed marked increases in survivals in glioma xenograft models [76]. However, the use of non-antibody based extracellular domain remains a theoretical risk to generate antibodies against junctional elements within the CAR ectodomain as its non-self antigen characteristic [79].

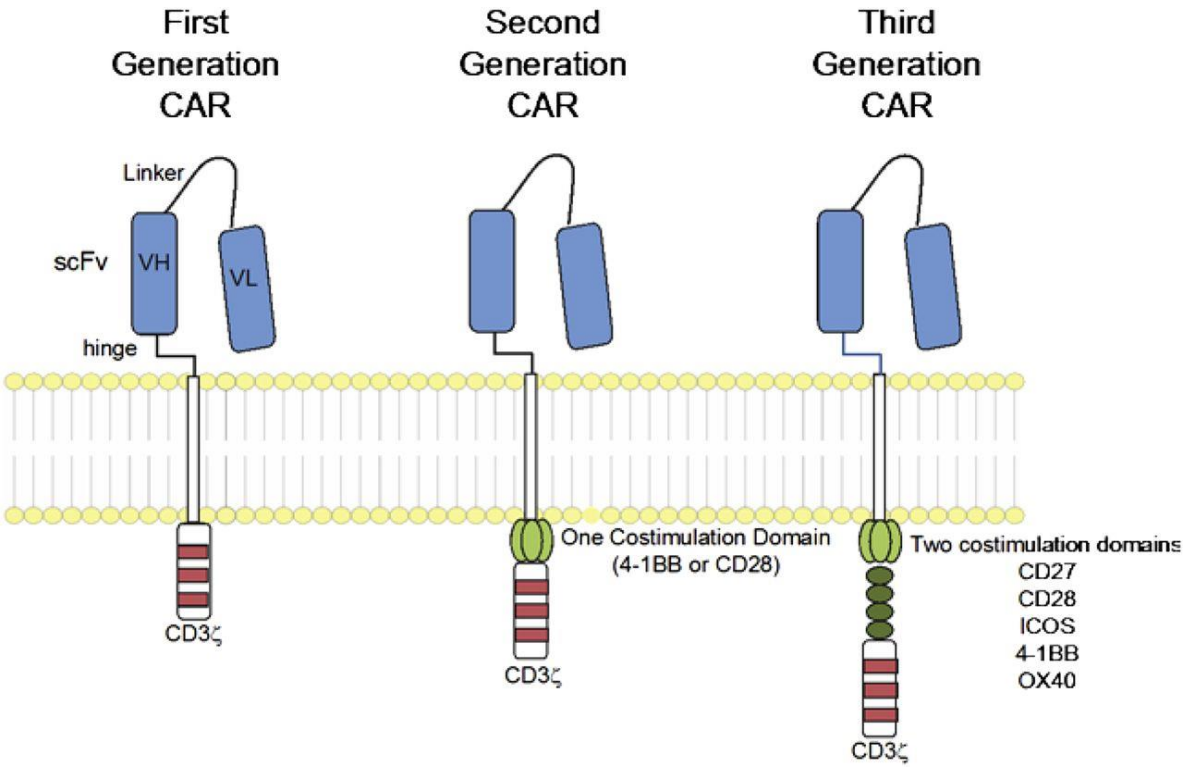

Figure 1.3 Schematic overview of CAR structure

The antigen binding, non-signalling and signalling elements can be modified to optimise the potency of CAR-T cells, such as tumour antigen recognition and activation signalling. First-generation CARs only contain a single CD3ζ activation domain, while second- and third- generations have one or two co-stimulatory domains respectively, such as CD28 and 41BB. Co-stimulation acts to enhance T cell proliferation, persistence and function by fully achieving T cell activation. Adapted from Maude et al., 2015 [80].

1.4.1.2 Hinge/spacer and transmembrane domain

The spacer region of CARs physically separates the antigen-binding domain from the T cell membrane. When the target antigen lies close to the cell membrane or it is complex in size and glycosylation status, a spacer seems to be required to enable efficient target recognition [79]. However, the optimal length of spacer is likely to be different based on the position of the target antigen [81].

The spacer is commonly derived from human IgG, typically IgG1 or IgG4, due to their stable expression. However, the IgG Fc portion of the spacer can bind with Fc gamma receptors (FcγRs) expressed on myeloid cells, resulting in limited persistence and reduced anti-tumour activity of CAR-T cells due to activation-induced cell death (AICD) [81]. But strategies like deleting or modifying the constant heavy (CH2) domain that is responsible for FcγR binding can be applied to tackle this problem [81].

The function of the transmembrane domain is to anchor the extracellular domain to the plasma membrane. The most commonly used are CD3ζ, CD28 and CD8α. Generally, CD28 would be used in the transmembrane region if it also serves as the co-stimulatory domain, while CD8α has been used when 4-1BB provides the co-stimulation [82].

1.4.1.3 Signalling domain

After antigen recognition, the activation signal from the CAR to the T cell is transmitted via the signalling domain. First-generation CAR-T cells only have a single stimulatory domain of which the most commonly used is the CD3ζ that is derived from the TCR/CD3 complex, as its three immunoreceptor tyrosine-based activation motifs (ITAMs) provide a sufficiently potent "signal one" [83]. However, although first-generation CAR-T cells are able to induce anti-tumour activity, additional co-stimulatory domains are applied to enhance T cell proliferation and efficacy, as in the absence of further signal ("signal two" or co-stimulation), T cells cannot be fully activated and thus become unresponsive or undergo activation induced cell death through apoptosis. Therefore, second-generation and third-generation CARs have been designed to contain one or two co-stimulatory domains in conjunction with CD3ζ respectively.

Second-generation CAR-T cells designed to incorporate co-stimulatory domains, such as CD28, 4-1BB (CD137), OX40 (CD134) and ICOS, can enhance cytokine release and T cell proliferation and persistence *in vivo* [84]. The most studied co-stimulatory signalling domains are CD28 and 4-1BB. In particular, the CD28 co-stimulatory domain can eliminate the suppressive function of TGF-β on T cell proliferation, reflected by a more pronounced

anti-tumour efficacy against TGF-β-secreting tumours by T cells armed with CD28-CD3ζ domain compared with T cells with CD3ζ *in vivo* [85]. Furthermore, the modification of the CD28 endodomain by deletion of the lymphocyte-specific protein kinase (LCK) binding moiety can abrogate IL-2 secretion upon CAR engagement, which results in reduced Treg persistence, and thus the improvement of anti-tumour efficacy of CAR-T cells in the presence of Tregs [86]. As for 4-1BB co-stimulation, its use enhances long-term persistence and effector function of CD19-specific CAR-T cells [80], which may be achieved by ameliorating the T cell exhaustion induced by persistent signalling of CARs [87]. However, it is still difficult to determine the best CAR co-stimulation for purpose due to variation in constructs, protocols and targets at different institutions that have contributed to the prevalent literature to date.

The incorporation of two co-stimulatory modules such as CD28 and 4-1BB in the third-generation CAR-T cells is likely to promote overall T cell activity, as CD28 and 4-1BB initiate PI3K and tumour necrosis family receptor-associated factor (TRAF) adaptor proteins signalling pathways respectively [88]. However, it remains too soon to judge if the efficacy of third-generation CAR-T cells will be better than second-generation CAR-T cells, as the number of clinical studies so far are limited.

1.4.2 Target selection

Target selection is of great importance in CAR technology. An antigen which is only expressed on cancer cells is an ideal target for CAR-T cells, which means that normal tissues would not be recognized and destroyed by CAR-T cells. For instance, the EGFR mutant, EGFRvIII, due to a mutation in glioblastoma [89], is absent in healthy tissues. However, those ideal antigens are limited and the majority of target cell surface antigens show at least some expression in normal tissues. Therefore, the majority of target antigens under research for CAR-T cell immunotherapy have high expression in tumours but lower levels in normal tissues, including CD19, CEA, mesothelin, HER2, prostate-specific membrane antigen (PSMA) and MUC-1. For example, CD19 is present on all B cell malignancies and at almost all stages of B-lineage differentiation but, crucially, is not present at haematopoietic stem cells or other tissues [79]. Although CD19-targeting CAR-T cell therapy might lead to B cell aplasia, patients' long term tolerance showed that CD19 is still an attractive target for selection [90]. Apart from protein antigens, carbohydrate and glycolipid tumour antigens can serve as potential targets as well [91].

1.4.2.1 CEA as target antigen

CEA is one of the carcinoembryonic antigen-related cell adhesion molecule (CEACAM) family members, termed as CEACAM5 or CD66e, belonging to the Ig superfamily. It is a glycosylated protein of approximately 150-180 kDa. Its structure contains one variable (V)-like domain, identified as the N domain, followed by three pairs of constant C2-like Ig domains [92]. Its structure also contains 28 complex N-linked glycosylation sites in line with the multi-antennary carbohydrate structures. CEA is anchored to the cell membrane through a glycosylphosphatidylinositol (GPI) linkage, which is achieved by post-translational modification of a small hydrophobic C-terminal region consisting of 26 amino acids. In addition, CEA can be secreted from cells.

CEA is present early in human embryonic and foetal development, but not in mouse, and is expressed at low levels on healthy tissues such as colon, stomach, tongue, cervix, sweat glands, esophagus and prostate [93]. However, CEA is significantly overexpressed in nearly 90 % of colorectal, gastric, pancreatic carcinomas, approximately 70 % of non-small-cell lung cancers and 50 % of breast cancers [94]. CEA is used clinically as a tumour marker in monitoring colorectal carcinoma (CRC) and has also been used in combination with other markers for a number of cancers such as breast and lung.

CEA plays a significant role in tumour progression and metastasis by several mechanisms. While membrane-bound CEA can directly bind a cell surface receptor on a target cell through homophilic or heterophilic association, secreted CEA can stimulate secretion of pro-tumorigenic and pro-metastatic cytokines via a paracrine manner [95]. For instance, CEA expressed on epithelial cells may directly influence tumour development through CEA-CEA bridges between tumour cells and stromal cells via bindings between the N and A3B3 domains, allowing the aggregation of tumour cells and the formation of a multi-layered structure of malignant epithelium. Also, heterophilic interactions of CEA and CEACAM1 expressed on the surface of NK cells via their N-terminal domains can lead to MHC-independent inhibition of NK cell killing, while the involvement of C2-like Ig domains within CEA enhance the intensity of the CEA binding with CEACAM1 [96]. In addition, Lewis X and Lewis Y carbohydrates, which are present on CEA, can interact with dendritic cell intercellular adhesion molecule 3-grabbing nonintegrin (DC-SIGN) and may suppress DC functions [97].

Secreted CEA can bind with a putative CEA receptor (CEAR) identified as heterogeneous nuclear ribonucleoprotein M (hnRNP M) on the surface of liver macrophages (Kupffer cells). This leads to Kupffer cell activation and release of pro-inflammatory cytokines including IL-1α, IL-1β, IL-6 and TNF-α [98]. These cytokines cause hepatic sinusoidal endothelial

cells to upregulate the expression of a number of cell adhesion molecules such as ICAM-1, VCAM-1, and E-selectin which in turn facilitate the binding of circulating tumour cells to the endothelium and support metastatic development. The secretion of the anti-inflammatory cytokine IL-10 by Kupffer cells activated by CEA also protects tumour cells against cytotoxicity by nitric oxide (NO) [99]. In addition, by heterophilic association with death receptor 5 (DR5) or TGF-βR1 on tumour cells, CEA can increase metastasis by decreased anoikis (cell death upon detachment from the matrix) or resistance to TGF-β-mediated growth inhibition respectively [100, 101].

As CEA has a critical function in tumour growth and metastasis, CEA can be a good target for CAR-T cell therapy. Apart from its overexpression on tumour cells, its role on liver metastasis is an important factor. In particular, although tumour cells may manage to escape from CEA-specific CAR-T cell responses and become CEA-negative, those variants will have a compromised ability to metastasise to other tissues such as the liver and therefore become less deadly.

1.4.3 Clinical studies of CAR-T cell therapy

In the context of haematological malignancies, most clinical studies involve the use of CD19-targeted CARs. Notably, T cells armed with CD19-specific CARs have resulted in complete remission (CR) rates of 70 – 90 % in patients with refractory B-cell Acute Lymphoblastic Leukaemia (B-ALL) [102-105]. Several clinical trials have reported that the overall rate response including partial response (PR) and CR of 57 – 88 % in patients with chronic lymphocytic leukaemia (CLL) [106-108]. Despite lower CR rates in CLL treatment, CD19-specific CAR-T cells appear to persist longer compared to some ALL treatments [109]. CAR-T cell persistence varies depending on CAR designs. While CD19-specific CAR-T cells with CD28 co-stimulatory domain were reported to persist by 1-3 months [102], longer persistence reached up to 2 years in CAR-T cells with 41BB co-stimulatory domain [104]. Recently, two CD19-specific CAR-T cell treatments were approved by FDA, the European Medicines Agency (EMA) and the National Institute for Health and Care Excellence (NICE). Kymriah™ (tisagenlecleucel), with the 41BB-CD3ζ signalling domains, was approved for refractory or relapsed B-ALL and diffuse large B cell lymphoma (DLBCL) [110, 111]. Yescarta™ (axicabtagene ciloleucel), with the CD28-CD3ζ signalling domain, was approved for patients with relapsed or refractory aggressive non-Hodgkin lymphoma and DLBCL [112]. More clinical trials of CAR-T cell therapy targeting other antigens such as B cell maturation antigen (BCMA), CD20, CD22, CD30 are ongoing for haematological malignancies.

At present, a number of clinical trials employing CARs specific for solid tumour antigens including CEA, HER2, GD2, mesothelin and PSMA are on-going or completed. However, the efficacy of CARs specific for solid tumour antigens has largely been disappointing to date [113]. Aside from the paucity of tumour-specific target antigens, preclinical studies suggest that this is partly due to several immunosuppressive mechanisms in tumours as mentioned in section 1.2.3, which can hinder CAR-T cell homing, intra-tumoural penetration, persistence and effector function. For instance, the interaction of PD-1 with its ligand, PD-L1, over-expressed on tumour cells would inhibit T cell activation and cytokine production [114]. Furthermore, TGF-β also plays a critical role on suppressing anti-tumour responses by modulating the function of a wide range of immune cells including effector T cells and APCs [115]. To improve the efficacy of CAR-T cell therapy for solid tumours, multiple strategies have been investigated which are discussed in section 1.4.5.

1.4.4 Toxicities induced by CAR-T cells

While CAR-T cell immunotherapy shows promising efficacy in some clinical trials, its potential toxicity should also be considered. There are several aspects of toxicity induced by CAR-T cell therapy, including cytokine release syndrome (CRS), tumour lysis syndrome, neurotoxicity and on-target off-tumour toxicity.

1.4.4.1 Cytokine release syndrome

CRS is the most common toxicity induced by CAR-T cell therapy. This toxicity is associated with CAR-T cell activation and proliferation upon tumour recognition, which leads to the release of large numbers of pro-inflammatory cytokines such as TNF-α, IFN-γ and IL-6 [116]. While its symptoms are characterized by fevers and myalgias in most cases, severe CRS can lead to multiple organ failure and finally cause the death of patients. Morgan et al reported the fatality of a patient after HER2/neu-targeted CAR-T cell treatment for colon cancer, due to a release of inflammatory cytokines, which caused pulmonary oedema and led to a cascading cytokine storm that resulted in multiorgan failure [117].

Although clinical data show that some degree of cytokine release is frequently correlated with the activation of CAR-T cells and their effective responses [104], CRS toxicity needs to be better predicted, understood and effective treatment options in place. Determined by severity, several approaches are applied to the management of CRS, such as symptomatic treatment, fluid replacement, oxygen and vasopressor support and immunosuppression. For instance, elevated levels of serum IL-6 in patients have been

shown to correlate with severe CRS and the use of IL-6 receptor blocking monoclonal antibody, tocilizumab, has been demonstrated to effectively induce rapid reversal of severe CRS without inhibiting the efficacy of CD19 CAR-T cells [102]. If IL-6 receptor blockade alone is not sufficient to control CRS, corticosteroids can be a choice to blunt CRS by suppressing inflammatory responses, which also have the potential to reduce anti-tumour efficacy of CAR-T cell therapy through clearance of therapeutic T cells [118]. Alternative strategies that rapidly eliminate CAR-T cells can also be applied to control CRS, such as the use of a suicide system, which will be discussed below.

1.4.4.2 Tumour lysis syndrome

Tumour lysis syndrome occurs when large numbers of tumour cells are lysed rapidly, leading to systemic metabolic disturbances. It can be characterized by the abruptly elevated release of potassium, phosphate and uric acid, accompanied by hypocalcaemia and sometimes renal failure [119].

1.4.4.3 Neurotoxicity

Neurotoxicity, also referred to as CAR-related encephalopathy syndrome (CRES) [118] or immune effector cell-associated neurotoxicity syndrome (ICANS) [120], is another acute toxicity commonly observed with CAR-T cell therapy. It can occur during CRS or after CRS has abated. Symptoms of neurotoxicity are diverse and include encephalopathy, delirium, aphasia, headache, motor weakness, tremor, seizures, depressed level of consciousness, and, rarely, diffuse cerebral edema [120].

The cause of this toxicity is less well understood than CRS. Similar to CRS, the severity of neurologic toxicity is associated with the degree of CAR-T cell expansion, cytokines and chemokines [112, 121]. Furthermore, CAR-T cells are detected in the cerebrospinal fluid (CSF) of most patients with neurotoxicity. It has been reported that endothelial cell activation and blood-brain barrier disruption may result in CAR-T cell trafficking and neurotoxicity [121]. Since the mechanisms of neurotoxicity remain unclear, current management approaches focus on supportive care for low-grade toxicity and corticosteroids for more severe grades.

1.4.4.4 On-target off-tumour toxicity

The risk of on-target off-tumour toxicity is a major concern in CAR-T cell therapy. This is because CAR-T cells are unable to distinguish between tumours and normal tissues while

the targeted antigens are expressed in both of them, thus resulting in the destruction of normal tissues.

In the case of B cell malignancies, CD19 is present at all stages of B-lineage differentiation from pro-B cells to mature B cells but, crucially, is not present on haematopoietic stem cells. Therefore, although the treatment of CD19-targeted CAR-T cells leads to B cell aplasia, it is thought to be acceptable in the context of untreatable B cell malignancy. Also, such toxicity can be mitigated by immunoglobulin replacement therapy [122].

This toxicity remains challenging in the case of many solid tumours, as the majority of antigens overexpressed by tumour cells are also present at low expression, although at different levels, in some healthy tissues. These tissues are therefore recognized due to the high specificity of CAR-T cells and this poses a significant problem where these healthy tissues are not disposable [79].

1.4.5 Strategies to improve CAR-T cell therapy for solid tumours

Given multiple hurdles raised by solid tumour against T cells, CAR-T cell therapy has yet to show encouraging clinical outcome for solid tumours. In an attempt to achieve better therapeutic efficacy, combination with other therapies including chemotherapy pre-conditioning or immune checkpoint inhibitors has been investigated. Moreover, additional engineering of CAR-T cells has been developed to increase the trafficking and infiltration of CAR-T cells towards tumour sites, counteract the immunosuppressive TME, improve CAR-T cell function and mitigate potential toxicities.

1.4.5.1 Chemotherapy pre-conditioning

Chemotherapy provides a vast range of available therapies for cancer treatment, using cytotoxic drugs to disrupt the growth of tumour cells. The significant drawback is that most conventional chemotherapy also affects rapidly dividing cells, such as immune cells, gut epithelia, and the hair follicles. In addition, some chemotherapy agents such as cyclophosphamide, fludarabine, mitoxantrone and oxaliplatin can induce immunogenic cell death (ICD), which result in an effective anti-tumour immune response by activating DCs and then specific T cell responses [123, 124]. Chemotherapy also induces anti-tumour activity through other mechanisms such as sensitizing tumour cells [125], reducing PD-L2 expression on tumour cells [126], selectively depleting Tregs [127] and MDSCs [128] showing the differential sensitivity of immune cell types.

Due to the effects of chemotherapeutic agents on lymphodepletion, chemotherapy has been used as the standard pre-treatment for CAR-T cell therapy. In fact, chemotherapy pre-conditioning has been demonstrated to augment therapeutic efficacy by promoting the engraftment of CAR-T cells [129], mainly depleting existing T cells that compete for space and pro-proliferative and anti-apoptotic signalling cytokines particularly IL-7 and IL-15 and thus making room for adoptively transferred T cells; resulting in the spontaneous expansion of the remaining T cells to maintain homeostasis, a phenomenon known as rebound overshoot [130].

1.4.5.2 Improving CAR-T cell infiltration

Intravenous administration is the most common way to inject CAR-T cells. Once CAR-T cells are infused into the systemic circulation, an immediate obstacle is the ability of CAR-T cells to target and infiltrate into the solid tumour. This process is governed by the expression and pairing of adhesion molecules on both T cells and the tumour endothelium that sequentially mediate binding, induction of signalling cascades and extravasation of circulating lymphocytes towards a chemokine gradient produced by tumour cells. However, abnormal expression of adhesion molecules on the tumour endothelium as well as the mismatch between T cell chemokine receptor and tumour-associated chemokine lead to insufficient T cell infiltration.

One strategy to overcome this problem is to modify CAR-T cells to additionally express chemokine receptors complementary to tumour-associated chemokines. For example, it has been reported that anti-mesothelin CAR-T cells co-expressing CCR2b showed improved trafficking and subsequent tumour eradication in the model of malignant pleural mesothelioma where the chemokine CCL2 was highly secreted [131]. The forced expression of CCR4 by anti-CD30 CAR-T cells improved their migration to $CD30^+$ Hodgkin lymphoma and the anti-tumour efficacy [132]. However, the feasibility of this approach is limited by the fact that the chemokine landscape can be heterogenous across cancer types and patients, underscoring the need to discover the appropriate chemokine receptor candidates for different cancer types [133]. Moreover, chemokines are not restricted to the tumours, suggesting the possible infiltration of CAR-T cells to other tissues where the specific chemokine is present.

Local/regional delivery of CAR-T cells is also being explored. This strategy has the advantage of reducing the trafficking and infiltration restrictions without additional modification, while avoiding the transient pulmonary distribution of intravenously administered CAR-T cells which is likely to be highly associated with development of

pulmonary toxicity [134, 135]. Recent studies have reported that administration of CAR-T cells was performed via local/regional injection, showing improved anti-tumour activity compared to intravenous delivery in preclinical studies [136, 137] and extensive tumour cell death and other signs of anti-tumour inflammation such as macrophage recruitment in patients with metastatic breast cancer in a phase 0 clinical trial (NCT01837602) [138]. Notably, this approach is more technically challenging and probably not practical for patients with metastatic cancer at several sites.

1.4.5.3 Counteracting the immunosuppressive tumour microenvironment

Following infiltration into the solid tumour, CAR-T cells have to face a microenvironment rich in suppressor cytokines such as TGF-β, IL-10 and inhibitory molecules including PD-L1 as described in section 1.2.3. To endow CAR-T cells with the ability to resist immunosuppressive signalling and exert their effector function, there are several strategies which focus on neutralising the suppressive effects mediated by TGF-β, CTLA-4 or PD-1 signalling. For example, it can be achieved by deletion of TGF-β receptor II (TGF-βRII), CTLA-4 or PD-1 expression on CAR-T cells through gene editing such as CRISPR–Cas9 technology or small interfering RNA (siRNA) technology [139-142], and modification of T cells to co-express CAR constructs and transgenic immune checkpoint inhibitors such as anti-PD-1 scFv [143]. An alternative approach involves the transgenic expression of truncated receptors on CAR-T cells such as a dominant-negative form of TGF-βRII or PD-1, which competes with the active receptors for binding to TGF-β and PD-L1 respectively [144, 145].

Switch receptors have also been designed to convert the suppressive signal into the stimulatory signal for T cell response, which can extend CAR-T cell engineering beyond neutralisation of inhibitory receptors or suppressive mediators to the active reversal of their effects. In the chimeric switch-receptor approach, the extracellular ligand-binding domain of inhibitory receptors such as IL-4 receptor (IL-4R), PD-1 or CTLA-4 is fused with the transmembrane domain and cytoplasmic signalling domain derived from stimulatory receptors such as IL-7 receptor (IL-7R) and CD28. In several preclinical studies, T cells transduced with switch receptors including TGF-β:CD28, PD-1:CD28, CTLA:CD28 and IL-4R:IL-7R have shown improved in vivo anti-tumour efficacy [146-149].

Notably, as those inhibitory receptors are essential regulators of T cell homeostasis, the possibility for uncontrolled proliferation and activation of CAR-T cells should also be noted. However, the possibility for uncontrolled proliferation and activation of CAR-T cells should also be noted. In addition, given that systemic blocking of checkpoint receptors with

antibodies has the disadvantage of inducing systemic autoimmune side effects that are sometimes problematic [150, 151], the combination of immune checkpoint blockade and CAR-T cell therapy may greatly exacerbate the autoreactive toxicity.

An alternative strategy for overcoming the unfavourable TME involves the use of fourth-generation CAR-T cells, also known as TRUCKs (T cells redirected for universal cytokine-mediated killing). Specifically, CAR-T cells are utilised as production and delivery vehicles that constitutively or inducibly secrete pro-inflammatory cytokines, such as IL-12, IL-18 and IL-15, to the targeted tumour [152-154]. Whilst the release of transgenic cytokines can directly stimulate the transferred CAR-T cells for a more acute inflammatory response, it also supports the generation of new antigen-specific lymphocytes via epitope spreading as well as the recruitment and activation of innate immune cells including macrophages and NK cells in a locally restricted region, resulting in an attack towards tumour cells that cannot be recognized by CAR-T cells [155, 156]. These effects will consequently synergise with CAR-T cells for augmented anti-tumour activity.

The inducible cytokine expression, such as inducible IL-12 (iIL-12), is controlled by a nuclear factor of the activated T cell (NFAT)-responsive expression cassette [157]. Activated by target-initiated CAR CD3ζ signalling, the NFAT/IL-2 minimal promoter initiates IL-12 transcription and finally induced IL-12 accumulates to high levels in the targeted tumour lesion. Given its ability to restrict the concentration of transgenic cytokines, an inducible expression system may avoid overactivation of T cells which possibly fosters counterproductive exhaustion and may cause less systemic side effects than the constitutive release system [155]. However, the limitation is that the inducible release of transgenic cytokines is determined by CAR signalling and cannot be induced in the tumour lesions without CAR-T cell activation [153]. Whilst the inducible release system may be fine for CD19-targeting haematological malignancies where CAR-T cells are always in contact with B cells, it is possibly limited for solid tumours due to the potentially insufficient CAR-T cell activation.

1.4.5.4 Improving CAR-T cell specificity for tumour targets

As described in section 1.4.2, the majority of tumour antigens targeted are present at low levels in normal tissues, which will potentially lead to on-target off-tumour toxicity. Moreover, targeting of a single antigen correlates with immune escape due to down-regulation or mutation of tumour antigens. To improve the precision of tumour targeting and limit off-tumour recognition, several strategies have been applied in CAR design.

For example, a bispecific CAR is designed to have two distinct antigen-binding domains in tandem coupled to the same signalling endodomain (TanCAR). The TanCAR T cells co-expressing both CD19 and HER2 was demonstrated to have greater anti-tumour response than those CAR-T cells expressing either antigen alone, suggesting that it may be a means to minimise the risk of tumour escape [158].

In addition, a dual targeting strategy that may be used to enhance discrimination between tumour cells from normal cells is to co-express two separate CARs in T cells. Notably, those separate CARs only have a signalling domain (signal 1) and a co-stimulatory domain (signal 2) respectively. As the full activation of such CAR-T cells require both signal 1 and 2 delivered by the binding of double-positive target cells, normal cells that express only one of these antigens are unlikely to fully activate CAR-T cells. However, to achieve this targeting specificity, the signalling strength of the CAR delivering signal 1 may need to be attenuated, such as by utilizing low affinity of scFv [159], as it can still elicit strong enough cytotoxicity responses like first-generation CAR-T cells. Furthermore, if the expression of target antigens is abundant on normal tissues, activation induced cell death may occur and then lead to the short persistence of CAR-T cells.

Co-expression of inhibitory CARs (iCARs) together with activating CARs can be applied to regulate CAR recognition as well. Inhibitory CARs are designed to specifically recognize antigens that are expressed in normal tissues but are down-regulated or lost in tumours, in order to prevent T cells from carrying out cytotoxic effector functions against non-tumour tissues. This can be achieved using signalling domains from checkpoint molecules such as PD-1, CTLA-4 or a range of phosphatases that negatively regulate T cell signalling. As the feasibility of this approach has been demonstrated by co-expressing a CD19-specific activating CAR and a PSMA-specific inhibitory CAR [160], it is particularly attractive for improving the specificity of tumour recognition and reducing the risk of off-tumour toxicity.

1.4.5.5 CAR-T cell depletion to mitigate off-tumour toxicity

Apart from engineering approaches to improve specificity to solid tumour antigens, CAR-T cell depletion can be another strategy to reduce severe toxicities. For example, suicide gene technology has been utilised to deplete activated CAR-T cells. The most effective to date is the inducible caspase 9 (iCasp9) system, which consists of the intracellular portion of the human caspase 9 protein, a pro-apoptotic molecule, and human FK506 binding protein domain [161]. The advantage of this humanized protein is that it will not cause immune rejection of T cells from the host. Activated by the small-molecule, chemical induction of dimerization (CID) drug, AP1903, this fusion protein would be dimerised and

activates the downstream executioner caspase 3 molecule, leading to cellular apoptosis and clearance rapidly [162]. Preclinical and clinical studies have demonstrated the efficacy and safety of iCasp9 system, compared with other established methods that require prolonged treatment, remove a small proportion of transduced cells, or show low persistence of transferred T cells due to anti-transgene immune responses [163, 164]. Furthermore, the use of iCasp9 system has been shown to improve the safety of CAR-T cells in preclinical models [165] and several clinical trials are still ongoing (NCT01822652, NCT02992210).

1.5 Project aims

CAR-T cell therapy has shown spectacular objective clinical responses in haematological malignancies such as leukaemia. However, CAR-T cells have largely failed to deliver significant clinical responses in the solid tumour setting. Our key hypothesis is that CAR-T cell effector function is strongly inhibited by the immunosuppressive microenvironment within solid tumours. The central aim of this project is, therefore, to exploit genetic engineering solutions in anti-CEA CAR-T cells to counteract the suppressive effects of tumour microenvironment. Immune modulatory CAR-T cells, which additionally secrete pro-inflammatory cytokines IL-12 or scFv blocking TGF-β or PD-1 signalling, will be developed.

The specific aims of this study were:

- To design and generate retroviral vectors encoding first- and second- generation anti-CEA CAR constructs and IL-12 or scFv expression cassette
- To assess whether T cells could be successfully transduced to express anti-CEA CARs and secrete IL-12 or scFv
- To evaluate whether secretion of IL-12or scFv enhance anti-tumour effects of CEA-specific CAR-T cells *in vitro*
- To establish an immunocompetent *in vivo* model with subcutaneous CEA^+ tumours
- To evaluate whether anti-tumour efficacy of CAR-T cells could be enhanced by secreting IL-12 or scFv *in vivo*

2 Materials and Methods

2.1 Molecular biology

2.1.1 Plasmids

The plasmids shown below were kindly donated by Dr Gray Kueberuwa and were constructed by altering the scFv sequence or the co-stimulatory signalling domain to the desired sequence (Table 2.1). The 3TP-Lux plasmid was a kind gift from Dr Aalia Alamoudi.

Table 2.1 Summary of plasmids used in the experiments

Plasmids	Abbreviation
Plasmids donated by Dr Gray Kueberuwa	
pMP71.tCD34.2A.MFE23.hCD28.hCD3ζ	MFE23.hCD28z
pMP71.mCherry.2A.1D3.mCD3ζ	1D3.mCD3z
pMP71.mCherry.2A.1D3.mCD28.mCD3ζ	1D3.mCD28z
pMP71.mCherry.2A.1D3.m41BB.mCD3ζ	1D3.m41BBz
pMP71.mCherry.2A.1D3.mCD3ζ.mIL12	1D3.mCD3z.IL12
pMP71.mCherry.2A.1D3.mCD28.mCD3ζ.mIL12	1D3.mCD28z.IL12
pMP71.mCherry.2A.1D3.m41BB.mCD3ζ.mIL12	1D3.m41BBz.IL12
pMP71.mCherry.2A.1D3.mCD3ζ.hTA	1D3.mCD3z.TA
pMP71.mCherry.2A.1D3.mCD3ζ.hTA.CH2CH3	1D3.mCD3z.DTA
pUC57 mCD3ζ.NFAT.mIL12	pUC57 mCD3z.NFAT.mIL12
pMK-RQ mCD3ζ.mPA	pMK-RQ mCD3ζ.PA
pMK-RQ mCD3ζ.mPA.CH2CH3	pMK-RQ mCD3ζ.DPA
pkat	pkat
pcl-Eco	pcl-Eco
rkat.lucifease.IRES.GFP	rkat.luc.IRES.GFP
Plasmids constructed	
pMP71.mCherry.2A.MFE23.mCD3ζ	MFE.mCD3z
pMP71.mCherry.2A.MFE23.mCD28.mCD3ζ	MFE.mCD28z
pMP71.mCherry.2A.MFE23.m41BB.mCD3ζ	MFE.m41BBz
pMP71.mCherry.2A.MFE23.mCD3ζ.mIL12	MFE.mCD3z.mIL12
pMP71.mCherry.2A.MFE23.mCD28.mCD3ζ.mIL12	MFE.mCD28z.mIL12
pMP71.mCherry.2A.MFE23.m41BB.mCD3ζ.mIL12	MFE.m41BBz.mIL12
pMP71.mCherry.2A.MFE23.mCD3ζ.NFAT.mIL12	MFE.mCD3z.NFAT.mIL12
pMP71.mCherry.2A.MFE23.mCD28.mCD3ζ.NFAT.mIL12	MFE.mCD28z.NFAT.mIL12
pMP71.mCherry.2A.MFE23.m41BB.mCD3ζ.NFAT.mIL12	MFE.m41BBz.NFAT.mIL12
pMP71.mCherry.2A.MFE23.mCD3ζ.hTA	MFE.mCD3z.TA
pMP71.mCherry.2A.MFE23.mCD28.mCD3ζ.hTA	MFE.mCD28z.TA
pMP71.mCherry.2A.MFE23.mCD3ζ.hTA.CH2CH3	MFE.mCD3z.DTA
pMP71.mCherry.2A.MFE23.mCD28.mCD3ζ.hTA.CH2CH3	MFE.mCD28z.DTA
pMP71.mCherry.2A.MFE23.mCD3ζ.mPA	MFE.mCD3z.PA
pMP71.mCherry.2A.MFE23.mCD28.mCD3ζ.mPA	MFE.mCD28z.PA
pMP71.mCherry.2A.MFE23.mCD3ζ.mPA.CH2CH3	MFE.mCD3z.DPA
pMP71.mCherry.2A.MFE23.mCD28.mCD3ζ.mPA.CH2CH3	MFE.mCD28z.DPA

2.1.2 Restriction enzyme digestion

For each digestion, 5 - 10 µg of DNA, 5 - 10 µl of reaction buffer, 25 - 50 U of each restriction enzyme and distilled water (dH_2O) were added and mixed in a sterile 1.5 ml microcentrifuge tube for a final volume of 50 - 100 µl. After incubation at 37°C water bath for 1 hour, backbone plasmid was de-phosphorylated to prevent re-ligation using 1 - 2 µl calf intestinal phosphatase (CIP) (New England Biolabs, UK) and both of plasmids were incubated for a further 1 hour at 37°C water bath. Digestion efficacy and fragment separation was assessed by gel electrophoresis.

2.1.3 Gel electrophoresis

1 - 2 % agarose gel was prepared using ultrapure agarose (Invitrogen, US) in tris-acetate EDTA (TAE) buffer (90mM TRIS base, 90mM acetic acid, 2mM EDTA). The agarose solution was heated until the agarose is completely dissolved and then cooled down for 5 min. Midori green (Nippon Genetics, Germany) was added at a concentration of 0.1 µl/ml before pouring into a gel tray. Once the gel was solidified, the DNA samples were prepared by mixing with DNA loading buffer blue (Bioline, UK) at 1: 5 ratio and loaded, along with the Hyperladder I marker (Bioline, UK). Running at 100 V for 45 - 60 min, the gel was imaged to identify and excise the required bands using a Visi-Blue transilluminator (UVP, US).

2.1.4 Gel purification

Isolation and purification of the target DNA fragments was performed using the Qiaquick gel extraction kit (Qiagen, UK) according to manufacturer's protocol. DNA concentration and purity were determined by Nanodrop (Labtech International, UK).

2.1.5 DNA ligation

Ligation of the target insert and the appropriate vector after restriction digest was performed. For each ligation, 14 µl of insert DNA, 3 µl of vector, 2 µl of T4 DNA ligase buffer (10x), 1 µl of T4 DNA ligase (New England Biolabs, UK) were added and mixed in a sterile 1.5 ml microcentrifuge tube for a final volume of 20 µl. A control ligation was added with 14 µl of dH_2O instead of insert DNA. The ligation reactions were incubated for 30 min at room temperature or 24 - 48 hours at 4°C.

2.1.6 Bacterial cell transformation

XL1-Blue or Dam^-/Dcm^- (JM110) competent cells were thawed on ice for 10 min. 5 µl of DNA ligation product was added to 100 µl of competent cells for ligation transformation, whereas 1 µg of plasmid DNA was added to 50 µl of competent cells for re-transformation. The competent cells containing the DNA were incubated on ice for 30 min, followed by heat shock at a 37°C water bath for 3 min and then incubation on ice for 2 min. Following this, 500 µl of Lysogeny Broth (LB) media without antibiotic was added and the samples were incubated in 37°C shaking incubator at 250 rpm for 1 hour. After that, bacteria were plated on pre-warmed agar ampicillin or kanamycin LB plates and the plates were incubated at 37°C overnight.

2.1.7 Plasmid DNA-Miniprep

Single colonies were selected and inoculated into 5 ml of LB media with the addition of ampicillin or kanamycin (Sigma Aldrich, UK) at 100 µg/ml. The cultures were incubated in 37°C shaking incubator at 250 rpm for 12 - 16 hours. Following this, the bacterial cells were harvested by centrifugation at 9000 rpm for 3 min at room temperature (15 - 25°C). Purification of plasmid DNA was performed using QIAprep Spin Miniprep Kit (Qiagen, UK) according to manufacturer's protocol. DNA concentration and purity were determined by absorbance at wavelength of 280 nm using a Nanodrop (Labtech International, UK).

2.1.8 Plasmid DNA-Maxiprep

To amplify a plasmid of interest, the bacterial cells containing plasmid DNA were inoculated into 400 ml LB media with the addition of ampicillin or kanamycin (Sigma Aldrich, UK) at 100 µg/ml. The cultures were incubated in 37°C shaking incubator at 250 rpm for 16 - 20 hours. Following this, the bacterial cells were harvested by centrifugation at 6000rpm for 15 min at 4°C. Purification of plasmid DNA was performed using QIAGEN Plasmid Maxiprep Kit (Qiagen, UK) according to manufacturer's protocol. DNA concentration and purity were determined by absorbance at wavelength of 280 nm using a Nanodrop (Labtech International, UK).

2.1.9 DNA sequencing

For sample sequencing, 350 - 500 ng of DNA, 3 - 15 pmol of the 5’ and 3’ sequencing primers and dH_2O were added and mixed in a sterile 1.5 ml microcentrifuge tube for a

final volume of 12 - 20 µl. The sequencing was determined by ABI PRISM® 3100-avant genetic Analyzer (Applied Biostystems, UK) and results were analysed using Lasergene software (DNASTAR, USA).

2.2 Tissue culture

2.2.1 Cell lines and culture media

The tumour cell lines, MC38 (kindly provided by Dr Jeffrey Schlom, NIH, US) and CT26 (ATCC, US) expressing human CEA extracellular domain and murine transmembrane domain (CEA^+ MC38 and CEA^+ CT26 cell line respectively), were generated by our laboratory. Tumour cells and the retroviral packaging cell line 293T (ATCC, US) were maintained in Dulbecco's Modified Eagle medium (DMEM) (Sigma Aldrich, UK) supplemented with 10 % heat inactivated foetal calf serum (FCS) (Gibco, US) and 2 mM L-glutamine (Sigma Aldrich, UK).

The retroviral packaging cell line, Platinum-E (Plat-E) (Cell Biolabs, Inc., US) were maintained in DMEM supplemented with 10 % heat inactivated FCS, 2 mM L-glutamine, 1 µg/ml puromycin and 10 µg/ml blasticidin (Sigma Aldrich, UK).

Mouse T cells were maintained in complete T cell media (TCM), which consists of Roswell Park Memorial Institute (RPMI)-1640 medium (Gibco, US) supplemented with 10 % FCS, 200 mM penicillin-streptomycin-glutamine (PSG) (Gibco, US), 25 mM HEPES (Sigma Aldrich, UK) and 50 µM 2-mercaptoethanol (Invitrogen, US).

All media were sterile filtered through 0.2 µm filters (Scientific Laboratory Supplies, UK) prior to use.

2.2.2 Culturing of adherent cell lines

Adherent cells were maintained in appropriate medium at 37°C, 5% CO_2 for incubation. Passaging was performed upon reaching 80 % confluency by incubation in trypsin (Sigma Aldrich, UK) followed by centrifugation at 500xg for 5 min. Cells were resuspended, enumerated and further cultured at the required cell density.

2.2.3 Culturing of mouse T cells

To isolate mouse splenic T lymphocytes, the spleen was dissected from BALB/c wild type (WT) mice or C57BL/6 WT or CEA transgenic mice, transferred into sterile phosphate-buffered saline (PBS) and mashed using a syringe plunger under manual force. The cell suspension was filtered through 100 µm pore cell strainer (VWR, US) and centrifuged at 400xg for 5 min. For red blood cell lysis, the pellet was resuspended in a 1x PharmLyse RBC lysis buffer (BD Biosciences, UK) and incubated for 3 min, followed by another centrifugation at the same settings. Cells were then resuspended in PBS, enumerated and cultured at 5 x 10^6 cells/ml. T cells were activated with 30 ng/ml anti-CD3ε antibody (clone: 145-2C11), anti-CD28 antibody (clone: 37.51) (αCD3ε and αCD28 antibodies) (both BD Biosciences, US), 100 IU/ml recombinant human IL-2 (hIL-2) (Novartis, Switzerland) and 2 ng/ml murine IL-7 (mIL-7) (BioLegend, US). Mouse splenic T cells were transferred to a tissue culture flask (Falcon) in complete TCM and incubated at 37°C, 5% CO_2 overnight. After 24-hour activation and subsequently 2-day transduction as described in section 2.3.2, transduced T cells were cultured at a density of 0.3 - 1 x 10^6 cells/ml with the addition of hIL-2 and mIL-7 at 100 IU/ml and 2 ng/ml respectively every other day.

2.2.4 Cell enumeration

Cells were brought into suspension as described above. 10 µl of cell suspension was mixed with trypan blue at a dilution of 1: 10 and the cell number in 4 squares of a 1/400 mm^2 hemocytometer (Appleton Woods, UK) was counted using a microscope and averaged. The number of cells per ml = average count per square x dilution factor (10) x 10^4.

2.2.5 Cryopreservation of cell lines

Cell freezing media was prepared using 10 % Dimethyl Sulfoxide (DMSO) (Sigma Aldrich, UK) and 90 % heat inactivated FCS. Cells were collected and centrifuged at 400xg for 5 min. The cell pellet was resuspended in 1 ml of cell freezing media and transferred to a Nunc cryovial (Sigma Aldrich, UK). Cells were stored at -80°C in the short term. For long term storage, cells were kept in liquid nitrogen at -196°C.

2.3 Retroviral transduction of T cells

2.3.1 Plat-E Retroviral Packaging Cell Line Transfection

On day 1, 6 x 10^6 Plat-E cells were seeded in 15 cm^2 tissue culture dishes in 16 ml of complete DMEM for incubation overnight at 37°C, 5% CO_2. On day 2, the DMEM media was removed from dishes and replaced by 12 ml of pH7.9 media (DMEM + 10 % FCS + 25 mM HEPES). 20.4 µg of pcl-Eco packaging vector DNA, 39.6 µg of plasmid DNA encoding retroviral CAR construct and 150 µl of 1M $CaCl_2$ was added and mixed with 3 ml of pH7.1 media (DMEM + 25 mM HEPES). The pH7.1 media containing DNA was added into the plates and the plates were gently rocked to mix and incubated at 37°C, 5% CO_2 overnight. The next day (day 3) media was removed and replaced with 16 ml of complete TCM. On day 4, viral supernatant was harvested from plates and filtered through a 0.45 µm filter (Appleton Woods, UK) for use on the first day of T cell transduction (section 2.3.1). 18 ml of fresh complete TCM was added and the incubation continued for a further 24 hours. On day 5, viral supernatant was harvested and filtered through 0.45 µm filter for use on the second day of T cell transduction (section 2.3.1). Successful transfection was confirmed using Leica DMi8 fluorescence microscope (Leica Microsystems, Germany).

2.3.2 Transduction of mouse T cells

Mouse T cell transduction was carried out using non-tissue culture 6-well plates coated with 2 ml 10 µg/ml RetroNectin (Takara Bio, Japan) overnight at 4°C. On day 1 of transduction, 2 ml of TCM was added to each well of previously RetroNectin coated plates to block non-specific binding and the plates were left for 30 min at room temperature. Retroviral-containing supernatant from Plat-E producer cells transfected with CAR construct and gag, pol and env encoding plasmid was collected and passed through a 0.45 µm filter to discard any non-adherent packaging cells. Following this, TCM was removed and 2.5 ml of filtered supernatant was added to each well. Plates were centrifuged at 1200xg for 30 min at room temperature. Activated T cells were collected, counted and centrifuged at 400xg for 5 min. T cells were resuspended in 2.5 ml of filtered supernatant at 5 x 10^6 cells/well and added into the coated plates with 100 IU/ml rhIL-2 and 2 ng/ml mIL-7 following centrifugation above. Plates were centrifuged at 1200xg for 90 min at room temperature and then incubated at 37°C, 5% CO_2 overnight. The transduction procedure repeated on day 2 using the day 1 transduced T cells. After 1.5-hour centrifugation and 3 - 4 hour incubation, T cells were seeded at a density of 1 x 10^6 cells/ml in TCM with 100 IU/ml rhIL-2 and 2 ng/ml mIL-7.

2.4 Retroviral transduction of CEA$^+$ tumour cells

The retroviral supernatant was prepared in a similar method in section 2.3.1. 20.4 µg of pkat packaging vector DNA, 39.6 µg of plasmid DNA encoding luciferase and GFP gene (rkat.luc.IRES.GFP) were used for this transduction.

Either CEA$^+$ MC38 cells or CEA$^+$ CT26 cells were seeded in a 6-well plate at a density of 1 x 10^5 cells/well 24 hours before transduction. On day 1 transduction, viral supernatant of transfection group was collected and passed through a 0.45µm filter to discard any non-adherent packaging cells. 5 ml/well of filtered supernatant was used to replace the DMEM media on CEA$^+$ tumour cells. Polybrene was added to each well at 4 µg/ml. The plate was centrifuged at 1200xg for 90 min at room temperature and then incubated at 37°C, 5% CO_2 overnight. The transduction procedure repeated on day 2 using the day 1 transduced tumour cells. After overnight incubation, CEA$^+$ tumour cells were grown in culture for a week and GFP expressing producers were sorting by FACSAria II or III (BD Biosciences, US). The analysis was performed by Novocyte (ACEA Biosciences, US) and results were analysed with FlowJo software.

After sorting and cell expansion, luciferase and GFP expressing CEA$^+$ tumour cells were seeded at different densities from 1 x 10^5 to zero cells in 200 µl DMEM/well in a 96-well U-bottom TC treated plate. Each condition was performed in triplicate. Cells were cultured at 37°C, 5% CO_2 for 20 hours. Following this, 150 µl of supernatant was discarded and the plate was added with 100 µl of luciferin solution (Perkin Elmer, US) diluted in PBS at a final concentration of 1.5 mg/ml and incubated for 10 min at 37°C, 5% CO_2. The luminescence intensity of each well was measured at 5 second exposure using the POLARstar Omega (BMG LABTECH, US). A linear standard curve was generated by plotting the average value of each standard.

2.5 Single cell cloning

CEA$^+$ MC38 cells with or without luciferase and GFP expression were counted and diluted to a concentration of 1 x 10^6 cells/ml. Further dilutions were performed to achieve a final concentration of 1.5 cells/ml in 25 ml. Mathematically, 0.3 cell in 200 µl was added to each well of a 96-well U-bottom TC treated plate. The assay therefore should contain roughly 1 cell every 3 wells. The diluted cells were allowed to grow for 7 - 14 days. Wells containing colonies identified under a microscope were marked and replaced with fresh media every 3 - 4 days. Cells were expanded until there were enough numbers for assessment of CEA and GFP expression by flow cytometry.

2.6 Flow cytometry

2.6.1 Cell surface staining

For the surface staining of CAR-T cells, 1 x 10^5 mock T cells or CAR-T cells were plated in a 96-well U-bottom plate and washed once with PBS, followed by staining with 100 µl of Zombie Violet dye (1: 100 dilution in PBS) (BioLegend, US) for 15 min at room temperature in dark. Cells were washed in 200 µl of FACS buffer (PBS, 1 % FCS) and centrifuged at 1300xg for 1.5 min. Then cells were resuspended and incubated with 50 µl of anti-mouse CD16/CD32 antibodies (clone: 2.4G2) (1: 100 dilution in FACS buffer) (BD Biosciences, US) for Fc receptor blocking for 10 min at 4°C. Another centrifugation and wash step were performed. Following this, 100 µl of surface marker antibodies (1: 100 dilution in FACS buffer) including anti-mouse CD4-BV785 (clone: RM4-5), CD4-APC (clone: GK1.5), CD8-BV711 (clone: 53-6.7) or PD-1-PE (clone: 29F.1A12) antibodies (BioLegend, US) were added, incubated for 30 min at 4°C and then washed in 200 µl of FACS buffer. Cells were fixed in 200 µl of 1 % paraformaldehyde (PFA) (Sigma Aldrich, UK) and kept in dark at 4°C until analysis.

For CEA surface staining of tumour cell lines, 1 x 10^5 tumour cells were plated in a 96-well U-bottom plate and washed in 200 µl of FACS buffer. 100 µl of primary mouse anti-human CEA antibodies (clone: Col-1, Invitrogen) (1: 100 dilution in FACS buffer) was added and incubated for 30 min at 4°C. Another centrifugation and wash step were performed. 100 µl of secondary anti-mouse IgG (whole molecule)-PE antibodies (1: 100 dilution in FACS buffer) (Sigma Aldrich, UK) was added and incubated for 30 min at 4°C. Unstained cells and cells stained with secondary antibodies only were used as negative control. For PD-L1 surface staining, similarly, 100 µl of anti-mouse PD-L1-BV421 antibodies (clone: 10F.9G2) or corresponding isotype antibodies (1: 100 dilution in FACS buffer) (BD Biosciences, US) were added, incubated for 30 min at 4°C and then washed in 200 µl of FACS buffer. Cells were washed in 200 µl of FACS buffer, fixed in 200 µl of 1 % PFA and kept in dark at 4°C until analysis.

2.6.2 Intracellular staining

Intracellular staining was performed to detect TGF-β production. MC38 tumour cells with or without CEA expression were incubated with 1 µl/ml Brefeldin A (eBioscience Inc., US) for 4 hours and then transferred to a 96-well U-bottom plate. Cells were washed in 200 µl

of FACS buffer and fixed and permeabilised using the FoxP3 / transcriptional factor staining buffer set (eBioscience Inc., US) for 60 min at 4°C. Following a wash step with 200 µl of 1X permeabilisation buffer, cells were incubated with 100 µl of anti-mouse TGF-β1-APC antibodies (clone: TW7-16B4) or isotype antibodies (1: 100 dilution in permeabilisation buffer**)** (BioLegend, US) for 30 min at 4°C. Cells were washed in 1X permeabilisation buffer and fixed in 1 % PFA until analysis.

Cytometric analysis was performed by BD LSRFortessa X-20 or ThermoFisher Attune™ NxT Flow Cytometer and subsequent data was analysed on FlowJo software.

2.7 Western blot

Western blot was performed to determine whether αTGF-β or αPD-1 scFv was expressed. Plat-E cells were transfected with the retroviral vectors encoding CAR constructs and the scFv expression cassette, as described in section 2.3.1. Notably, FCS-free DMEM was used for media replacement on the next day. After 24-hour cell culture, scFv-containing supernatant from transfected Plat-E cells was collected and passed through a 0.45 µm filter to discard any non-adherent packaging cells. The supernatant was transferred to a centrifugal filter unit (10 kDa molecular weight cutoff, Merck Millipore, US) and centrifuged at 4000 x g for 30 min at 4°C. The concentrated supernatant was collected and stored at -80°C for scFv detection by western blot or evaluation of scFv blocking assay.

20 µl of concentrated supernatant was diluted with 4 µl of 6x laemmli sample buffer and heated at 98°C for 5 min. Samples were loaded into the wells of a 12 % precast sodium dodecyl sulphate-polyacrylamide (SDS-PAGE) gel (Bio-Rad, US), along with the colour prestained protein standard (11 – 245 kDa) (New England Biolabs, UK). Electrophoresis was performed at 100 V for 90 - 120 min to separate the proteins. The proteins were transferred from the gel to the PVDF membrane using semi-dry transfer apparatus at 15 V for 60 min. The membrane was then blocked with 5% non-fat milk in PBS with agitation for 1 hour. After blocking, the membrane was incubated with the anti-His-tag antibody (BioLegend, US) diluted in 5 % non-fat milk in PBS at the 1: 1000 ratio overnight at 4°C. Following incubation with the primary antibody, the membrane was washed for 10 min with 0.1 % Tween-20 in PBS three times and incubated with peroxidise-conjugated anti-mouse IgG (Sigma Aldrich, UK) diluted in 5 % non-fat milk in PBS at the 1: 2500 ratio at room temperature for 1 hour. After another wash step, the membrane was developed with ECL substrates (Bio-Rad, US) following manufacturer's instruction and visualisation of the proteins was performed by chemiluminescence using ChemiDoc™ Imaging Systems (Bio-Rad, US).

2.8 αTGF-β scFv blocking assay

The blocking assay was performed to determine the binding and blocking capacity of αTGF-β scFv to TGF-β. The rationale of this assay is that 293T cells transfected with p3TP-Lux reporter plasmids can be induced to express luciferase by the induction of Smad signalling initiated by TGF-β1 proteins, whilst the addition of αTGF-β scFv can inhibit the binding of TGF-β1 and TGF-β receptor and consequently lead to reduced luciferase activity.

On day 1, 5 x 10^6 293T cells were seeded in 15 cm^2 tissue culture dishes in 16 ml of complete DMEM for incubation overnight at 37°C, 5% CO_2. On day 2, the DMEM media was removed from dishes and replaced by 12 ml of pH7.9 media (DMEM + 10 % FCS + 25 mM HEPES). 60 µg of reporter plasmids 3TP-Lux (p3TP-Lux) and 150 µl of 1M $CaCl_2$ was added and mixed with 3 ml of pH7.1 media (DMEM + 25 mM HEPES). The pH7.1 media containing DNA was added into the plates and the plates were gently rocked to mix and incubated at 37°C, 5% CO_2 overnight. On day 3, transfected 293T cells were trypsinised and re-seeded at a density of 3 x 10^4 cells in 200 µl DMEM/well in a 96-well flat-bottom TC treated plate.

On day 4, media was removed from each well and replaced with 100 µl of the concentrated supernatant containing αTGF-β scFv collected from transfected Plat-E cells following the protocol 2.7. 20 µl of recombinant human TGF-β1 protein (PeproTech, US) at various concentrations (2.5, 5, 10, 20 ng/ml) were added into wells respectively. Fresh DMEM without TGF-β1 protein was used as negative control. Each condition was performed in triplicate. The plate was incubated at 37°C, 5% CO_2 for 16 hours. Following this, a luciferase assay was performed. After the supernatant was discarded, the plate was added with 100 µl of luciferin solution diluted in PBS at a final concentration of 1.5 mg/ml and incubated for 3 min at 37°C. The luminescence intensity of each well was measured at 1 second exposure using the POLARstar Omega luminometer or equivalent.

2.9 αPD-1 scFv blocking assay

Plat-E cells were transfected with the retroviral vectors encoding CAR constructs and the scFv expression cassette, as described in section 2.3.1. TCM was used for media replacement on the next day. After 2-day cell culture, scFv-containing supernatant from transfected Plat-E cells was collected and passed through a 0.45 µm filter to discard any non-adherent packaging cells. A co-culture assay of CEA^+ MC38 cells and MFE.mCD3z CAR-T cells was performed in the absence or presence of scFv-containing supernatant

following the protocol in section 2.10.1. Simultaneously, the scFv-containing supernatant only was used as negative control. The supernatant post co-culture was collected for analysis of IFN-γ production by ELISA.

2.10 *In vitro* function of CAR-T cells

2.10.1 Co-culture assay

For assessment of cytokine release, CEA^+ tumour cells and parental tumour cells were seeded at a density of 1 - 2 x 10^4 cells in 100 µl TCM/well in a 96-well U-bottom TC treated plate (Falcon). Non-transduced T cells or CAR-T cells were added at E: T ratio of 1: 1 in 100 µl TCM/well. Simultaneously, CAR-T cells were cultured alone as negative control and with 50 ng/ml phorbol 12-myristate 13-acetate (PMA) and 1 µg/ml ionomycin (both Sigma Aldrich, UK) as positive control. Each condition was performed in triplicate. Cells were co-cultured at 37°C, 5% CO_2 for 20 hours. Following this, plates were centrifuged at 500xg for 5 min and the supernatant was collected and stored at -80°C for cytokine analysis by ELISA.

For assessment of cytotoxicity, CEA-specific CAR-T cells were co-incubated in a similar way with 1 - 2 x 10^4 of CEA^+ target cells expressing luciferase and GFP at various E: T ratios for 20 hours. Simultaneously, CEA^+ target cells expressing luciferase and GFP were cultured alone as negative control and with 50 µl of 1 % Triton™ X-100 solution (Sigma Aldrich, UK) as positive control.

Given the variable levels of transduction efficiency among CAR-T cell groups, non-transduced T cells were added into each group to ensure that the number of both total T cells and CAR-expressing T cells remained consistent.

2.10.2 Luciferase assay

The CEA^+ MC38 tumour cell line expressing luciferase and GFP was co-cultured with CAR-T cells following the protocol 1.4.1. After the supernatant was collected, the plate was added with 100 µl of luciferin solution diluted in PBS at a final concentration of 1.5 mg/ml and incubated for 10 min at 37°C. The luminescence intensity of each well was measured at 1 second exposure using the POLARstar Omega luminometer or equivalent. Percentage lysis was calculated using the following formula:

$$\%\ of\ killing = \left[1 - \frac{(CAR\ T\ cells\ RLU\ ) - (Triton\ RLU)}{(target\ cells\ alone\ RLU) - (Triton\ RLU)}\right] x\ 100$$

2.10.3 IFN-γ enzyme-linked immunosorbent assay (ELISA)

The concentration of murine IFN-γ (mIFN-γ) after co-culture was determined using an ELISA kit (Invitrogen, US) according to the manufacturer's protocol. All reagents were supplied in the kit, apart from 1 M H_2SO_4 stopping buffer. The absorbance value of each well was measured using the plate reader and SoftMax Pro software at 450 nm. A non-linear standard curve was generated by plotting the average value of each standard. The concentration of mIFN-γ in each sample was determined by interpolating absorbance values from a standard curve.

2.10.4 IL-12 p70 ELISA

The concentration of murine IL-12 p70 (mIL-12p70) after co-culture was determined using an ELISA kit (Invitrogen, US) according to the manufacturer's protocol. All reagents were supplied in the kit, apart from 1 M H_2SO_4 stopping buffer. The absorbance value of each well was measured using the plate reader and SoftMax Pro software at 450 nm. A non-linear standard curve was generated by plotting the average value of each standard. The concentration of mIL-12p70 in each sample was determined by interpolating absorbance values from a standard curve.

2.11 *In vivo* function of CAR-T cells

All *in vivo* experiments were performed under the auspices of the Animals (Scientific Procedures) Act 1986 and under UK Coordinating Committee for Cancer Research guidelines. All animal studies were carried out at the Manchester Cancer Institute, which was approved by the CRUK-Manchester institute local animal welfare & ethics review body (CRUK-MI AWERB). These studies were conducted under the home office personal licence (PIL) number IA4E15152 and the home office project license (PPL) number P4657F6CD. Animals were housed under specific pathogen–free conditions.

For evaluation of tumour engraftment, six- to eight-week-old BALB/c or C57BL/6 mice (Harlan Laboratories, UK) were injected subcutaneously with MC38 or CT26 cells with or without CEA expression at various cell doses. For assessment of anti-CEA CAR-T cell therapy, C57BL/6 WT or CEA transgenic (CEAtg) mice were used. CEAtg mice were

obtained from the CRUK Manchester institute. Tumour-bearing mice were pre-conditioned with 5Gy TBI or chemotherapy regimens including 100 mg/Kg cyclophosphamide monohydrate (Merck Millipore, US) and 100 mg/Kg fludarabine phosphate (Selleck Chemicals LLC, US) by intraperitoneal injection. Two days later, mock T cells or CAR-T cells were injected intravenously into mice at varying doses, as detailed in the figure legends. Growth of subcutaneous tumours was monitored twice a week by calliper measurements and calculated by the formula: $W^2 \times L/2$. Mice were euthanized when tumours ulcerated or reached over 1,000 mm^3 or they experienced lethal toxicities such as 20 % severe body weight loss (BWL), emaciation or pale extremities. Tumours were collected and fixed with formalin. Spleens were collected to assess the functional activity of CEA-specific immune cells *in vitro*. Splenocytes were isolated following the protocol 2.2.3 and cryopreserved in cell freezing media in liquid nitrogen without αCD3ε and αCD28 antibody activation for later analysis by co-culture assays.

To determine the efficiency of lymphodepletion pre-conditioning, peripheral blood samples were collected from tail vein bleeds at various time points post T cell infusion and blood counts were determined using the Sysmex™ automated hematology analyser. In addition, serum was isolated from blood samples by centrifugation at 1,000–2,000xg for 10 min at 4°C and stored at -80°C until use. 1 – 5 µl of serum samples diluted with PBS were measured for IL-12 production by ELISA.

2.12 Immunohistochemistry (IHC)

All tumour samples for IHC assays were fixed with formalin overnight and embedded in paraffin was. 4 µm thick tumour sections were cut and used for assessment of CEA expression and $CD8^+$ T cell infiltration. Automated IHC staining was performed using the Leica Bond Max (Leica Biosystems, Germany). To detect human CEA expression, tumour sections from tumour-bearing mice were immunostained with mouse anti-CEA monoclonal antibody (clone: 1106; Invitrogen) at 1: 1000 dilution and the ARK™ (animal research kit) Peroxidase (Dako, Denmark) was used. The mouse IgG1 antibody was used as negative control at the same dilution as the primary antibody. To detect the level of mouse $CD8^+$ T cells, tumour sections from treated mice were immunostained with anti-mouse CD8a monoclonal Antibody (clone: 4SM15; Invitrogen) at 1: 750 dilution and the ImmPRESS™ HRP anti-rat IgG (mouse adsorbed) polymer detection kit (Vector Laboratories, US) was used. The rat IgG2a antibody was used as negative control at the same dilution as the primary antibody. The Bond™ Polymer Refine Detection Kit (Leica Biosystems, Germany), which contains the 3,3'-Diaminobenzidine (DAB) chromogen and haematoxylin, was used

for antibody and cell nuclei visualisation respectively. Images were acquired using the EVOS™ FL Auto Imaging System (magnification x10) (Thermo Fisher Scientific, US).

2.13 Quantitative polymerase chain reaction (QPCR)

The QIAamp DNA Mini Kit (Qiagen, UK) was used to extract total DNA from blood samples collected via tail vein on day 1, 7 post T cell infusion according to manufacturer's protocol.

QPCR was conducted to quantify the amount of mCherry sequence in 10 ng of DNA samples extracted using the HotStarTaq Plus Master Mix Kit (Qiagen, UK) according to manufacturer's protocol. Custom primer pairs and corresponding probe for detection of mCherry were synthesised by Sigma, UK and are shown in Table 2.2. QPCR was carried out on QuantStudio 5 Real-Time PCR Systems and the setting are shown in Table 2.3. Results were analysed using QuantStudio™ Design & Analysis software (Thermo Fisher Scientific, US).

A stander curve ranging from 1 x 10^{-8} to 1 µg were produced for each experiment by 10-fold serial dilutions of the MFE.CD3z plasmid. 1 - 100 ng of genomic DNA extracted from CD3z CAR-T cells and water only were used as positive control and negative control respectively.

Table 2.2 QPCR primer and probe sequences for the detection of mCherry

Target gene	Oligonucleotide	Sequence	Amplicon length (bp)
mCherry	Forward primer	5'-AGACCACCTACAAGGCCAAGAAGC-3'	99
	Reverse primer	5'-TCAAGTTGGACATCACCTCCCACA-3'	
	Probe	[JOE] 5'-CCGGCGCCTACAACGTCAAC-3' [BHQ1]	

Table 2.3 QPCR setting for the detection of mCherry

Initial activation	Denaturation	Annealing	Extension	Final extension
1 cycle	3-step cycling x 35 cycles			1 cycle
95°C	94°C	55.7°C	72°C	72°C
5 min	30 sec	30 sec	1 min	10 min

2.14 *In vitro* function of splenocytes from treated mice

On day 0, a co-culture assay was performed for expansion of CEA-specific T cells. CEA^+ MC38 tumour cells were irradiated with 50 Gy and seeded at a density of 1 x 10^6 cells in 2 ml TCM/well in 6-well TC treated plates. Splenocytes of each treated mouse were isolated as mentioned in section 2.2.3 and resuspended at 3.5 x 10^6 cells/ml. When irradiated tumour cells were completely adherent to the plate, 3.5 x 10^6 splenocytes were added into each well. TCM was added to top up to 4 ml and 100 IU/ml hIL-2 and 2 ng/ml mIL-7 were added into each well. Plates were incubated at 37°C, 5% CO_2 for 5 days.

On day 5, activated splenocytes were re-cultured with 5 × 10^5 irradiated CEA^+ MC38 cells at E: T ratio of 1: 1 in 24-well TC treated plates. Cells were co-cultured at 37°C, 5% CO_2 for 20 hours. Following this, plates were centrifuged at 500xg for 5 min and the supernatant was collected and stored at -80°C for the measurement of IFN-γ by ELISA.

2.15 Statistical analysis

GraphPad Prism 8.0 was used to perform statistical analysis of the conducted experiments. Results were generally shown as the mean ± standard deviation, unless otherwise stated. For comparison of one variable with more than two sets of data one-way analysis of variance (ANOVA) was performed and where the effects of two variables were compared two-way ANOVA was employed. Data was considered to be statistically significant when the P value was less than 0.05.

3 Construction and Assessment of anti-CEA CAR-T cells secreting IL-12

3.1 Introduction

3.1.1 Anti-CEA CAR-T cell therapy

Anti-CEA CAR-T cells have shown anti-tumour efficacy in pre-clinical studies [166-168]. With regards to clinical efficacy, a phase I trial reported that local delivery of second-generation CD28-CD3ζ CAR-T cells by hepatic artery infusion showed increased CEA^+ liver metastasis necrosis and fibrosis in some patients, although there were no partial or complete responses [169]. Another two clinical trials have also reported some clinical efficacy but no objective clinical responses in the treatment of gastrointestinal adenocarcinoma with metastases by systemic administration of autologous T cells engineered with a first-generation CD3ζ CAR [170] and a second-generation CD28-CD3ζ CAR [171] respectively. Furthermore, decline of serum CEA levels was observed in these trials, strongly indicating that the CEA-specific CAR-T cells mediated productive anti-tumour responses.

It is of note that these CAR-T cell trials did not observe severe treatment-related colitis in most patients, compared to treatment of TCR-T cells against CEA [172]. This is probably because CEA protein is expressed in a polarized fashion on the lumen side of normal epithelial cells in gastrointestinal tracts [173], which therefore cannot be recognized by CAR-T cells unless CEA distribution collapses due to tissue injury [174]. In contrast, given the non-polarized expression of CEA peptides bound to HLA molecules on cell surfaces, CEA-expressing healthy cells can be recognized by TCR-T cells as well, resulting in severe transient colitis. Additionally, the CD3ζ CAR trial observed transient pre-conditioning-dependent respiratory toxicity, which may be due to the expression of CEA on lung epithelium, whilst other two trials using CD28-CD3ζ CAR did not report this toxicity. The underlying reason remains unknown due to multiple factors across different trials, such as chemotherapy pre-conditioning, IL-2 administration, variation in the scFv affinity for its target, cell doses and manufacturing differences.

Collectively, encouraging clinical responses of anti-CEA CAR-T cells for the treatment of solid tumours has yet to be achieved. Based on the current findings, CEA is still a potential

target for CAR-T cell therapy and more strategies need to be explored to improve anti-tumour efficacy of anti-CEA CAR-T cells in the treatment of solid tumours.

3.1.2 IL-12

IL-12 is a multifunctional, pro-inflammatory cytokine which bridges innate and adaptive immunity. It is mainly produced by APCs such as monocytes, macrophages and DCs in response to antigen stimulation. Structurally, IL-12 is a heterodimeric cytokine of 70 kDa (p70) which consists of two covalently linked p35 and p40 subunits. The biological functions of IL-12 are mediated via the heterodimeric IL-12 receptor (IL-12R) composed of IL-12Rβ1 and IL-12Rβ2 chains. The IL-12R complex is expressed mainly on NK cells and activated T cells but has also been detected on other cell types such as DCs [175] and B cell lines [176].

In anti-tumour immunity, IL-12 mainly acts as a pivotal orchestrator of Th1-type immune response against tumour [177]. The most crucial mediator of IL-12-induced responses is IFN-γ, which is produced from NK cells and T cells upon IL-12 stimulation alone or synergy with other activating stimuli such as IL-2 and IL-18 [178, 179]. The release of IFN-γ, in turn, stimulates APCs to secret IL-12 in a positive feedback loop [180]. IL-12 also induces other cytokine production, such as IL-2, TNF-α and granulocyte-macrophage colony-stimulating factor (GM-CSF).

IL-12 released by APCs enhances proliferation and cytotoxicity of NK cells and $CD8^+$ T cells and promotes the differentiation of naïve $CD4^+$ T cells towards the Th1 effector cell phenotype [181, 182]. It also programs effector T cells for optimal progression into effector memory T cells [183]. Moreover, IL-12 enhances the activation and production of Th1-associated classes of immunoglobulin such as IgG2a and suppresses IgE production in B cells and augments antibody-dependent cellular cytotoxicity (ADCC) against tumour cells [184, 185]. IL-12 also increases capability of APCs to present poorly immunogenic tumour peptides [186, 187]. Apart from tumour-specific immune responses, IL-12 has been reported to mediate anti-tumour activities through other mechanisms. For example, IL-12 mediates potent anti-angiogenic effects via induction of IFN-γ-inducible protein 10 (IP-10, CXCL10) and monokine induced by IFN-γ (MIG, CXCL9) [188]. Additionally, IL-12 regulates the tumour vasculature by upregulating expression of the adhesion molecule, such as ICAM and VCAM, which is thought to facilitate leukocyte recruitment [189]. In some cases, IL-12 has direct inhibitory effects on tumour growth, such as AML, lung adenocarcinoma [190, 191].

Notably, IL-12 appears to exhibit more potent anti-tumour responses when secreted or applied locally in the tumour, rather than given systemically. Systemic administration of IL-12 showed severe toxicities so that therapeutic levels of IL-12 could not be safely achieved [192, 193].

In light of the potent anti-tumour properties of IL-12, modification of tumour-specific T cells, including CAR-T cells, to secret IL-12 has been used as a strategy to improve therapeutic effects of T cells. This approach allows IL-12 to be delivered locally into tumour sites, where it can exert its function without the toxicities observed in systemic administration. The release of IL-12 by engineered T cells in a constitutive and inducible manner has been demonstrated to improve cytolytic activity and persistence of T cells [194, 195], recruit and activate innate immune cells such as macrophages [153]. Moreover, functional changes of resident repressor cells by IL-12 may enhance the efficacy of engineered T cells in an indirect manner. Accumulated IL-12 re-programmed $CD11b^+$ myeloid-derived tumour stromal cells, in particular MDSCs, dendritic cells and macrophages, towards functional antigen-presenting cells, enabling them to cross-present naturally occurring tumour antigens to tumour infiltrating T cells [196]. It can also induce collapse of the tumour stroma through increasing Fas expression [197]. In addition, IL-12-secreting T cells acquired intrinsic resistance to the repressive functions of Treg cells [198].

3.1.3 Hypothesis and aims

The secretion of IL-12 by CAR-T cells has been reported to not only enhance anti-tumour responses of CAR-T cells, but also recruit and activate innate immune cells like NK cells and macrophages which can attack antigen-negative tumour cells invisible to CAR-T cells. It is therefore hypothesised that secretion of IL-12 by murine anti-CEA CAR-T cells may enhance anti-tumour activity of T cells *in vitro*. Murine anti-CEA CAR-T cells secreting IL-12 might also show better efficacy against solid tumours by stimulating CAR-T cells and recruiting other immune cells in an immunocompetent model. Therefore, the main aims of this chapter were:

- To design and generate retroviral vectors encoding murine first- and second-generation CAR constructs and murine IL-12 gene
- To assess whether murine T cells could be successfully transduced to express anti-CEA CARs and secrete IL-12
- To establish a CEA positive tumour cell line expressing GFP and luciferase for evaluation of CAR-T cell cytotoxicity

- To evaluate whether secretion of IL-12 enhance anti-tumour effects of CEA-specific CAR-T cells *in vitro*

3.2 Results

3.2.1 Generation of retroviral vectors encoding anti-CEA CAR gene

The MP71 retroviral vectors formed the backbone of CAR encoding plasmids, as it has stable, high-level transgene expression in T cells [199] and has been well developed for CAR construction in our lab. Constructs were constructed by altering the scFv or intracellular signalling domain sequence to the desired sequence from pre-existing vectors in the lab via DNA cloning methods. Briefly, the CAR construct consisted of an oncostatin M leader sequence (OM1) fused to the MFE23 scFv targeting human CEA [200] followed by fully mouse intracellular signalling domains (Figure 3.1). OM1 was used for scFv transport to the cell membrane. In order to detect CAR expression, the mCherry reporter gene was placed upstream by means of a 2A cleavage sequence which allows equal co-expression of mCherry and CAR genes [201]. Another 2A cleavage sequence was placed downstream of the CAR to initiate the translation of murine IL-12 gene for constitutive secretion.

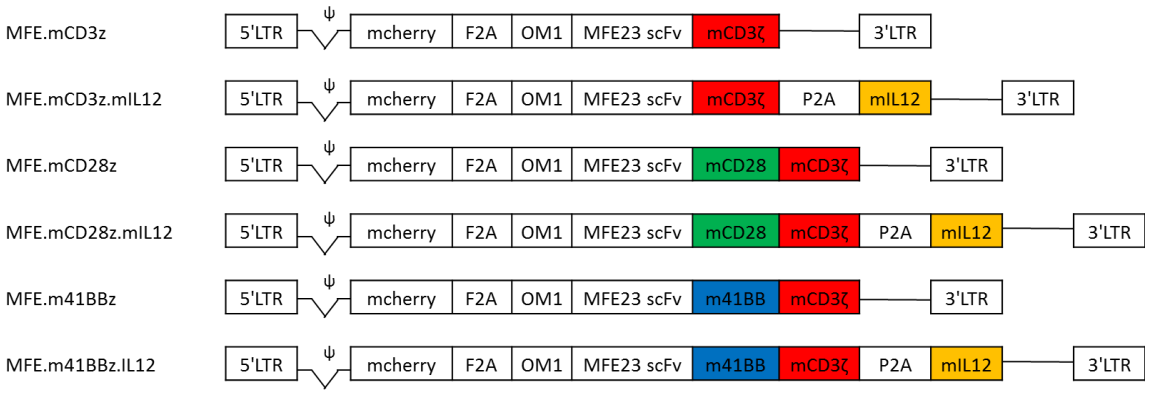

Figure 3.1 Schematic diagram of anti-human CEA CAR constructs

CEA-specific CAR consists of a mouse anti-human CEA MFE23 scFv linked to different murine signalling moieties. The first-generation CAR only contains a CD3ζ stimulatory domain, while second-generation CARs have one additional co-stimulatory domain CD28 or 41BB followed by CD3ζ. Murine IL-12 gene was inserted in the CAR constructs to generate the fourth-generation CARs. (LTR, long terminal repeat; OM1, oncostatin M leader sequence)

To generate the retroviral vector pMP71.mCherry.2A.MFE23.mCD3ζ (MFE23.mCD3z), the MFE23 scFv from the vector encoding MFE23 with truncated CD34 (tCD34) marker gene and human CD3ζ and CD28 signalling gene (pMP71.tCD34.2A.MFE23.hCD28.hCD3ζ) was cloned as a ClaI, NotI fragment replacing the anti-mouse CD19 scFv (1D3 scFv) in the retroviral vector pMP71.mCherry.2A.1D3.mCD3ζ (Figure 3.2 A & B). Following this, the pMP71 vectors containing MFE23.mCD28.mCD3ζ sequence (MFE23.mCD28z) and MFE23.m41BB.mCD3ζ (MFE23.m41BBz) sequence respectively were generated by replacing mCD3ζ sequence from MFE23.mCD3z construct with mCD28.mCD3ζ and m41BB.mCD3ζ sequence from anti-mouse CD19 CAR constructs as NotI, NheI fragment (Figure 3.3 A & B).

To generate fourth-generation anti-CEA CARs encoding murine IL-12, the mCherry.2A.MFE23 sequence was cut out of the plasmid MFE23.mCD3z with NcoI, NotI restriction enzymes to replace the mCherry.2A.1D3 sequence in first- and second-generation anti-mouse CD19 CARs encoding murine IL-12 (Figure 3.4 A & B).

Confirmation of successful ligation of the CAR encoding vector was performed by Sanger DNA sequencing of samples. Primers for detecting mCherry, MFE23, CD3z, CD28z, 41BBz and IL-12 sequences are shown in Table 3.1.

A.

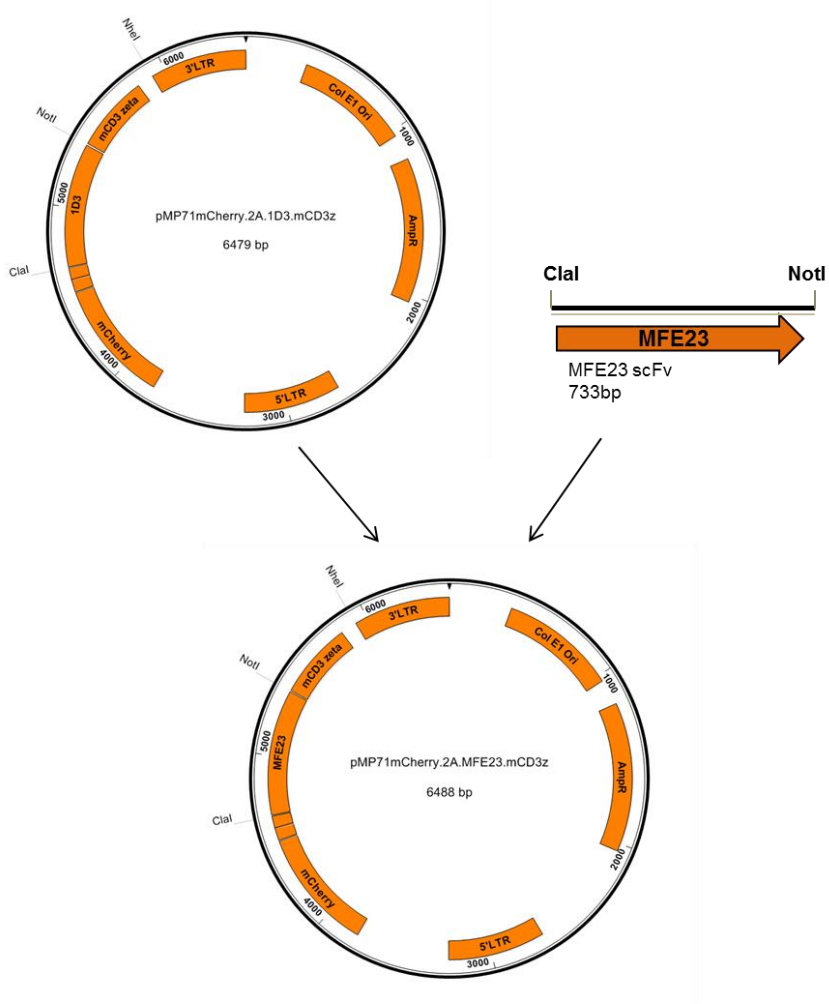

B.

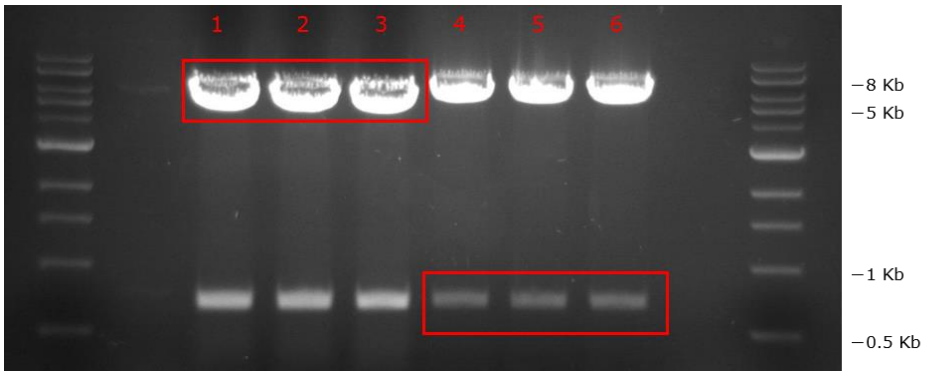

Figure 3.2 Schematic diagram of first-generation anti-CEA CAR constructs

(A) Overview of cloning strategies for generation of MFE.CD3z plasmid. **(B)** Agarose gel electrophoresis of backbone vector MP71 and target MFE23 DNA fragments. The DNA samples were digested with ClaI, NotI restriction enzymes. Lane 1 - 3 shows the CAR backbone from the vector pMP71.mCherry.2A.1D3.mCD3ζ at ~5.8 kb; Lane 4 - 6 shows the MFE23 insert from the vector pMP71.tCD34.2A.MFE23.mCD28.mCD3ζ at ~0.7 kb;

A.

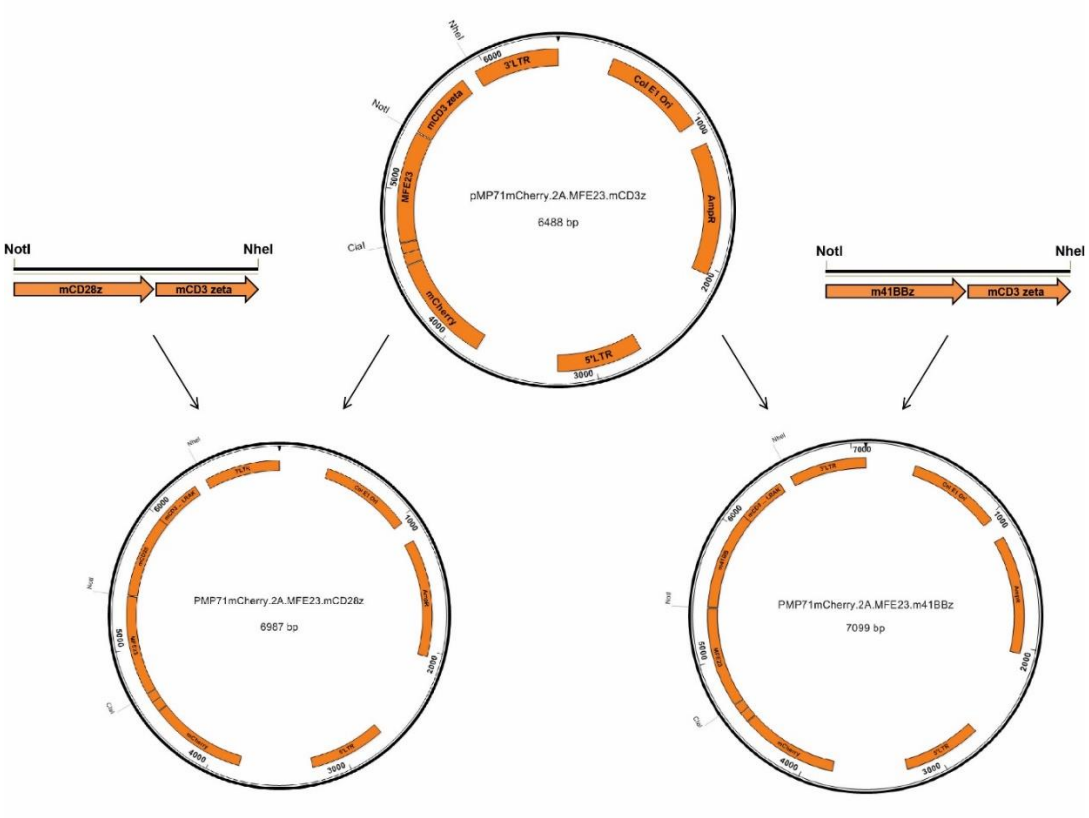

B.

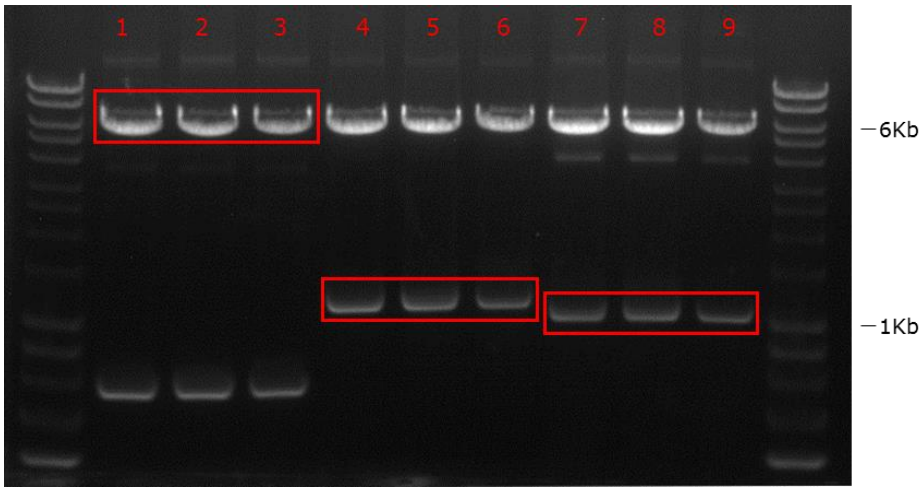

Figure 3.3 Schematic diagram of second-generation anti-CEA CAR constructs

(A) Overview of cloning strategies for generation of MFE.CD28z and MFE.41BBz plasmids. **(B)** Agarose gel electrophoresis of backbone vector MP71 and target CD28 and 41BBz DNA fragments. The DNA samples were digested with NotI, NheI restriction enzymes. Lane 1 - 3 represents the MFE23 backbone from the vector MFE23.mCD3z at ~6 kb; Lane 4 - 6 shows the m41BBz insert from the vector pMP71.mCherry.2A.1D3.m41BB.mCD3ζ at ~1.1 kb; Lane 7-9 shows the mCD28z insert from the vector pMP71.mCherry.2A.1D3.mCD28.mCD3ζ at ~1 kb.

A.

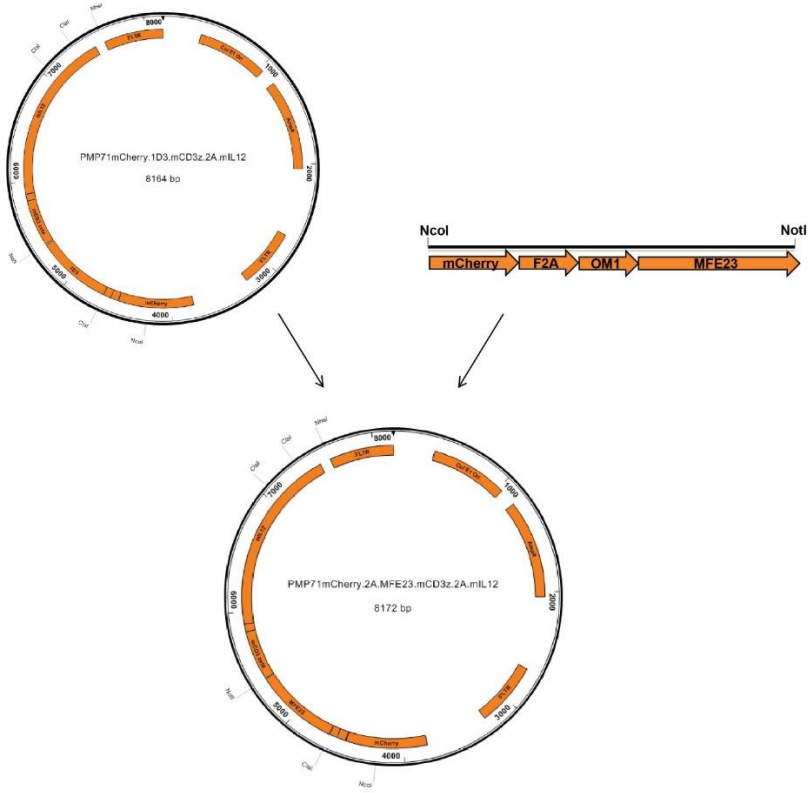

B.

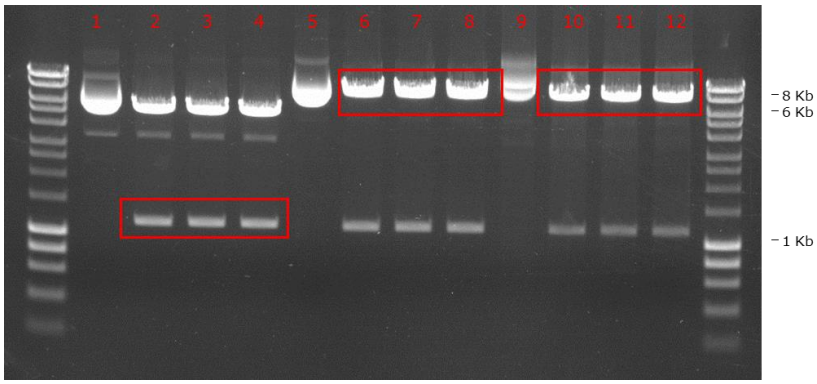

Figure 3.4 Schematic diagram of fourth-generation anti-CEA CAR constructs encoding murine IL-12

(A) Overview of cloning strategies for generation of anti-CEA CARs encoding murine IL-12 plasmids; **(B)** Agarose gel electrophoresis of target mCherry.2A.MFE23 and backbone CD28z.IL12 and 41BBz.IL12 DNA fragments. Lane 2 - 4 represents the mCherry.2A.MFE23 insert from the vector MFE23.mCD3z at ~1.2 kb; Lane 6 - 8 represents the mC28z.IL12 backbone from the vector pMP71.mCherry.2A.1D3.mCD28.mCD3ζ.IL12 (1D3.mCD28z.mIL12) at ~7.5 kb; Lane 10 - 12 represents the m41BBz.IL12 backbone from the vector pMP71.mCherry.2A.1D3.m41BB.mCD3ζ.IL12 (1D3.m41BBz.mIL12) at ~7.6 kb. Lane 1, 5 and 9 represents MFE23.mCD3z, 1D3.mCD28z.mIL12 and 1D3.m41BBz.mIL12 without restriction digest respectively.

Table 3.1 Primers for Sanger Sequencing

Primers	**Sequence**
mCherry fwd	5’ CAACATCAAGTTGGACATCACCTC 3’
MFE23 fwd	5’ GAAGATGCTGCCACTTATTAC 3’
mCD3z fwd	5’ CCAGGAAGGCGTATACAATGCACTGCAG 3’
MP rev	5’ CTTAAGCTAGCTTGCCAAACCTACAGG 3’

3.2.2 Efficient retroviral transduction of mouse T cells with anti-CEA CARs

In this study, the Plat-E cell line was used as a helper cell due to its efficient and stable ability to package retroviral particles [202]. Plat-E packaging cells were transfected with pMP71 vectors encoding anti-CEA CARs and pcl-Eco packaging vector as described in section 2.4.1. Efficient transfection was observed by the expression of mCherry fluorescence using fluorescence microscopy (Figure 3.5 A).

On day 2 post CAR transfection, Plat-E cells were collected to detect mCherry expression by flow cytometry (Figure 3.5 B). Whilst MFE23.mCD3z, MFE23.mCD28z and MFE23.m41BBz constructs had similar transfection efficiency which was 34.4 ± 6.5, 41.0 ± 14.8, 37.2 ± 8.8 % respectively, all IL-12 constructs showed lower transfection efficiency (22 % on average). Notably, there was an inverse correlation between CAR construct length and transfection efficiency ($R^2 = 0.776$, $P < 0.05$) (Figure 3.5 C), which was consistent with the study reported [203]. It is possible that the efficiency of DNA uptake was decreased because of an increase in plasmid size.

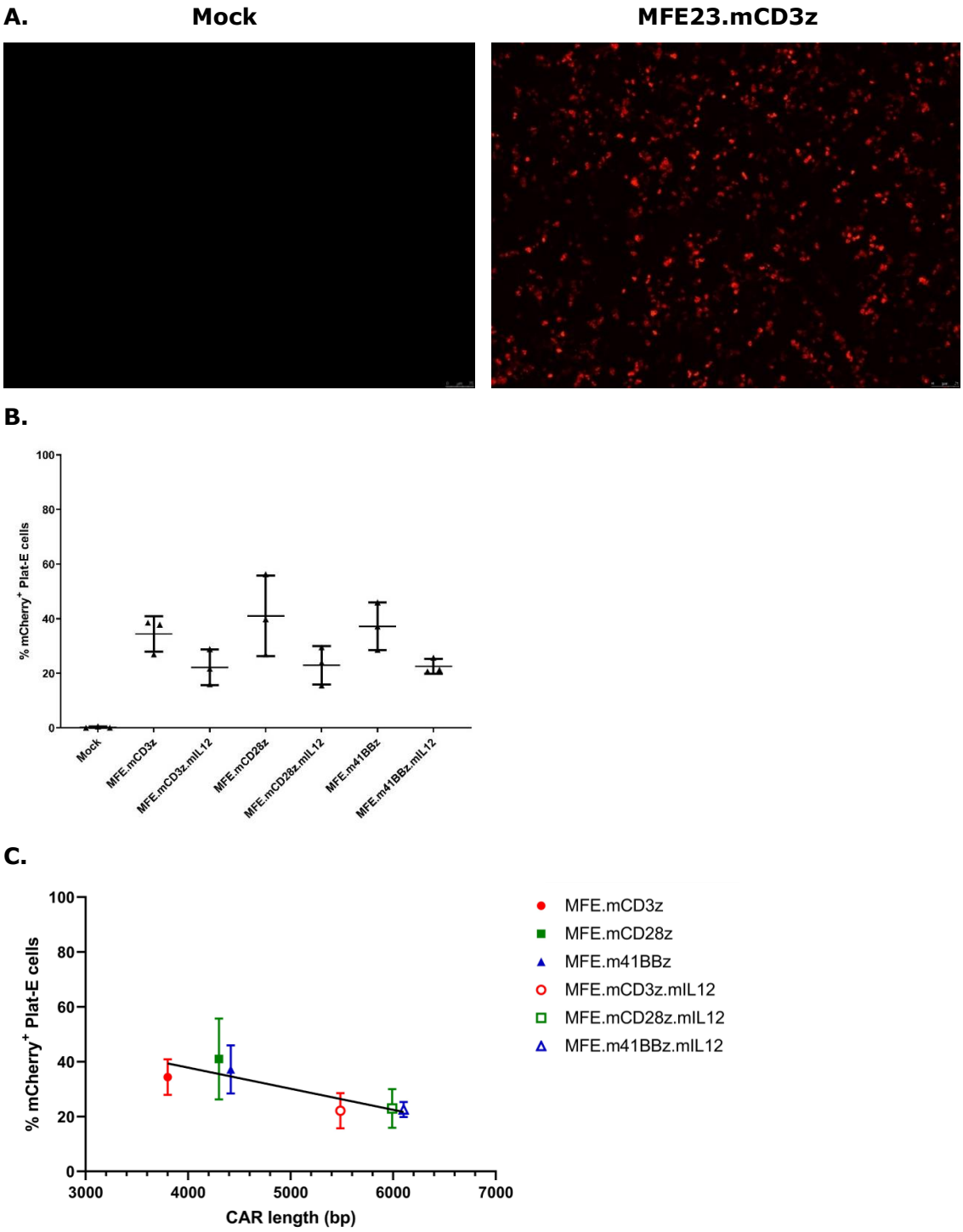

Figure 3.5 mCherry expression of transfected Plat-E cells

(A) Representative images of mCherry fluorescence of Plat-E cells post transfection by fluorescence microscopy; Magnification = 50X; **(B)** Transfection efficiency was determined via mCherry expression on transfected Plat-E cells by flow cytometry. Data are mean ± SD of 3 independent experiments. **(C)** Correlation between the length of CAR constructs and transfection efficiency, Spearman's correlation, $R^2 = 0.776$, $P < 0.05$.

After 24-hour stimulation by soluble αCD3 and αCD28 antibodies, mouse T cells were transduced to express different CAR constructs by spinning and co-incubating with retroviral containing supernatant. Transduced T cells were cultured at a density of 1×10^6 cells/ml with the addition of hIL-2 and mIL-7 at 100 IU/ml and 2 ng/ml respectively every other day. Following 4 days of culture, to confirm retroviral integration and expression of CAR, $CD4^+$ and $CD8^+$ T cells were then analysed for the presence of surface markers mCherry by flow cytometry. For cytometric analysis, mock transduced T cells were used to set gates for background fluorescence intensity in order to analyse the percentage of surface marker expression of CAR-expressing T cells in each of the transduced groups.

The gating strategy of mock T cells for analysis is represented in Figure 3.6 A - E. Briefly, the initial gate was drawn on the single population based on FSC-A/FSC-H plot. Zombie Violet, a live/dead cell discrimination dye, was used to identify dead cells and exclude them from analysis. Live singlets were then analysed for the percentage of $mCherry^+$ cells within CD4 and CD8 subsets. The detectable mCherry fluorescence indicated that T cells were successfully transduced (Figure 3.6 F & G). However, the transduction efficiency of mouse T cells transduced with different CAR constructs was poor (Figure 3.7 A). MFE23.mCD3z, MFE23.mCD28z, MFE23.m41BBz groups had only 27.8 ± 10.4, 18.9 ± 10.0, 15.1 ± 6.1 % $mCherry^+$ T cells respectively. The addition of IL-12 gene resulted in a slightly decrease in transduction efficiency of CD3z, CD28z and 41BBz CAR constructs, which was 23.3 ± 12.1, 13.2 ± 9.1, 13.4 ± 8.0 % respectively. It is of note that the transduction efficiency of CD3z.mIL12 CARs (5485 bp) was slightly higher than that of either CD28z or 41BBz CARs (4300 and 4416 bp respectively). There is no strong correlation between CAR construct length and transduction efficiency (Figure 3.7 B). It seems that the impact of the inclusion of CD28 or 41BB signalling domain in the CAR on transduction efficiency is stronger than that for the total length of CAR construct.

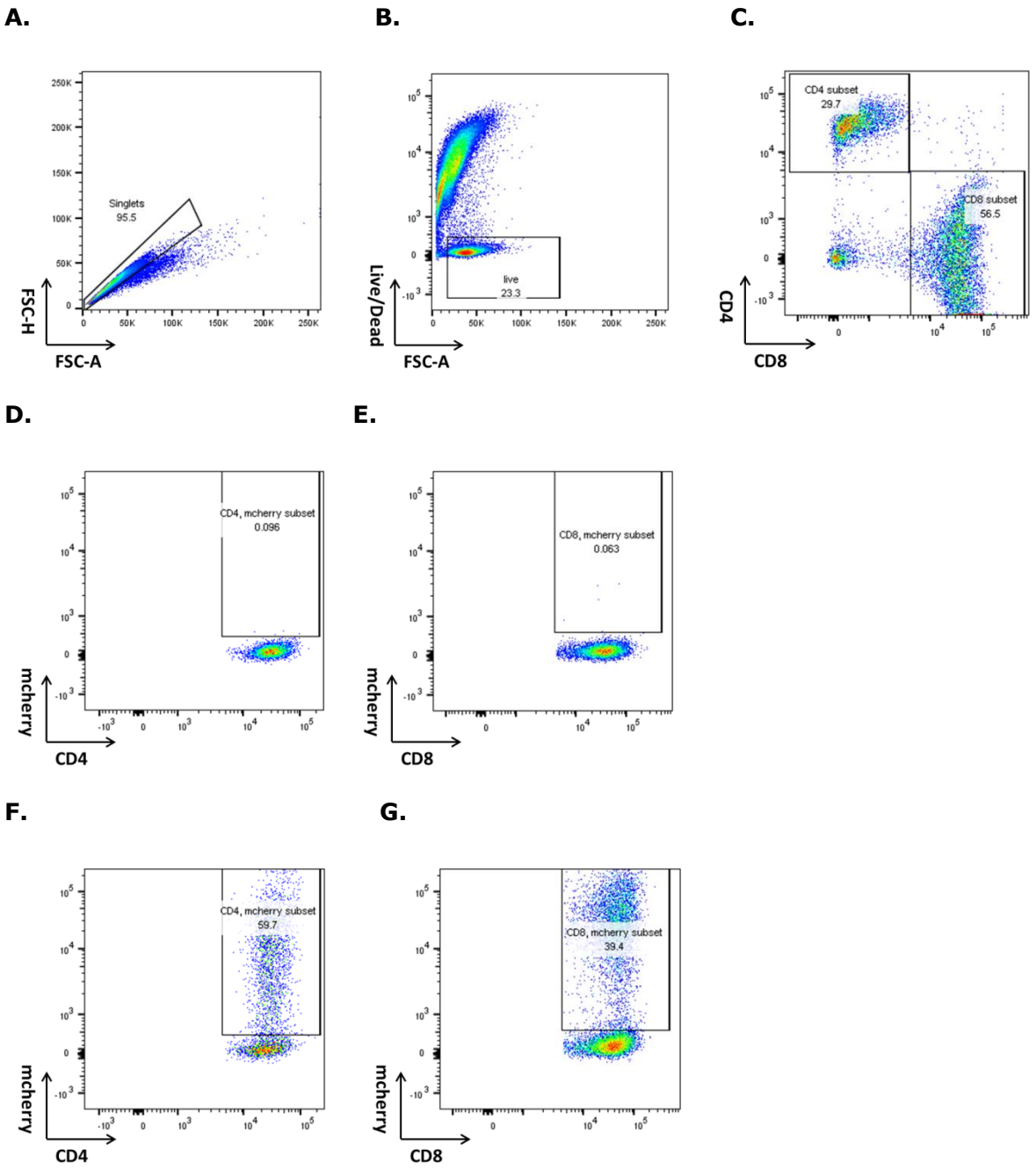

Figure 3.6 Gating strategy for flow cytometry analysis of surface marker expression of CAR-expressing T cells

Gating strategy used to define mCherry$^+$ population in CD4$^+$ and CD8$^+$ T cells. **(A)** The single cells were identified on the FSC-A/FSC-H plot. **(B)** Live cells were identified by Zombie Violet negative staining of single cell population. **(C)** T cells were determined by gating on the CD4$^+$ and CD8$^+$ populations. **(D & E)** mCherry$^+$ T cells were gated on the CD4$^+$ and CD8$^+$ subsets of mock T cells. **(F & G)** Representative dot plots are shown for mCherry expression on the CD4 and CD8 subsets of CAR-T cells respectively.

A.

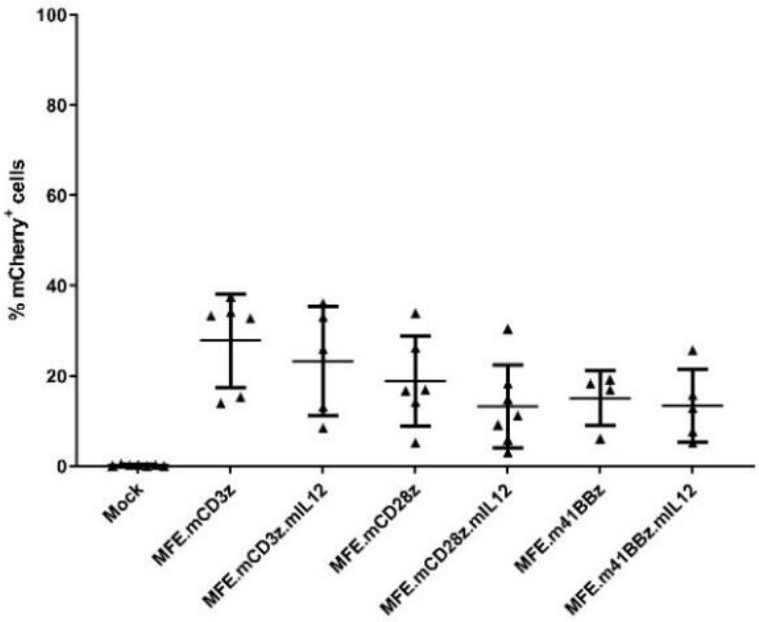

B.

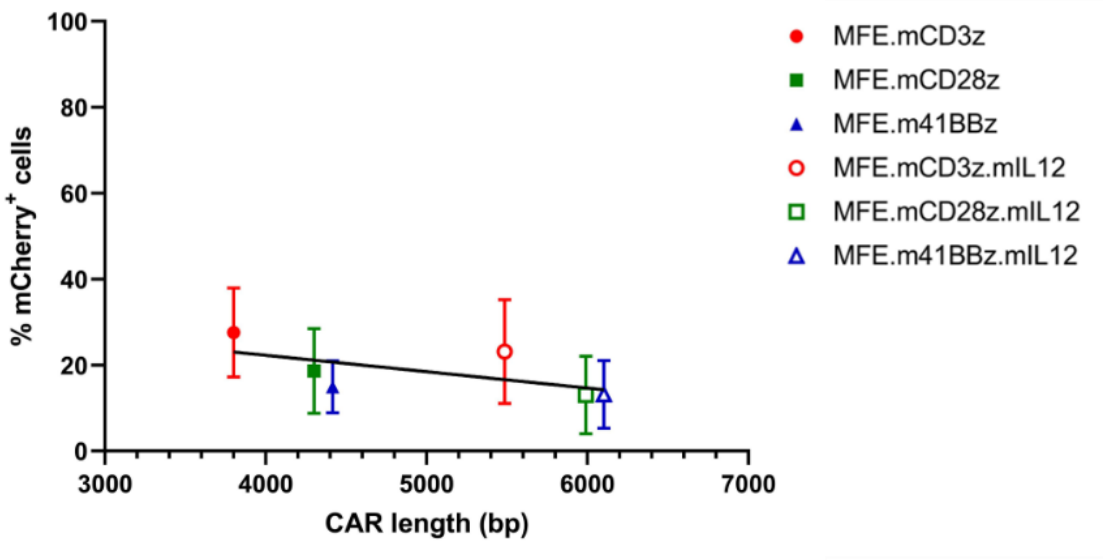

Figure 3.7 Transduction efficiency of anti-CEA CAR-T cells

(A) Transduction efficiency was determined by the detection of mCherry expression on CD4 and CD8 subsets on day 4-5 post transduction by flow cytometry. **(B)** Correlation between the length of CAR constructs and transduction efficiency, Spearman's correlation, $R^2 = 0.3906$.

3.2.3 *In vitro* culture optimization of IL-12-secreting CAR-T cells

During 4-day *in vitro* culture post transduction, the number of Mock and MFE23.m41BBz T cells (7.5 ± 2.4 and 7.3 ± 1.5-fold increase from day 0 to day 4 respectively) was higher than MFE23.mCD3z and MFE23.mCD28z T cells (4.9 ± 1.9 and 4.4 ± 1.9 -fold increase respectively) (Figure 3.8 A). Thus, it seems possible that retroviral transduction can reduce cell expansion but the incorporation of 41BB signalling domain is able to minimise the effect, as both MFE.mCD28z and MFE.m41BBz T cells had similar transduction efficiency (18.9 ± 10.0 and 15.1 ± 6.1 %) (Figure 3.7 A). However, whilst the mean expansion was lower with MFE23.mCD3z and MFE23.mCD28z T cells, there is no significant difference in expansion, except the comparison between Mock and MFE23.mCD28z T cells on day 4 ($P < 0.05$). As for IL-12-secreting T cells, a significantly lower fold expansion was observed on day 4, which indicated that the secretion of IL-12 possibly had a negative effect on T cell expansion. It also corresponded with a lower percentage of viable cells in the IL-12-secreting CAR-T cell cultures observed by flow cytometry, although there is no significant difference compared to parental T cells (Figure 3.8 B). It was observed that upon centrifugation the cell pellet was larger in the IL-12-secreting CAR-T cells (no figure shown), leading to the hypothesis that IL-12 could stimulate T cells to rapidly expand followed by activation induced cell death (AICD). However, culturing IL-12-secreting T cells at 1×10^6 cells/ml with fresh cytokines every 2 days did not provide sufficient growth signals to maintain cell viability, resulting in cell death and poor expansion. Additionally, IL-12 has been reported to induce dose-dependent apoptosis in human T cells *in vitro* [204]. Therefore, lowering cell density for T cell culture to provide more culture medium and cytokines and dilute IL-12 concentration might be a strategy to circumvent this problem.

A.

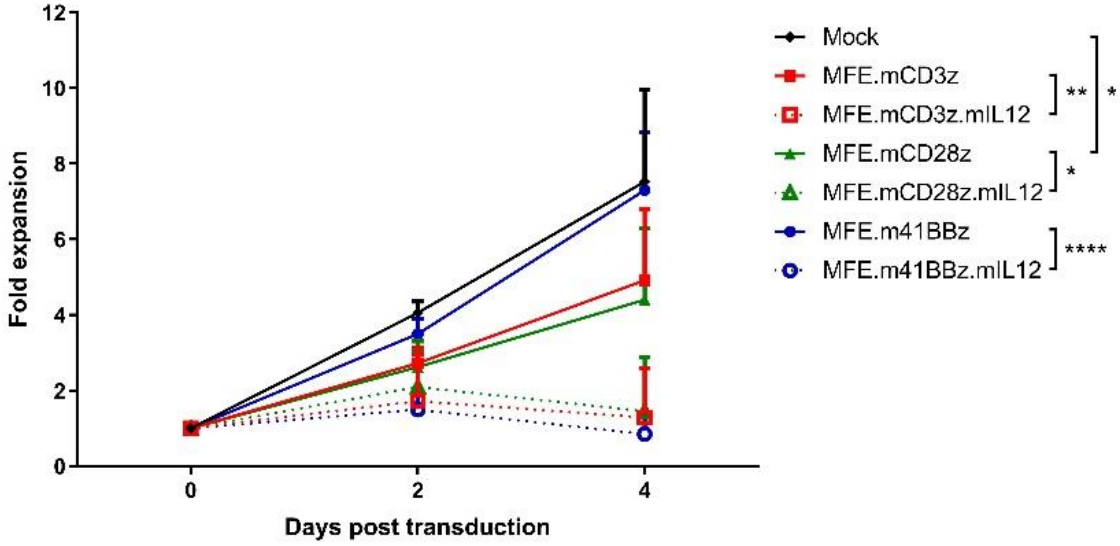

B.

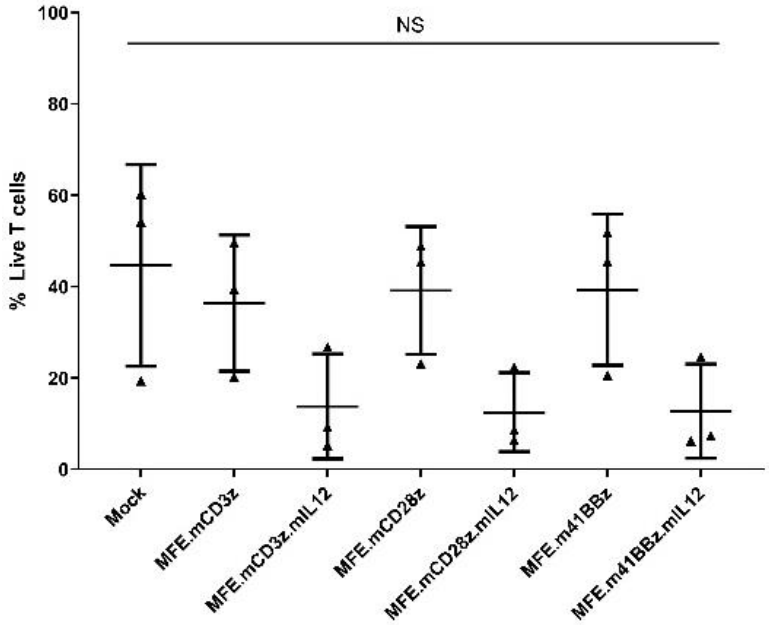

Figure 3.8 Expansion of transduced T cells with different CAR constructs

(A) Fold expansion of transduced T cells cultured at 1 x 10^6 cells/ml from day 0 to day 4 post transduction. Viable cells were enumerated every 2 days by bright field microscopy using trypan blue exclusion. **(B)** The percentage of live cells in each group identified by zombie violet dye by flow cytometry. The data are plotted as mean ± SD of three independent experiments. Statistically significant difference was analysed using two-way ANOVA with Tukey's multiple comparisons test. ∗ $P < 0.05$; ∗∗ $P < 0.01$; ∗∗∗∗ $P < 0.0001$.

To investigate cell culture conditions for the reliable expansion of CAR-T cells, CD3z T cells with or without IL-12 co-expression were cultured at different cell densities, 1 x 10^6 cells/ml and 0.3 x 10^6 cells/ml respectively. During 8-day *in vitro* culture, transduced T cells at 0.3 x 10^6 cells/ml showed significantly higher fold expansion compared to that at 1 x 10^6 cells/ml from day 4 post transduction (Figure 3.9 A). On day 4, the cell number of CD3z.mIL12 T cells was remarkably more than that of CD3z T cells at 0.3 x 10^6 cells/ml. However, reduced fold expansion was observed in CD3z.mIL12 T cells at both cell densities after day 4, while the number of CD3z T cells increased gradually and significantly overtook that of CD3z.IL12 T cells at 0.3 x 10^6 cells/ml on day 6 and day 8. It indicated that T cells stimulated by IL-12 could rapidly proliferate for several days post transduction and then failed to expand after 4 days in culture regardless of cell culture density. Whilst lowering cell density could provide more culture medium for expansion and dilute the concentration of IL-12 accumulated within 2-day culture, T cells still underwent apoptosis which was probably caused by IL-12 stimulation. Although this approach was not ideal for maintaining T cells survival, it enabled IL-12-secreting CAR-T cells to proliferate rapidly, reaching sufficient numbers for adoptive transfer.

In the following experiments, IL-12-secreting T cells were cultured at 0.3 x 10^6 cells/ml to improve viability during *in vitro* expansion and showed similar expansion pattern (Figure 3.9 B), whilst non-IL-12-secreting T cells were still cultured at 1 x 10^6 cells/ml to save TCM.

A.

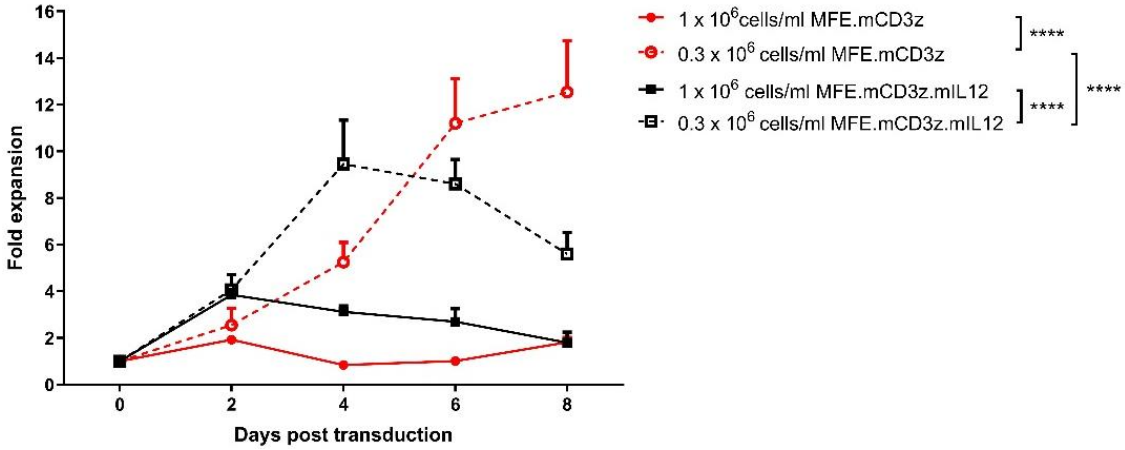

B.

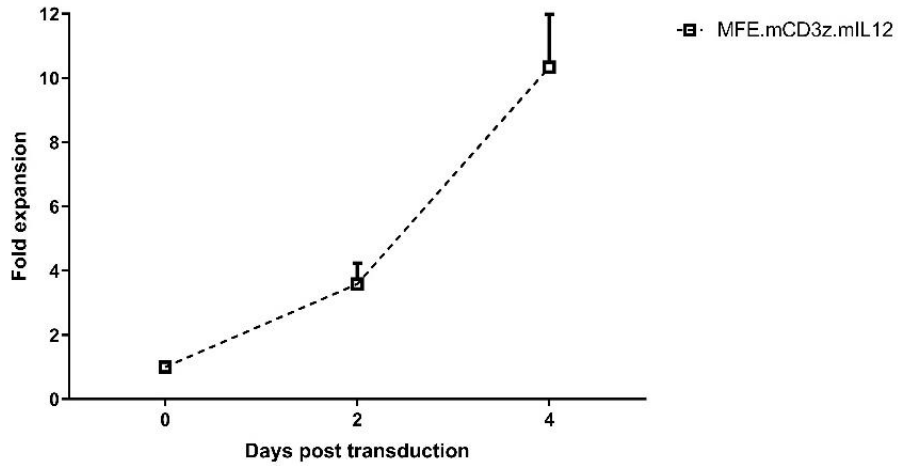

Figure 3.9 Expansion of transduced T cells at different cell densities

(A) Comparison of fold expansion of MFE23.mCD3z.IL12 T cells at two cell culture densities. The data are plotted as mean ± SD of triplicates of one experiment. **(B)** Fold expansion of MFE23.mCD3z.IL12 T cells cultured at 0.3 x 10^6 cells/ml in the following experiments. The data are plotted as mean ± SD of three independent experiments. Viable cells were enumerated every 2 days by bright field microscopy using trypan blue exclusion. Statistically significant difference was analysed using two-way ANOVA with Sidak's multiple comparisons test. **** $P < 0.0001$.

3.2.4 Establishment of GFP and luciferase expressing CEA$^+$ tumour cell lines

To assess the anti-tumour responses of MFE23 CAR-T cells, two widely used colorectal cell lines CT26 and MC38, syngeneic to BALB/c and C57BL/6 mouse strains respectively, were chosen as target cells. The derivative cell lines CT26.CEAdo.mtm (CEA$^+$ CT26) and MC38.CEAdo.mtm (CEA$^+$ MC38) cell lines were made previously in our laboratory by transducing CT26 and MC38 cells with retroviral vectors encoding a truncated part of human CEA molecule linked to an anchoring transmembrane domain. The CEA domain used is the N terminal region to which MFE23 scFv binds. The non-cleavable transmembrane domain was used to replace the GPI linkage of the whole CEA molecule prevents the release of CEA into the surroundings and circulation. This design could therefore avoid an underestimation of the anti-tumour functions of anti-CEA CAR-T cells due to reduced CEA expression on the tumour cell surface.

To determine the level of CEA expression, CEA$^+$ target cell lines were stained with anti-CEA antibody, followed by anti-mouse IgG antibody conjugated to PE. Staining CEA$^+$ target cells with anti-mouse IgG antibody conjugated to PE only was used as negative control (Figure 3.10 A). Both transduced CT26 and MC38 cell lines showed high levels of CEA expression, which was 98.4 ± 0.9 and 88.3 ± 1.9 % respectively (Figure 3.10 B & C). These CEA-expressing cell lines were subsequently used as target cells to evaluate the anti-tumour activity of MFE23 CAR-T cells *in vitro and in vivo*.

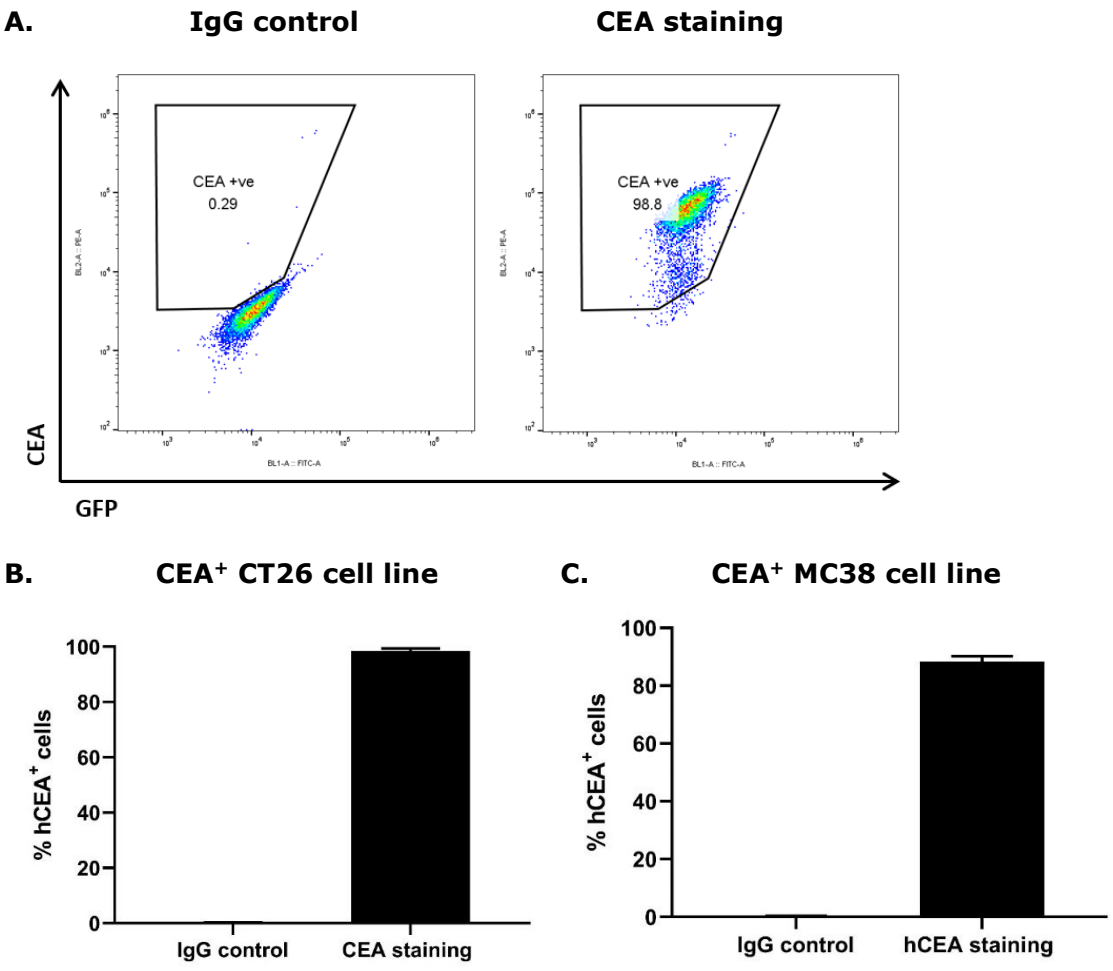

Figure 3.10 Expression of CEA on CEA$^+$ tumour cell lines

(A) Representative dot plots are shown for CEA expression of CEA$^+$ CT26 cell line. **(B)** The percentage of CEA$^+$ CT26 cells is plotted as mean ± SD of three independent experiments determined by flow cytometry. **(C)** The percentage of CEA$^+$ MC38 cells is plotted as mean ± SD of three independent experiments determined by flow cytometry.

In order to assess cytotoxicity of CAR-T cells *in vitro*, a luciferase assay was performed using CEA^+ tumour cell lines transduced to express luciferase and GFP (CEA^+ CT26.Luc.GFP and CEA^+ MC38.Luc.GFP). To establish these cell lines, a retroviral vector encoding luciferase and GFP (rkat.Luc.IRES.GFP) was used for retroviral transduction. GFP was used as a marker protein to determine if tumour cells were efficiently transduced with the luciferase encoding vector.

Efficient transfection of Plat-E cells was confirmed by the detection of GFP fluorescence using fluorescence microscopy (Figure 3.11 A). Retroviral transduction for CEA^+ tumour cells was performed by spinfection in the presence of polybrene. To measure the level of CEA and GFP co-expression, transduced CEA^+ target cell lines were stained with anti-CEA antibody, followed by anti-mouse IgG antibody conjugated to PE. Staining non-transduced CEA^+ target cells with anti-mouse IgG antibody conjugated to PE only was used as negative control. Cell sorting was performed to obtain high levels of CEA and GFP co-expression by collecting CEA^+ and GFP^+ double positive cells.

It can be seen that 92 % of transduced CT26 cells were double positive for CEA and GFP post transduction (Figure 3.11 B). The proportion of CEA^+ and GFP^+ double positive CT26 cells was further increased to 98 % after cell sorting (Figure 3.11 C). Furthermore, brighter GFP fluorescence could be observed from transduced CT26 cells post sorting by fluorescence microscopy (Figure 3.11 D). The percentage of CEA^+ and GFP^+ CT26 cells remained stable at 96.2 ± 3.7 % from three independent experiments (Figure 3.11 E).

A. **Mock** **GFP transfected**

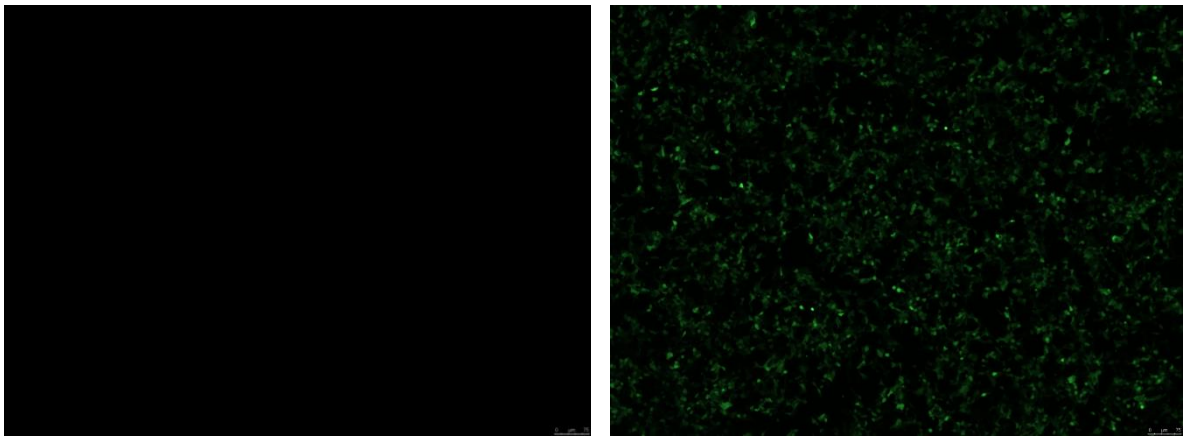

B. **IgG control** **CEA staining**

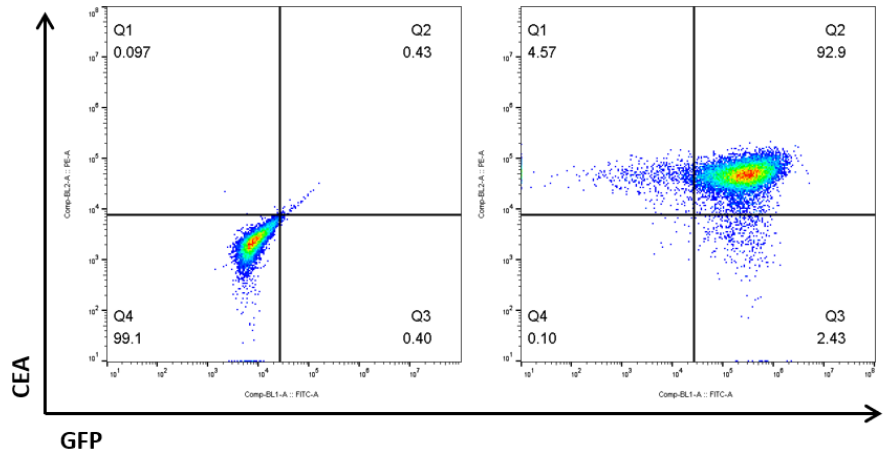

C. **IgG control** **CEA staining**

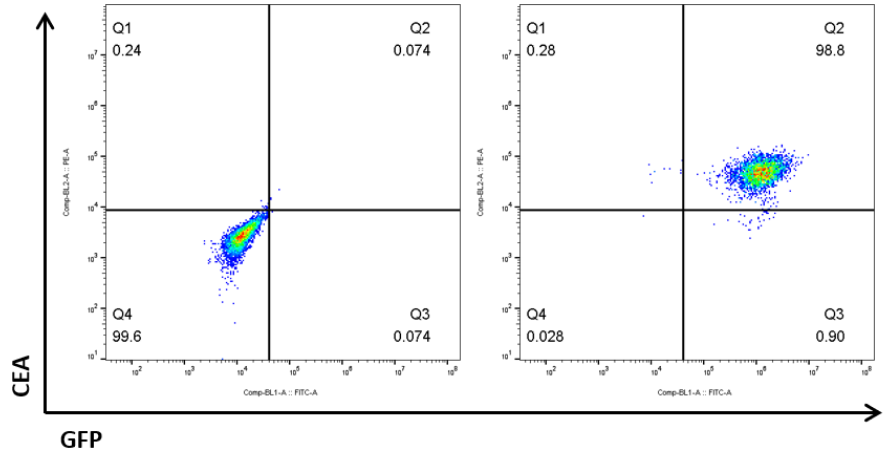

D. **before sorting** **after sorting**

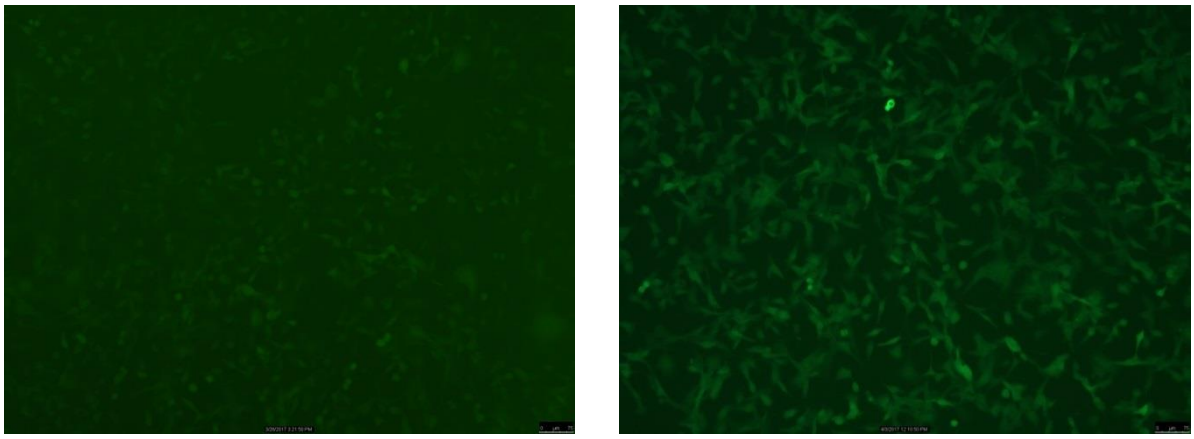

E.

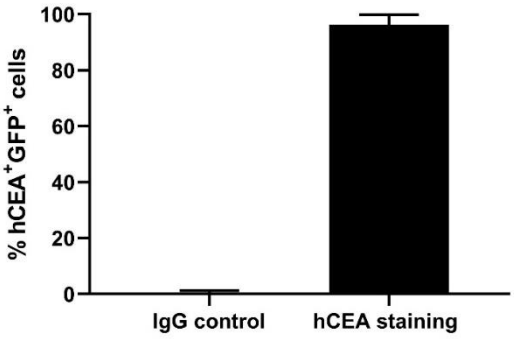

Figure 3.11 Expression of GFP and CEA on transduced CT26 tumour cells before and after cell sorting

(A) Representative images of GFP fluorescence of Plat-E cells post transfection by fluorescence microscopy. **(B)** Representative dot plots are shown for GFP and CEA expression of transduced GFP^+ CEA^+ CT26 cell line before sorting. **(C)** Representative dot plots are shown for GFP and CEA expression of transduced GFP^+ CEA^+ CT26 cell line after sorting. **(D)** Representative images of GFP fluorescence of transduced GFP^+ CEA^+ CT26 cells before and after cell sorting by fluorescence microscopy, Magnification = 50X. **(E)** The percentage of GFP^+ and CEA^+ CT26 cells is plotted as mean ± SD of three independent experiments determined by flow cytometry.

Compared to CT26 cells, MC38 cells were more difficult to transduce. Only 25 % of them co-expressed CEA and GFP (Figure 3.12 A). Even though the level of co-expression was increased to around 40 % by cell sorting, it was back down to 23 % after 10 passages (Figure 3.12 B). As two retroviral vectors encoding CEA and GFP and luciferase respectively were separately put into both CT26 and MC38 cell lines, there is probably a competition for gene expression between those vectors, resulting in untable CEA and GFP co-expression in MC38 cell line. Also, the non-transgene-expressing cells were likely to overpopulate the culture over time. Those situations may lead to the low level of co-expression.

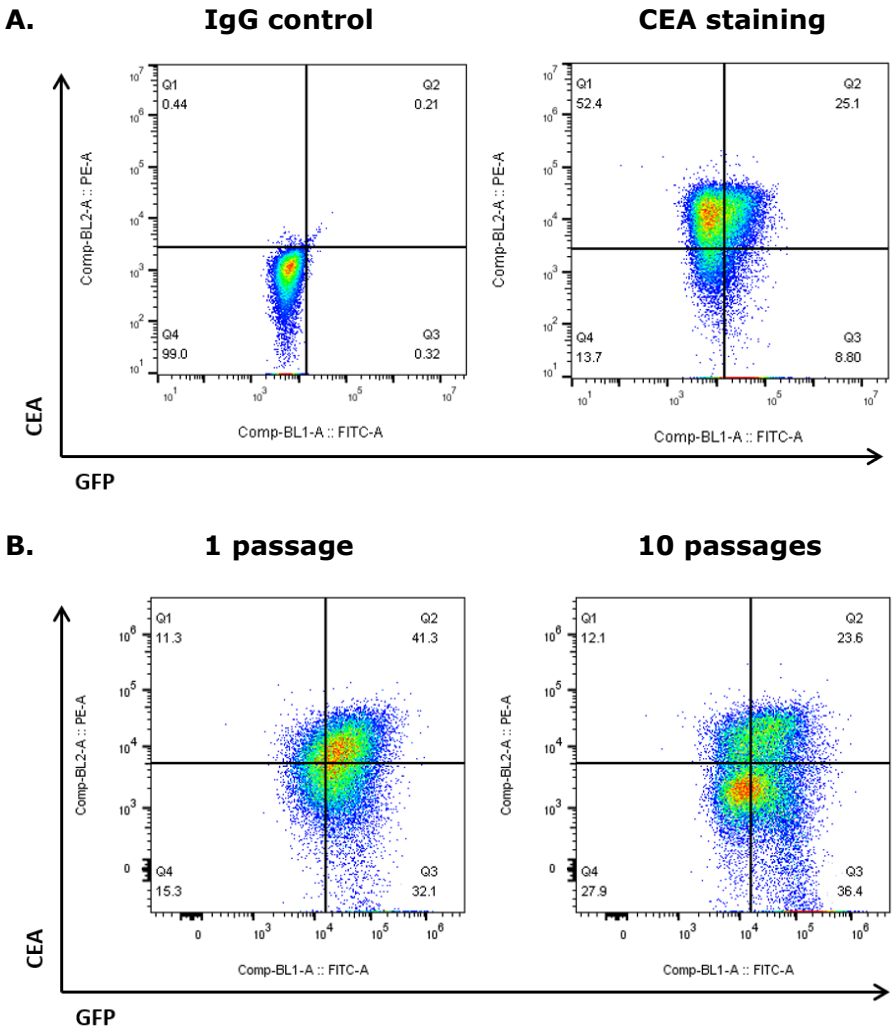

Figure 3.12 Expression of GFP and CEA on transduced MC38 tumour cells before and after cell sorting

(A) Representative dot plots are shown for GFP and CEA expression of transduced GFP^+ CEA^+ MC38 cell line before sorting. **(B)** Representative dot plots are shown for GFP and CEA expression of transduced GFP^+ CEA^+ MC38 cell line at different passages after sorting.

In order to retain stable transgene co-expression, single cell cloning for GFP^+ CEA^+ MC38 cells were performed three times. Additionally, in an attempt to reach higher CEA expression, CEA^+ MC38 cells without luciferase or GFP expression which had been established to have 88.3 ± 1.9 % of CEA expression underwent single cell cloning.

The CEA and GFP expression of single cell clones expanded was determined by flow cytometry (Figure 3.13). It was seen that CEA and GFP were stably co-expressed in 98.5 % of GFP^+ CEA^+ MC38 cells after the third time of single cell cloning, whilst it was 25 % before cloning. The CEA expression level of CEA^+ MC38 cells without luciferase or GFP expression was increased slightly from 88.3 to 94.5 %. Performing single cell cloning three times also minimised the possibility that non-transgene-expressing cells overpopulate the culture.

The luciferase activity of CEA^+ MC38.Luc.GFP cells was validated by luciferase assays with the addition of luciferin. Efficient luciferase expression was demonstrated by the detection of relative light units (RLU). A non-linear increase in RLU was observed following the increasing number of transduced cells seeded from 0 to 1 x 10^5 cells (Figure 3.14 A). The possible reason is that the 96-well plate used has limited space to allow CEA^+ MC38.Luc.GFP cells at high density (5 x 10^4 cells/well) to seed, resulting in the plateau of luminescence intensity detected. When excluding higher cell densities 5 x 10^4 and 1 x 10^5 cells/well, RLU showed a linear correlation with the increase of cell density from 0 to 2 x 10^4 cells (R^2 =0.994) (Figure 3.14 B). As such, the 1 x 10^4 or 2 x 10^4 of transduced tumour cells was used for the co-culture with CAR-T cells to assess CAR-T cell activity.

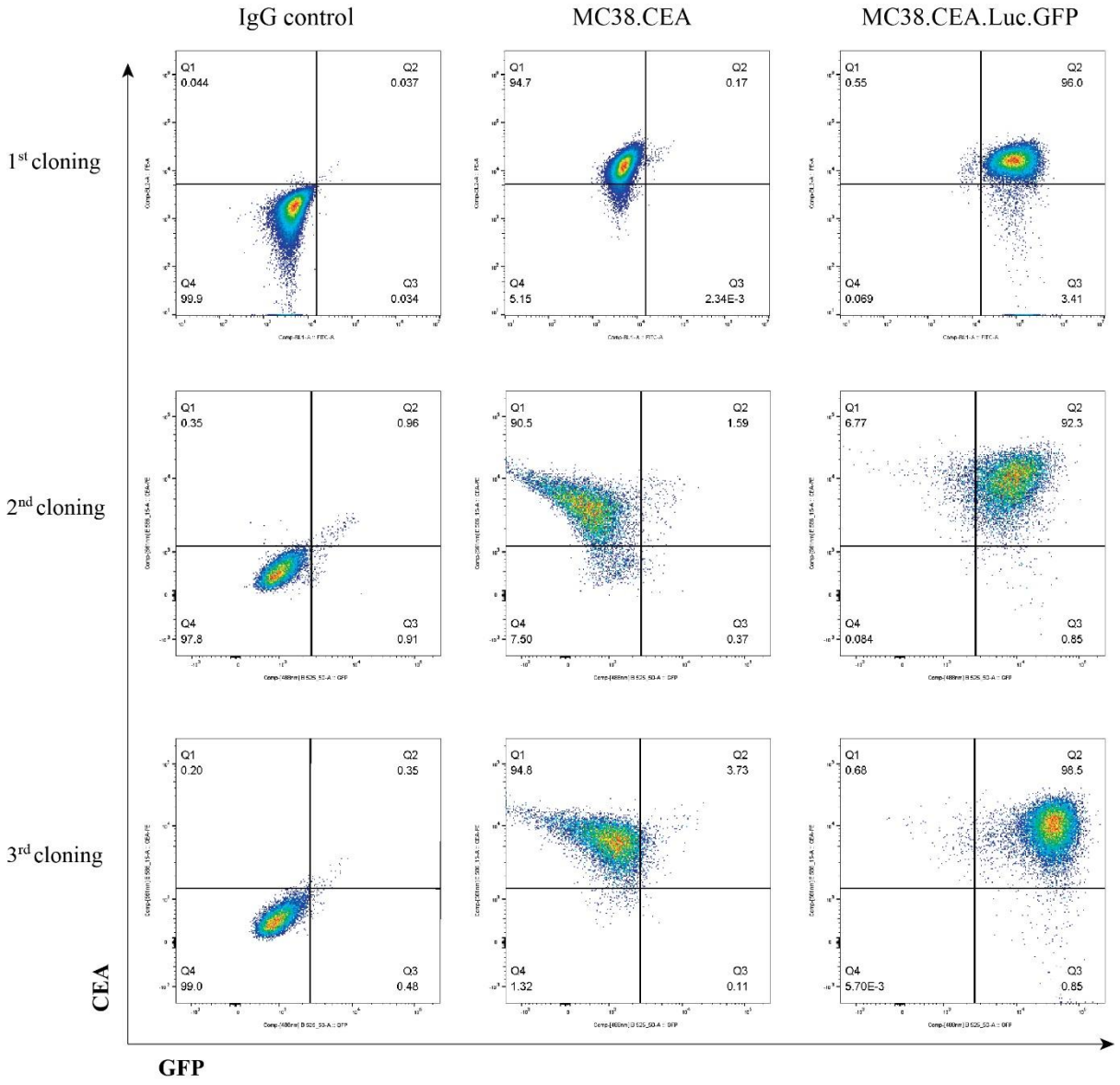

Figure 3.13 Single cell cloning for CEA$^+$ MC38 cells with or without luciferase and GFP expression

Single cell clones were generated by limiting dilution. Transduced MC38 cells were counted and serially diluted to a final concentration of 1.5 cells/ml. 0.3 cell was seeded per well in 200 µl in a 96-well plate. The diluted cells were allowed to grow and form clonal colonies undisturbed for 1 week. Single cell clones were then identified and transferred sequentially into larger culture plates until there are enough cells to assess transgene expression. To measure the level of CEA and GFP co-expression, the single cell clones were stained with anti-CEA antibody, followed by anti-mouse IgG antibody conjugated to PE. Staining CEA$^+$ MC38 cells with anti-mouse IgG antibody conjugated to PE only was used as negative control.

A.

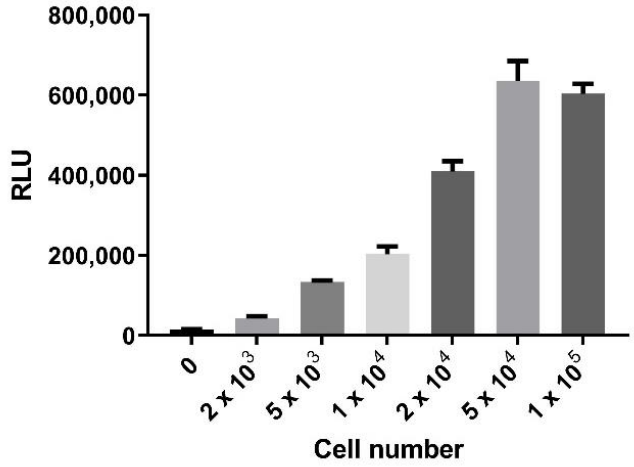

B.

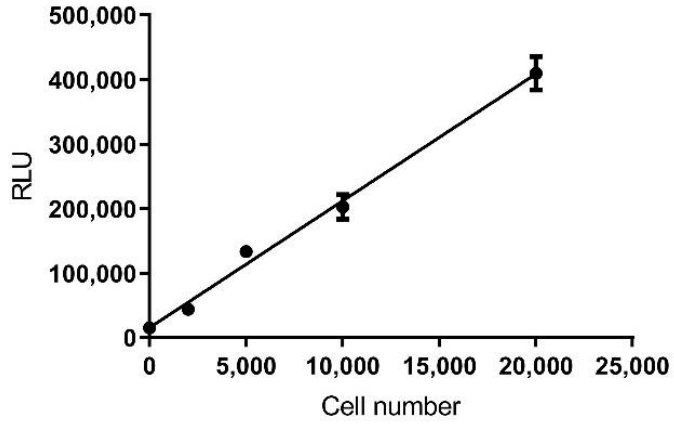

Figure 3.14 RLU of luciferase-labelled CEA$^+$ MC38 cells seeded at different densities

CEA$^+$ MC38 cells expressing GFP and luciferase post single cell cloning were seeded at the densities of 1 x 10^5, 5 x 10^4, 2 x 10^4, 1 x 10^4, 5 x 10^3, 2 x 10^3 and 0 cells/well respectively and incubated for 20 hours. Each condition was performed in triplicate. **(A)** The RLU of luciferase-labelled cells seeded at different densities was measured by luminometry. **(B)** Linear regression was calculated to generate the best fit line based on the RLU of cell number from 0 to 2 x 10^4 (R^2 =0.994).

3.2.5 Cytokine release by anti-CEA CAR-T cells secreting IL-12

To assess whether IL-12 enhanced the *in vitro* anti-tumour function of CAR-T cells, CEA-specific CAR-T cells with or without constitutive IL-12 expression were co-incubated with CEA^+ target cells and parental target cells at effector: target (E: T) ratio of 1: 1 for 20 hours. Syngeneic mouse T cells were isolated from the BALB/c and C57BL/6 mice when co-cultured with CEA^+ CT26 and MC38 cell lines respectively. Due to the variable levels of transduction efficiency among CAR-T cell groups, non-transduced T cells were added into each group to ensure that the number of both total T cells and CAR-expressing T cells remained consistent. The supernatant was collected post co-culture and measured for IFN-γ and IL-12 release by ELISA.

A representative experiment using CEA^+ CT26 cell line showed that IL-12 could be significantly produced by IL-12-expressing CAR-T cells alone, but not parental CAR-T cells (Figure 3.15 A). In the presence of target antigen, CD3z.mIL12 secreted the most amount of IL-12 (5,682.7 ± 1,070.3 pg/ml), followed by CD28z.mIL12 (1,985.0 ± 131.0 pg/ml) and 41BBz.mIL12 (1,749.0 ± 147.0 pg/ml). This suggests that the addition of the CD28 or 41BB co-stimulatory domain had a negative impact on the production of IL-12 from CAR-T cells. However, while CEA-specific stimulation resulted in significantly increased IL-12 production in CD3z.mIL12 and CD28z.mIL12 CARs ($P < 0.0001$), there was no significant increase in IL-12 production for 41BBz.mIL12 CARs compared to production on culture with non-CEA-expressing CT26 cells. Similar secretion patterns could be seen in the mean ± SD values of 2 independent experiments, although statistical significance was reduced (Figure 3.15 B).

A.

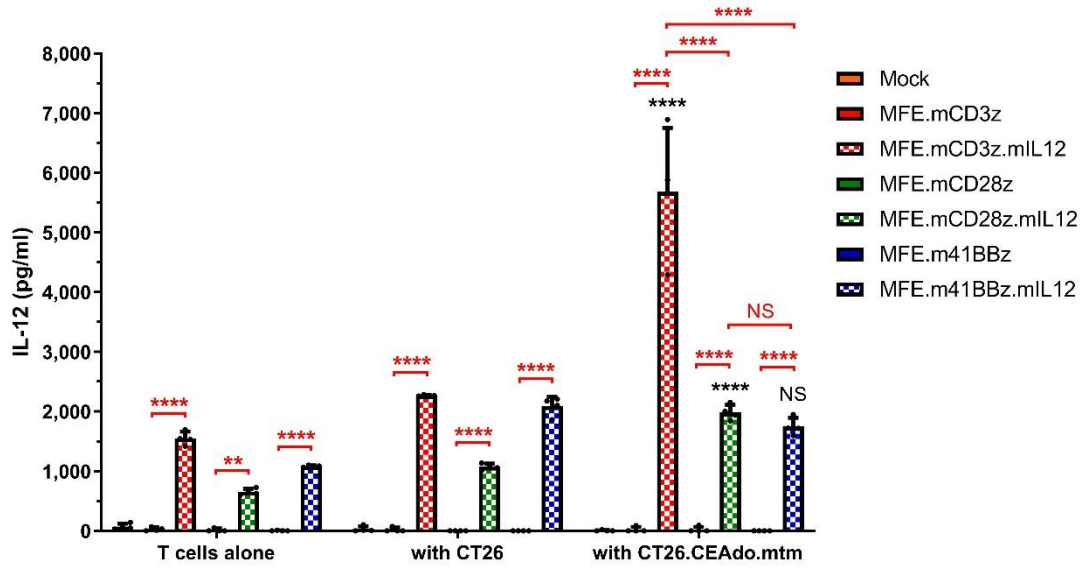

B.

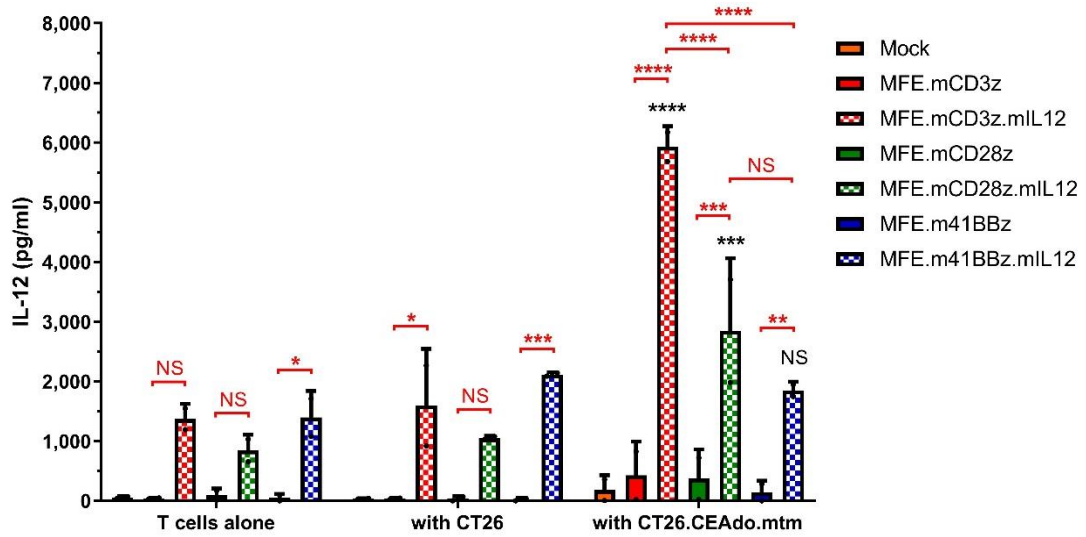

Figure 3.15 IL-12 secretion by anti-CEA CAR-T cells in response to CEA$^+$ CT26 cell line

Transduced T cells were co-cultured for 20 hours with 1×10^4 CEA$^+$ CT26 cells and CT26 cells at E: T ratio of 1:1. The supernatant collected post incubation was measured for IL-12 production by ELISA. **(A)** The data are representative of two independent experiments and values are presented in mean ± SD of triplicates. **(B)** The data are plotted as mean ± SD of two independent experiments. Statistically significant difference was analysed using two-way ANOVA with Tukey's multiple comparisons test. NS, no significant difference; $*$ $P < 0.05$; $**$ $P < 0.01$; $***$ $P < 0.001$; $****$ $P < 0.0001$. Red stars represent comparison between two constructs. Black stars represent comparison of each construct co-cultured with CEA$^+$ CT26 cells and parental CT26 cells.

With regard to the C57BL/6 T cells, more IL-12 was produced as the cell number for co-culture was increased to 2×10^4 cells. Similarly, a representative experiment showed that all CAR-T cells expressing IL-12 could constitutively produce IL-12 (Figure 3.16 A). The highest levels of IL-12 were still produced by CD3z.mIL12 T cells. Notably, compared to the panel of CAR-T cells alone, IL-12 production was significantly reduced in CD3z.mIL12 and CD28z.mIL12 CAR-T cells co-cultured with non-CEA-expressing MC38 cells ($P < 0.05$ and $P < 0.01$ respectively). Due to the expression of IL-12Rβ1 on MC38 cells [205], it is hypothesised that IL-12 might be taken up by tumour cells. It is further supported by other studies showing that IL-12 directly inhibits the angiogenic activity of human tumour cells expressing IL-12Rβ1 and IL-12Rβ2 *in vitro* through down-regulation of different pro-angiogenic molecules such as IL-6, VEGF-C [190, 191]. Because of this, there is a significant difference in IL-12 production for CD3z.mIL12 and CD28z.mIL12 CAR-T cells post co-culture with CEA^+ MC38 cells compared to co-culture with parental MC38 cells ($P < 0.0001$ and $P < 0.001$ respectively), whilst statistical significance was reduced when compared to the panel of CD3z.mIL12 and CD28z.mIL12 CAR-T cells alone ($P < 0.01$ and NS respectively). 41BBz.mIL12 CAR-T cells failed to secret more IL-12 upon CAR engagement with CEA-expressing target cells. A similar trend but less significance was seen in the mean ± SD values of 2 independent experiments due to donor variability (Figure 3.16 B).

A.

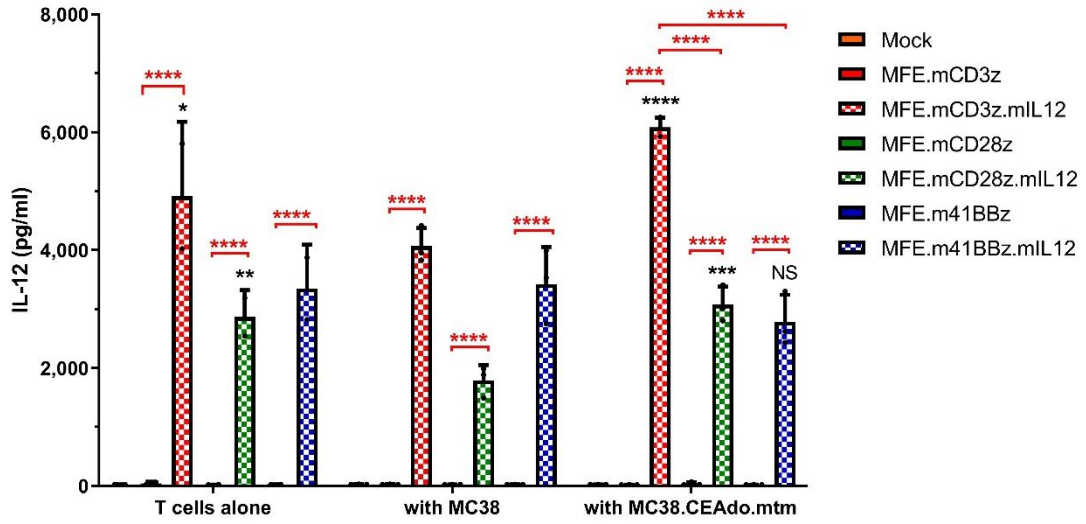

B.

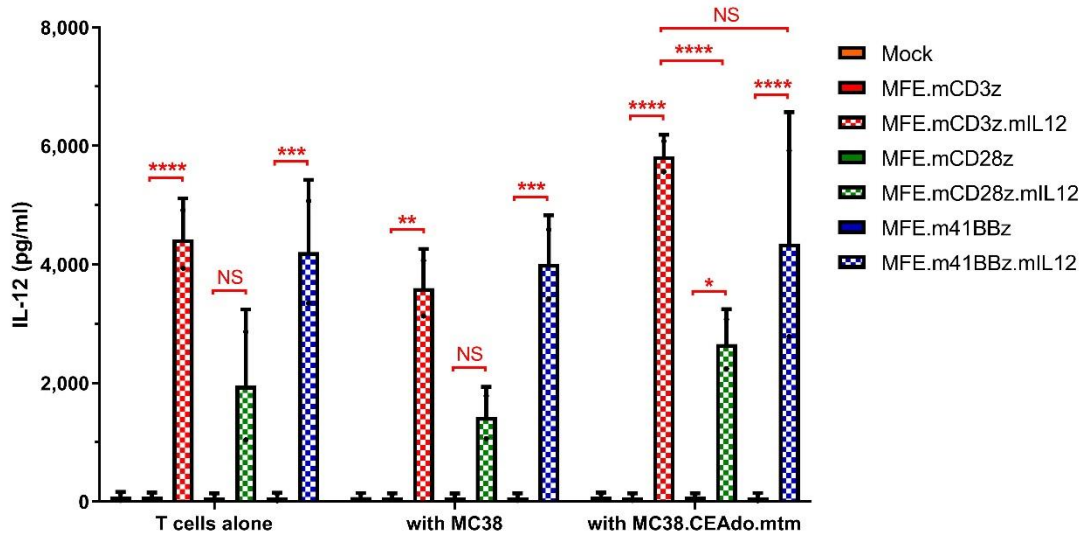

Figure 3.16 IL-12 secretion by anti-CEA CAR-T cells in response to CEA$^+$ MC38 cell line

Transduced T cells were co-cultured for 20 hours with 2 × 10^4 CEA$^+$ MC38 cells and MC38 cells at E: T ratio of 1:1. The supernatant collected post incubation was measured for IL-12 production by ELISA. **(A)** The data are representative of two independent experiments and values are presented in mean ± SD of triplicates. **(B)** The data are plotted as mean ± SD of two independent experiments. Statistically significant difference was analysed using two-way ANOVA with Tukey's multiple comparisons test. NS, no significant difference; ∗ $P < 0.05$; ∗∗ $P < 0.01$; ∗∗∗ $P < 0.001$; ∗∗∗∗ $P < 0.0001$. Red stars represent comparison between two constructs. Black stars represent comparison between MC38 cell panel and T cell alone or CEA$^+$ MC38 cell panels.

In terms of IFN-γ secretion in the BALB/c model (Figure 3.17 A), a representative experiment showed that much less IFN-γ (527.2 ± 89.9 pg/ml) was detected in CD3z CARs, whilst the additional secretion of IL-12 (CD3z.mIL12 CARs) and the incorporation of co-stimulatory domain CD28 only (CD28z CARs) could increase IFN-γ production significantly when transduced CAR-T cells were co-cultured with CEA^+ CT26 cells compared to parental CT26 cells (4,359.5 ± 210.0 pg/ml, 21,406.5 ± 970.9 pg/ml respectively) ($P < 0.0001$). Importantly, the combination of IL-12 cytokine and co-stimulatory domain CD28 achieved the highest IFN-γ secretion (57,660.8 ± 1,946.6 pg/ml) ($P < 0.0001$). In contrast, the use of another co-stimulatory domain 41BB led to less IFN-γ production than first-generation CD3z CAR (203.1 ± 12.7 pg/ml). As for 41BBz.mIL12 CARs, there is no significant difference in IFN-γ production between CEA^+ CT26 group versus CT26 group, which is similar to IL-12 production. Despite this, it is notable that all IL-12-secreting CAR-T cell cells had a higher amount of IFN-γ production compared to parental CAR-T cells. A similar but less prominent trend was seen in the mean ± SD values of 2 independent experiments due to donor variability (Figure 3.17 B).

A.

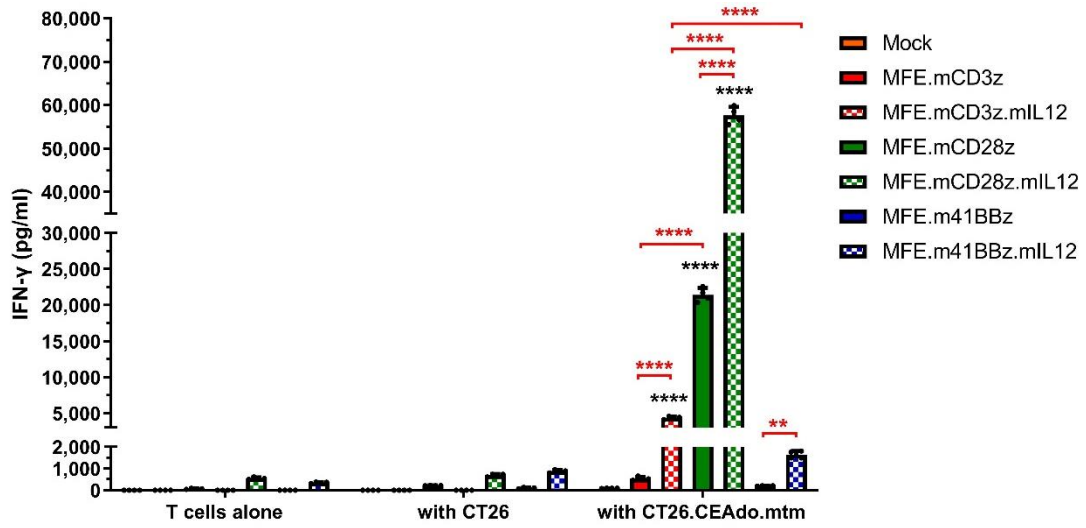

B.

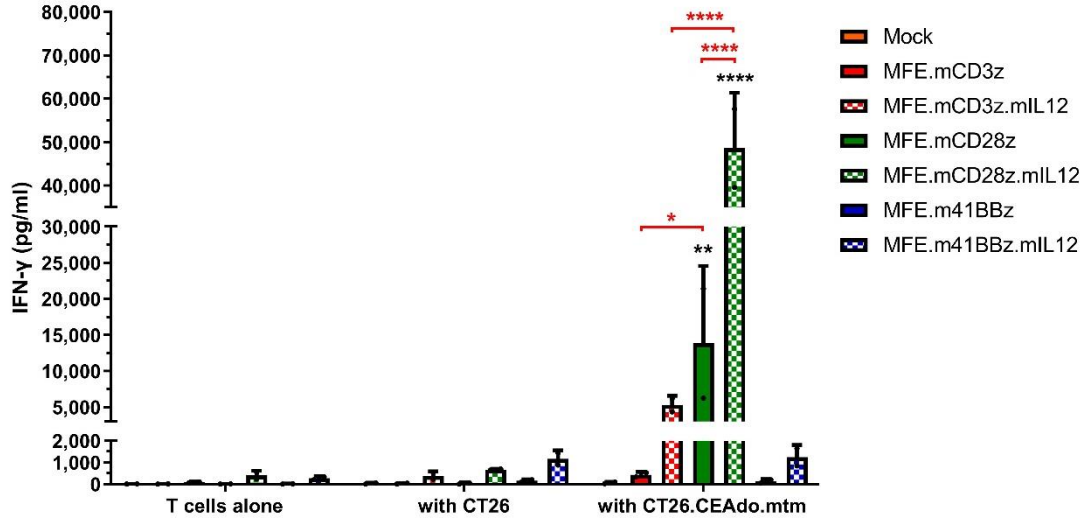

Figure 3.17 IFN-γ secretion by anti-CEA CAR-T cells in response to CEA$^+$ CT26 cell line

Transduced T cells were co-cultured for 20 hours with 1×10^4 CEA$^+$ CT26 cells and CT26 cells at E: T ratio of 1:1. The supernatant collected post incubation was measured for IFN-γ production by ELISA. **(A)** The data are representative of two independent experiments and values are presented in mean ± SD of triplicates. **(B)** The data are plotted as mean ± SD of two independent experiments. Statistically significant difference was analysed using two-way ANOVA with Tukey's multiple comparisons test. NS, no significant difference; * $P < 0.05$; ** $P < 0.01$; **** $P < 0.0001$. Red stars represent comparison between two constructs. Black stars represent comparison of each construct co-cultured with CEA$^+$ CT26 cells and parental CT26 cells.

As for the C57BL/6 model, a similar pattern can be observed in IFN-γ secretion from a representative experiment (Figure 3.18 A). CAR-T cells with different CAR constructs with the exception of 41BBz produced more IFN-γ in response to CEA-expressing MC38 cells. Whilst second-generation CD28z CARs showed higher levels of IFN-γ production than first-generation CD3z CARs, the addition of IL-12 in CEA-specific CAR-T cells could significantly facilitate CAR-T cells to produce more IFN-γ. Notably, similar to IL-12 production, IFN-γ production was reduced in IL-12-secreting CAR-T cells co-cultured with non-CEA-expressing MC38 cells, compared to production of IL-12-secreting CAR-T cells alone, although the reduction was not significant. In the absence of CEA antigen, IFN-γ was only produced from T cells by IL-12 stimulation. It has been reported that IFN-γ has direct anti-tumour effects on tumour cells such as upregulating the expression of MHC class I molecules to enhance antigen presentation and inhibiting cell proliferation, as well as potential pro-tumour effects [206]. This suggests that IFN-γ is likely to act on MC38 tumour cells, resulting in the reduction in IFN-γ levels in cultures with MC38. Again, a similar secretion pattern could be seen in the mean ± SD values of 2 independent experiments, although statistical significance was reduced (Figure 3.18 B).

A.

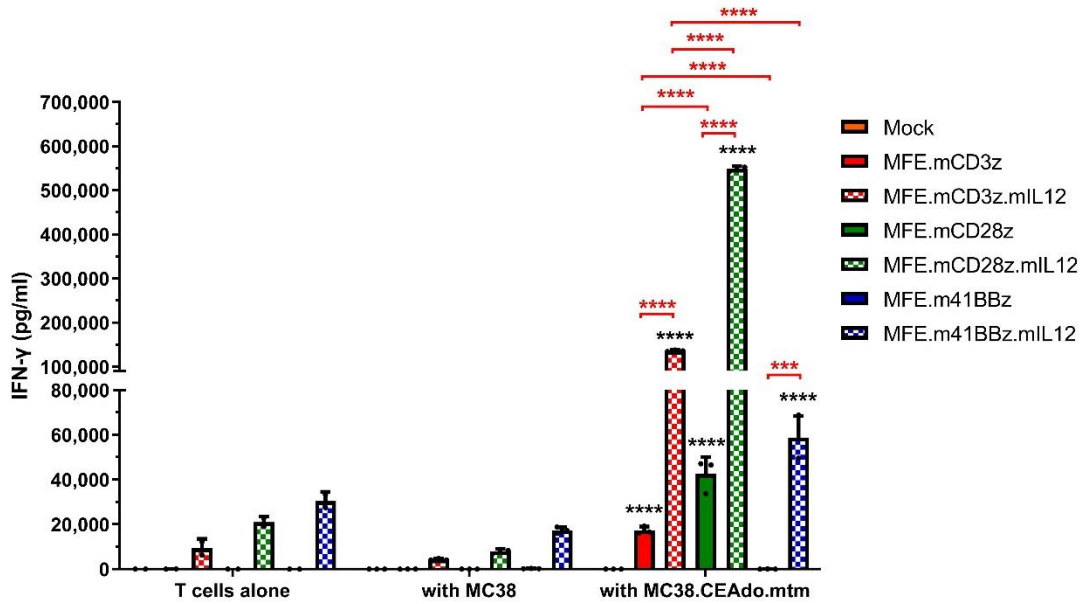

B.

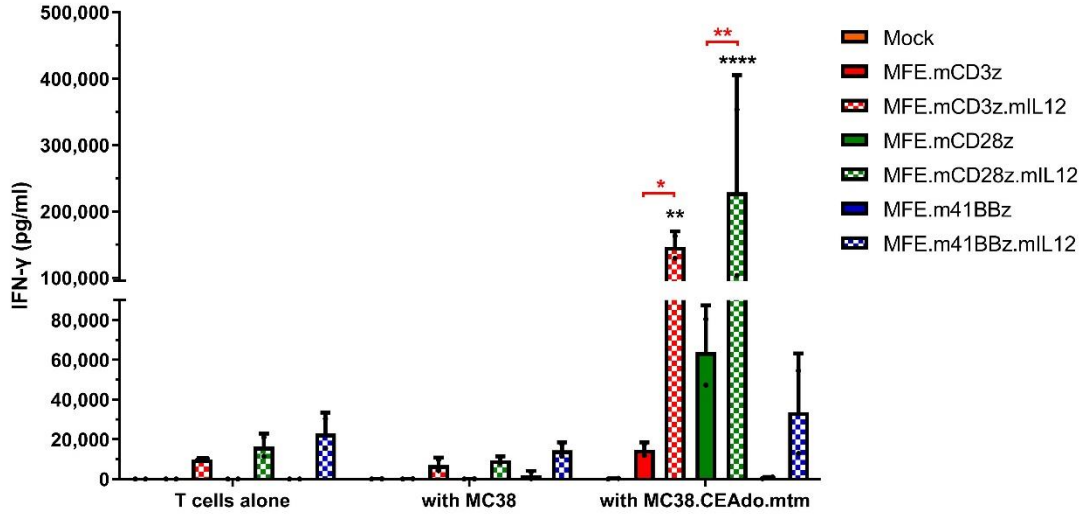

Figure 3.18 IFN-γ secretion by anti-CEA CAR-T cells in response to CEA$^+$ MC38 cell line

Transduced T cells were co-cultured for 20 hours with 2 × 10^4 CEA$^+$ MC38 cells and MC38 cells at E: T ratio of 1: 1. The supernatant collected post incubation was measured for IFN-γ production by ELISA. **(A)** The data are representative of two independent experiments and values are presented in mean ± SD of triplicates. **(B)** The data are plotted as mean ± SD of two independent experiments. Statistically significant difference was analysed using two-way ANOVA with Tukey's multiple comparisons test. NS, no significant difference; * $P < 0.05$; ** $P < 0.01$; *** $P < 0.001$; **** $P < 0.0001$. Red stars represent comparison between two constructs. Black stars represent comparison of each construct co-cultured with CEA$^+$ MC38 cells and parental MC38 cells.

3.2.6 Cytotoxicity of anti-CEA CAR-T cells secreting IL-12

To assess the cytotoxicity of CAR-T cells, luciferase assays were performed by measuring the luciferase activity of target cell lines post 20-hour co-culture with CAR-T cells.

Two experiments using the BALB/c model showed that all CAR-T cell groups exhibited cytotoxicity against luciferase-expressing CEA^+ target cells in comparison with mock T cells ($P < 0.0001$) (Figure 3.19 A). In donor one, IL-12-secreting CAR-T cells mediated significant target cell lysis in comparison with parental CAR-T cells ($P < 0.0001$). The CD28z.mIL12 T cells showed the highest specific lysis (92.4 ± 0.6 %) which was consistent with IFN-γ secretion, compared to the lysis caused by CD28z T cells (56.9 ± 0.4 %). Similarly, more tumour cell killing with CD3z.mIL12 T cells (87.7 ± 0.6 %) was detectable than that with CD3z T cells (64.5 ± 0.4 %). In donor two, as both CD3z and CD28z CAR-T cells with or without IL-12 expression mediated full lysis of CEA^+ CT26 cells within the 20-hour co-culture ($P < 0.0001$), any significant improvement in cytotoxicity by IL-12 cannot be observed. This was partially due to the unspecific cytotoxicity of non-CAR-expressing T cells, which was reflected by high background lysis by mock T cells (44.6 ± 3.3 %). It is of interest that 41BBz and 41BBz.mIL12 T cells also showed killing in two donors, albeit weaker (35.9 ± 1.1 % versus 81.5 ± 1.2 %; 70.8 ± 2.8 % versus 85.8 ± 1.0 % respectively). Given no significant IFN-γ production in the presence of target antigen, it suggests that killing of 41BBz CAR-T cells might be mediated by other mechanisms such as via the TNF family. It is necessary to determine what other cytokines such as IL-2, TNF-α and IL-10 were secreted from $CD8^+$ or $CD4^+$ CAR-T cells to fully understand the mechanisms of CD28 or 41BB co-stimulation. Notably, whilst CD28z.mIL12 T cells exhibited greater cytotoxicity than CD3z.mIL12 T cells ($P < 0.01$), CD3z T cells without IL12 secretion exerted more tumour cell killing than CD28z T cells in donor one ($P < 0.0001$). In donor two, CD28z T cells exhibited better cytotoxicity than CD3z T cells ($P < 0.01$). This was probably due to donor variability as there was no significant difference between them in the mean ± SD values of 2 independent experiments (Figure 3.19 B).

A.

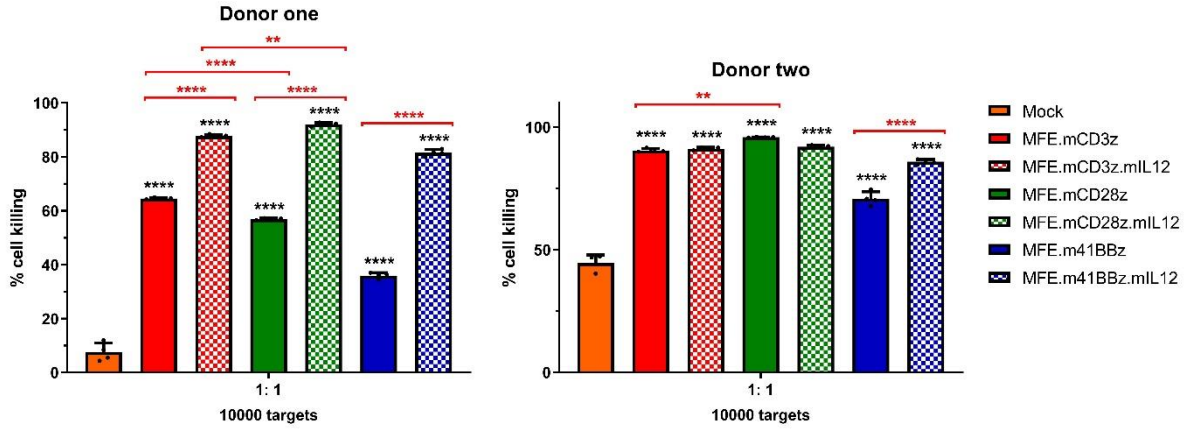

B.

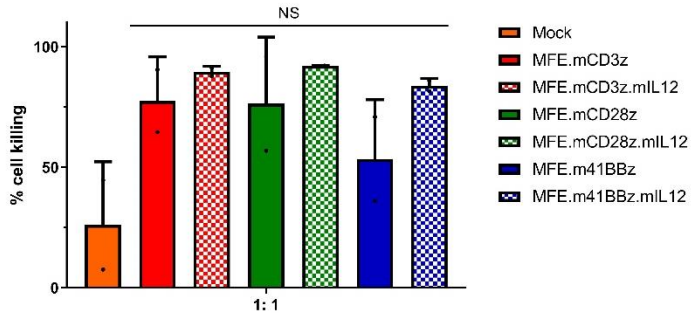

Figure 3.19 Cytotoxicity of anti-CEA CAR-T cells in response to luciferase-labelled CEA$^+$ CT26 cell line

Transduced T cells were co-cultured for 20 hours with 1 × 10^4 CEA$^+$ CT26 cells expressing luciferase and GFP at E: T ratio of 1: 1. Luminometry was performed to assess the cytotoxicity post co-culture. **(A)** The data are presented in mean ± SD of triplicates from two donors respectively. **(B)** The data are plotted as mean ± SD of two independent experiments. Statistically significant differences were analysed using one-way ANOVA with Tukey's multiple comparisons test. NS, no significant difference; ** P < 0.01; **** P < 0.0001. Red stars represent comparison between IL-12-secreting CAR and parental CAR constructs. Black stars represent comparison between mock and CAR constructs.

In terms of the C57BL/6 model, transduced T cells with different CAR constructs with the exception of 41BBz showed significant killing of CEA^+ MC38 cells compared to mock T cells at different E: T ratios ranging from 5: 1 to 0.125: 1 (Figure 3.20 A). The enhanced killing efficiency was correlated with the increase in E: T ratios. At the E: T ratio of 1: 1 in a representative experiment, IL-12-secreting CAR-T cells mediated significant target cell lysis in comparison with the parental non-IL-12-secreting CAR-T cells with the exception of the CAR CD28 construct (Figure 3.20 B). The incorporation of CD28 but not the 41BB co-stimulatory domain was able to enhance tumour cell killing ability of anti-CEA CAR-T cells, which was consistent with the increased IFN-γ secretion seen with this construct. In this model, no significant difference in cytotoxicity was seen between CD28z.mIL12 and CD3z.mIL12 or CD28z T cells. This is probably because these CAR-T cells were functional enough to lyse CEA^+ MC38 cells completely within 20-hour co-culture. Similar results with less significance were seen when the mean of two independent experiments was analysed (Figure 3.20 C).

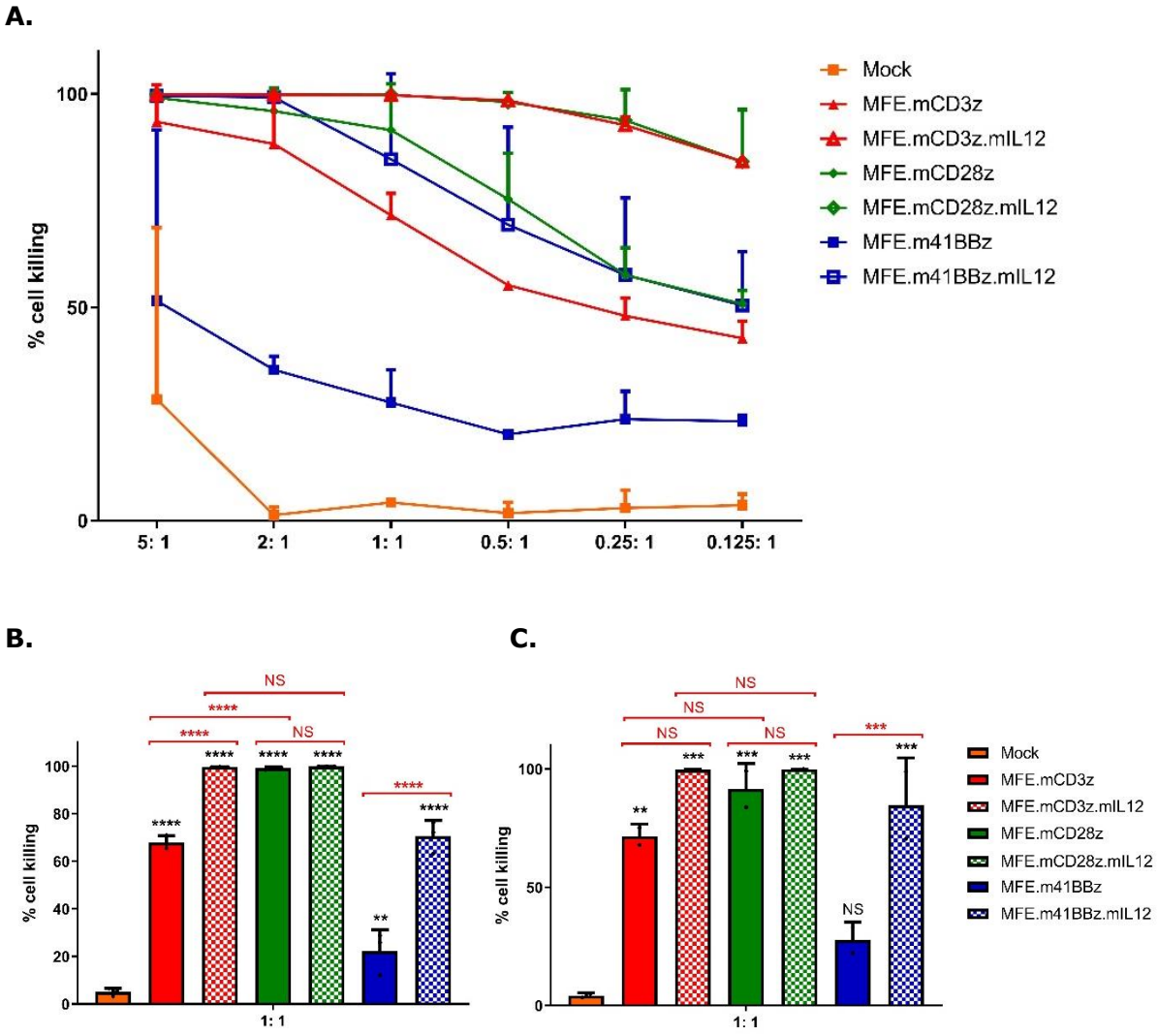

Figure 3.20 Cytotoxicity of anti-CEA CAR-T cells in response to luciferase-labelled CEA$^+$ MC38 cell line

Transduced T cells were co-cultured for 20 hours with 2 × 10^4 CEA$^+$ MC38 cells expressing luciferase and GFP at different E: T ratios from 5: 1 to 0.125: 1 (n = 3). Luminometry was performed to assess the cytotoxicity post co-culture. **(A)** The data at different ratios are shown as mean ± SD of two independent experiments. **(B)** The data at E: T ratio of 1: 1 are representative of two independent experiments and values are presented in mean ± SD. **(C)** The data at E: T ratio of 1: 1 are plotted as mean ± SD of two independent experiments. Statistically significant differences were analysed using one-way or two-way ANOVA with Tukey's multiple comparisons test. NS, no significant difference; ** P < 0.01; *** P < 0.001; **** P < 0.0001. Red stars represent comparison between IL-12-secreting CAR and parental CAR constructs. Black stars represent comparison between mock and CAR constructs.

3.3 Discussion

The main aims of this chapter were to generate first- and second-generation anti-CEA CAR-T cells with or without IL-12 co-expression and assess their anti-tumour activity *in vitro*. The results demonstrated that mouse T cells could be successfully transduced to express different CAR constructs. However, poor transduction efficiency of CAR-T cells was observed, as determined by mCherry expression. Furthermore, there was significant correlation between CAR construct length and transfection efficiency (R^2 = 0.776) but not transduction efficiency (R^2 = 0.3906). In contrast, one study has reported that an increase in the length of CAR constructs correlated with a decrease in transduction efficiency of CAR-T cells, using the same CAR constructs with the exception of anti-mouse CD19 scFv in the MP71 vector (R^2 = 0.9192) [156]. This study suggests that IL-12 expression did not have direct effects on transduction efficiency by causing AICD specific for CAR-T cells. It is therefore hypothesised that the difference of extracellular scFv might be responsible for non-correlated transduction efficiency, by affecting several factors during CAR integration and expression such as the site of transgene insertion into the host genome and the number of transgene copies, the level of transgene transcription, the stability of the mRNA transcript [207]. Additionally, during the formation of pseudotyped retroviral particles, inefficient RNA encapsidation might occur at variable levels among different CAR constructs, resulting in non-correlation between transduction efficiency and CAR construct length. To confirm this, retroviral titer or the amount of vector RNA present in particles should be further examined.

After retroviral transduction, mock and CAR-T cells were usually kept at 1 x 10^6 cells/ml in culture. While CAR expression was likely to affect T cell expansion, IL-12-expressing CAR-T cells significantly failed to expand to large numbers in culture compared to parental CAR-T cells. It has been reported that constitutively expressed IL-12 had anti-proliferative effects on engineered T cells without antigen stimulation *in vitro* [157, 208]. Similar to the results presented here, IL-12-expressing CAR-T cells were able to proliferate slowly for several days post transduction and then underwent apoptosis. It was found that IL-12 caused activation-induced cell death (AICD) of human T cells by simulating high levels of IFN-γ production but not upregulating FasL, as IL-12-induced apoptosis could be partially blocked by anti-IFN-γ or anti-IL12Rβ2 antibodies [157]. However, it was also reported that 50 ng/ml of IL-12 induced human T cell apoptosis mediated by FasL upregulation and increased IFN-γ secretion in the absence of antigen after 24 hours [204]. Perhaps the contradictory results about FasL upregulation is due to the different concentrations of IL-12 used for investigation. In this study, high levels of IFN-γ production from IL-12-secreting CAR-T cells without antigen stimulation were detected as well (Figure 3.17 & 3.18 A), suggesting that IFN-γ plays a role in T cell apoptosis. It would be interesting to

investigate whether IFN-γ directly induces T cell apoptosis mediated by the Fas/FasL interaction.

In the present study, IL-12-expressing CAR-T cells cultured at 0.3 x 10^6 cells/ml expanded significantly better than at 1 x 10^6 cells/ml, most likely due to more culture media provided and the diluted IL-12 accumulation. Notably, when cultured at 0.3 x 10^6 cells/ml on day 4, IL-12-expressing CAR-T cells showed greater expansion than parental CAR-T cells. This suggests that IL-12 could induce murine CAR-T cells to rapidly expand before apoptosis without antigen stimulation, which has not been reported yet. However, further experiments are required to confirm this observation. Furthermore, while it has been reported that IL-12 could significantly enhance either human or murine T cell proliferation with antigen stimulation *in vitro* [195, 209] and *in vivo* [210], this was not investigated in the present study. It would be of interest to perform cell proliferation assays to further determine whether murine anti-CEA CAR-T cells expressing IL-12 would rapidly expand upon CAR engaging target.

In this study, the *in vitro* anti-tumour responses of anti-CEA CAR-T cells were evaluated using CEA^+ CT26 and MC38 cell lines. Similar cytotoxicity outcomes and cytokine secretion levels were observed between them. Due to the individual difference among mouse T cells isolated, the amounts of cytokines secreted post co-culture were variable.

Overall, following CAR engagement with CEA^+ target cells, T cells expressing different CAR constructs exhibited antigen-specific cytotoxicity and produced abundant amounts of IFN-γ at variable levels. The inclusion of the murine CD28 co-stimulatory domain significantly improved the functional activity of CAR-T cells. However, the addition of the murine 41BB domain failed to enhance T cell function, which was consistent with other studies reported using anti-mouse CD19 CAR-T cells [156, 211], whilst the anti-tumour efficacy of the second-generation human 41BBz CAR-T cells has been widely validated [212, 213]. Perhaps the sequence differences between human and mouse 41BB domain, which are 60 % identical [214], led to the different outcomes. While human 41BB domain could bind TNF receptor–associated factor (TRAF) 1-3 which are all critical for 41BB co-stimulation in CAR-T cells, mouse 41BB domain only binds TRAF 1-2 [215, 216]. The substitution of the first 5 N-terminal amino acid mismatches of mouse 41BB with human 41BB amino acids, which have been identified for increased TRAF3 binding and optimal NF-κB signalling, could improve cytokine production and antiapoptotic protein expression as well as *in vivo* CAR-T cell persistence [211].

Modification of CAR-T cells to constitutively secrete IL-12 was able to improve their anti-tumour efficacy, as demonstrated by significantly enhanced cell killing and cytokine secretion. However, there is no significant enhancement of IL-12 and IFN-γ production in 41BBz.IL12 T cells when co-cultured with CEA^+ tumour cells in comparison with parental tumour cells, which indicated that perhaps 41BBz.IL12 T cells were not activated as well as CD3z.IL12 and CD28z.IL12 T cells. Given that 41BBz.IL12 T cells exhibited significant cell lysis compared to 41BBz T cells in the presence of target antigen, it was most likely that IFN-γ, which was produced by IL-12 stimulation, induced direct tumour cell apoptosis [217], rather than cell death through scFv CAR engagement. To determine if this is the case, CAR-T cells would also need to be co-cultured with luciferase-labelled CEA-negative target cells or a control of non-CEA-specific 41BBz.mIL12 CAR-T cells included. It is also necessary to determine the level of other cytokines such as IL-2, TNF-α and IL-10 secreted from CAR-T cells to fully understand the mechanisms of CD28 or 41BB co-stimulation and IL-12 stimulation.

In summary, the results shown in this chapter demonstrated that first- and second-generation CEA-specific CAR-T cells with or without IL-12 co-expression have successfully been generated. Cell culture conditions were optimized to maintain T cell proliferation. Furthermore, the constitutive secretion of IL-12 and the incorporation of the co-stimulatory domain CD28 could improve anti-tumour activities of CEA-specific CAR-T cells *in vitro*.

4 *In vivo* function of anti-CEA CAR-T cells secreting IL-12

4.1 Introduction

4.1.1 Preclinical mouse models in CAR-T cell therapy

Establishment of an appropriate preclinical mouse model is crucial for prediction of both efficacy and toxicity of CAR-T cell treatment in clinic. One of the most common models used is the human xenograft mouse model, which utilises immunocompromised mice that do not reject human tumours or CAR-T cells. Several immunocompromised mouse strains have been developed for this purpose, such as athymic nude mice that are T-cell deficient, severely compromised immunodeficient (SCID) mice that lack mature B and T cells and NOD SCID gamma (NSG) mice that lack mature B, T and NK cells [218, 219]. Either human tumour cell lines or patient-derived tumours can be used to establish xenograft models. The main advantages of cell-line-derived xenograft (CDX) models are their high availability and better tumour take rates and lower costs compared to patient-derived xenograft (PDX) models. PDX tumours are established by implanting patient-derived tumour tissue explants. These can better reflect underlying tumour biology and heterogeneity of individual human cancers, such as cellular morphology, gene expression profiles and cell proliferation rates, compared to tumours derived from tumour cell lines which have been exposed in artificial environments and passaged for long periods [220]. The main advantage of human tumour xenograft models is that they can directly demonstrate the basic efficacy of human CAR-T cells on clinically relevant human tumour cells. However, human T cells transferred into immunocompromised mice would attack mouse cells and sometimes cause xenogeneic GvHD [221, 222]. These models also cannot predict on-target off-tumour effects due to the lack of human target antigen expressed on normal tissues. Additionally, because of non- or partial host immunity and lack of overlap in mouse and human biology, a less realistic tumour microenvironment where stromal components involved in tumourigenesis are of mouse origin is provided and the interactions between CAR-T cells and other immune cells during tumour regression are limited [223].

It is thought that the unsatisfactory efficacy of CAR-T cell therapy for solid tumours in clinical trials is partly due to the immunosuppressive tumour microenvironment as described in section 1.2.3. However, this immunosuppression on CAR-T cells cannot be comprehensively elucidated in immunocompromised mouse models bearing human

tumours, due to the limitations mentioned above. In an attempt to reflect full influence of the tumour microenvironment and the involvement of endogenous immune cells on CAR-T cell efficacy in the clinically relevant situation, immunocompetent mouse models with intact murine immune systems are commonly utilised. In this model, CAR-T cells, tumour cells and target antigens are all murine-derived [224]. Given that murine normal tissues may have low levels of target antigen expression, the immunocompetent model also has the advantage of evaluating potential on-target off-tumour toxicities of CAR-T cells. In addition, several human tumour-associated antigens (TAAs) which are not detected in mice, such as CEA and HER2, can also be used as target antigens in immunocompetent mouse models [83, 225]. In this experimental model, murine T cells are engineered to express CAR targeting human TAAs and syngeneic tumour cell lines transduced to express the targeted antigens are utilised for tumour establishment. However, endogenous immune responses against human TAAs might be elicited in mice and contribute to tumour eradication in CAR-T cell therapy, which requires investigation in tumour-bearing mice.

Alternatively, immunocompetent transgenic mice can be employed if available for the study of murine CAR-T cells targeting human TAAs, such as CD19, CEA and HER2 [226-228]. These mice are genetically modified to express a human TAA transgene such that TAA expression patterns and levels are similar to that seen in humans and the host immune system is tolerant to the TAA transgene. This transgenic model therefore not only enables the evaluation of CAR-T cells targeting human TAAs *in vivo* in mice with a fully functional murine immunity and syngeneic tumours, but also avoids the potential occurrence of endogenous immune responses against the targeted human antigens. Most importantly, compared to immunocompetent wild-type mouse model targeting murine TAAs, transgenic mice mirroring the expression patterns of human TAAs in human patients is more valuable to predict potential on-target off-tumour toxicity of CAR-T cell therapy in clinical studies.

It is of note that the main limitation of syngeneic immunocompetent model is the crucial difference between mouse and human immunity, which impact the predictive power in clinical activity. For example, the differences between murine and human T cell signalling pathways [229] might make mouse models poor predictors of CRS which is a side effect of CAR-T cell therapy that can be life threatening in clinical studies as discussed in section 1.4.4. Furthermore, mouse CAR-T cells are more susceptible to AICD and have poorer persistence compared to human CAR-T cells [230, 231]. The number of mouse tumour cell lines is also limited compared to that of human tumour lines, and some lines are strongly immunogenic resulting in spontaneous regression.

The most common immunocompetent mouse strains used to model cancer are BALB/c and C57BL/6 mouse strains and others derived from them. Whilst both strains are fully immunocompetent, there are important differences in immune responses between them, which need to be considered when evaluating the anti-tumour efficacy and potential toxicity of CAR-T cell therapy. For example, T cells in BALB/c mice at 2 to 3 months of age have a higher percentage of CD4 expression (29.3 ± 1.7 %) compared to that in C57BL/6 mice (13.3 ± 0.6 %) [232]. Furthermore, BALB/c mice have a much higher levels of M2 macrophage and Th2-like T cell responses leading to stronger humoral immunity. Conversely, C57BL/6 mice display M1-dominant macrophage and, therefore, favour Th1-like T cell responses for cell-mediated immunity [233, 234]. A syngeneic model of lymphoma in BALB/c mice showed that anti-CD19 CAR-T cells with CD28 co-stimulatory domain induced chronic toxicity, associated with prolonged expression of Th2 cytokines, whilst such toxicity was not apparent in C57BL/6 mice treated with T cells expressing the same CAR construct [235].

Transplantable tumour models have been commonly used to assess the anti-tumour efficacy of CAR-T cells against solid tumours in mice. Subcutaneous implantation of tumours derived from intraperitoneal organs on the dorsal area of mice is frequently used to model disease progression and intervention, due to the ease of administration and measuring tumour volume. Orthotopic implantation into a given organ can be an alternative option, such as intrapancreatic injection of pancreatic adenocarcinoma, intracranial injection for glioblastoma cell lines [166, 236]. Compared to subcutaneous transplantation, this approach is more physiologically relevant in terms of tumour microenvironment, morphology, angiogenesis and tissue invasion and metastasis, thus being considered as better predictors of clinical response [237]. However, it is technically challenging and difficult for monitoring tumour growth. Transplantable tumour models have the advantages of fast speed and reproducibility of tumour formation. It therefore means that they do not recapitulate the tumour microenvironment and the multistep processes of spontaneous tumour development, which can be in months and years in the human situation [238]. These limitations likely lead to the difference in therapeutic effects between mice and patients.

4.1.2 Hypothesis and aims

The release of IL-12 has shown improved effector function of murine anti-CEA CAR-T cells *in vitro* in section 3.2.5 & 3.2.6, especially second-generation CAR-T cells with CD28 co-stimulatory domains. It is therefore hypothesised that the release of IL-12 can potentially facilitate second-generation anti-CEA CD28-CD3ζ CAR-T cells to mediate tumour

regression or even eradication *in vivo*. To present a more immunologically relevant tumour microenvironment, an immunocompetent mouse model with established subcutaneous CEA^+ tumours will be utilised as a cancer disease model. In this system, the effects of IL-12 secretion on the potency of CAR-T cells targeting CEA will be assessed. Furthermore, host lymphodepletion prior to CAR-T cell treatment has been commonly utilised to enhance CAR-T cell engraftment *in vivo* as mentioned in section 1.3.5. It is hypothesised that host lymphodepletion would be able to further improve anti-tumour efficacy of anti-CEA CAR-T cells secreting IL-12. Therefore, the main aims of this chapter were:

- To establish subcutaneous CEA^+ tumours in an immunocompetent mouse model
- To assess the potential immunogenicity towards CEA by host immune system
- To evaluate the effects of IL-12 on improving anti-tumour efficacy of CEA-specific CD28-CD3ζ CAR-T cells *in vivo*
- To assess whether the combination of host lymphodepletion and IL-12 secretion could facilitate anti-tumour efficacy of CEA-specific CD28-CD3ζ CAR-T cells
- To investigate the safety of CEA-specific CD28-CD3ζ CAR-T cells with or without IL-12 secretion in tumour-bearing mice in the presence or absence of lymphodepletion
- To assess the persistence of CEA-specific CAR-T cells in blood post infusion

4.2 Results

4.2.1 Establishment of syngeneic tumour-bearing mouse model

To assess the anti-tumour responses of CEA-specific CAR-T cells *in vivo*, a subcutaneous CEA-expressing tumour model was established using syngeneic immunocompetent mouse strain. One concern is that the expression of human CEA on the surface of murine cell lines may be immunogenic in immunocompetent mice. Non-transduced tumour cells, therefore, were included to determine if CEA is immunogenic in mice. Briefly, female mice at 6 to 8 weeks of age were injected subcutaneously with tumour cells with or without CEA expression at different cell doses. Growth of subcutaneous tumours was monitored twice a week by calliper measurements and calculated by the formula: $W^2 \times L/2$. Mice were euthanized when tumours ulcerated or reached over 1,000 mm^3 or they displayed 20 % weight loss.

The BALB/c mouse strain was utilised for the establishment of syngeneic subcutaneous CT26 tumour model. As shown in Figure 4.1 A, while CT26 tumours at 2×10^6 cell dose displayed a similar growth rate, most CEA^+ CT26 tumours showed slower growth rate and failed to engraft in some mice. A similar pattern could be observed in mice receiving 1×10^6 cells dose (Figure 4.1 B). As for 5×10^5 cell dose, while CT26 tumours grew to around 1,000 mm^3 in 30 days, CEA^+ CT26 tumours failed to engraft in all mice (Figure 4.1 C). Most importantly, there is a statistically significant difference in survival between mice receiving CT26 cells and those receiving CEA^+ CT26 cells at 3 different cell doses (Figure 4.1 D). Collectively, CEA^+ CT26 tumours were difficult to be established in BALB/c mice and showed variable and slower growth patterns when established, compared to parental CT26 tumours. These results suggested that BALB/c mice are likely generating obvious immune responses towards human CEA. Therefore, the BALB/c mouse strain is not an appropriate choice for the establishment of subcutaneous CEA^+ tumour model for *in vivo* evaluation of anti-CEA CAR-T cells. Even though CEA^+ tumours were established with higher tumour cell dose, endogenous immune responses of the host towards CEA could also possibly contribute to tumour regression during CAR-T cell treatment, which subsequently influences the evaluation of anti-tumour activities of CAR-T cells *in vivo*.

A.

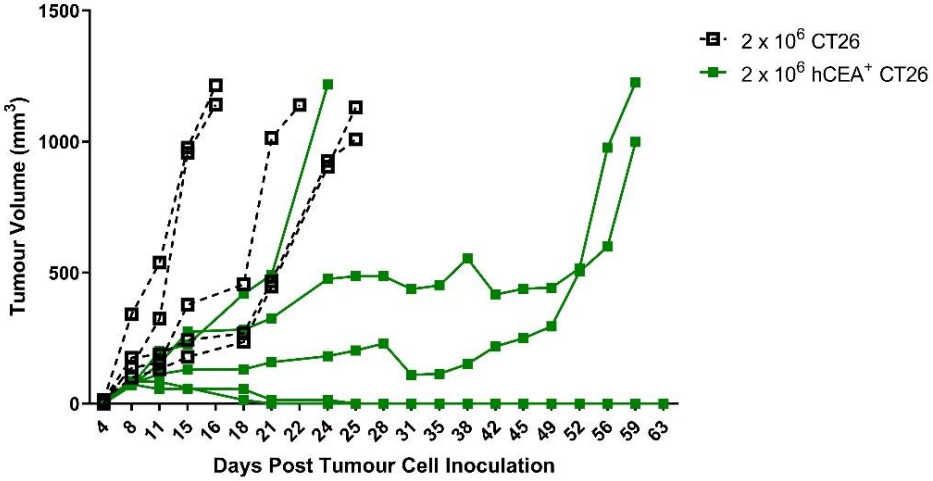
1500
1000
500
0
Tumour Volume (mm3)
4 8 11 15 16 18 21 22 24 25 28 31 35 38 42 45 49 52 56 59 63
Days Post Tumour Cell Inoculation
2 x 10^6 CT26
2 x 10^6 hCEA+ CT26

B.

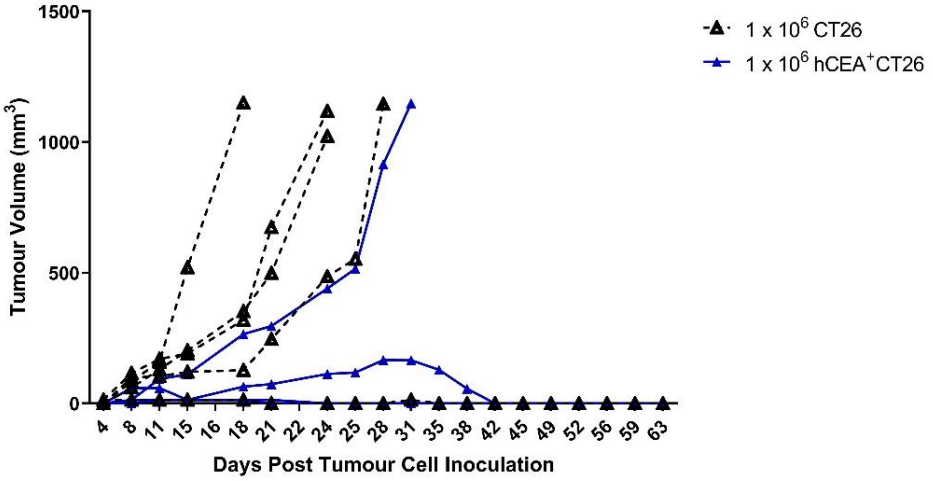
1500
1000
500
0
Tumour Volume (mm3)
4 8 11 15 16 18 21 22 24 25 28 31 35 38 42 45 49 52 56 59 63
Days Post Tumour Cell Inoculation
1 x 10^6 CT26
1 x 10^6 hCEA+CT26

C.

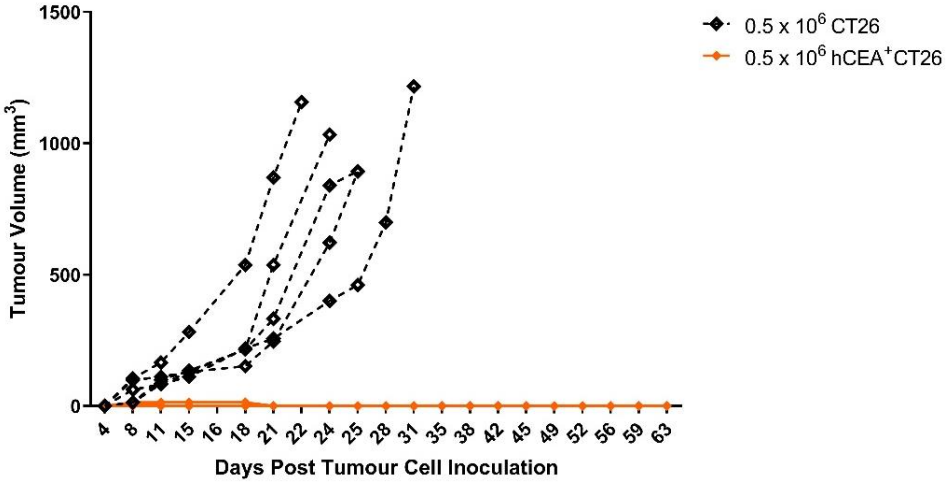
1500
1000
500
0
Tumour Volume (mm3)
4 8 11 15 16 18 21 22 24 25 28 31 35 38 42 45 49 52 56 59 63
Days Post Tumour Cell Inoculation
0.5 x 10^6 CT26
0.5 x 10^6 hCEA+CT26

D.

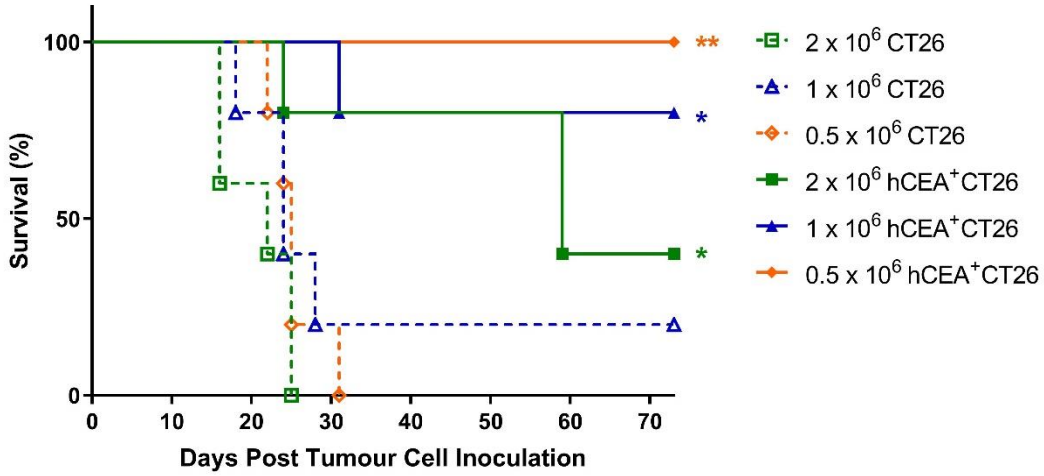

Figure 4.1 Engraftment of CEA$^+$ and CEA$^-$ CT26 tumours in BALB/c mice

The growth curves of subcutaneous CEA$^+$ and CEA$^-$ CT26 tumour model at **(A)** 2 × 10^6, **(B)** 1 × 10^6 or **(C)** 0.5 × 10^6 cell doses respectively. **(D)** Survival of BALB/c mice injected with tumour cells at different doses (n = 5). Statistically significant differences were analysed using log rank (Mantel-Cox) test. ∗ $P < 0.05$; ∗∗ $P < 0.01$.

Alternatively, the C57BL/6 mouse strain was utilised to investigate whether this strain is tolerant to human CEA. Therefore, C57BL/6 mice were subcutaneously inoculated with syngeneic MC38 tumour cells with or without CEA transgene expression. The maximum cell number for injection was increased to 5×10^6, in an attempt to avoid the potential poor tumour engraftment seen in BALB/c mouse strain. Another two cell doses (2×10^6 or 1×10^6 tumour cells per mouse) were given to C57BL/6 mice in line with that in BALB/c mice.

In tumours that were successfully transplanted at 5×10^6 and 2×10^6 cell doses, the growth rate of CEA^+ MC38 tumour was as similar to that of parental MC38 tumour, which indicated that C57BL/6 mice were tolerant to human CEA (Figure 4.2 A and B). In addition, parental MC38 tumour growth was slower in some mice than the CEA^+ MC38 at both cell doses, which seems to be a non-CEA-specific immune response against MC38 tumours during tumour engraftment, as it was not observed in CEA^+ MC38 tumours and is potentially due to the high cell doses used as no delay in tumour growth was seen with 1 x 10^6 cells.

At 1×10^6 cell dose, both CEA^+ MC38 and parental MC38 tumours engrafted well in all mice, although MC38 tumours grew slightly slower compared to CEA^+ MC38 tumours (Figure 4.2 C). Despite that, there is no significant difference in survival rate between CEA^+ MC38 and parental MC38 tumours at this cell dose as well as other two higher cell doses (Figure 4.2 D).

Overall, tumour growth rate was correlated with tumour cell dose injected, as it required 5, 8 and 12 days post injection to reach 100 mm^3 on average from 5×10^6 to 1×10^6 cell doses respectively. Unlike the BALB/c mouse model, good engraftment of CEA^+ MC38 tumour was observed at all cell doses in C57BL/6 mouse model.

A.

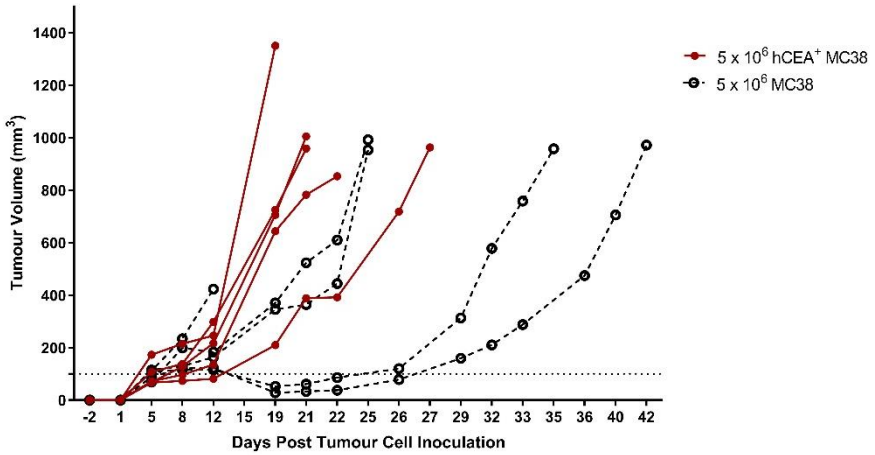
Tumour Volume (mm3)
Days Post Tumour Cell Inoculation
5 x 10^6 hCEA+ MC38
5 x 10^6 MC38

B.

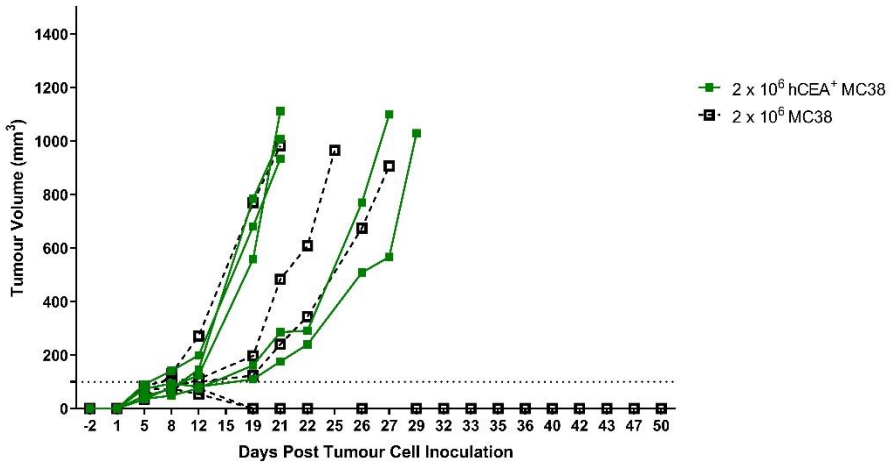
Tumour Volume (mm3)
Days Post Tumour Cell Inoculation
2 x 10^6 hCEA+ MC38
2 x 10^6 MC38

C.

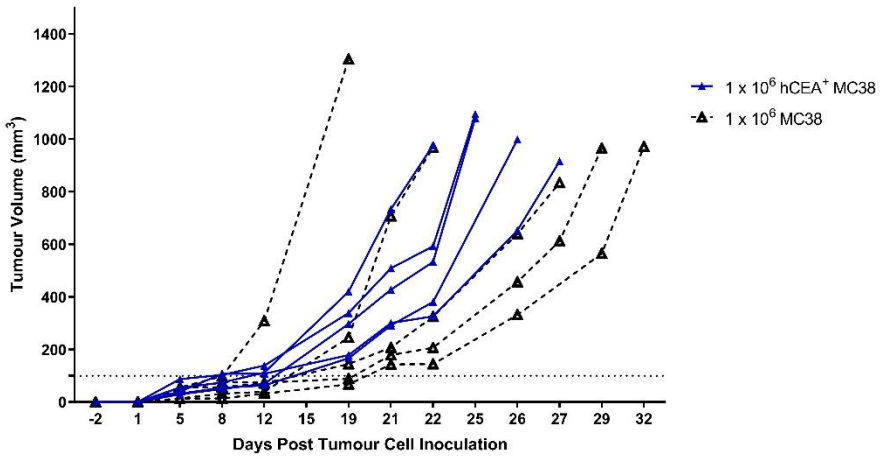
Tumour Volume (mm3)
Days Post Tumour Cell Inoculation
1 x 10^6 hCEA+ MC38
1 x 10^6 MC38

D.

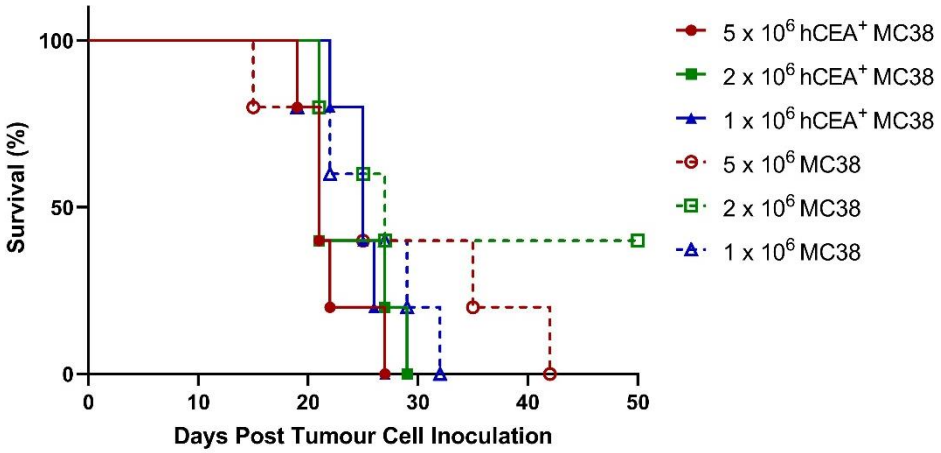

Figure 4.2 Engraftment of CEA$^+$ and CEA$^-$ MC38 tumours in C57BL/6 mice

The growth curves of subcutaneous CEA$^+$ and CEA$^-$ MC38 tumour models at **(A)** 5 × 10^6, **(B)** 2 × 10^6 or **(C)** 1 × 10^6 cell doses respectively. **(D)** Survival of C57BL/6 mice injected with tumour cells with different doses (n = 5). Statistically significant differences were analysed using log rank (Mantel-Cox) test.

To further investigate the level of immune responses towards CEA in mice receiving 1 × 10^6 tumour cells, splenocytes were isolated when mice needed to be culled and were stimulated with irradiated CEA^+ MC38 cells for a 5-day expansion. Activated splenocytes were re-cultured with irradiated CEA^+ MC38 cells at E: T ratio of 1: 1 for 24 hours in the presence of Brefeldin A. Stimulation by PMA/I and splenocytes alone were used as positive and negative controls respectively. The level of IFN-γ expression in splenocytes post co-culture was measured by flow cytometry. As shown in Figure 4.3 A, splenocytes in both MC38 and CEA^+ MC38 models showed high levels of IFN-γ by PMA/I stimulation (74.2 ± 12.4 and 82.6 ± 7.9 % respectively). When stimulated by irradiated CEA^+ MC38 cells, there was only 6.2 ± 1.8 and 6.8 ± 1.0 % of cells producing IFN-γ respectively. Most importantly, no significant difference in IFN-γ production in splenocytes post CEA stimulation was seen between MC38 and CEA^+ MC38 tumour models. These results indicated that there was no significant cellular immunity towards CEA in C57BL/6 mice bearing CEA^+ MC38 tumour. Notably, the use of Brefeldin A for intracellular IFN-γ staining led to a reduction in CEA expression by inhibiting protein transport when co-cultured with CEA^+ MC38 cells for 24-hour (Figure 4.3 B). This potentially suggests that there may be reduced expression of CEA derived antigens on MHC-I and subsequent IFN-γ production from CEA specific T cells. But the difference in CEA-specific responses of activated splenocytes between MC38 and CEA^+ MC38 models was unlikely to be affected.

In addition, CEA expression on tumours was determined by immunohistochemistry. It can be seen that high levels of CEA were detected in CEA^+ MC38 tumour sections, but not negative mouse IgG controls and parental MC38 tumour sections (Figure 4.4). Compared to the poor engraftment of CEA^+ CT26 in BALB/c mice, CEA^+ MC38 tumours could successfully engraft into C57BL/6 mice without causing obvious immunogenicity.

Consequently, the syngeneic C57BL/6 mouse strain was therefore adopted to assess the *in vivo* anti-tumour responses of anti-CEA CAR-T cells. A subcutaneous CEA^+ MC38 tumour model would be established at a dose of 1 × 10^6 cells due to its relatively slow growth rate, which would provide enough time for CAR-T cells to fully exhibit their anti-tumour functions before mouse culling endpoints as it has been previously shown that tumours can continue to increase in size for up to 7 days before regression after CAR-T cell transfer [239]. CAR-T cell injection would be applied within 7 – 12 days post tumour cell inoculation when the average tumour size reached over 50 mm^3 but below 150 mm^3.

A.

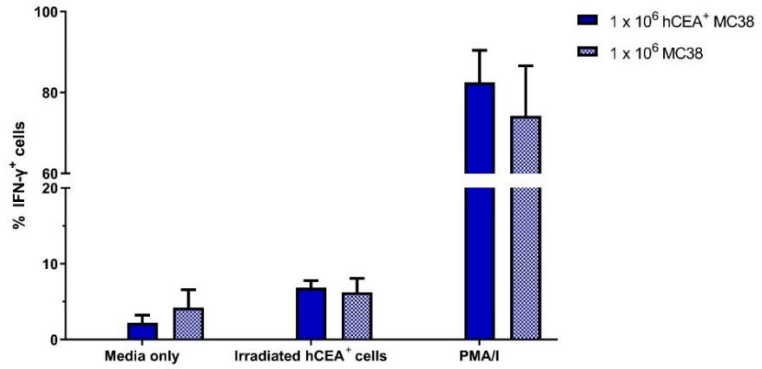

B.

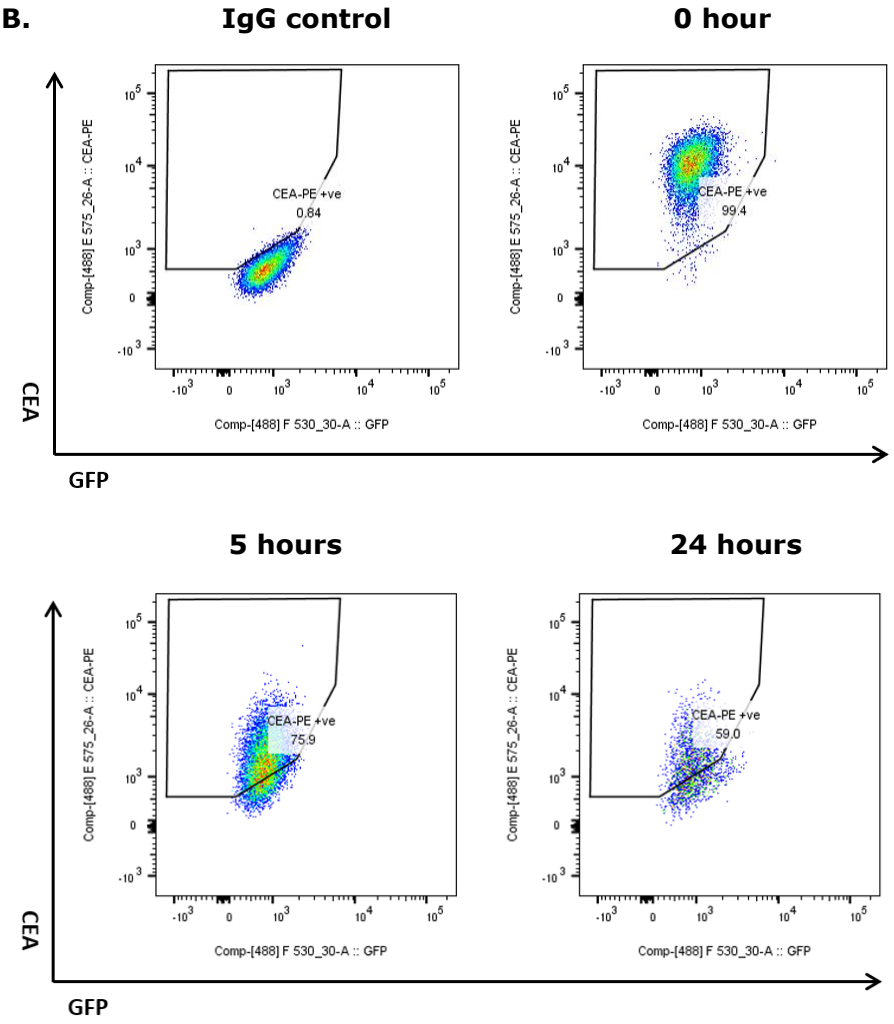

Figure 4.3 IFN-γ expression of splenocytes co-cultured with irradiated CEA$^+$ MC38 cells

(A) The percentage of IFN-γ$^+$ splenocytes is plotted as mean ± SD of four or five mice each group determined by flow cytometry. Statistically significant differences were analysed using two-way ANOVA with Tukey's multiple comparisons test. **(B)** Representative dot plots are shown for CEA expression of CEA$^+$ MC38 cell line cultured with Brefeldin A for 0, 5 and 24 hours respectively.

A. **mouse IgG control** **B.** **CEA$^+$ MC38**

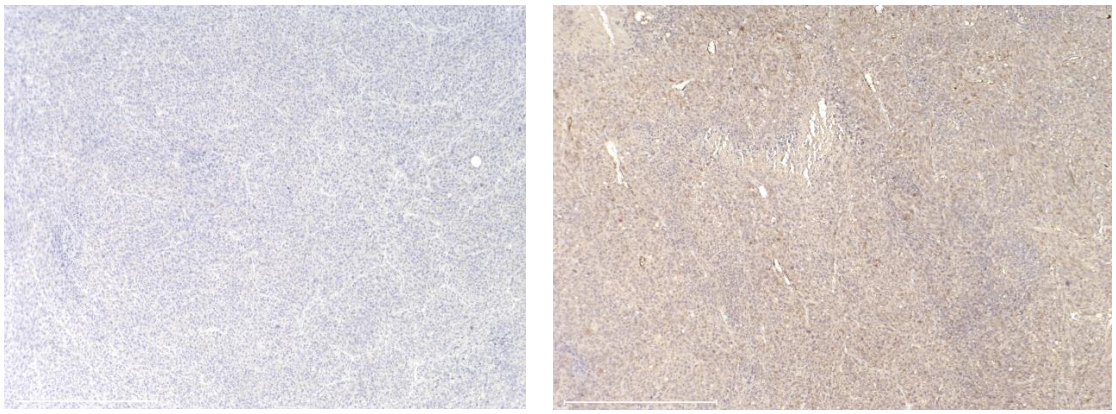

C. **MC38**

Figure 4.4 CEA expression on CEA$^+$ and parental tumour sections by light microscopy

(A) Representative image of CEA$^+$ MC38 section stained with mouse IgG isotype control antibody. **(B) and (C)** Representative images of CEA$^+$ MC38 and MC38 tumour sections with CEA antibody staining respectively. Magnification = 10X; Scale bar represents 500 µm.

4.2.2 Anti-tumour Efficacy of anti-CEA CAR-T cells secreting IL-12 *in vivo*

It was previously found that the introduction of murine CD28 co-stimulatory domain in combination with constitutive murine IL-12 expression could endow anti-CEA CAR-T cells with improved effector cell functions *in vitro* (section 3.2.5 & 3.2.6). To further assess their anti-tumour efficacy *in vivo*, CD28z CAR-T cells with or without constitutive IL-12 co-expression were adoptively transferred into immunocompetent C57BL/6 mice bearing subcutaneous CEA^+ MC38 tumour.

A preliminary experiment using a dose of 7 x 10^6 total T cells was tested, which contains 1 x 10^6 mock and CD28z T cells respectively (Figure 4.5 A). However, only 0.5 x 10^6 MFE.mCD28z.mIL12 T cells were infused into each mouse, as insufficient number was obtained. Tumour-bearing mice were treated with CAR-T cells at indicated cell doses on day 7 when tumour size reached between 50 and 100 mm^3 on average. Tumour volume was measured every 3-4 days. As shown in Figure 4.5 B, 1 x 10^6 mock and CD28z CAR-T cells did not have an efficacious impact on tumour growth. Interestingly, even at a lower cell dose of 0.5 x 10^6 CD28z.mIL12 CAR-T cells mediated a slightly delay on tumour growth for 2 weeks and complete regression of tumour in one mouse. Mice treated with CD28z.mIL12 CAR-T cells showed a significant prolonged survival compared to mice receiving mock T cells or CD28z CAR-T cells ($P = 0.0231$ & $P = 0.0439$ respectively) (Figure 4.5 C). Furthermore, no obvious toxicity was observed in mice treated with CD28z T cells or CD28z.mIL12 T cells.

Overall, these results indicated that the secretion of IL-12 was able to enhance the anti-tumour responses of CD28z CAR-T cells against CEA^+ MC38 tumour *in vivo*. For subsequent experiments, the dose of IL-12-secreting T cells was increased to determine whether better anti-tumour efficacy could be achieved and to test for IL-12-related toxicity which is seen in systemic IL-12 therapy [192].

A.

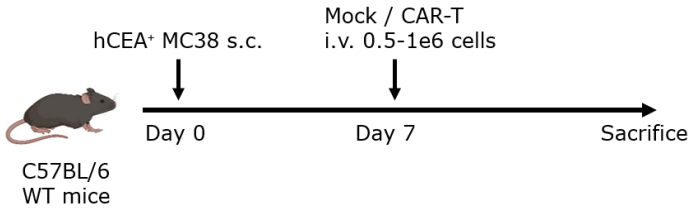

B.

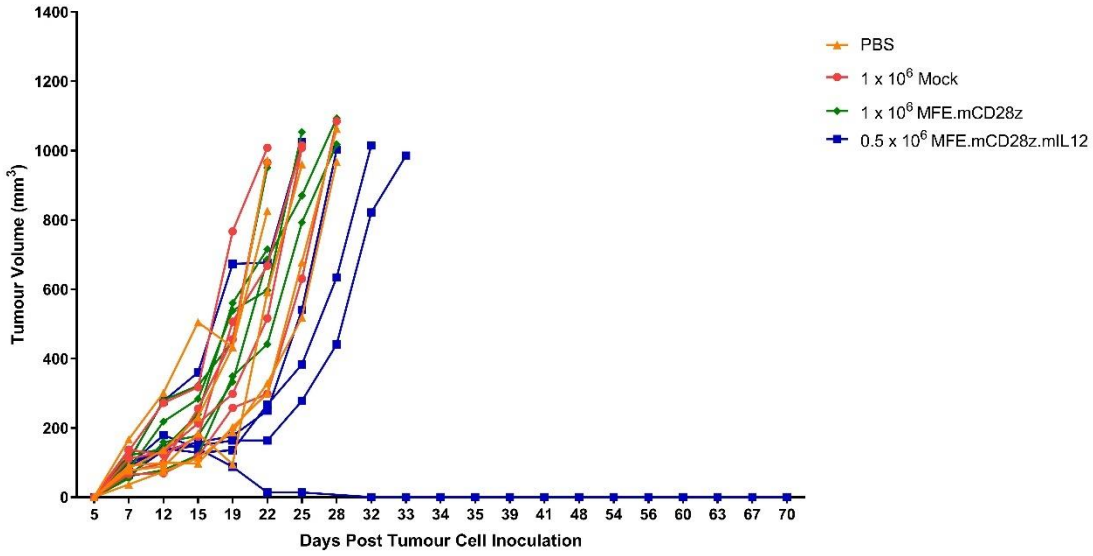

C.

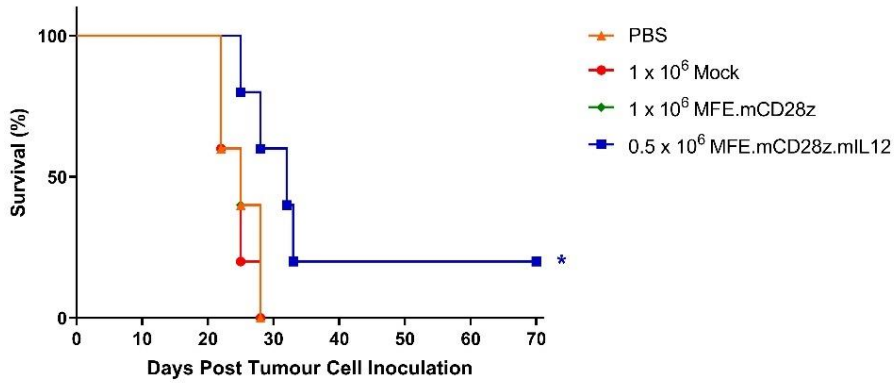

Figure 4.5 Evaluation of anti-tumour responses of CEA-specific CAR-T cells

(A) Schematic diagram of the experimental procedure applying CAR-T cell treatment *in vivo*. Tumour-bearing C57BL/6 WT mice were treated with PBS, mock, MFE.mCD28z and MFE.mCD28z.mIL12 CAR-T cells respectively at indicated cell doses on day 7 when tumour size reached between 50 and 100 mm^3 on average (n=5). **(B)** Tumour volume of C57BL/6 mice post cell transfer in each group. **(C)** Survival of C57BL/6 mice post cell transfer. Statistically significant differences were analysed using log rank (Mantel-Cox) test. $* P < 0.05$.

4.2.3 Effect of Lymphodepletion for anti-CEA CAR-T cell treatment

Host lymphodepletion pre-conditioning has been widely used prior to adoptive transfer of CAR-T cells. It aims to augment therapeutic efficacy of CAR-T cell therapy by promoting CAR-T cell engraftment and expansion, as described in section 1.4.5. Therefore, the use of lymphodepletion pre-conditioning by 5Gy TBI has been performed to assess whether it could enhance anti-tumour efficacy of anti-CEA CAR-T cells with or without IL-12 secretion.

A schematic diagram of the experimental procedure giving CAR-T cell treatment with 5Gy TBI was shown in Figure 4.6 A. Mice bearing 50 – 100 mm^3 tumours were treated with 5Gy TBI 2 days before i.v. administration of 2 x 10^6 CAR-T cells within 2.5 x 10^7 total T cells. To determine the efficiency of lymphodepletion by 5Gy TBI, peripheral blood samples were collected via tail vein bleeds on day 7, 16 and 22, and blood cell counts were performed. In addition, to monitor the release of cytokines and the persistence of CAR-T cells in blood post treatment, serum was isolated and genomic DNA was extracted from blood samples collected via tail vein bleeds listed above and cardiac puncture at terminal day. Mice were euthanized when tumours ulcerated or reached over 1,000 mm^3 or they displayed 20 % severe body weight loss (BWL), emaciation or pale extremities. Spleens were collected and used to assess the functional activity of immune cells *in vitro*.

As shown in Figure 4.6 B, levels of both white blood cells and lymphocytes in mice treated with TBI decreased significantly and not recovered to normal levels for 9 days. However, lethal toxicities, which were mainly reflected by severe BWL, emaciation and pale extremities, occurred in pre-conditioned mice receiving CAR-T cells shown in Table 4.1. While all the pre-conditioned mice treated with CD28z.mIL12 CAR-T cells had to be culled due to severe BWL, there were only 25 % and 33 % of mice experiencing BWL post administration of mock and CD28z CAR-T cells plus 5Gy TBI respectively. No severe BWL was observed in mice treated with CD28z.mIL12 CAR-T cells only. There was a significant survival advantage for mice receiving CD28z T cells with 5Gy TBI or CD28z.mIL12 T cells only relative to that receiving CD28z.mIL12 T cells with 5Gy TBI ($P = 0.0295$) (Figure 4.6 C). Interestingly, mice receiving 5Gy TBI plus CD28z.mIL12 CAR-T cells had begun to undergo regression at the tumour site at the time they had to be culled due to severe BWL, suggesting that the T-cells were mediating anti-tumour efficacy (Figure 4.6 D). Based on these results, it was hypothesised that CD28z.mIL12 CAR-T cells were likely to proliferate and eradicate tumours post host lymphodepletion, but high levels of IL-12 secreted by expanded T cells resulted in lethal toxicities. In addition, transfer of non-targeted mock T cells also appeared to mediate tumour regression in some mice treated with 5Gy TBI.

In this study, although numbers were small, administration of 2 x 10^6 CD28z.mIL12 CAR-T cells alone led to a reduction in tumour burden even after tumours reached 600 mm^3 (Figure 4.6 D). While one mouse failed to eradicate tumour completely, the other two remained tumour-free until the experiment ended. Notably, tumour burden was decreased in some pre-conditioned mice treated with mock T cells as well, although tumours relapsed eventually. As large numbers of total T cells were adoptively transferred into mice, the level of non-transduced T cell killing on CEA^+ MC38 tumour might be more obvious and was probably enhanced by host lymphodepletion.

A.

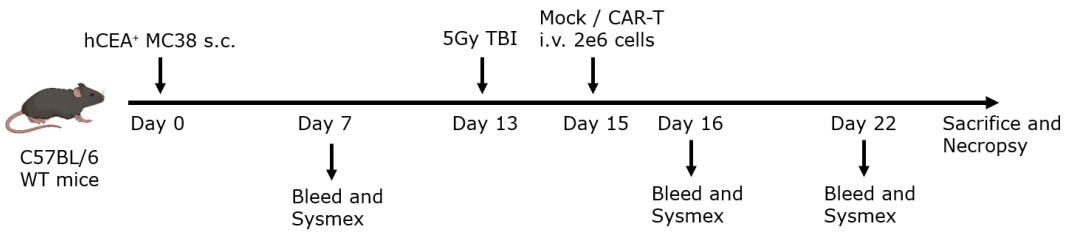
hCEA+ MC38 s.c.
5Gy TBI
Mock / CAR-T
i.v. 2e6 cells
C57BL/6
WT mice
Day 0
Day 7
Day 13
Day 15
Day 16
Day 22
Sacrifice and
Necropsy
Bleed and
Sysmex
Bleed and
Sysmex
Bleed and
Sysmex

B.

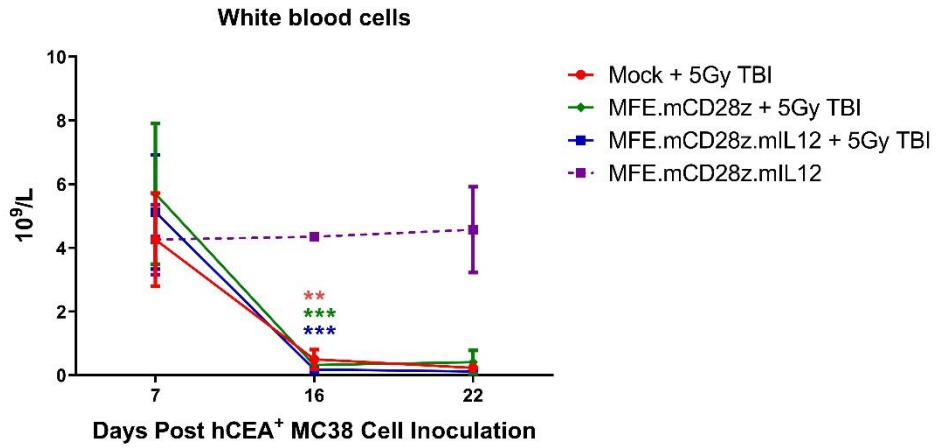
White blood cells
10⁹/L
Days Post hCEA+ MC38 Cell Inoculation
Mock + 5Gy TBI
MFE.mCD28z + 5Gy TBI
MFE.mCD28z.mIL12 + 5Gy TBI
MFE.mCD28z.mIL12

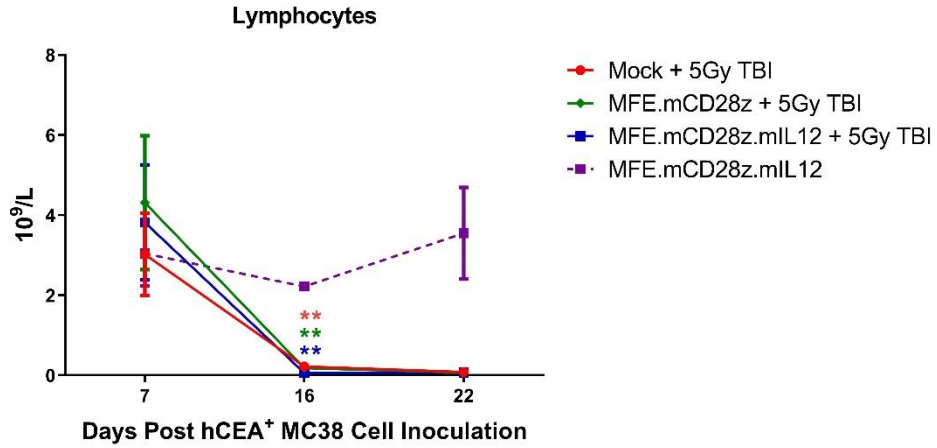
Lymphocytes
10⁹/L
Days Post hCEA+ MC38 Cell Inoculation
Mock + 5Gy TBI
MFE.mCD28z + 5Gy TBI
MFE.mCD28z.mIL12 + 5Gy TBI
MFE.mCD28z.mIL12

C.

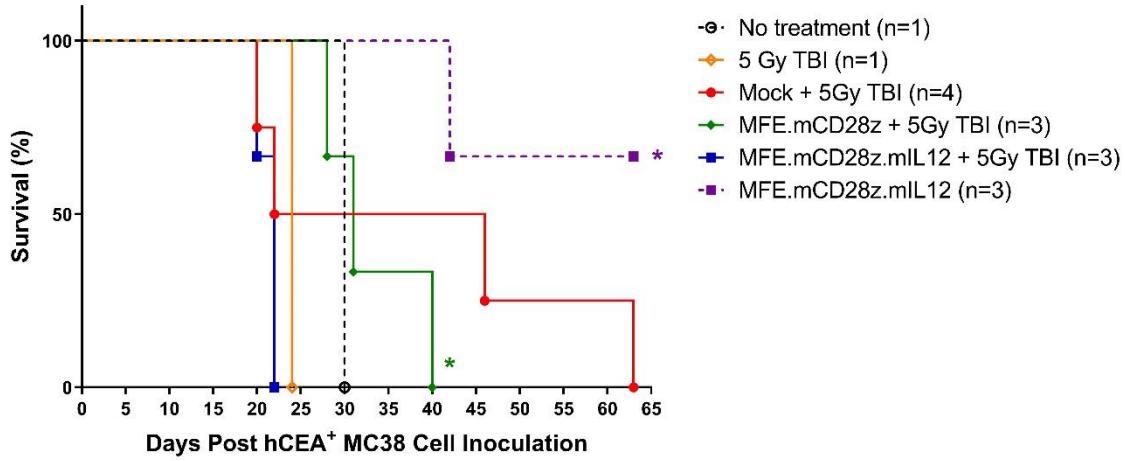
Survival (%)
Days Post hCEA+ MC38 Cell Inoculation
No treatment (n=1)
5 Gy TBI (n=1)
Mock + 5Gy TBI (n=4)
MFE.mCD28z + 5Gy TBI (n=3)
MFE.mCD28z.mIL12 + 5Gy TBI (n=3)
MFE.mCD28z.mIL12 (n=3)

D.

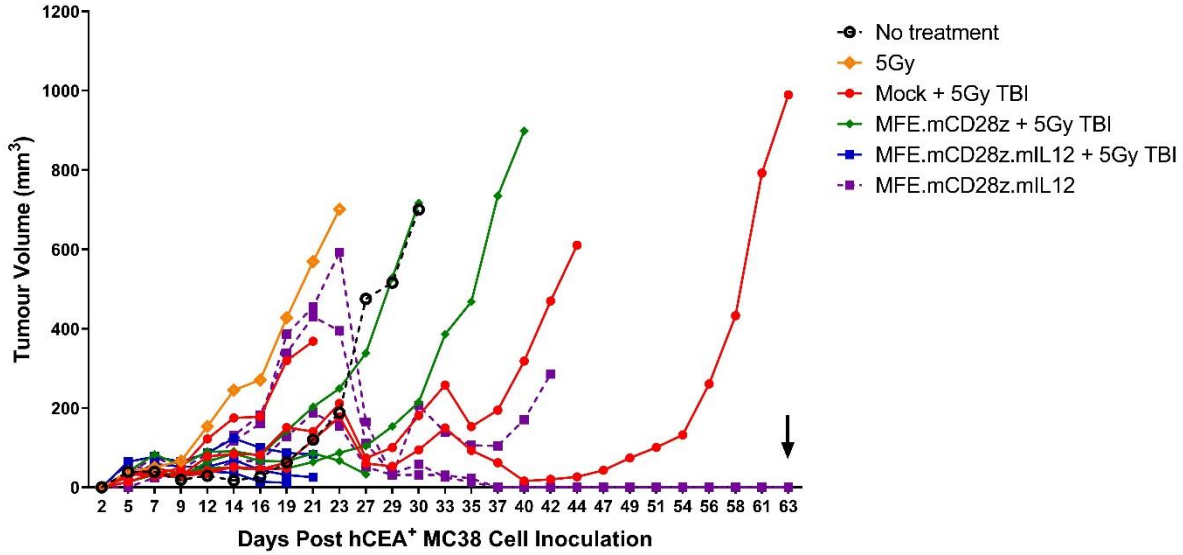

Figure 4.6 Evaluation of anti-tumour responses of CEA-specific CAR-T cells post host lymphodepletion

(A) Schematic diagram of the experimental procedure applying CAR-T cell treatment with or without 5Gy TBI *in vivo*. Tumour-bearing C57BL/6 WT mice were treated with 5Gy TBI 2 days before i.v. administration of 2 x 10^6 mock T cells or CAR-T cells within 2.5 x 10^7 total T cells (n = 3 - 4). Peripheral blood samples were collected via tail vein bleeds on day 7, 16 and 22 for analysis. **(B)** The amount of white blood cells and lymphocytes of individual mice before and after 5Gy TBI. **(C)** Survival of individual mice post cell transfer treatment. Statistically significant differences were analysed using log rank (Mantel-Cox) test. $* P < 0.05$. **(D)** Tumour volume of individual mice in each treatment.

Table 4.1 Details of the cause of death for CEAtg mice receiving CAR-T cells

Group	Reasons for culling		Tumour-free (%)	% culled due to body weight loss
	Severe body weight loss; Emaciation; pale extremities	Tumour condition (over 1,000 mm^3, ulceration, holed or bleeding)		
No treatment (n=1)	0	1	0	0
5Gy TBI (n=1)	0	1	0	0
Mock T cells + 5Gy TBI (n=4)	1	3	0	25
CD28z T cells + 5Gy TBI (n=3)	1	2	0	33
CD28z.mIL12 T cells + 5Gy TBI (n=3)	3	0	0	100
CD28z.mIL12 T cells (n=3)	0	1	66	0

To further confirm whether lethal toxicity was caused by high levels of secreted IL-12, serum samples were measured for IL-12 production by ELISA. It can be seen that similar amounts of IL-12 were detected from blood in pre-conditioned and parental mice receiving CD28z.mIL12 CAR-T cells on day 16 24-hour post T cell transfer (488.8 ± 95.5 and 491.0 ± 145.2 pg/ml respectively), which were higher than levels in TBI treated mice receiving mock or CD28z T cells (48.8 ± 3.0 and 59.5 ± 20.7 pg/ml respectively) (Figure 4.7). However, a significant increase in serum IL-12 levels (3,870.2 ± 1,309.6 pg/ml) was observed in pre-conditioned mice receiving CD28z.mIL12 CAR-T cells on day 7 post T cell treatment which was the time point when the mice had to be culled because of BWL. In contrast, IL-12 production reduced to 319.8 ± 178.8 pg/ml at day 7 post transfer in mice receiving CD28z.mIL12 without TBI and levels gradually decreased to background levels by the time of cull from day 42 to 63. These data strongly suggest that constitutive expression of IL-12 by 2 x 10^6 CAR-T cells can cause lethal toxicity when combined with host lymphodepletion by TBI. One strategy to avoid this issue might be to lowering the number of CAR-T cells transferred when given with host lymphodepletion.

A.

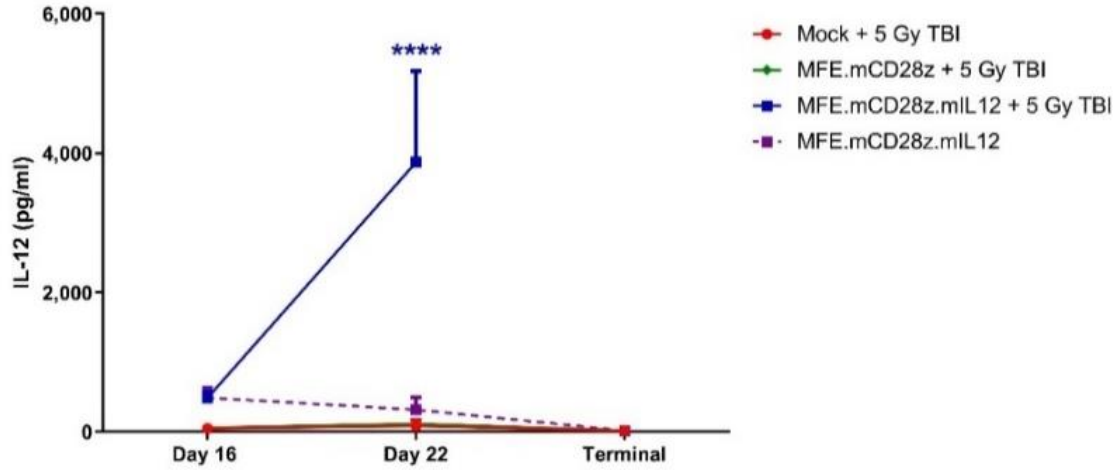

Figure 4.7 IL-12 secretion by CAR-T cells in peripheral blood

The level of IL-12 post CAR-T cell administration in blood samples was measured by ELISA. The data are plotted as mean ± SD of blood samples that could be successfully collected (n = 2 - 4). Statistically significant differences between day 16 and day 22 were analysed using two-way ANOVA with Sidak's multiple comparisons test. **** $P < 0.0001$.

To monitor the engraftment of CAR-T cells at day 1 post injection, genomic DNA was extracted from blood samples and then tested for mCherry marker gene by probe-specific qPCR. Using MFE.mCD3z DNA plasmid as a template, a standard curve ranging from 1 x 10^{-8} to 1 µg (R^2 = 0.993) with a sensitivity of 1500 genomes/well was generated by linear regression analysis, showing the successful binding of mCherry-specific primers and probe (Figure 4.8 A). Transduced T cells which had 30 % CD3z CAR expression and mock T cells were lysed to extract CAR gene as positive and negative control respectively. It was seen that 1 - 100 ng of genomic DNA extracted from CD3z CAR-T cells could be detected and 10 and 100 ng of DNA were within the range of standard curve. Although 1 ng of genomic DNA was beyond the range of detection, which equated to 1.5 x 10^{-9} µg based on the regression equation Y = -3.018X + 7.784, it indicated that the sensitivity of this assay could be as low as 225.35 genomes/well.

As shown in Figure 4.8 B, DNA samples extracted from blood were below the limit of quantification, which was 1 x 10^{-8} µg, indicating that no mCherry marker gene could be detected via this method. As such, the subsequent detection of DNA samples collected on the other days was not performed. The fact no mCherry transcripts were detected was possibly due to the low percentage (8 %) of CAR-T cells in total T cells transferred into blood. It might also be affected by DNA extraction efficiency. To confirm this, a known number of transduced cells could be spiked into blood samples to determine whether DNA extraction was efficient. Additionally, instead of extracting genomic DNA, messenger RNA (mRNA) could be extracted and converted to complementary DNA (cDNA) via reverse-transcription for transgene quantification by qPCR. Because of higher amounts of mRNA compared to genomic DNA, this technique is more likely to allow amplification of the mCherry gene to reach the detection threshold within 35 cycles.

A.

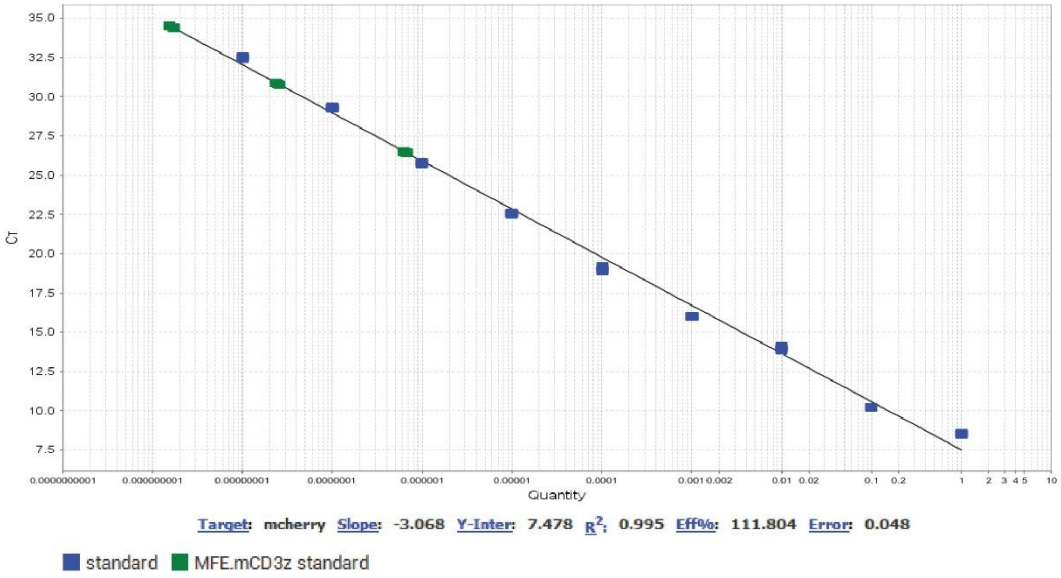

B.

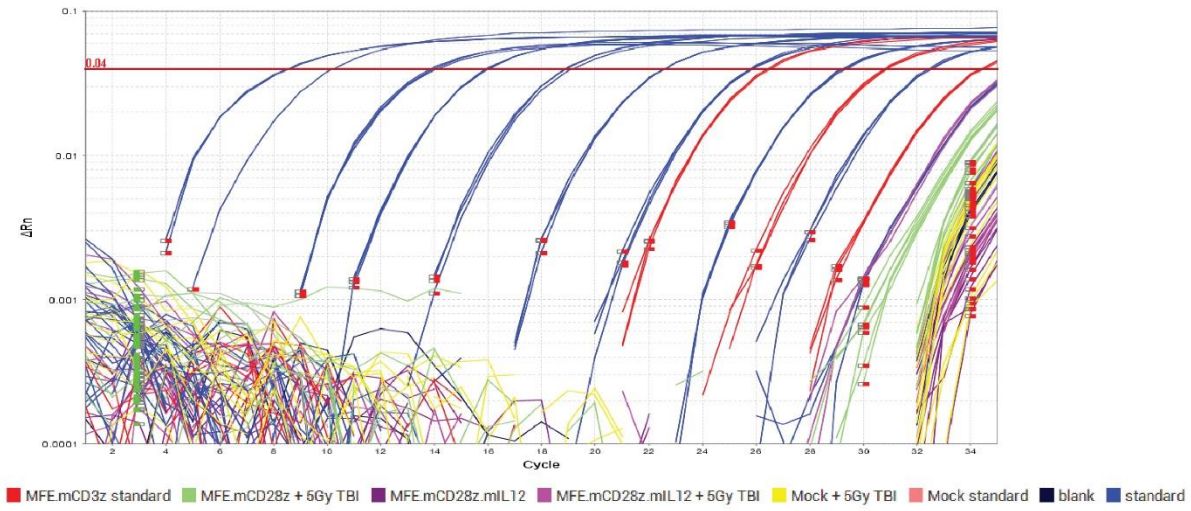

Figure 4.8 CAR-T cell persistence in peripheral blood measured by qPCR

The persistence of CAR-T cells post administration was determined by the fluorescence intensity of mCherry-specific gene in genomic DNA using probe-based qPCR. **(A)** A standard curve using linear regression was generated from serial dilutions of the MFE.CD3z plasmid (Y = -3.068X + 7.478, R^2 =0.995). **(B)** Amplication plot of DNA standards at 10-fold serial dilutions from 1 x 10^{-8} to 1 µg, DNA samples extracted from CD3z CAR-T cells and DNA samples extracted from peripheral blood in mice treated with T cell therapy is shown. Each diluted standard or sample was measured in triplicates. Two wells of 0.1 µg standard were omitted due to poor pipetting.

The *in vitro* functional activity of splenocytes from mice receiving T cell therapy was determined by IFN-γ production in response to CEA-expressing tumour cells. To achieve this, splenocytes were isolated when mice needed to be culled and subsequently stimulated with irradiated CEA^+ MC38 cells with the supplement of hIL-2 and mIL-7 for a 5-day CEA-specific expansion. Activated splenocytes were co-cultured with irradiated CEA^+ MC38 cells at E: T ratio of 1: 1 for 20 hours. The supernatant was measured for IFN-γ release by ELISA. Notably, due to host lymphodepletion, the number of splenocytes from pre-conditioned mice culled at early time points were not sufficient for expansion and co-culture, especially in the CD28z.mIL12 T cell therapy group. Splenocytes from these mice were thus cultured at a lower E: T ratio. In an attempt to compare the level of IFN-γ secretion among groups, cell number was normalised to 5×10^5 during statistical analysis.

Splenocytes from pre-conditioned mice receiving CD28z CAR-T cells showed significantly higher levels of IFN-γ secretion (6,900.8 ± 2,280.8 pg/ml) when co-cultured with irradiated CEA^+ MC38 cells, compared to splenocytes from pre-conditioned mice receiving mock T cells (1,457.1 ± 908.5 pg/ml) ($P < 0.001$) (Figure 4.9). This suggests that the administration of CAR-T cells contributed to the induction of CEA-specific immune responses, although CD28z CAR-T cells did not show any anti-tumour efficacy *in vivo*. High levels of IFN-γ were also produced in splenocytes from the CD28z.mIL12 CAR-T cell therapy group after cell number normalisation (6,146.9 ± 1,455.6 pg/ml), which was similar to levels produced in the CD28z CAR-T cell therapy group. It is of note that, due to insufficient cell number, splenocytes from the CD28z.mIL12 CAR-T cell therapy group was co-cultured with irradiated CEA^+ MC38 cells at lower E: T ratios, which was likely to affect the level of IFN-γ production. It is therefore difficult to conclude whether the production of IL-12 from CAR-T cells *in vivo* can improve immune responses against CEA^+ target cells, which might be through epitope spreading [156]. Furthermore, as the level of CAR-T cells present within the spleen was not measured, it remains unknown whether CEA-specific immune responses were mediated by the host immune system and/or CAR-T cells.

Without host lymphodepletion, splenocytes of mice treated with CD28z.mIL12 CAR-T cells alone released IFN-γ (1,222.4 ± 683.6 pg/ml) at levels similar to that produced by mice receiving mock T cells plus 5Gy TBI (1,457.1 ± 908.5 pg/ml), which was in contrast to the strong anti-tumour efficacy *in vivo*. To further confirm whether CD28z.mIL12 CAR-T cells alone could induce or even improve CEA-specific immune responses in mice, it requires the adoptive transfer of mock T cells and CD28z CAR-T cells into non-pre-conditioned mice as controls.

The main limitation of this assay is that the time of individual mouse survival and subsequent splenocyte isolation was different among T cell therapy groups. This situation is likely to influence the comparison in IFN-γ production among those groups. Better comparisons between the treatment groups could be made if splenocytes were isolated for assays on a certain day before tumour or treatment-related toxicity, such as one week after T cell infusion. In addition, to further confirm whether the functional activity of splenocytes was CEA-specific *in vitro*, co-culture with irradiated non-CEA-expressing MC38 cells should be included for comparison.

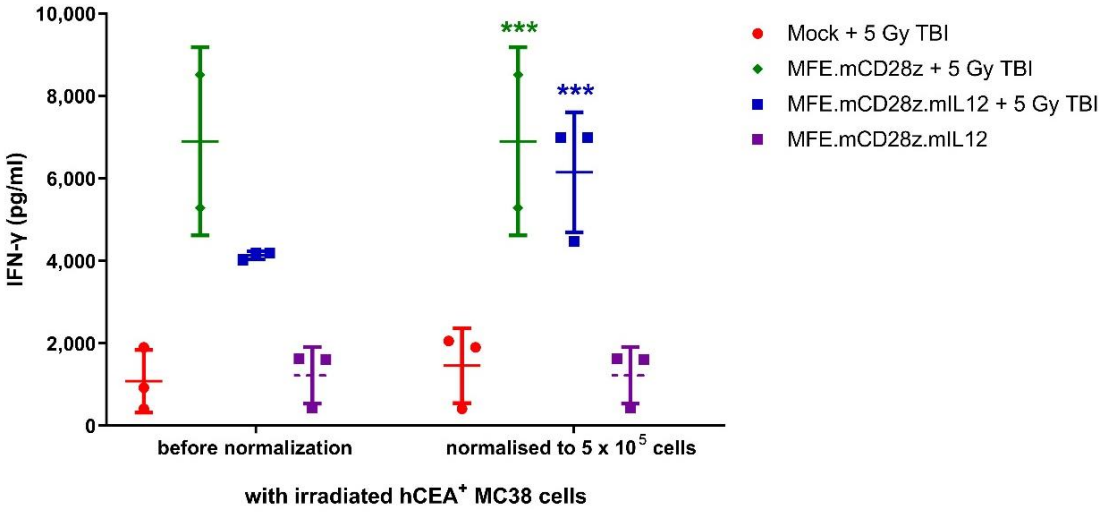

Figure 4.9 IFN-γ secretion by splenocytes in response to irradiated CEA$^+$ MC38 cells

Splenocytes were stimulated with irradiated CEA$^+$ MC38 cells with the supplement of hIL-2 and mIL-7 for 5-day CEA-specific expansion. Activated splenocytes were re-cultured with 5 × 10^5 irradiated CEA$^+$ MC38 cells at E: T ratio of 1: 1 for 20 hours. The supernatant collected post incubation was measured for IFN-γ production by ELISA. In some cases, splenocytes were cultured at lower E: T ratios due to insufficient number. To compare the level of IFN-γ production among therapy groups, cell number was normalised to 5 x 10^5 during statistical analysis. The data are plotted as mean ± SD of samples that could be collected in each group (n = 2 - 4). Statistically significant differences were analysed using two-way ANOVA with Tukey's multiple comparisons test. *** $P < 0.001$.

4.3 Discussion

The main aims of this chapter were to establish a murine subcutaneous tumour model and assess anti-tumour efficacy of anti-CEA CAR-T cells *in vivo*. As mouse MC38 and CT26 cell lines were modified to express CEA, it was necessary to determine whether CEA would be immunogenic in syngeneic immunocompetent mice. Whilst CEA^+ MC38 tumour progressively grew similar to the parental MC38 tumour, poor engraftment was found with CEA^+ CT26 tumours (Figure 4.1 & 4.2). This suggests that the immunogenicity of CEA was sufficient to trigger immune responses which led to tumour cell rejection in immunocompetent BALB/c mice, which is likely to be CEA-dependent. It has been reported that murine mammary adenocarcinoma 410.4 cells expressing human MUC-1 had poor engraftment compared to MUC-1-negative cells [240], while there is no obvious immunogenicity caused by CT26 cells expressing human HER2/neu in BALB/c mice [241].

Immunocompetent C57BL/6 mice bearing subcutaneous MC38 tumours expressing human CEA were utilised as an *in vivo* cancer model in which to test fourth-generation CAR-T cell therapy. Anti-tumour efficacy of CEA-specific CAR-T cells was evaluated using immunocompetent mice bearing subcutaneous 50 – 100 mm^3 tumours. In a preliminary experiment, a single dose of 5 x 10^5 CD28z.mIL12 CAR-T cells showed encouraging therapeutic activity, demonstrated as slower tumour growth or even tumour elimination, compared to non-IL-12-secreting CAR-T cells (Figure 4.5 B). This therefore provided a rationale that the release of IL-12 has the potential for improving anti-tumour efficacy of anti-CEA CAR-T cells in the model of subcutaneous CEA-expressing MC38 tumour.

Higher numbers of IL-12-secreting CAR-T cells were therefore administrated to try to achieve better anti-tumour control. It was found that 2 x 10^6 CD28z.mIL12 CAR-T cells alone could completely eradicate tumours which had grown to 200 – 400 mm^3 in size. As the reduced tumour growth was observed in one pre-conditioned mouse receiving mock T cells, it remains a concern that non-CAR-mediated T cell killing may be partially involved in CD28z.mIL12 T cell therapy due to large numbers of total T cells injected (2.5 x 10^7 cells) (Figure 4.6 D). To explore this, mock T cell therapy and MFE.mCD28z CAR-T cell therapy alone should be included as controls, as was done in Figure 4.5.

Previous studies have also reported improved anti-tumour efficacy of CAR-T cells constitutively secreting IL-12 without the need for pre-conditioning in immunocompetent mouse model, such as anti-CD19 CAR-T cells in the model of established systemic B cell lymphoma and local administration of anti-$MUC16^{ecto}$ CAR-T cells in the model of ovarian peritoneal carcinomatosis [156, 210]. In contrast to these studies, here anti-CEA IL-12-secreting CAR-T cells were given via i.v injection in a subcutaneous CEA^+ tumour model.

This model was more challenging as CAR-T cell trafficking and infiltration into tumour sites is an obstruction to achieving CAR-T cell efficacy. The results found in this study suggested that anti-CEA CD28-CD3ζ CAR-T cells constitutively secreting IL-12 could potentially overcome these obstacles and exhibit therapeutic effects against transplanted solid tumours without the need for pre-conditioning. Furthermore, no obvious toxicity was related to constitutive IL-12 expression by CAR-T cells, which was also consistent with other CAR-T cell studies without performing lymphodepletion pre-conditioning [156, 198, 210]. Taken together, these results suggested that genetic modification of CAR-T cells to constitutively secrete IL-12 could be a promising strategy to improve anti-tumour efficacy of CAR-T cell therapy without causing IL-12-related toxicity seen in systemic IL-12 therapy. Furthermore, this strategy overcomes the need for lymphodepletion pre-conditioning, which therefore allows for the application of CAR-T cell therapy to cancer patients intolerant to currently requisite toxic conditioning regimens.

Due to time limitations, the experiment was ended when the last tumour-bearing mouse was culled whilst two of three mice receiving CD28z.mIL12 T cells were still tumour-free. Therefore, long-term survival of these two tumour-free mice was not obtained. Otherwise it would be of interest to assess whether tumour would relapse in those tumour-free mice. Splenocytes could also be collected and adoptively transferred into mice bearing CEA^+ MC38 tumour to evaluate their anti-tumour potency.

In this study, lymphodepletion pre-conditioning was also given to investigate whether it could enhance anti-tumour efficacy of CAR-T cell treatment by improving the engraftment of CAR-T cells. However, there was still no significant therapeutic effects of non-IL-12-secreting CD28z CAR-T cells on tumours (Figure 4.6 D). As for CD28z.mIL12 CAR-T cells, despite a reduction in tumour burden in TBI treated mice, lethal IL-12 toxicity was observed, most likely due to high levels of IL-12 secreted in blood post 5Gy TBI (Figure 4.7). It is therefore suggested that IL-12-secreting CD28z CAR-T cells rapidly expanded in lymphodepleted hosts [156], although no mCherry marker gene could be detected in genomic DNA by qPCR (Figure 4.8 B). Similarly, the lethal toxicity caused by IL-12 has been reported in other studies which explored constitutive IL-12 secretion in combination with lymphodepletion pre-conditioning for CAR-T cell therapy [194, 208].

Despite that, these studies also showed that an appropriate dose of engineered T cells secreting IL-12 could mediate dramatic tumour regression when host lymphodepletion was given. These findings indicated that the use of tumour-specific IL-12-secreting T cells and TBI pre-conditioning has the potential for being a powerful combination therapy against tumour if IL-12-related toxicity could be mitigated. In an attempt to reduce the toxicity

associated with CD28z CAR-T cells constitutively secreting IL-12 without compromising their anti-tumour efficacy in the lymphodepleted hosts, restricting IL-12 expression and accumulation in tumour sites using an inducible expression system driven by CAR-specific T cell activation might be a suitable approach and is explored in the next chapter.

One of the limitations in this study is that the potential on-target off-tumour toxicity of anti-CEA CAR-T cell therapy could not be assessed, due to the lack of human CEA expressed on normal tissues in mice. In addition, more experimental data is required to support the findings mentioned above, especially the anti-tumour functions of IL-12-secreting CAR-T cells in the absence of host lymphodepletion as mouse numbers were limited.

In summary, the results outlined in this chapter indicated that a subcutaneous CEA^+ MC38 tumour model could be established in syngeneic immunocompetent C57BL/6 mouse strain, without endogenous immune responses against CEA. Conventional CD28z CAR-T cells failed to show any anti-tumour responses. But administration of CD28z.IL12 CAR-T cells alone demonstrated promising anti-tumour efficacy, suggesting the potent effects of IL-12 on anti-CEA CAR-T cell therapy. However, in combination with lymphodepletion pre-conditioning, severe toxicity was seen in CD28z.IL12 CAR-T cell therapy, probably because of high levels of IL-12 secreted. Experimental optimisations including dosing for anti-CEA CAR-T cells secreting IL-12 should be developed to achieve tumour eradication and avoid IL-12-related toxicity.

5 Construction and characterisation of anti-CEA CAR-T cells secreting inducible IL-12

5.1 Introduction

Inducible gene expression systems have the great benefit of controlling gene expression in a reversible and flexible manner, compared to constitutive gene expression systems. The most common method is to use the tetracycline (Tet)-inducible system which induces gene expression in the presence of tetracycline in mammalian cells. Alternatively, inducible gene expression can be regulated by some transcription factors which are driven by cell activation signalling. As mentioned in section 1.3.5, the inducible system under the control of nuclear factor of activated T cells (NFAT) has been used for the induction of transgene expression in immune cells such as NK and T cells [242].

NFAT is a family of transcription factors consisting of five members NFAT 1-5. Apart from NFAT 5 which is identified as tonicity response element binding protein (TonEBP), NFAT 1 - 4 are known as the classic members and regulated by calcium signalling [243]. These four remaining NFAT proteins play an important role in inducible gene transcription for immune responses [244]. While calcium-regulated NFAT (NFATc) proteins are widely expressed in many types of immune cells, NFAT 1, 2 and 4 are expressed in T cells.

NFATc proteins are phosphorylated and located in the cytoplasm of resting cells. The activation of NFATc proteins is induced by ligand binding of many receptors, such as the antigen receptors that are expressed on T and B cells, the Fcγ receptors that are expressed on NK cells and monocytes [245]. It is followed by the activation of phospholipase C-γ (PLC-γ) and release of inositol triphosphate (InsP3), which results in increased levels of Ca^{2+} from intracellular stores. Of note, the initial release of Ca^{2+} is not sufficient to promote long term immune responses. Instead, the depletion of intracellular stores triggers the influx of Ca^{2+} through calcium-release-activated calcium (CRAC) channels in the plasma membrane to maintain increased levels of intracellular calcium [246]. Calmodulin bound with calcium activates the calmodulin-dependent phosphatase calcineurin. Activated calcineurin dephosphorylates NFATc proteins, resulting in their translocation to the nucleus. In the nucleus, NFATc proteins couple to different transcription factors to form cooperative complexes and bind to DNA, thereby inducing NFAT-mediated gene expression. For instance, activator protein 1 (AP1) are the main transcriptional partners during T cell activation. Cooperative complexes of NFATc and AP1 bind to the distal ARRE2 elements of the human and murine IL-2 promoters to promote IL-2 expression [247].

CAR-T cells have been developed to inducibly produce cytokines such as IL-12 to improve their anti-tumour efficacy [153, 157, 208]. To achieve this, an NFAT-responsive promoter containing binding motifs of NFAT and a minimal IL-2 promoter is placed upstream of IL-12 transgene in CAR constructs. Under the transcriptional control of this promoter, IL-12 would only be expressed upon cell activation. In CAR-T cell therapy, IL-12 expression and accumulation was mostly restricted in tumour lesions where CAR-T cells were activated through antigen-specific recognition [155]. Therefore, the use of inducible IL-12 expression could minimise severe IL-12-related toxicity which has been observed in either systemic administration of IL-12 therapy in clinical trials or CAR-T cells constitutively secreting IL-12 in lymphodepleted hosts as mentioned in section 3.1.2 and 4.2.3.

5.1.1 Hypothesis and aims

The inducible release of IL-12 has been demonstrated to enhance anti-tumour efficacy of CAR-T cells without causing IL-12-related toxicities in lymphodepleted hosts, compared to the constitutive expression of IL-12 in some studies. It is therefore hypothesised that the local delivery of IL-12, which is controlled by a NFAT composite promoter following CAR-triggered T cell activation, could facilitate anti-CEA CAR-T cells to eradicate tumour and avoid potential IL-12-related toxicities when host lymphodepletion was applied *in vivo*. The main aims of this chapter were:

- To generate retroviral vectors containing first- or second-generation anti-CEA CAR constructs and the inducible IL-12 expression cassette
- To assess whether the induction of IL-12 expression could be triggered by T cell activation through CAR engagement
- To evaluate *in vitro* function of inducible IL-12-secreting CAR-T cells
- To evaluate anti-tumour efficacy of inducible IL-12-secreting CAR-T cells *in vivo*
- To investigate potential toxicities of inducible IL-12-secreting CAR-T cells in combination with host lymphodepletion pre-conditioning *in vivo*

5.2 Results

5.2.1 Generation of CAR-triggered IL-12 expression vectors

A schematic diagram of retroviral vectors containing CAR constructs and the inducible IL-12 expression cassette is shown in Figure 5.1 A. First- and second- generation anti-CEA CAR constructs, as shown in Figure 3.1, were further modified to express IL-12 under the transcriptional control of an NFAT-responsive promoter, which contains six repeats of NFAT binding motif followed by a minimal IL-2 promoter, designated as MFE.mCD3z.NFAT.mIL12, MFE.mCD28z.NFAT.mIL12 and MFE.m41BBz.NFAT.mIL12 respectively. To avoid the promoter activity from the 5' LTR, a sequence (TAGTTAGTTAG) which encodes for the stop codon in 3 reading frames was placed between CD3z sequence and the NFAT-responsive promoter.

The cloning strategy to construct the CAR-triggered IL-12 expression vectors is shown in Figure 5.1 B. First- and second- generation anti-CEA CAR constructs with constitutive IL-12 expression were used as backbone vectors. The fragment, which contains partial sequences of CD3z and IL-12 linked by the NFAT-responsive promoter, was synthesised by GenScript and cloned into BspEI/BstZ17I sites of backbone vectors to generate CAR-triggered IL-12 expression vectors (Figure 5.1 C & D). Confirmation of successful ligation of the CAR encoding vector was performed by Sanger DNA sequencing of samples.

A.

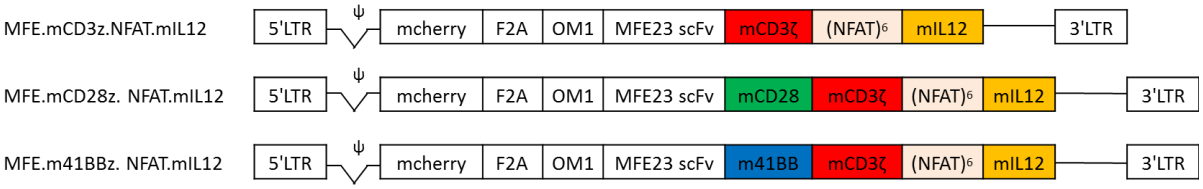
MFE.mCD3z.NFAT.mIL12
5'LTR
ψ
mcherry
F2A
OM1
MFE23 scFv
mCD3ζ
(NFAT)6
mIL12
3'LTR
MFE.mCD28z. NFAT.mIL12
5'LTR
ψ
mcherry
F2A
OM1
MFE23 scFv
mCD28
mCD3ζ
(NFAT)6
mIL12
3'LTR
MFE.m41BBz. NFAT.mIL12
5'LTR
ψ
mcherry
F2A
OM1
MFE23 scFv
m41BB
mCD3ζ
(NFAT)6
mIL12
3'LTR

B.

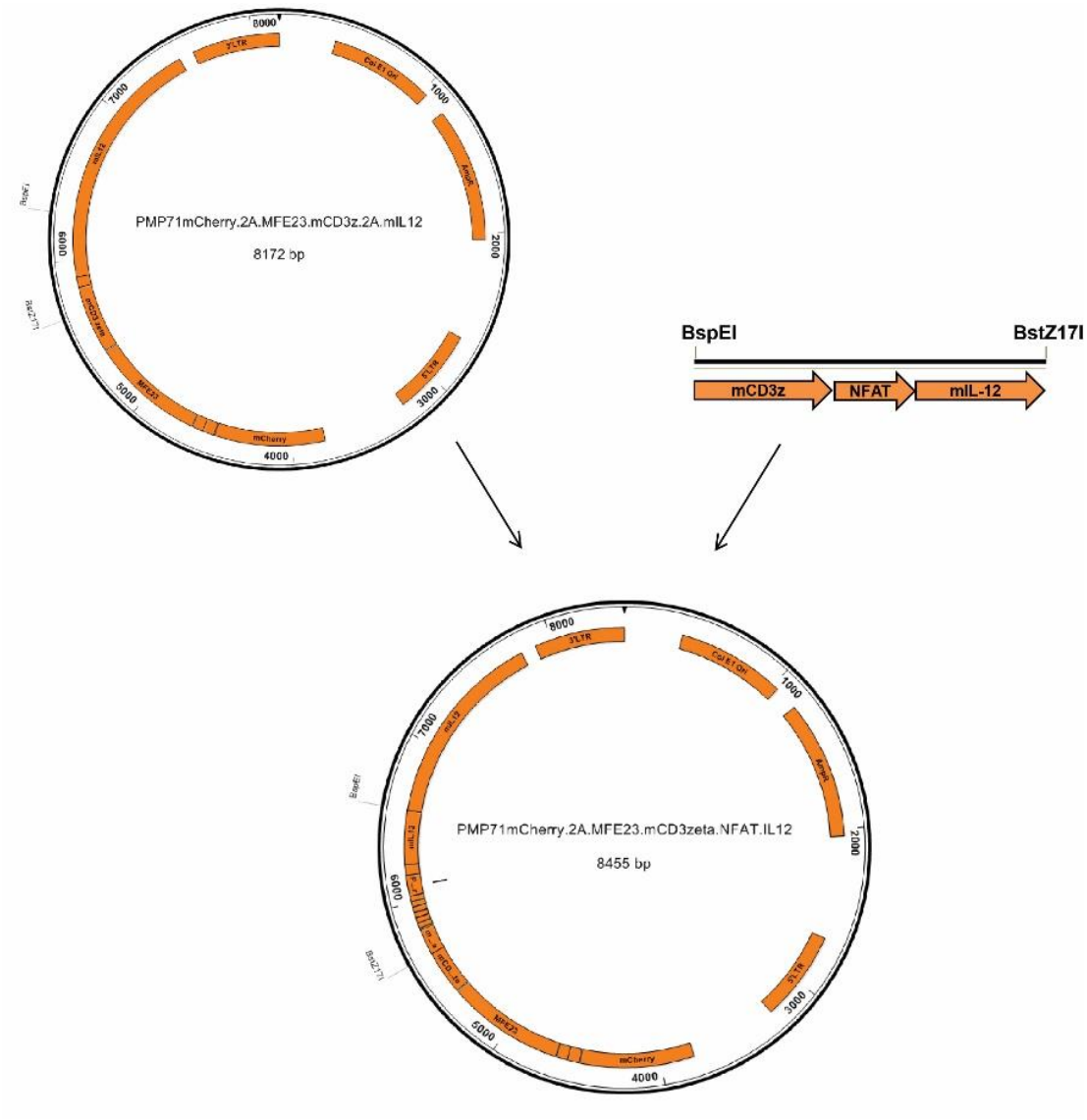
PMP71mCherry.2A.MFE23.mCD3z.2A.mIL12
8172 bp
BspEI
BstZ17I
mCD3z
NFAT
mIL-12
PMP71mCherry.2A.MFE23.mCD3zeta.NFAT.IL12
8455 bp

C.

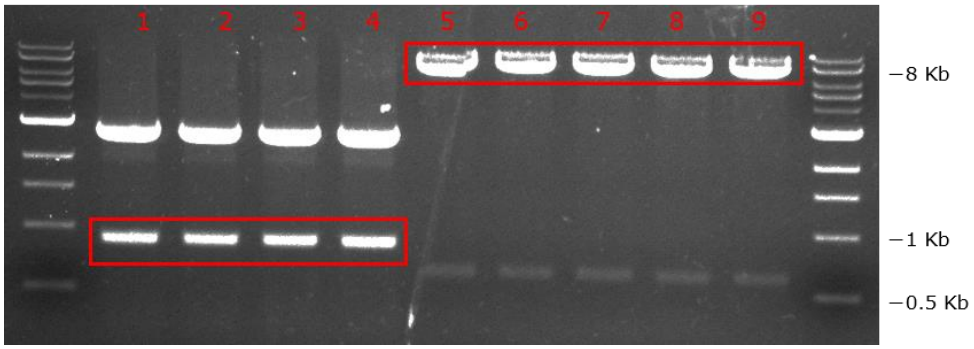
1
2
3
4
5
6
7
8
9
8 Kb
1 Kb
0.5 Kb

D.

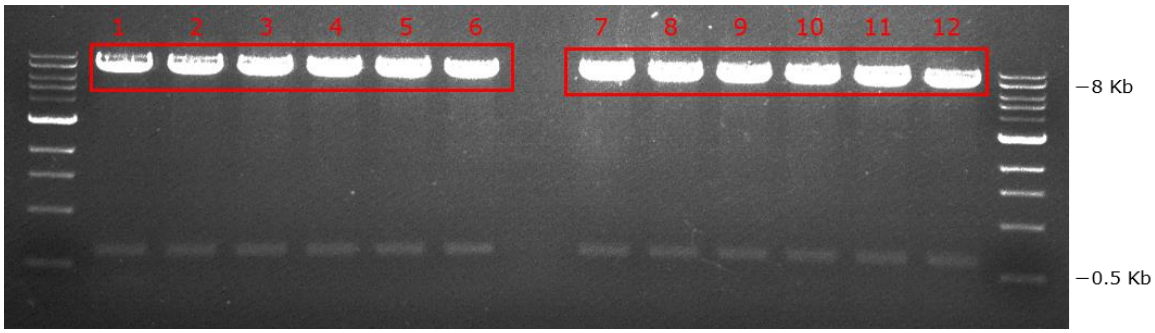

Figure 5.1 Generation of anti-CEA CAR constructs encoding NFAT-responsive IL-12 expression cassette

(A) Schematic diagram of anti-CEA CAR constructs: MFE.mCD3z.NFAT.mIL12, MFE.mCD28z.NFAT.mIL12 and MFE.m41BBz.NFAT.mIL12; **(B)** Overview of cloning strategies for generation of CAR-triggered IL-12 expression vectors. The vectors were digested with BspEI, BstZ17I restriction enzymes. **(C)** Agarose gel electrophoresis of backbone MFE.mCD3z.mIL12 and target mCD3z.NFAT.mIL12 DNA fragments. Lane 1 - 4 shows the mCD3z.NFAT.mIL12 insert from the intermediate pUC57 vector at ~0.9 kb; Lane 5 - 9 shows the CAR backbone from the vector MFE.mCD3z.mIL12 at ~7.5 kb. **(D)** Agarose gel electrophoresis of backbone MFE.mCD28z.mIL12 and MFE.m41BBz.mIL12 DNA fragments. Lane 1 - 6 shows the CAR backbone from the vector MFE.mCD28z.mIL12 at ~8.0 kb. Lane 7 - 12 shows the CAR backbone from the vector MFE.m41BBz.mIL12 at ~8.1 kb. NFAT, composite NFAT-responsive promoter; LTR, long terminal repeat; OM1, oncostatin M leader sequence.

5.2.2 Generation of anti-CEA CAR-T cells secreting inducible IL-12

CD3/CD28-activated mouse T cells were transduced to express different CAR constructs and cultured at a density of either 0.3×10^6 or 1×10^6 cells/ml with the addition of hIL-2 and mIL-7 at 100 IU/ml and 2 ng/ml respectively every other day. To confirm successful CAR-T cell transduction, the expression of surface marker mCherry was analysed on day 4-5 post transduction by flow cytometry.

As shown in Figure 5.2 A, MFE23.mCD3z, MFE23.mCD28z, MFE23.m41BBz CAR-T cells had 55.8 ± 17.8, 26.3 ± 12.0, 40.8 ± 11.2 % $mCherry^+$ T cells respectively. A reduction in transduction efficiency was shown in CD3z, CD28z and 41BBz CAR-T cells constitutively secreting IL-12, which was 28.1 ± 17.6, 19.9 ± 4.6, 15.6 ± 2.8 % respectively. When a NFAT-responsive promoter (335 bp only) for inducible IL-12 expression was further inserted into vectors, the proportion of $mCherry^+$ T cells was further decreased to 10.0 ± 5.3, 9.1 ± 6.3, 5.8 ± 3.1 % in CD3z, CD28z and 41BBz CAR-T cells respectively. Similar results were also seen in the median fluorescent intensity (MFI) of mCherry among transduced T cells (Figure 5.2 B).

The total length of MFE.mCD28z.NFAT.mIL12 (6.3 kb) and MFE.m41BBz.NFAT.mIL12 (6.4 kb) did not exceed the maximum length of an allowable DNA insert which is usually about 8-10 kb in a retroviral vector. Transduction efficiency was probably affected by RNA encapsidation during retroviral particle formation, several factors during CAR integration and expression such as the site of transgene insertion into the host genome and the number of transgene copies, the level of transgene transcription, the stability of the mRNA transcript, which have been discussed in section 3.3. Given low levels of transduction efficiency, large numbers of non-transduced T cells would be included when a certain CAR-T cell dose was given, which therefore presents a limitation to the suitability of use *in vivo* without a selection method of purification.

A.

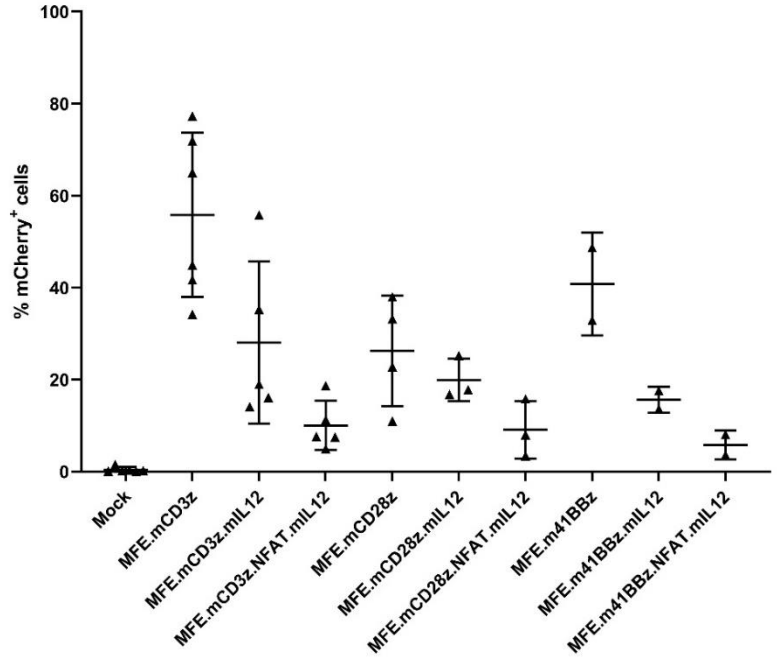

B.

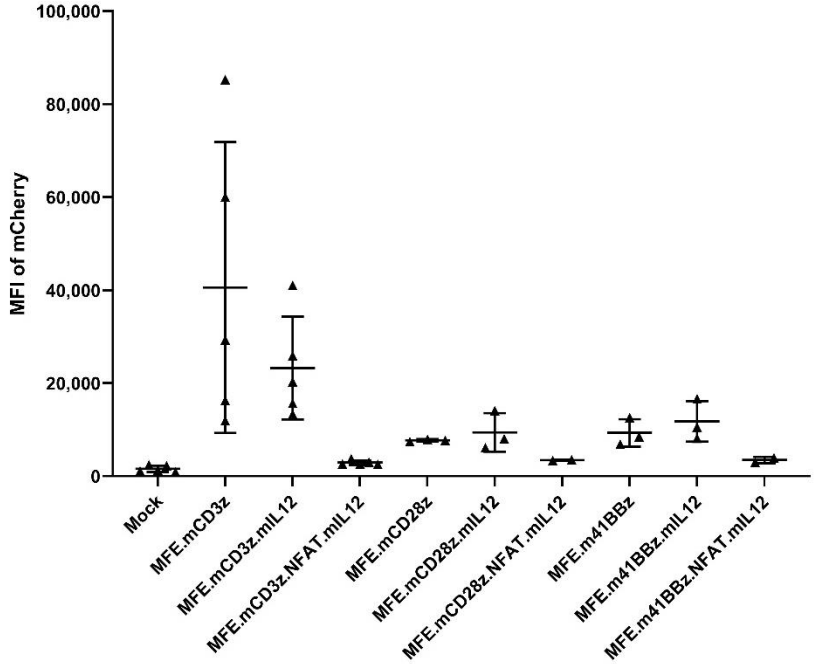

Figure 5.2 Transduction efficiency of transduced T cells

Transduction efficiency was determined by the detection of mCherry expression on both CD4 and CD8 subsets on day 4-5 post transduction by flow cytometry. **(A)** The percentage of mCherry$^+$ T cells and **(B)** the MFI value of mCherry were shown. The data are plotted as mean ± SD of all independent transduction experiments performed.

5.2.3 *In vitro* function of anti-CEA CAR-T cells secreting inducible IL-12

To assess the level of IL-12 production induced by CAR-triggered T cell activation, transduced CAR-T cells with inducible IL-12 expression were co-incubated with CEA^+ target cells and parental target cells at E: T ratio of 1: 1 for 20 hours. Parental CAR-T cells with or without constitutive IL-12 expression were used for comparison. Due to the variable levels of transduction efficiency among CAR-T cell groups, non-transduced T cells were added into each group to ensure that the number of both total T cells and CAR-expressing T cells remained consistent. The supernatant was collected from co-cultures and measured for IL-12 release by ELISA.

Similar to results in section 3.2.5 (Figure 3.16), a representative experiment showed that mouse T cells transduced with CD3z.mIL12, CD28z.mIL12 and 41BBz.mIL12 vectors respectively could produce IL-12 constitutively in the absence of target antigen (Figure 5.3 A). IL-12 production was significantly increased in CD3z.mIL12 and CD28z.mIL12 CAR-T cells in response to CEA-expressing MC38 cells ($P < 0.0001$). In terms of CAR-T cells inducibly secreting IL-12, without CEA-specific stimulation, the amount of IL-12 secreted was below the limit of detection (48 pg/ml). When co-cultured with CEA-expressing MC38 cells, IL-12 production was slightly increased to 93.7 ± 3.1, 70.0 ± 6.6 and 65.2 ± 7.5 pg/ml for CD3z.NFAT.mIL12, CD28z.NFAT.mIL12 and 41BBz.NFAT.mIL12 CAR-T cells respectively, whilst IL-12 production by mock and non-IL-12-secreting T cells was still below the limit of detection. It suggested that IL-12 expression might be induced upon cell activation resulting from CAR engagement. However, there is no significant difference in IL-12 production between inducible-IL-12-secreting CAR-T cells and non-IL-12-secreting CAR-T cells in response to CEA-expressing MC38 cells. Similar secretion pattern could be seen in the mean ± SD values of 2 independent experiments, although statistical significance was reduced (Figure 5.3 B).

A.

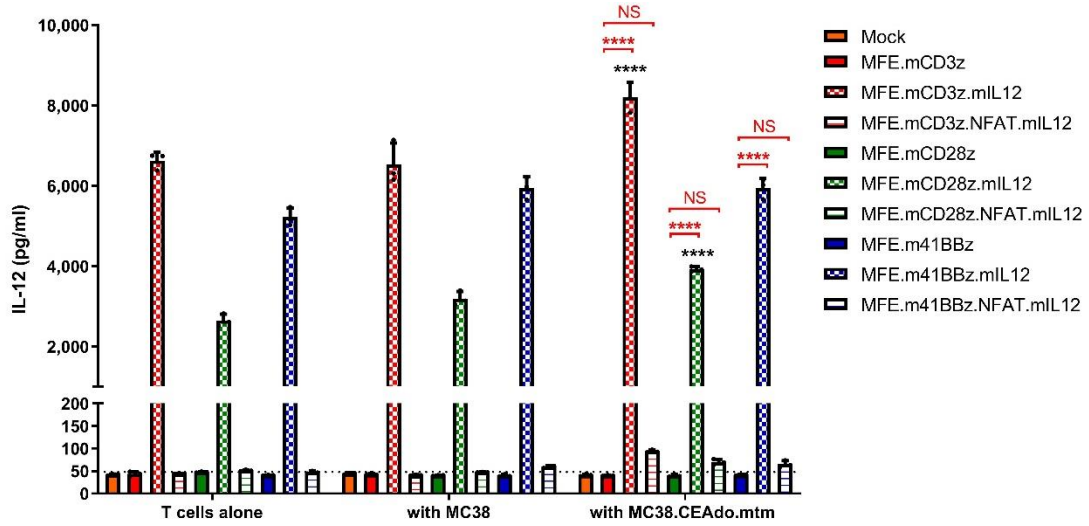

B.

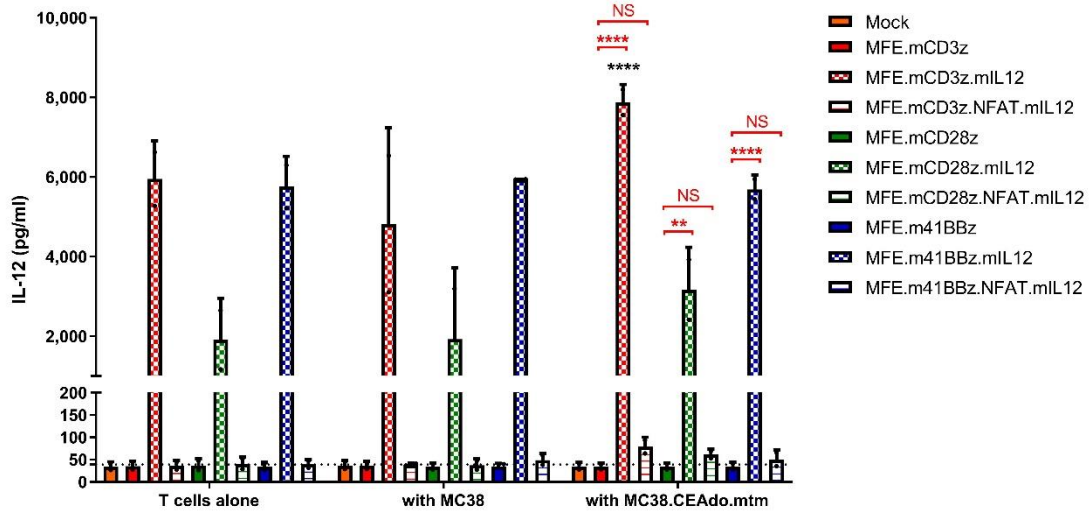

Figure 5.3 IL-12 secretion by anti-CEA CAR-T cells in response to CEA$^+$ MC38 cell line

Transduced T cells were co-cultured for 20 hours with 2 × 10^4 CEA$^+$ MC38 cells and MC38 cells at E: T ratio of 1: 1. The supernatant collected post incubation was measured for IL-12 production by ELISA. **(A)** The data are representative of two independent experiments and values are presented in mean ± SD of triplicates. **(B)** The data are plotted as mean ± SD of two independent experiments. Statistically significant difference was analysed using two-way ANOVA with Tukey's multiple comparisons test. NS, no significant difference; ** $P < 0.01$; **** $P < 0.0001$. Red stars represent comparison between two constructs. Black stars represent comparison of each construct co-cultured with CEA$^+$ MC38 cells and parental MC38 cells. The dotted line represents the limit of detection (LOD) of IL-12 concentration.

To further confirm whether the NFAT-responsive promoter was functional to induce IL-12 expression in activated CAR-T cells, phorbol myristate acetate (PMA)/ionomycin stimulation was used for comparison with CAR-specific activation. As shown in Figure 5.4, IL-12 was produced by CD3z.NFAT.mIL12 CAR-T cells when co-cultured with CEA-expressing MC38 cells or activated by PMA/ionomycin stimulation, which were 136.1 ± 7.9 and 902.7 ± 32.2 pg/ml respectively, but not by mock and CD3z T cells. There was a significant difference in IL-12 production between CD3z and CD3z.NFAT.mIL12 CAR-T cells with both conditions ($P < 0.0001$). These results suggested that IL-12 expression driven by the NFAT-responsive promoter in CAR-T cells could be successfully triggered by either CEA-specific or non-specific T cell stimulation. The non-specific T cell stimulation via PMA/ionomycin induced more IL-12 production than CEA-specific T cell activation through CAR engagement ($P < 0.0001$). This is because PMA could bypass surface receptor stimulation and directly activate protein kinase C (PKC) in the cytoplasm, whilst ionomycin as a calcium ionophore could trigger the release of intracellular calcium in T cells which is required for NFAT signalling [248, 249].

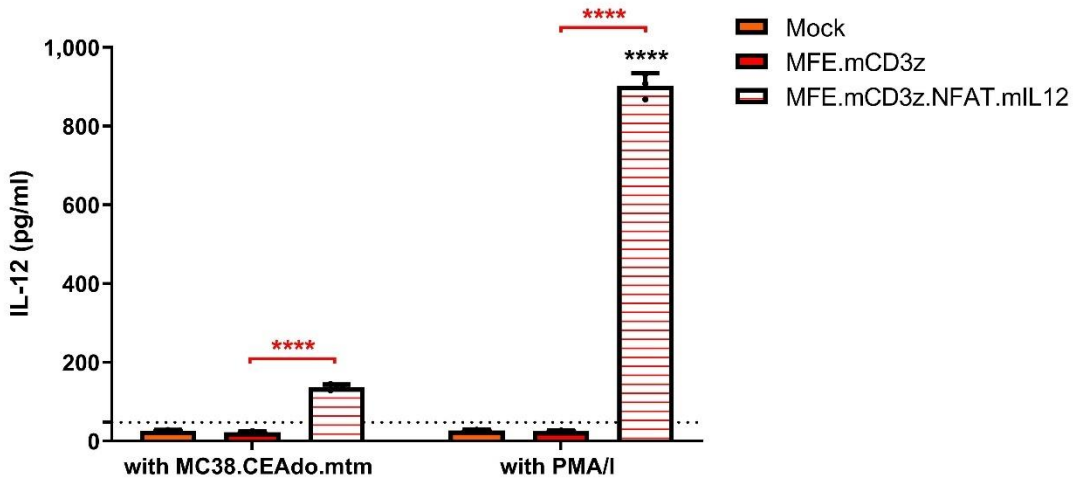

Figure 5.4 IL-12 secretion by anti-CEA CAR-T cells in response to PMA/I stimulation

Transduced T cells were co-cultured with 2 × 10^4 CEA^+ MC38 cells or MC38 cells at E: T ratio of 1: 1 or stimulated by PMA/ionomycin for 20 hours. The supernatant collected post incubation was measured for IL-12 production by ELISA. The data are plotted as mean ± SD of triplicates from one experiment. Statistically significant difference was analysed using two-way ANOVA with Tukey's multiple comparisons test. NS, no significant difference; * $P < 0.05$; **** $P < 0.0001$. Red stars represent comparison between two constructs. Black stars represent comparison of each construct at two conditions. The dotted line represents the LOD of IL-12 concentration.

Release of IFN-γ was also measured by ELISA following co-culture of transduced T cells with tumour cells. Similar to results in section 3.2.5 (Figure 3.18), constitutive expression of IL-12 significantly enhanced IFN-γ production of transduced T cells with CD3z and CD28z CAR constructs, whilst the level of IFN-γ production was further improved in the presence of target antigen ($P < 0.0001$) (Figure 5.5 A). Notably, compared to parental non-IL-12-expressing CAR-T cells, IFN-γ production was also increased significantly in CD3z.NFAT.mIL12 and CD28z.NFAT.mIL12 CAR-T cells (48,641.6 ± 1,008.0 and 73,581.6 ± 759.0 pg/ml respectively) in response to CEA-expressing MC38 cells ($P < 0.0001$). This suggests that the inducible IL-12 expression driven by T cell activation through CAR engagement could facilitate CAR-T cells to secret more IFN-γ, although low levels of IL-12 production were detected. Moreover, without CEA-specific stimulation, the amount of IFN-γ was much reduced in CAR-T cells inducibly secreting IL-12, probably due to the lack of IL-12 secretion. As for 41BBz.NFAT.mIL12 T cells, although the amount of IFN-γ was slightly increased when co-cultured with CEA^+ tumour cells in comparison with parental tumour cells, there is no significant difference between them (8,033.0 ± 200.0 versus 6,902.9 ± 283.1 pg/ml), which was similar to the results found in 41BBz.mIL12 T cells. A similar secretion pattern could be seen in the mean ± SD values of 2 independent experiments, although statistical significance was reduced (Figure 5.5 B).

A.

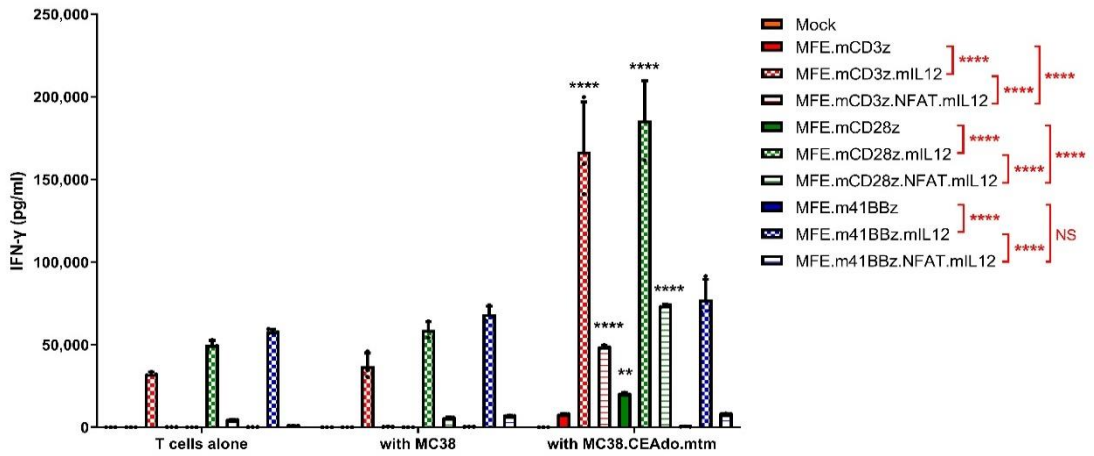

B.

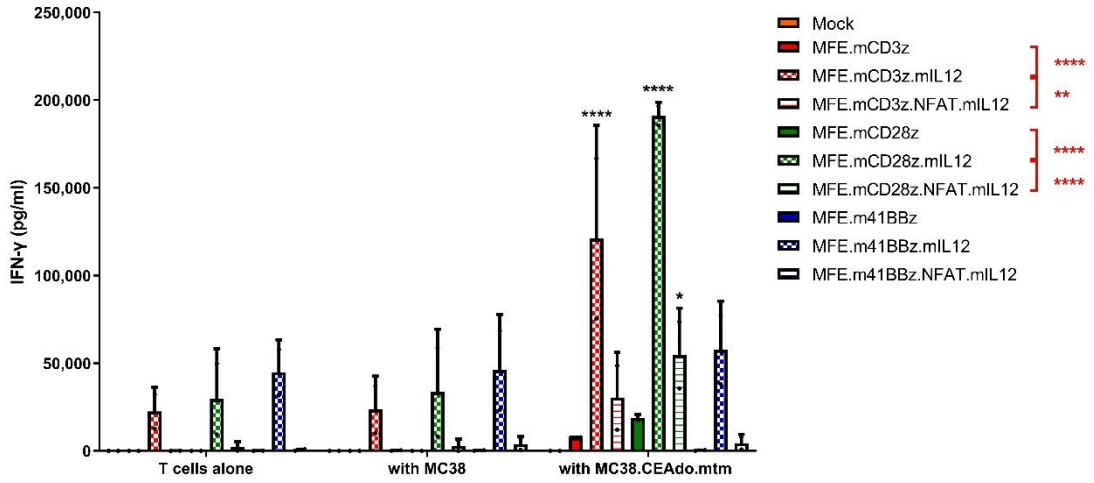

Figure 5.5 IFN-γ secretion by anti-CEA CAR-T cells in response to CEA$^+$ MC38 cell line

Transduced T cells were co-cultured for 20 hours with 2 × 10^4 CEA$^+$ MC38 cells or MC38 cells at E: T ratio of 1: 1. The supernatant collected post incubation was measured for IFN-γ production by ELISA. **(A)** The data are representative of two independent experiments and values are presented in mean ± SD of triplicates. **(B)** The data are plotted as mean ± SD of two independent experiments. Statistically significant difference was analysed using two-way ANOVA with Tukey's multiple comparisons test. NS, no significant difference; * P < 0.05; ** P < 0.01; **** P < 0.0001. Red stars represent comparison between two constructs. Black stars represent comparison of each construct co-cultured with CEA$^+$ MC38 cells and parental MC38 cells.

To assess the cytotoxicity of CAR-T cells, luciferase assays were performed by measuring the luciferase activity of target cell lines post 20-hour co-culture with CAR-T cells. T cells transduced with different CAR constructs with the exception of 41BBz exhibited cytotoxicity against luciferase-expressing CEA^+ target cells in comparison with mock T cells in 2 donors ($P < 0.0001$) (Figure 5.6 A & B). In donor one (Figure 5.6 A), both CD3z.mIL12 and CD3z.NFAT.mIL12 T cells showed improved cytotoxicity (99.4 ± 1.7 % and 95.2 ± 1.1 % respectively) compared to CD3z T cells (61.3 ± 5.4 %) ($P < 0.0001$), suggesting that both constitutive and inducible expression of IL-12 was able to enhance cytotoxicity of CAR-T cells. Similar results were observed in 41BBz CAR-T cell variants. Given that 41BBz.mIL12 and 41BBz.NFAT.mIL12 T cells did not produce IFN-γ significantly in response to CEA-expressing MC38 cells compared to MC38 cells, it is hypothesised that the enhancement of cytotoxicity was caused by direct effects of IFN-γ on tumour cell apoptosis, which has been discussed in section 3.3. Furthermore, 100 % of cell killing among CD28z, CD28z.mIL12 and CD28z.NFAT.mIL12 T cells were observed. It was probably due to their high functional activity to lyse target cells completely within a 20-hour co-culture period.

In donor two (Figure 5.6 B), however, there is no significant difference in cytotoxicity between inducible IL-12-secreting CAR-T cells and parental non-IL-12-secreting T cells. Apart from donor variability, the main difference was the lowest transduction efficiency between these two donors, which was 8.05 % and 3.43 % in donor one and two respectively. It required 2.48×10^5 and 5.83×10^5 of total T cells containing 2×10^4 CAR-T cells for co-culture. As the number of non-transduced T cells in donor two was 2.5-fold higher than that in donor one, it is hypothesised that small amounts of inducible IL-12 secreted were more likely to be taken up by non-transduced T cells rather than CAR-T cells, resulting in no enhancement of cytotoxicity for CAR-T cells post direct antigen recognition. Additionally, high number of total T cells might also lead to increased non-specific tumour cell killing, reflected by 18.3 ± 6.0 % of cell killing in mock T cells in donor two.

A.

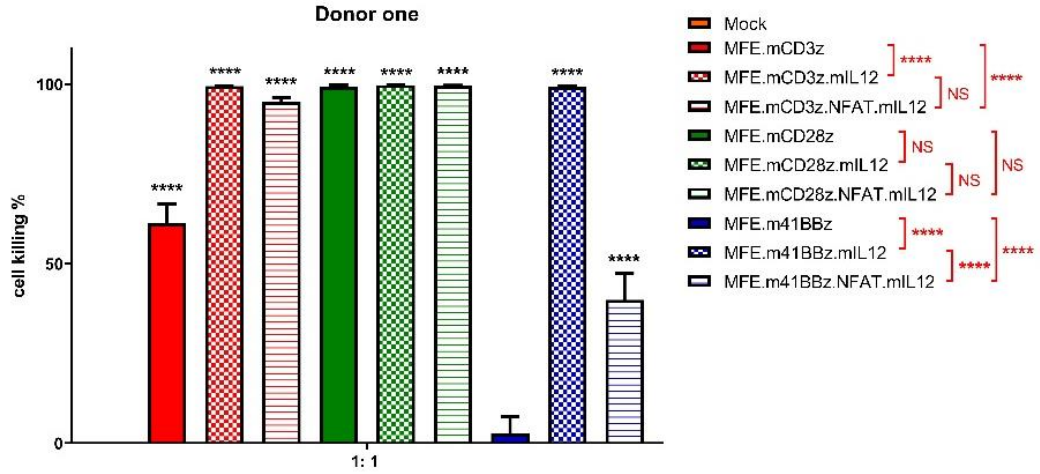

B.

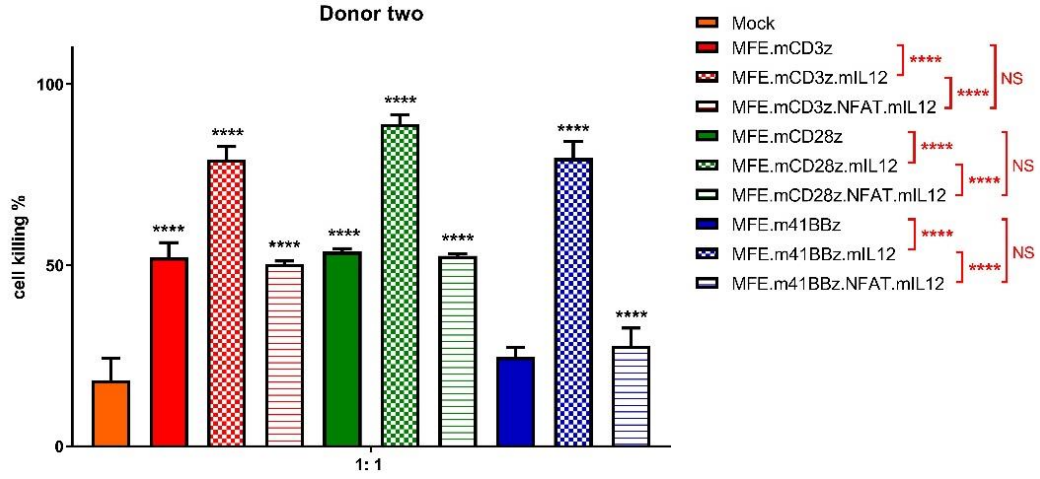

Figure 5.6 Cytotoxicity of anti-CEA CAR-T cells in response to luciferase-labelled CEA$^+$ MC38 cell line

Transduced T cells were co-cultured for 20 hours with 2 × 10^4 CEA$^+$ MC38 cells expressing luciferase and GFP at different E: T ratios from 5: 1 to 0.125: 1 (n = 3). Luminometry was performed to assess the cytotoxicity post co-culture. The data are plotted as mean ± SD of triplicates from two donors **(A)** and **(B)** respectively. Statistically significant difference was analysed using one-way ANOVA with Tukey's multiple comparisons test. NS, no significant difference; ** P < 0.01; *** P < 0.001; **** P < 0.0001. Red stars represent comparison between two CAR constructs. Black stars represent comparison between mock and CAR constructs.

5.2.4 *In vivo* function of anti-CEA CAR-T cells secreting inducible IL-12

The previous study in section 4.2.3 showed that severe toxicity was seen in lymphodepleted mice treated with a single dose of 2 x 10^6 CD28z.mIL12 CAR-T cells, with high levels of IL-12 in serum. High levels of IL-12 in serum were considered the cause of death. A strategy of inducible IL-12 expression has been developed to restrict IL-12 secretion to the tumour microenvironment and therefore reduce systemic IL-12 toxicity. To assess whether the inducible expression of IL-12 could reduce toxicity and facilitate anti-tumour efficacy of anti-CEA CAR-T cells, CD28z.NFAT.mIL12 CAR-T cells were adoptively transferred into immunocompetent mice bearing subcutaneous CEA^+ tumour with or without host lymphodepletion. Additionally, as CEA is also expressed at low levels on normal tissues in human, there is a concern that anti-CEA CAR-T cells might induce on-target off-tumour toxicity. To further assess this possibility, CEA transgenic C57BL/6 mouse (CEAtg) model, which expresses human CEA in the esophagus, small intestine, trachea, and lung, soluble CEA in serum and consequently have immunological tolerance to CEA [226], would be utilised in this study, closely reflecting the human situation.

A schematic diagram of the experimental procedure giving CAR-T cell treatment with 5Gy TBI was shown in Figure 5.7 A. CEAtg mice bearing 50 – 100 mm^3 tumour were treated with 2.5 x 10^7 total T cells containing 2 x 10^6 CAR-T cells by i.v. injection on day 2 post 5Gy TBI. To monitor the release of cytokines in blood post treatment, serum was isolated from blood samples collected via tail vein bleeds on day 7, 16 and 22 and cardiac puncture at terminal day. Mice were euthanized when tumours ulcerated or reached over 1,000 mm^3 or they experienced lethal toxicities such as 20 % severe BWL, emaciation or pale extremities. Spleens were collected and used to assess the functional activity of immune cells *in vitro*.

It can be seen that the number of white blood cells, lymphocytes and neutrophils in mice treated with TBI were decreased and not recovered to normal levels for 9 days (Figure 5.7 B). A reduction in these cell numbers was also seen in CD28z.mIL12 T cell therapy without TBI pre-conditioning. Since only one mouse was treated with CD28z.mIL12 T cells, it was probably because of donor variability. As shown in Table 5.1, there were only 33 % of mice treated with mock T cells and 5Gy TBI showing severe BWL. This suggests that mice treated with 5Gy TBI might be in part sensitive to CAR-T cells or large numbers of total T cells transferred. Notably, severe morbidity and mortality were observed in all pre-conditioned CEAtg mice receiving CD28z.mIL12 and CD28z.NFAT.mIL12 CAR-T cells. Whilst there was no anti-tumour activity, there was a significant survival advantage for mice receiving CD28z T cells with 5Gy TBI or CD28z.NFAT.mIL12 T cells only relative to

that receiving CD28z.NFAT.mIL12 T cells with 5Gy TBI who had to be culled early due to body weight loss and ill health ($P < 0.05$ and $P < 0.01$ respectively) (Figure 5.7 C). It indicated that IL-12 which was produced in an inducible manner by CAR-T cells still possibly triggered IL-12-related toxicities in pre-conditioned mice, although there was a slight increase in survival compared to pre-conditioned mice receiving constitutive IL-12-secreting CAR-T cells. Additionally, although only one mouse was treated, administration of 0.3×10^6 CD28z.mIL12 T cells still caused toxicity in combination with pre-conditioning, suggesting that cell dose should be further reduced.

Without 5Gy TBI pre-conditioning, no lethal toxicity was observed post infusion of 2×10^6 CAR-T cells with constitutive or inducible IL-12 expression (Table 5.1). Nevertheless, administration of 2×10^6 CD28z.mIL12 and CD28z.NFAT.mIL12 CAR-T cells did not show any therapeutic effect on tumour (Figure 5.7 D). Notably, only one mouse was treated with 2×10^6 CD28z.mIL12 CAR-T cells, as T cells did not expand to sufficient number *in vitro*. More experimental data is required to determine whether the administration of 2×10^6 CD28z.mIL12 in the CEAtg model was as efficacious as same therapy in the WT model which has been shown in section 4.2.3.

A.

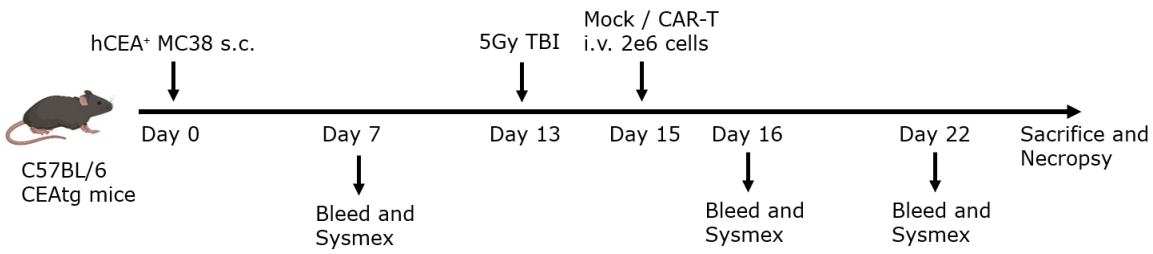
hCEA+ MC38 s.c.
5Gy TBI
Mock / CAR-T
i.v. 2e6 cells
Day 0
Day 7
Day 13
Day 15
Day 16
Day 22
Sacrifice and
Necropsy
C57BL/6
CEAtg mice
Bleed and
Sysmex
Bleed and
Sysmex
Bleed and
Sysmex

B.

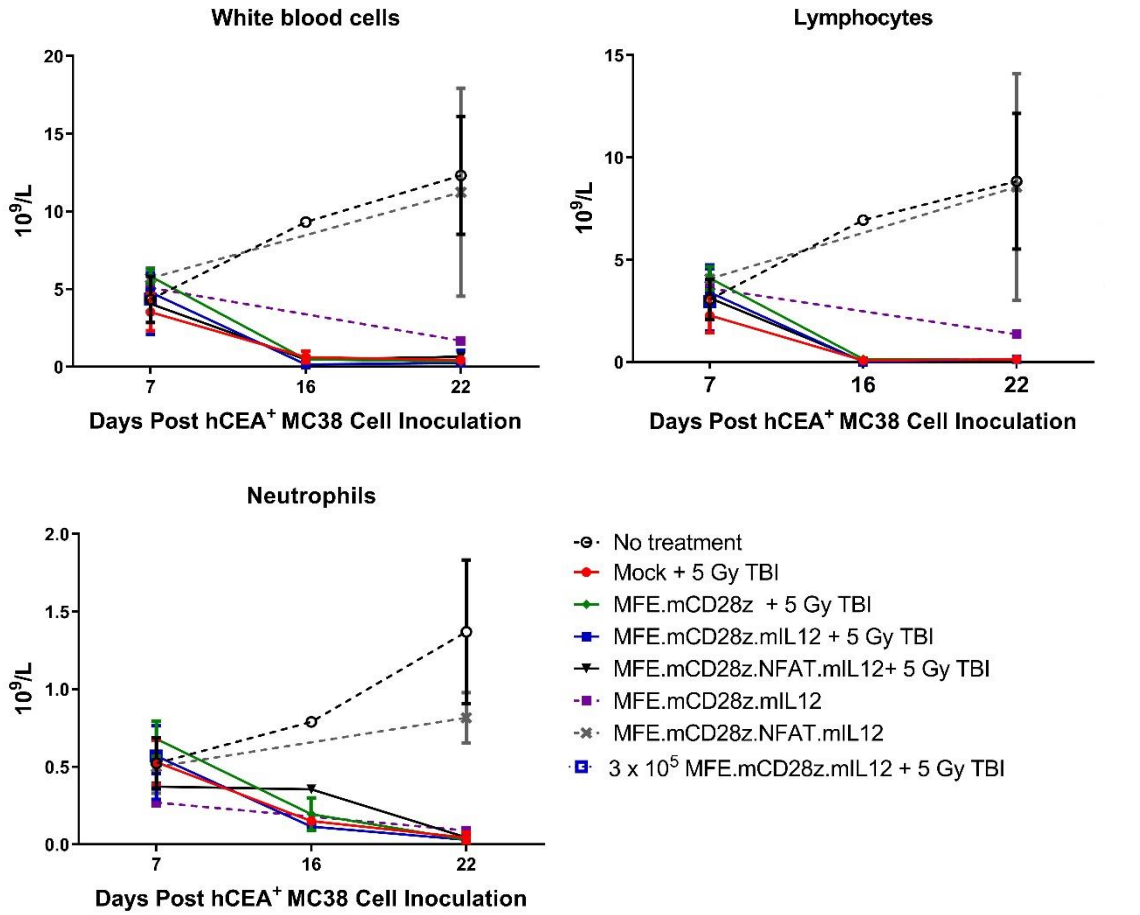
White blood cells
Lymphocytes
Neutrophils
10^9/L
Days Post hCEA+ MC38 Cell Inoculation
No treatment
Mock + 5 Gy TBI
MFE.mCD28z + 5 Gy TBI
MFE.mCD28z.mIL12 + 5 Gy TBI
MFE.mCD28z.NFAT.mIL12+ 5 Gy TBI
MFE.mCD28z.mIL12
MFE.mCD28z.NFAT.mIL12
3 x 10^5 MFE.mCD28z.mIL12 + 5 Gy TBI

C.

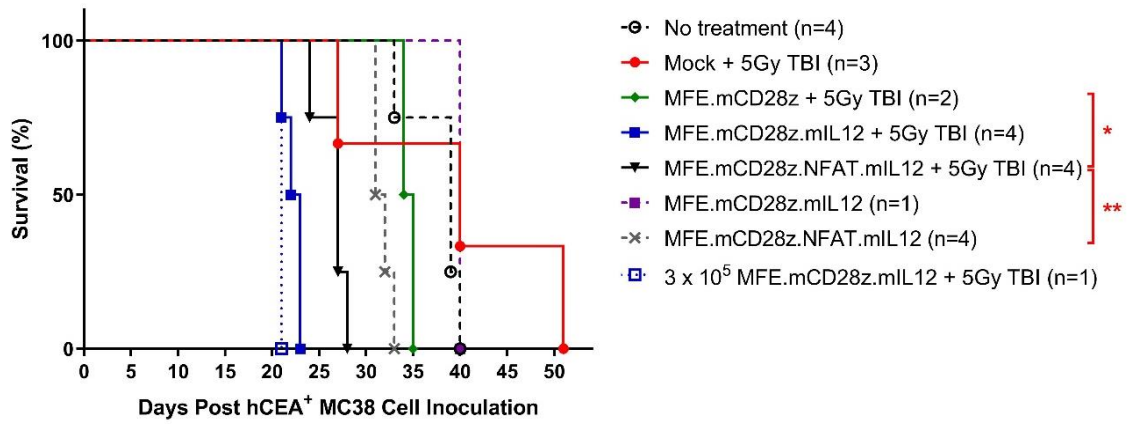
Survival (%)
Days Post hCEA+ MC38 Cell Inoculation
No treatment (n=4)
Mock + 5Gy TBI (n=3)
MFE.mCD28z + 5Gy TBI (n=2)
MFE.mCD28z.mIL12 + 5Gy TBI (n=4)
MFE.mCD28z.NFAT.mIL12 + 5Gy TBI (n=4)
MFE.mCD28z.mIL12 (n=1)
MFE.mCD28z.NFAT.mIL12 (n=4)
3 x 10^5 MFE.mCD28z.mIL12 + 5Gy TBI (n=1)
*
**

D.

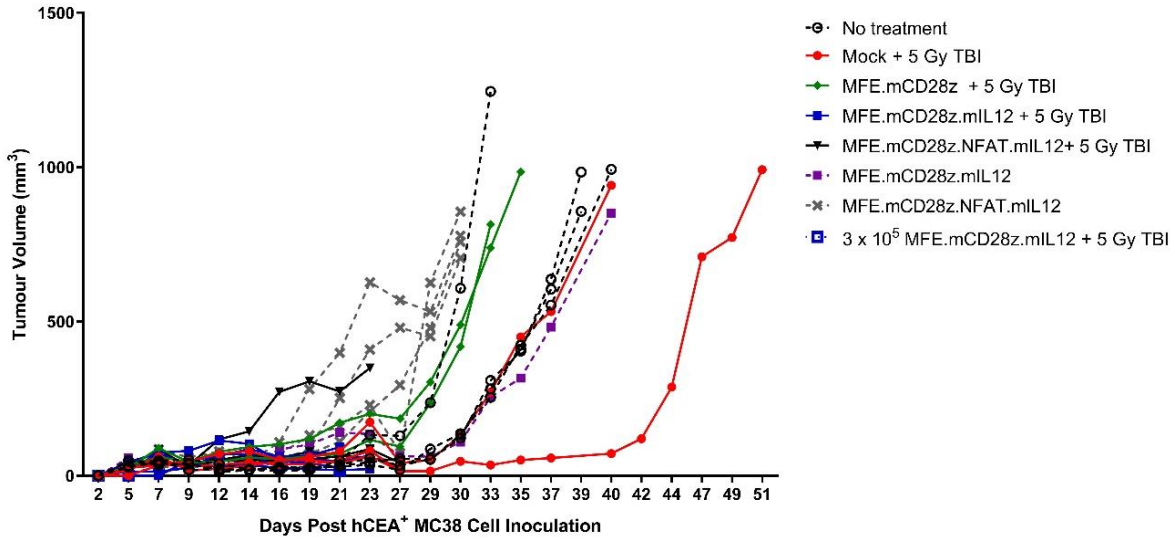

Figure 5.7 Evaluation of anti-tumour responses of CEA-specific CAR-T cells post host lymphodepletion

(A) Schematic diagram of the experimental procedure applying CAR-T cell treatment with or without 5Gy TBI *in vivo*. Tumour-bearing C57BL/6 CEAtg mice were treated with 5Gy TBI 2 days before i.v. administration of 2 x 10^6 mock T cells or CAR-T cells within 2.5 x 10^7 total T cells (n = 1 - 4). Peripheral blood samples were collected via tail vein bleeds on day 7, 16 and 22 for analysis. **(B)** The amount of white blood cells, lymphocytes and neutrophils of individual mice before and after 5Gy TBI. **(C)** Survival of individual mice post cell transfer treatment. Statistically significant difference was analysed using log rank (Mantel-Cox) test. $*$ $P < 0.05$; $**$ $P < 0.01$. **(D)** Tumour volume of individual mice in each T cell therapy group.

Table 5.1 Details of the cause of death for CEAtg mice receiving CAR-T cells

CEAtg mouse model	Reasons for culling		Tumour-free (%)	% culled due to body weight loss
	Severe body weight loss; Emaciation; pale extremities	Tumour condition (over 1,000 mm^3, ulceration, holed or bleeding)		
No treatment (n=4)	0	4	0	0
Mock T cells + 5Gy TBI (n=3)	1	2	0	33
CD28z T cells + 5Gy TBI (n=2)	0	2	0	0
CD28z.mIL12 T cells + 5Gy TBI (n=3)	3	0	0	100
CD28z.NFAT.mIL12 T cells + 5Gy TBI (n=4)	4	0	0	100
CD28z.mIL12 T cells (n=1)	0	1	0	0
CD28z.NFAT.mIL12 T cells (n=4)	0	4	0	0
3 x 10^5 CD28z.mIL12 T cells + 5Gy TBI (n=1)	1	0	0	100

High serum levels of IL-12 were detected in lymphodepleted WT mice treated with CAR-T cells constitutively secreting IL-12 in section 4.2.3 (Figure 4.7), which was probably the cause of lethal toxicity. To assess whether the level of inducible IL-12 was also increased post host lymphodepletion and subsequently led to lethal toxicity, serum samples were measured for IL-12 production by ELISA. Similar to serum IL-12 levels in C57BL/6 WT model (Figure 4.7), whilst increased levels of IL-12 were detected in pre-conditioned mice receiving 2 x 10^6 and 0.3 x 10^6 CD28z.mIL12 CAR-T cells from day 16 to day 22 (428.8 ± 236.4 versus 3,776.0 ± 1,929.3; 140.2 ± 0.0 versus 2,591.0 ± 0.0 pg/ml respectively), IL-12 amount was gradually reduced to background in the mouse receiving 2 x 10^6 CD28z.mIL12 CAR-T cells only (Figure 5.8 A & B). With regards to CD28z.NFAT.mIL12 CAR-T cells with or without 5Gy TBI, however, the amount of IL-12 was below background at all timepoints. Given poor levels of IL-12 production in the co-culture of CD28z.NFAT.mIL12 CAR-T cells with CEA^+ MC38 cells, it is again possible that IL-12 induced in mice was taken up by immune cells and thus was not detectable. In addition, since the release of IL-12 was restricted at tumour sites, this is most likely why serum IL-12 level were not raised.

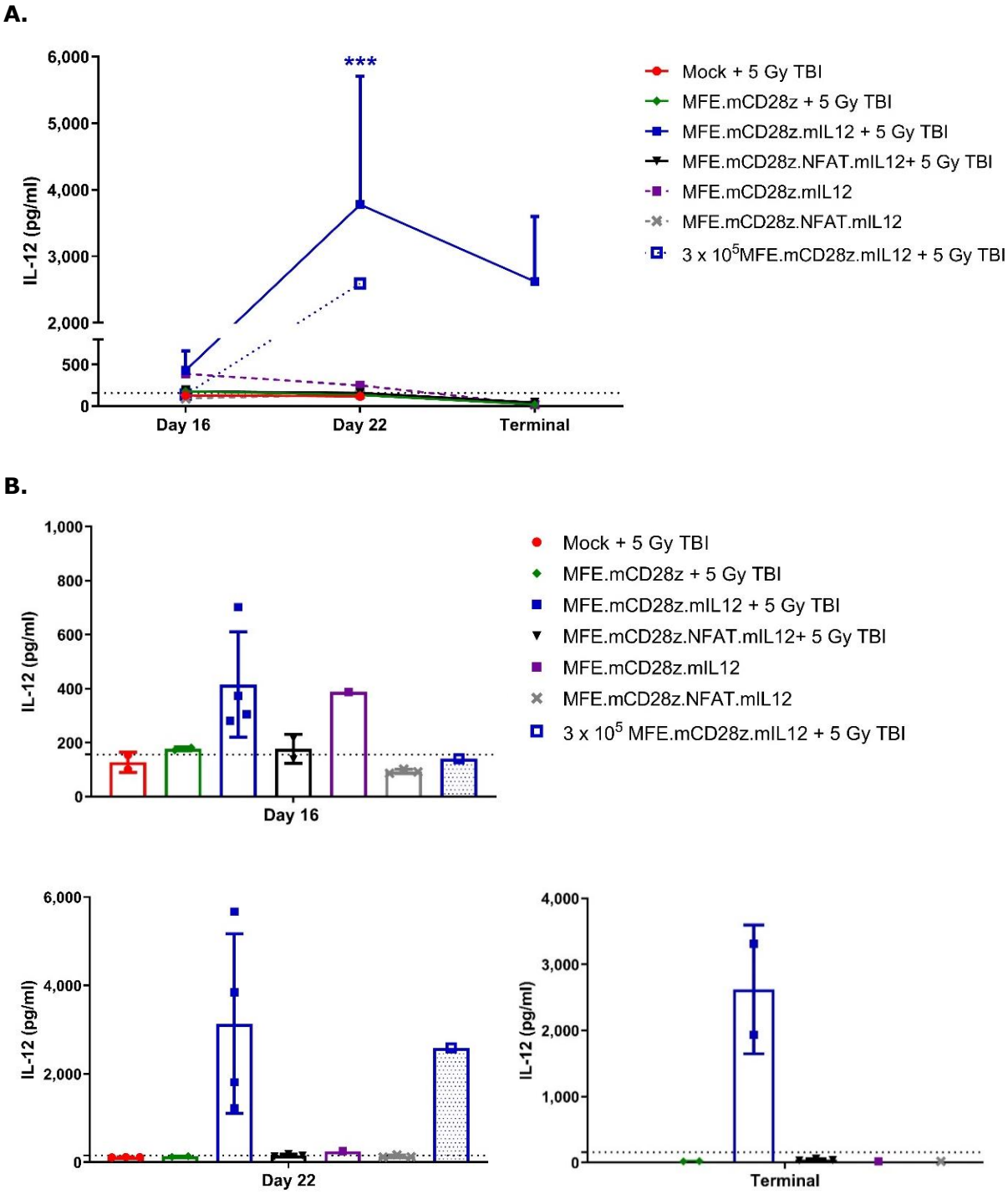

Figure 5.8 IL-12 production in the serum of mice receiving T cells

The level of IL-12 post CAR-T cell administration in blood samples was measured by ELISA. **(A)** The data are plotted as mean ± SD of blood samples that could be successfully collected. Statistically significant difference between day 16 and day 22 was analysed using two-way ANOVA with Sidak's multiple comparisons test. *** $P < 0.001$. **(B)** The serum levels of IL-12 on day 16, 22 and on terminal day are shown in bar graphs separately. The dotted line represents the LOD of IL-12 concentration.

5.3 Discussion

The main aims of this chapter were to genetically modify anti-CEA CAR-T cells to express IL-12 through an inducible expression system driven by T cell activation through CAR recognition of target antigen and to assess anti-tumour activity *in vitro* and *in vivo*. Compared to the constitutive expression of IL-12, the inducible release of IL-12, which is under the transcriptional control of an NFAT-responsive promoter, has the advantage of being able to minimise systemic IL-12-related toxicity. It also could avoid T cell apoptosis during *in vitro* culture, which is one of the obstacles in CAR-T cells constitutively secreting IL-12 as described in section 3.3.

Mouse T cells were successfully transduced with the retroviral vectors encoding anti-CEA CAR constructs and the NFAT-responsive IL-12 expression cassette. However, one of the major issues was low levels of transduction efficiency (Figure 5.2 A). Nevertheless, IL-12 secretion was successfully induced following activation of T cells through either PMA/ionomycin stimulation or CAR-specific stimulation *in vitro* (Figure 5.3 & 5.4). However, compared to CAR-T cells constitutively secreting IL-12, CAR-T cells with inducible IL-12 expression produced IL-12 at much lower levels in the presence of target antigen, which was just slightly above the limit of detection (48 pg/ml). This could potentially be because IL-12 was mainly taken up by T cells once secreted, resulting in low levels of IL-12 accumulation in the supernatant. To determine if this is the case, intracellular staining could be performed to detect IL-12 expression followed by flow cytometry analysis. In addition, since the MFI value of mCherry expressed in CAR-T cells with inducible IL-12 expression was much lower than that in parental CAR-T cells (Figure 5.2 B), it is hypothesised that the amount of CAR constructs and NFAT-responsive promoters integrated into a single T cell was probably low. This situation could also result in low levels of inducible IL-12 production.

Recently, several studies have also combined CAR construct and inducible IL-12 construct in a single lentiviral vector for transduction of T cells and reported high levels of transduction efficiency [250, 251]. Therefore, although the total length of CAR construct is within the maximum length of retroviral vector in this study, re-design of anti-CEA CAR construct in a lentiviral vector which can carry more transgenic payloads could be a strategy to improve transduction efficiency. Lentiviral vectors have the advantage of infecting both dividing and non-dividing cells through nuclear pore complexes, whilst γ-retroviral vectors can only infect actively dividing cells as they can only cross the nuclear envelope during mitosis. Moreover, altering the vector for better CAR expression would presumably give increased number of CARs and NFAT-responsive promoters per cell and, therefore, increased levels of inducible IL-12 upon CEA recognition. Once transduction

efficiency has been significantly improved, a dose-escalation schedule could be performed to determine which dose of CAR-T cells secreting inducibly IL-12 would achieve anti-tumour efficacy without causing unacceptable toxicity.

With regards to *in vitro* anti-tumour function, there was significant difference in IFN-γ production between inducible-IL-12-secreting CAR-T cells and non-IL-12-secreting CAR-T cells (Figure 5.5). This suggests that the inducible expression of IL-12 upon CAR-triggered cell activation, albeit at low levels, could enhance anti-tumour effects of CAR-T cells *in vitro*. However, the improvement in cytotoxicity by inducible IL-12 was only seen in one of two donors (Figure 5.6). In the other donor, no significant difference in cytotoxicity was thought to be due to a higher proportion of non-transduced T cells as discussed in section 5.2.3. To further demonstrate whether inducible IL-12 expression could also enhance CEA-specific cytotoxicity of CAR-T cells, more donors are needed for investigation.

A previous study showed that subcutaneous co-injection of first-generation CEA-specific CAR-T cells inducibly secreting IL-12 and tumour cells could efficiently eradicate tumour without pre-conditioning *in vivo* [153]. Furthermore, first-generation CEA-specific CAR-T cells inducibly secreting IL-12 significantly prevented the growth of CEA^+ and CEA^- mixed MC38 tumour lesion in comparison to CEA^- subcutaneous tumour lesion. The regression of CEA^- tumours was accompanied by accumulation of activated macrophages and elevated levels of TNF-α, although tumour volume still reached 1,000 mm^3 and no long-term survival was revealed. These findings formed the basis of the rationale for this work that further modification of anti-CEA CAR-T cells with a co-stimulatory signalling domain and inducible IL-12 expression might be able to achieve better anti-tumour efficacy and even reach long term survival in subcutaneous tumour model.

In this study, however, a single dose of 2 x 10^6 CD28z.NFAT.mIL12 CAR-T cells did not show anti-tumour efficacy for CEA^+ MC38 tumours in CEAtg mouse model without lymphodepletion pre-conditioning. In contrast, a recent study reported that 1 - 2 x 10^6 murine glypican-3 (GPC3)-specific CD28-CD3ζ CAR-T cells inducibly secreting IL-12 could efficiently eradicate subcutaneous tumours and did not show obvious toxicity in immunocompetent C57BL/6 hosts without lymphodepletion pre-conditioning, with the elevated levels of IFN-γ and IL-12 in serum and significant CAR-T cell infiltration in tumours [251]. Whilst both studies assessed murine CAR-T cells targeting human antigen at similar cell dose in immunocompetent C57BL/6 mouse model, several factors, such as the antigens targeted, CAR constructs, may contribute to the difference in anti-tumour efficacy between the studies. Most importantly, the efficacy of inducible-IL-12-secreting CAR-T cells heavily depends on whether these CAR-T cells infiltrated into tumours and

inducible IL-12 production reached sufficient levels that could efficiently improve anti-tumour responses of CAR-T cells. To further confirm this, assessment of CAR-T cell persistence in blood and their infiltration in tumours are needed. Additionally, the level of IFN-γ production in serum should be measured to reflect whether anti-CEA CAR-T cells could recognise CEA^+ MC38 tumour cells *in vivo*. For future experiments, administration of higher cell doses could be a strategy to further investigate the therapeutic effects of inducible-IL-12-secreting CAR-T cells if transduction efficiency was improved.

To assess the on-target off-tumour toxicity of anti-CEA CAR-T cells, CEAtg mice with tissue-specific CEA expression was utilised as an *in vivo* model. A previous study has shown that therapy with 1 x 10^7 anti-CEA CD28-CD3ζ CAR-T cells via i.v. injection did not induce autoimmune pathology in the CEAtg mouse model, whilst infiltration of CAR-T cells was observed in CEA^+ tissues such as the gastrointestinal tract and the lung [166]. Chemotherapy pre-conditioning did not favour autoimmune pathology. In this study, similarly, severe morbidity and mortality were not observed in all CEAtg mice in the therapy of 2 x 10^6 CD28z.mIL12 and CD28z.NFAT.mIL12 CAR-T cells without TBI pre-conditioning, or in the therapy of CD28z CAR-T cells with TBI pre-conditioning. This suggests that anti-CEA CAR-T cells presumably did not induce on-target off-tumour toxicity in the CEAtg mouse model. However histopathologic analysis of various tissues in CEAtg mice is required to confirm this.

In combination with host lymphodepletion via 5Gy TBI, however, severe mortality of mice with high levels of IL-12 in serum was observed post infusion of either 0.3 x 10^6 or 2 x 10^6 CD28z.mIL12 CAR-T cells in CEAtg model. This observation is in line with other reports studying CAR-T cells constitutively secreting IL-12 in lymphodepleted hosts [157, 194, 208]. Whilst further reducing cell number could be a strategy to minimise the toxicity caused by constitutive expression of IL-12, the corresponding anti-tumour efficacy was probably compromised. Local delivery of IL-12 expressed in an inducible manner in tumour site offers an alternative to overcome this obstacle.

In this study, pre-conditioned mice treated with 2 x 10^6 CD28z.NFAT.mIL12 CAR-T cells also had observable toxicities. Given that significant survival advantage for lymphodepleted mice receiving CD28z T cells was observed in comparison to that receiving CD28z.NFAT.mIL12 T cells, this toxicities were probably associated with inducible expression of IL-12. However, the level of IL-12 in serum was not detectable in CD28z.NFAT.mIL12 CAR-T cells post infusion. Furthermore, whilst neutropenia was one of the common hematologic toxicities in IL-12 therapy [192, 252], it is difficult to determine whether the reduction of neutrophils was caused by IL-12 in this study, due to the

lymphodepletion effects of 5Gy TBI. The mechanisms underlying IL-12-related toxicity induced by CD28z.NFAT.mIL12 CAR-T cells remain unknown. It has been reported that the toxicity of IL-12 also correlated to the secondary production of IFN-γ [192, 253]. It is therefore worth evaluating whether serum IFN-γ levels were increased in lymphodepleted mice treated with CD28z.NFAT.mIL12 CAR-T cells in future studies.

As no toxicity was observed in non-lymphodepleted mice treated with CD28z.NFAT.mIL12 T cells, the use of 5Gy TBI for lymphodepletion prior to CAR-T cell therapy seemed to be one of the factors that causes the IL-12-mediated toxicity. It was probably caused by improving the engraftment and expansion of adoptively transferred CAR-T cells. To determine this, mCherry-specific qPCR could be performed to compare the level of CAR copy numbers in peripheral blood samples among CAR-T cell therapy groups with or without pre-conditioning. The results in this study suggested that decreasing cell number of CD28z.NFAT.mIL12 T cells is required to assess therapeutic effects and minimise IL-12-related toxicity when host lymphodepletion is given.

A previous study demonstrated that T cells engineered with anti–VEGFR-2 CAR and inducible IL-12 mediated long-term tumour regressions at all doses from 1 – 12 x 10^6 in lymphodepleted hosts bearing subcutaneous B16 tumour, associated with enhanced expansion, persistence and infiltration of transferred T cells [208]. Most importantly, there were no dose-limiting toxicities determined by body weight loss and histopathologic analysis of normal tissues. The immunohistochemical results revealed that VEGFR-2 expression was restricted to tumour vascular endothelial cells but not on B16 tumour cells in subcutaneous B16 melanoma [224]. It is therefore hypothesised that higher density of target antigen for CAR-T cell activation in tumour lesions likely correlates to higher levels of inducible IL-12 production, increasing the risk of IL-12-related toxicity.

The main limitations in this study are that CEA expression and CAR-T cell infiltration in tumours was not investigated by performing IHC. The presence of CEA and the level of CAR-T cell infiltration largely contributes to inducible IL-12 production, which subsequently affect the anti-tumour efficacy of inducible-IL-12-secreting CAR-T cells and even IL-12-related toxicity observed in lymphodepleted mice. Confirmation of the level of infiltrated CAR-T cells and CEA expressed on tumours would be greatly helpful to understand the findings mentioned above. Additionally, more information would have been provided if the level of serum IFN-γ was measured. However, the volume of serum collected from blood samples via tail veins was limited. It was difficult to measure both IL-12 and IFN-γ production in serum by ELISA. Most importantly, sufficient mouse numbers for assessment of CAR-T cell therapy is needed to make the findings more convincing in this study.

In summary, the results shown in this chapter revealed that first- and second- generation CEA-specific CAR-T cells with inducible IL-12 expression have successfully been generated. The induction of IL-12 release could be triggered by activation of T cells through CAR engagement with target antigen or PMA/ionomycin stimulation. IL-12 expressed in an inducible manner could improve anti-tumour functions of CEA-specific CAR-T cells *in vitro*. However, administration of 2 x 10^6 CD28z.NFAT.mIL12 CAR-T cells alone failed to show any therapeutic benefit for subcutaneous CEA^+ MC38 tumour in the CEAtg mouse model. In combination with TBI pre-conditioning, lethal toxicity was observed in CD28z.NFAT.mIL12 CAR-T cell therapy. It appears to be associated with IL-12, although serum levels of IL-12 were not increased. Additionally, anti-CEA CAR-T cells did not induce apparent on-target off-tumour toxicity. To better understand the unsatisfactory efficacy and IL-12-related toxicity of CD28z.NFAT.mIL12 CAR-T cell therapy, evaluation of CEA expression on tumours, CAR-T cell infiltration and persistence and the level of IFN-γ in serum should be performed in future studies. Moreover, future work should focus on improving transduction efficiency of inducible-IL-12-secreting CAR-T cells, perhaps through the use of lentiviral vectors [250]. It is also worth applying a dose-escalation schedule for anti-CEA CAR-T cells with inducible IL-12 expression to assess their therapeutic window, which shows the highest anti-tumour efficacy without causing unacceptable toxicity.

6 Construction and characterisation of anti-CEA CAR-T cells secreting scFv

6.1 Introduction

6.1.1 Blockade of TGF-β signalling

As described in section 1.2.3, TGF-β acts as either a tumour suppressor or a tumour promoter during carcinogenesis. In early stages, TGF-β suppresses proliferation and induces apoptosis of normal epithelial and lymphoid cells from which most tumours arise [254]. However, in advanced stages, tumour cells can evade growth inhibitory effects of TGF-β by mutation and/or functional inactivation in the TGF-β receptors (TGF-βRI and TGF-βRII) and/or downstream Smad signalling proteins [255], while leaving intact TGF-β-mediated cellular signalling that promote tumour progression and metastasis. TGF-β, which is overexpressed in various tumour types, can promote epithelial-to-mesenchymal transition (EMT), contribute to the formation of CAFs, upregulate the synthesis of many ECM proteins and induce tumour angiogenesis [256]. TGF-β also mediates immunosuppressive effects on all arms of the immune system due to the antagonistic functions in various immune cells, which leads to compromised tumour cell recognition and clearance [257]. For instance, high levels of TGF-β in the tumour microenvironment suppress T cell proliferation and reduce T cell effector function. It also inhibits the differentiation of T helper cells and instead stimulates the differentiation of immune-suppressive Tregs. Additionally, TGF-β induces the polarisation of macrophages and neutrophils into the pro-tumour M2 and N2 phenotype respectively and inhibits the maturation of DCs and NK cells [258-260]. It is evident that increased production of TGF-β is correlated with advanced metastasis and poor patient prognosis for breast cancer, gastric cancer and hepatocellular carcinoma [261].

Given the crucial role of TGF-β on the immunosuppressive tumour microenvironment, targeting TGF-β signalling has been used in CAR-T cell treatment as a therapeutic strategy to modify the tumour microenvironment and thus enhance their anti-tumour effects for advanced solid tumours. For example, the dominant-negative TGF-βRII (dnTGF-βRII), which is a truncated receptor binding TGF-β without downstream signalling, has been introduced to CAR-T cells. This design can block the active TGF-βRII from binding TGF-β, thus counteracting effects of TGF-β specifically in T cells. It has been demonstrated that modification of CAR-T cells targeting PSMA to express the dnTGF-βRII can significantly

enhance infiltration, proliferation, persistence and efficacy of CAR-T cells in the presence of TGF-β [145]. Based on these promising preclinical results, a phase I clinical trial has been initiated to evaluate the safety and preliminary efficacy of PSMA-directed/TGFβ-insensitive CAR-T cells in patients with refractory castration-resistant metastatic prostate cancer (NCT03089203). However, as it has been reported that dnTGF-βRII T cell transgenic mice experienced severe lymphoproliferative disorder which showed enlarged spleen and lymph nodes (LNs) and moderate infiltration of lymphocytes in other organs [262], the potential risk in clinical trials still needs to be assessed. Additionally, a recent study reported that a CAR was constructed to target TGF-β and activate the modified T cells through CD28-CD3ζ signalling, which therefore not only inhibits the immunosuppressive signalling of TGF-β but also converts this cytokine into a potent T cell stimulant [146]. TGF-β CAR-T cells could proliferate remarkably and secret pro-inflammatory Th1 cytokines in response to TGF-β *in vitro*. Most importantly, this strategy also has the advantage to protect neighbouring immune cells from TGF-β-mediated suppressive effects [263]. Specifically, TGF-β CAR-T cells enabled tumour-targeted $CD8^+$ T cells to maintain their cytolytic activities and prevented $CD4^+$ T cells from TGF-β-induced Treg differentiation *in vitro*.

6.1.2 Blockade of PD-1 signalling

Given their remarkable clinical responses, the addition of PD-1 or PD-L1 inhibitors in CAR-T cell therapy are a logical approach to augment the potency of CAR-T cells especially in solid tumours. It has been shown that the PD-1-blocking antibodies enhanced *in vitro* T cell proliferation and cytokine secretion and *in vivo* tumour regression of CAR-T cells targeting HER2, mesothelin or IL-13Rα2 in pre-clinical studies [144, 264, 265]. At present, several clinical trials are exploring the combination therapy of immune checkpoint inhibitors and CAR-T cells for the treatment of diffuse large B cell lymphoma (NCT02706405, NCT02926833, NCT02650999), mesothelioma (NCT02414269) and glioblastoma (NCT03726515, NCT04003649). Notably, systemic administration of immune checkpoints inhibitors could induce systemic autoimmune side effects, such as dermatologic toxicities, diarrhea/colitis and pneumonitis [151, 266]. The combination with CAR-T cell therapy may greatly exacerbate the autoreactive toxicity. To reduce the possible toxicities associated with systemic checkpoint inhibition, modification of CAR-T cells to secrete scFv blocking PD-1 or PD-L1 have been developed, which may have the advantage of mostly accumulating the secreted scFv within tumour sites.

Success with this approach has been observed in multiple experimental models. Anti-carbonic anhydrase IX (CAIX) CAR-T cells engineered to secrete anti-PD-L1 scFv have

improved anti-tumour activity in an orthotopic model of human renal cell carcinoma [267]. Anti-CD19 CAR-T cells that secrete anti-PD-1 scFv could efficiently eradicate subcutaneous tumour established in xenograft mouse models [143]. It has also been reported that anti-CD19 or anti-MUC16^{ecto} CAR-T cells secreting PD-1-blocking scFv could enhance the survival of mice in syngeneic and xenogeneic PD-L1^{+} hematologic and solid tumour models, showing similar or better efficacy compared to that achieved by combination therapy [268]. Several clinical trials have been initiated to investigate the safety and effectiveness of CAR-T cells secreting anti-PD-1 scFv for the treatment of EGFR positive advanced solid malignancies (NCT02873390 and NCT03182816).

Other strategies have also been developed to induce resistance to PD-1 signalling for CAR-T cells. For instance, a study reported that the expression of a PD-1 dominant negative receptor on anti-mesothelin CAR-T cells, which competed for PD-L1/PD-L2 with the endogenous PD-1 receptor, could restore effector functions of CAR-T cells *in vitro* and *in vivo* [144]. In the chimeric switch-receptor approach, CAR was constructed by fusing the extracellular domain of PD-1 with the transmembrane and intracellular domains of co-stimulatory molecules, which aims to turn the inhibitory signal into a positive co-stimulatory signal for anti-tumour activity of T cells. T cells engineered with PD-1: CD28 receptors showed the improvement of anti-tumour efficacy in a murine pancreatic tumour model [147]. Furthermore, genome-editing strategies to knock out PD-1 in CAR-T cells via CRISPR/Cas9 technology exhibited improved cytotoxic activity *in vitro* and cleared subcutaneous CD19^{+} PD-L1^{+} tumour in xenograft mouse models [139].

6.1.3 Hypothesis and aims

Approaches blocking TGF-β or PD-1 signalling have both been reported to improve effector functions of CAR-T cells *in vitro* and *in vivo* as described above. It is therefore hypothesised that the anti-tumour efficacy of CEA-specific CAR-T cells could be improved by inhibiting the immunosuppressive effects mediated by TGF-β or PD-1. This can be achieved by engineering CAR-T cells to constitutively secrete anti-TGF-β (αTGF-β) or anti-PD-1 (αPD-1) scFv. Therefore, the main aims of this chapter were:

- To generate retroviral vectors containing first- or second- generation anti-CEA CAR constructs and αTGF-β or αPD-1 scFv expression cassette
- To assess the production and binding capacity of αTGF-β or αPD-1 scFv
- To evaluate whether the level of cytotoxicity and cytokine release of scFv-secreting CAR-T cells was better than non-scFv-secreting CAR-T cells *in vitro*

- To evaluate whether anti-tumour efficacy of CAR-T cells could be enhanced by secreting αTGF-β or αPD-1 scFv in combination with host lymphodepletion pre-conditioning *in vivo*
- To assess whether any toxicity was observed in the therapy of scFv-secreting CAR-T cells
- To investigate whether the level of T cell infiltration in tumour lesions was improved in the therapy of scFv-secreting CAR-T cells

6.2 Results

6.2.1 Generation of retroviral vectors encoding scFv-expressing anti-CEA CAR

Target tumour cell lines were measured for the level of TGF-β production and PD-L1 expression by flow cytometry. Both CEA^+ MC38 cells and parental MC38 cells showed high levels of intracellular TGF-β production, which was 99.4 ± 0.7 % and 99.2 ± 1.1 % respectively (Figure 6.1 A & B). PD-L1 was also highly expressed on these cell lines (99.5 ± 0.6 %, 98.1 ± 1.3 %), without the need for additional IFN-γ stimulation to induce PD-L1 expression (Figure 6.1 C & D). The abundant expression of TGF-β and PD-L1 represents clinically relevant mechanisms of immune suppression mediated by PD-1 and TGF-β signalling. Therefore, these tumour cell lines were used as model to assess whether CAR-T cell secretion of scFv to block TGF-β or PD-1 signalling could improve the anti-tumour efficacy of CEA-specific CAR-T cells.

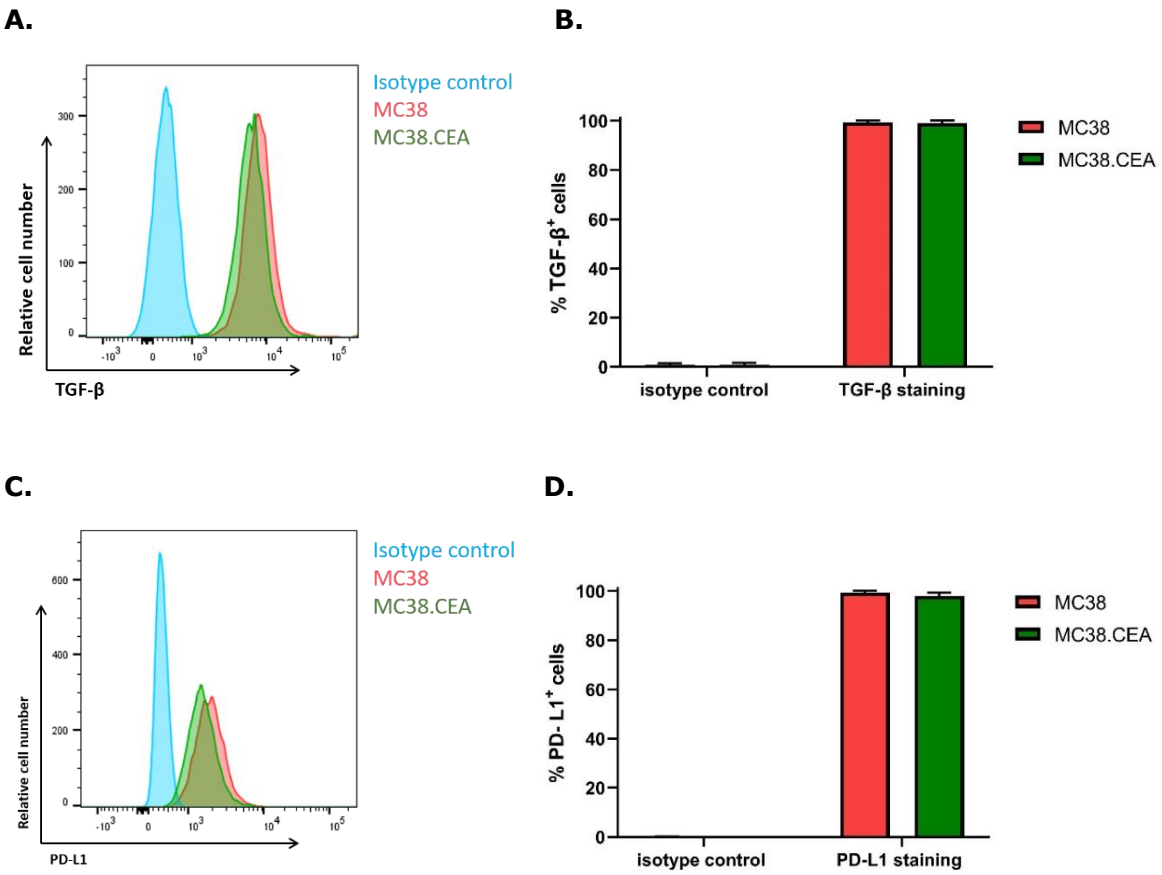

Figure 6.1 TGF-β and PD-L1 expression of target tumour cell lines

(A) Representative histogram is shown for intracellular TGF-β expression of MC38 and CEA$^+$ MC38 cell lines. **(B)** The percentage of TGF-β$^+$ cells is plotted as mean ± SD of two independent experiments determined by flow cytometry. **(C)** Representative histogram is shown for surface PD-L1 expression of MC38 and CEA$^+$ MC38 cell lines. **(D)** The percentage of PD-L1$^+$ cells is plotted as mean ± SD of two independent experiments by flow cytometry. The isotype antibody staining was used as negative control.

The schematic diagram of MP71 retroviral vectors containing CAR constructs and the αTGF-β scFv expression cassette is shown in Figure 6.2 A. Utilising a P2A cleavage element, the first- and second- generation anti-CEA CAR constructs were further modified to express a histidine (his)-tagged αTGF-β scFv, designated as MFE.mCD3z.TA, MFE.mCD28z.TA. The αTGF-β scFv is derived from variable heavy and light chains from anti-human monoclonal antibody fresolimumab (also known as GC1008), which neutralizes all isoforms of TGF-β [269]. The same strategy was used to construct the vectors encoding CAR constructs and the αPD-1 scFv derived from hamster anti-mouse mAb J43 [270], designated as MFE.mCD3z.PA, MFE.mCD28z.PA (Figure 6.2 B). Additionally, a mouse IgG1 CH2-CH3 sequence was inserted downstream of both αTGF-β and αPD-1 scFv sequence linked by a hinge fragment, designated as MFE.mCD3z.DTA, MFE.mCD28z.DTA, MFE.mCD3z.DPA and MFE.mCD28z.DPA, providing interaction sites for homodimer formation of scFv-Fc molecules (Figure 6.2 C). The scFv-Fc format has several advantages over monomer scFv including bivalent binding, longer half-life and Fc-mediated effector functions [271]. The αTGF-β or αPD-1 scFv and CH2-CH3 sequence were synthesised by Thermo Fisher Scientific.

A.

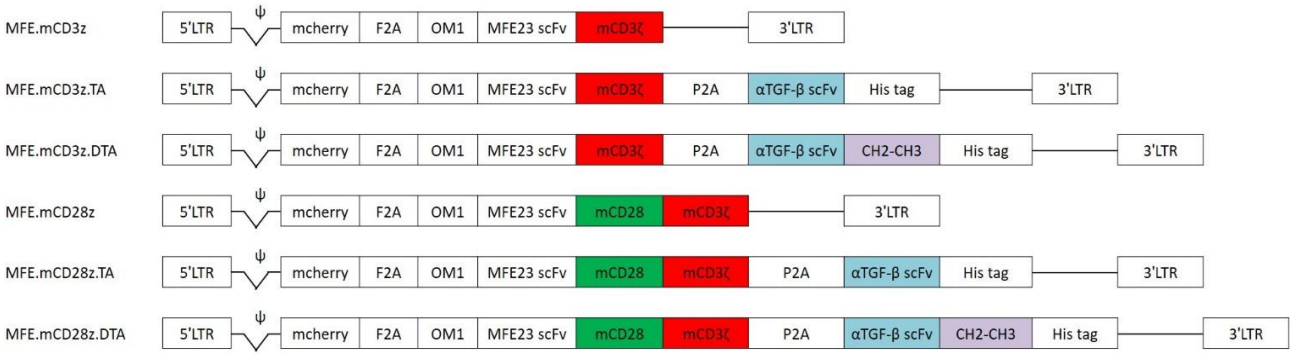

B.

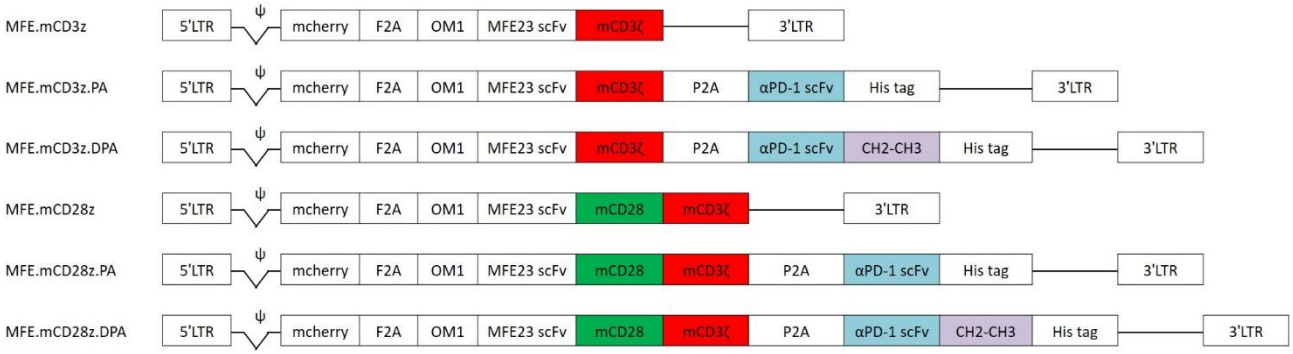

C.

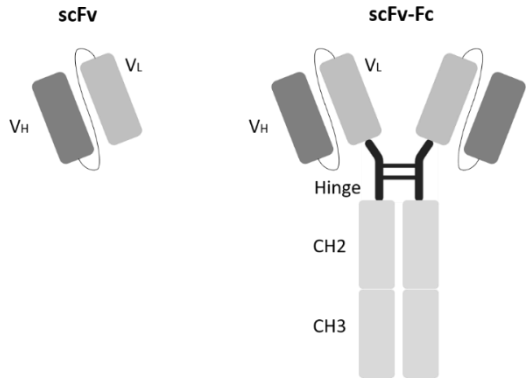

Figure 6.2 Schematic diagram of retroviral vectors encoding anti-CEA CAR constructs and scFv expression cassette

On the basis of the first- and second- generation anti-CEA CAR constructs, **(A)** αTGF-β scFv or **(B)** αPD-1 scFv sequence was placed downstream of the CAR via a P2A linker. The mouse IgG1 hinge and CH2-CH3 sequence were further inserted downstream of the scFv sequence to allow dimerization as scFv-Fc format. A histidine (his)-tag was included for the detection of scFv or scFv-Fc. **(C)** Schematic representation of the scFv and scFv-Fc antibodies. The scFv-Fc form a homodimer through two disulfide bonds in the hinge domain. (V_L, variable light chain; V_H, variable heavy chain; CH2, mouse IgG1 heavy chain constant domain 2; CH3, mouse IgG1 heavy chain constant domain 3).

The construction strategy for MFE.mCD3z.TA and MFE.mCD3z.DTA vectors is shown in Figure 6.3 A. The retroviral vectors encoding the first-generation anti-mouse CD19 CAR constructs and αTGF-β scFv expression cassette, designated as 1D3.mCD3z.TA and 1D3.mCD3z.DTA, were used as backbone vectors. By replacing the 1D3 sequence, the MFE23 sequence fragment from MFE.mCD3z vector was cloned into BsrGI/NotI sites of backbone vectors to generate MFE.mCD3z.TA and MFE.mCD3z.DTA (Figure 6.3 B). Following this, the MFE.mCD28z.TA and MFE.mCD28z.DTA vectors were constructed by replacing mCD3ζ sequence from MFE.mCD3z.TA and MFE.mCD3z.DTA with mCD28.mCD3ζ sequence from MFE.mCD28z vector as SbfI, SbfI fragment (Figure 6.3 C).

A.

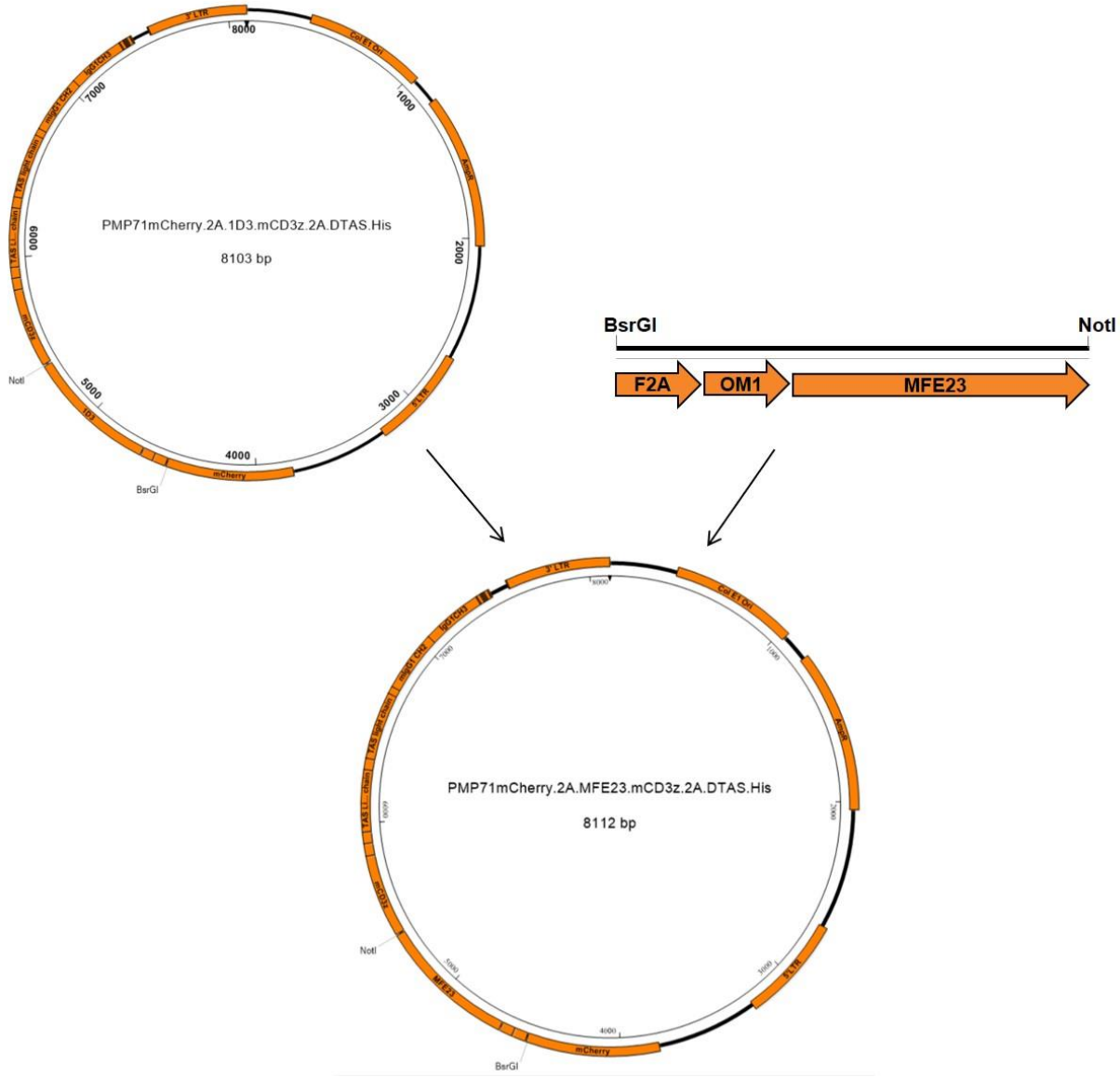
PMP71mCherry.2A.1D3.mCD3z.2A.DTAS.His
8103 bp
BsrGI
NotI
F2A
OM1
MFE23
PMP71mCherry.2A.MFE23.mCD3z.2A.DTAS.His
8112 bp

B.

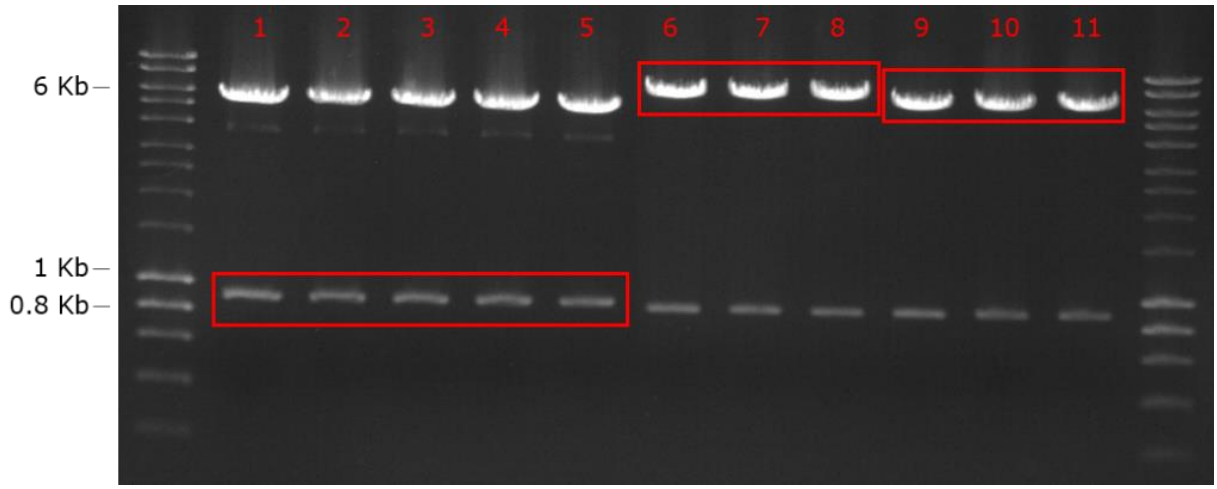
1
2
3
4
5
6
7
8
9
10
11
6 Kb
1 Kb
0.8 Kb

C.

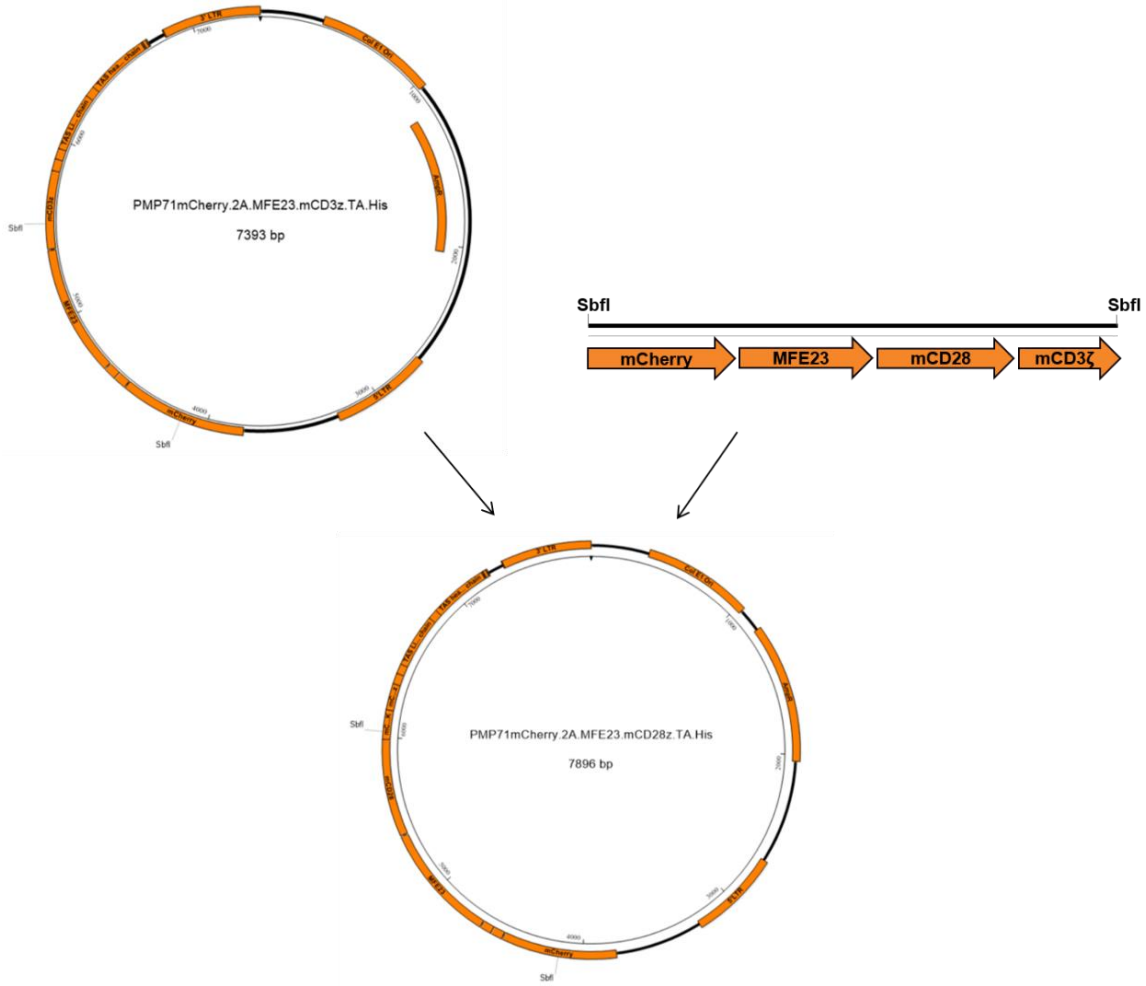

Figure 6.3 Generation of retroviral vectors encoding anti-CEA CAR constructs and αTGF-β scFv expression cassette

(A) Overview of cloning strategies for generation of either MFE.mCD3z.TA or MFE.mCD3z.DTA plasmid. **(B)** Agarose gel electrophoresis of backbone 1D3.mCD3z.TA and 1D3.mCD3z.DTA and target MFE23 DNA fragments. The DNA samples were digested with BsrGI, NotI restriction enzymes. Lane 1 - 5 shows the MFE23 insert from the vector MFE.mCD3z at ~0.9 kb; Lane 6 - 8 shows the mCD3z.DTA backbone from the vector 1D3.mCD3z.DTA at ~7.2 kb; Lane 9 - 11 shows the mCD3z.TA backbone from the vector 1D3.mCD3z.TA at ~6.5 kb. **(C)** Overview of cloning strategies for generation of either MFE.mCD28z.TA or MFE.mCD28z.DTA plasmid.

To generate MFE.mCD3z.PA and MFE.mCD3z.DPA vectors, the mCD3z.PA sequence and mCD3z.DPA sequence were cut out of the intermediate pMK-RQ vectors with NotI, NheI restriction enzymes respectively to replace the mCD3z sequence in MFE.mCD3z vector (Figure 6.4 A & B). Similarly, the MFE.mCD28z.PA and MFE.mCD28z.DPA vectors were constructed by inserting the mCD3z.PA sequence and mCD3z.DPA sequence respectively into BamHI/NheI sites of the backbone vector MFE.mCD28z (Figure 6.4 C).

Confirmation of successful ligation of the vectors was performed by Sanger DNA sequencing of samples. Primers for detecting MFE23, CD3z, CD28z, αPD-1 or αTGF-β scFv and CH2CH3 sequences are shown in Table 3.1 in Chapter 3.

A.

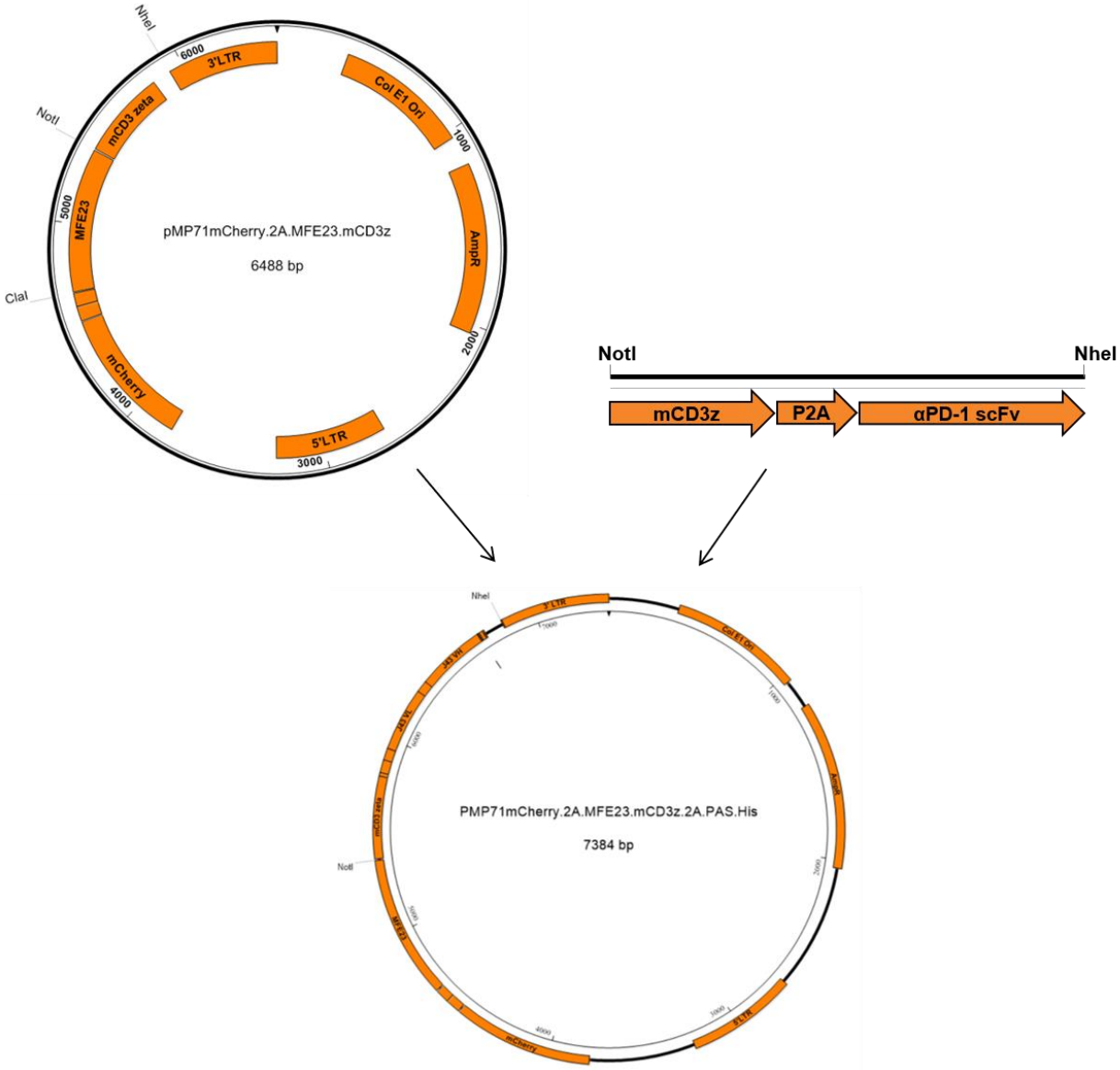
NheI
NotI
ClaI
6000
3'LTR
Col E1 Ori
1000
mCD3 zeta
5000
MFE23
pMP71mCherry.2A.MFE23.mCD3z
6488 bp
AmpR
2000
mCherry
4000
5'LTR
3000
NotI
NheI
mCD3z
P2A
αPD-1 scFv
PMP71mCherry.2A.MFE23.mCD3z.2A.PAS.His
7384 bp

B.

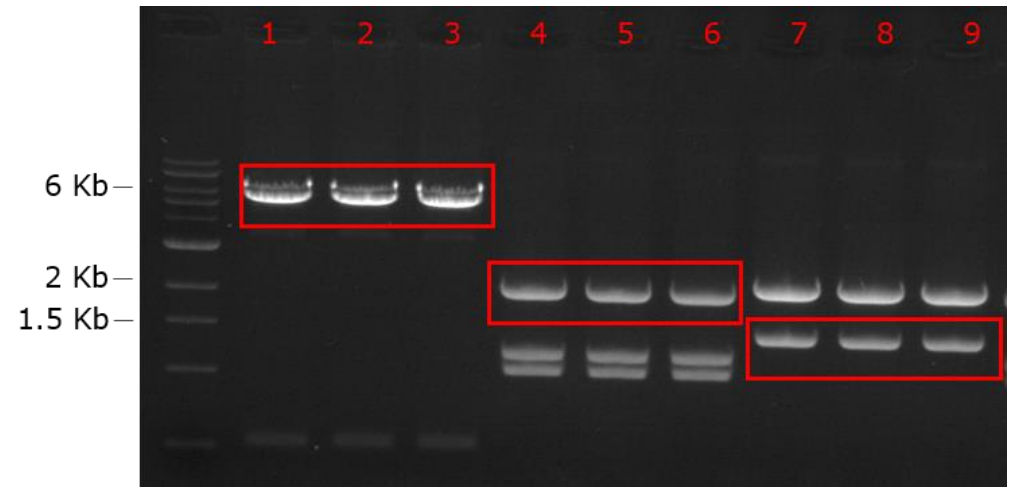
1
2
3
4
5
6
7
8
9
6 Kb
2 Kb
1.5 Kb

C.

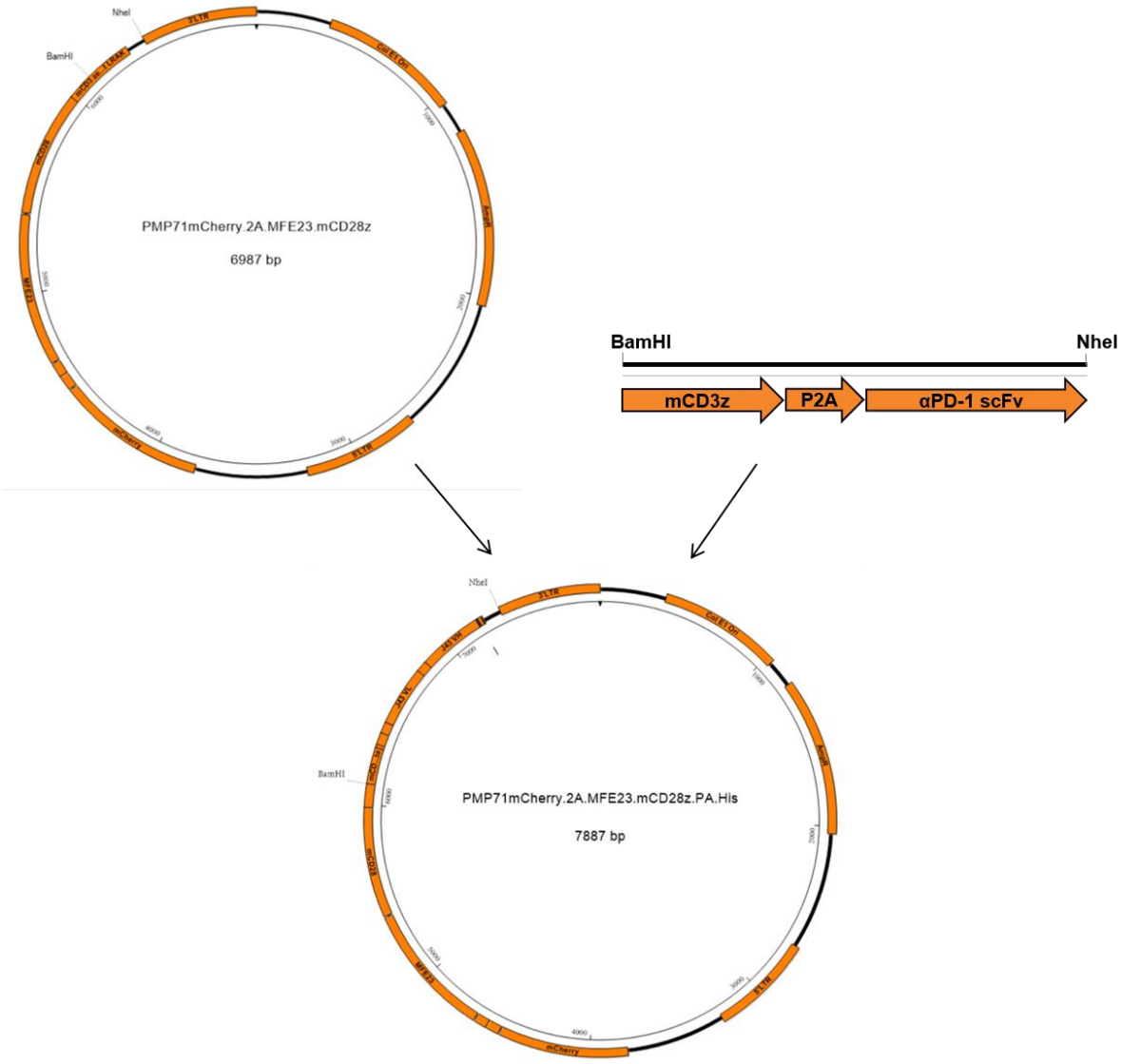

Figure 6.4 Generation of retroviral vectors encoding anti-CEA CAR constructs and αPD-1 scFv expression cassette

(A) Overview of cloning strategies for generation of either MFE.mCD3z.PA or MFE.mCD3z.DPA plasmid. **(B)** Agarose gel electrophoresis of backbone vector MFE.mCD3z and target mCD3z.PA and mCD3z.DPA DNA fragments. The DNA samples were digested with NotI, NheI restriction enzymes. Lane 1 - 3 shows the MFE23 backbone from the vector MFE23.mCD3z at ~6 kb; Lane 4 - 6 shows the mCD3z.DPA insert from the intermediate pMK-RQ vector at ~2.1 kb. Its backbone fragment was additionally digested by NcoI enzymes to distinguish from the desired insert due to the similar DNA size. Lane 7 - 9 shows the mCD3z.PA insert from the intermediate pMK-RQ vector at ~1.4 kb. **(C)** Overview of cloning strategies for generation of either MFE.mCD28z.PA or MFE.mCD28z.DPA plasmid.

6.2.2 Expression and binding capacity of scFv and scFv-Fc

To assess the secretion of scFv or scFv-Fc molecules, Plat-E cells packaging cells were transfected with the CAR constructs and the supernatant was collected, filtered and further concentrated for Western Blot analysis using anti-His-tag antibody. The supernatant from Plat-E cells transfected with parental non-scFv-expressing CAR constructs was used as negative control. As shown in Figure 6.5, both αTGF-β scFv and αPD-1 scFv (27 kDa) could be successfully detected in denatured supernatant samples from MFE.mCD3z.TA, MFE.mCD28z.TA and MFE.mCD3z.PA, MFE.mCD28z.PA Plat-E cells respectively. In terms of samples from MFE.mCD3z.DTA, MFE.mCD28z.DTA, MFE.mCD3z.DPA and MFE.mCD28z.DPA Plat-E cells, whilst the predicted molecular weight of scFv-Fc is 57 kDa, the actual band appeared at 46 kDa based on the protein ladder. This is possibly due to more hydrophobic interactions between CD2-CH3 domain and SDS resulting in faster migration [272]. Additionally, another weaker band at bigger molecular weight was seen in MFE.mCD3z.DTA and MFE.mCD28z.DTA samples, which was probably because of the incomplete protein denaturation of scFv-Fc. Various amounts of scFv and scFv-Fc were observed among supernatant from Plat-E cells transfected with different CAR constructs, which was likely caused by the difference in the confluence or viability of Plat-E cells and transfection efficiency.

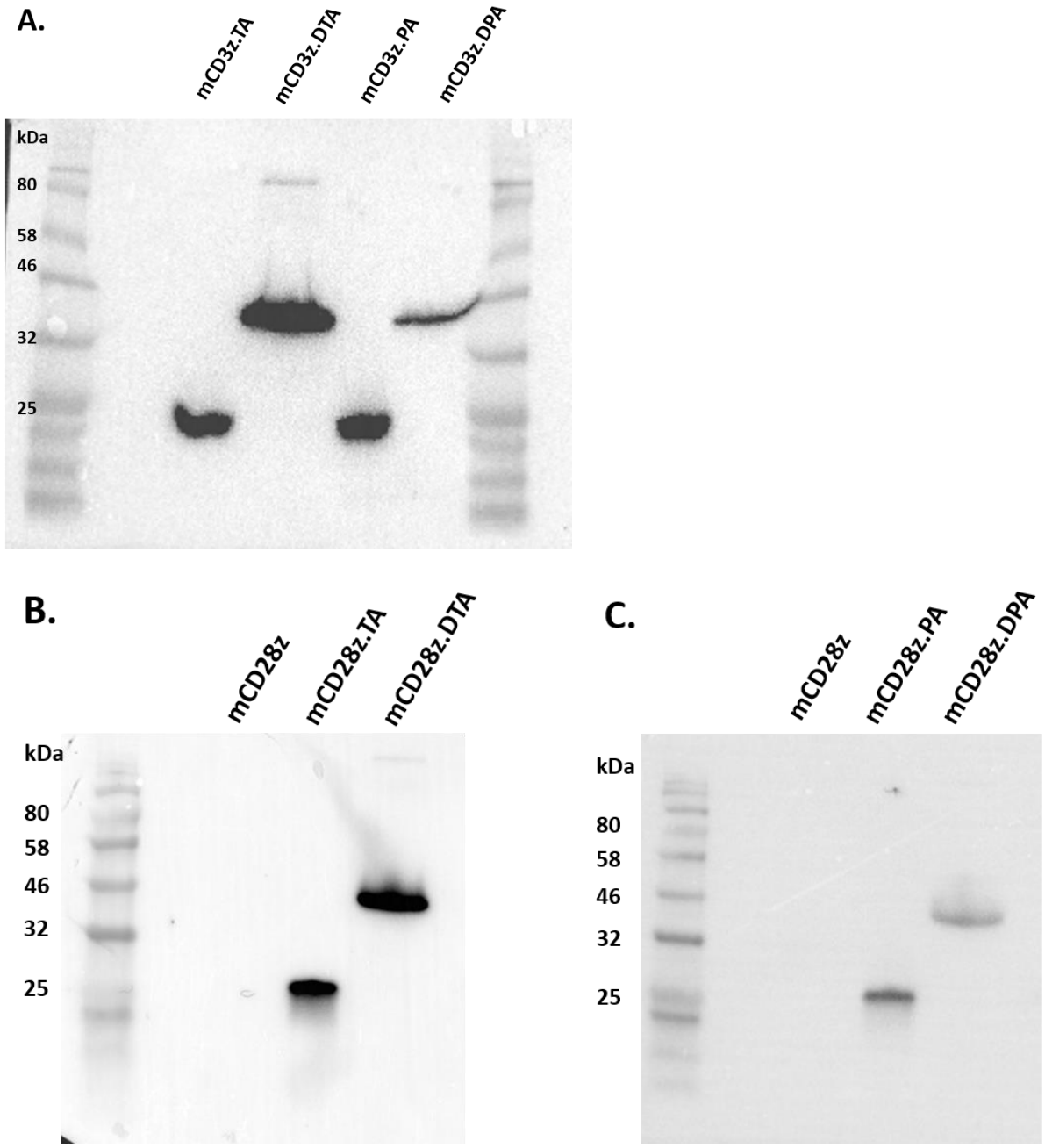

Figure 6.5 Expression of scFv and scFv-Fc targeting TGF-β or PD-1 in the supernatant from transfected Plat-E cells

Plat-E cells were transfected with the indicated CAR constructs: **(A)** MFE.mCD3z.TA, MFE.mCD3z.DTA, MFE.mCD3z.PA, MFE.mCD3z.DPA; **(B)** MFE.mCD28z, MFE.mCD28z.TA, MFE.mCD28z.DTA; **(C)** MFE.mCD28z.PA, MFE.mCD28z.DPA. Expression of scFv and scFv-Fc in the serum-free supernatant was analysed by Western Blot, detected with anti-his-tag antibody. The predicted molecular weight of scFv targeting either TGF-β or PD-1 is 27 kDa, whilst that of scFv-Fc is 57 kDa post protein denaturation.

The binding capacity of secreted αTGF-β scFv and scFv-Fc to TGF-β was assessed by a luciferase assay using reporter plasmids 3TP-Lux (p3TP-Lux) which can be induced to express luciferase by TGF-β signalling. Luciferase activity of Plat-E cells transfected with p3TP-Lux is regulated by TGF-β signalling. The addition of αTGF-β scFv and scFv-Fc, by binding to TGF-β proteins, could inhibit TGF-β signalling required for inducing luciferase expression, which consequently results in the reduction in relative light units (RLU) shown in the luciferase assay.

As shown in Figure 6.6 A, the 293T cells transfected with p3TP-Lux showed an increase in RLU in the presence of TGF-β1 recombinant protein from 2.5 to 20 ng/ml, which indicated that the luciferase activity of transfected 293T cells was efficiently induced by TGF-β1. Following this, transfected 293T cells was co-incubated with TGF-β1 protein and the supernatant from Plat-E cells transfected with indicated CAR constructs. It was seen that the luciferase activity of transfected 293T cells was significantly reduced by MFE.mCD3z.TA and MFE.mCD3z.DTA supernatant which contained scFv and scFv-Fc respectively in comparison with MFE.mCD3z supernatant, in the presence of 2.5, 5, 10, 20 ng/ml of TGF-β ($P < 0.0001$) (Figure 6.6 B). No significant difference in reduction of luciferase activity was seen between αTGF-β scFv and scFv-Fc. These results suggested that both scFv and scFv-Fc secreted had similar ability to bind to TGF-β1 and inhibit TGF-β1-induced luciferase activity.

A.

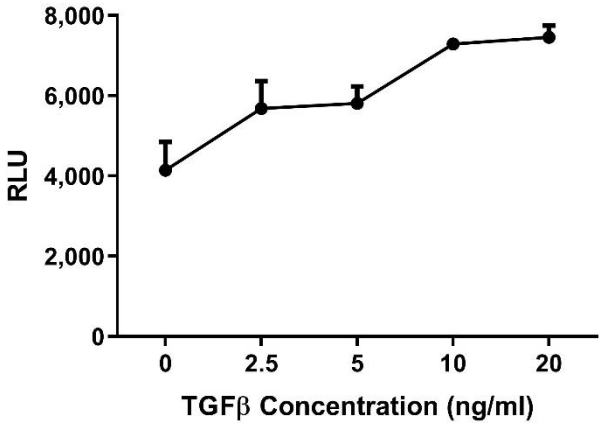

B.

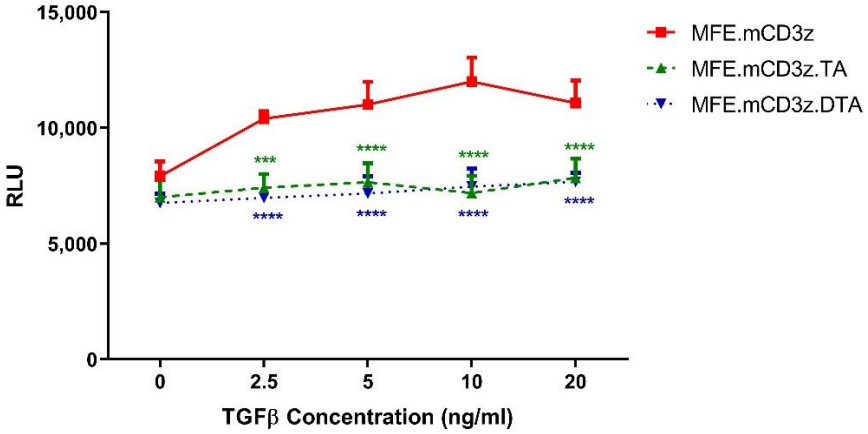

Figure 6.6 Inhibition of TGF-β1-induced luciferase activity by αTGF-β scFv and scFv-Fc

The 293T cells transfected with p3TP-Lux reporter plasmids could express luciferase induced by TGF-β1 recombinant protein. Luciferase activity was measured post 16-hour co-incubation with indicated amounts of TGF-β1 in the absence **(A)** or presence **(B)** of concentrated supernatant from Plat-E cells transfected with indicated CAR constructs. The data are plotted as mean ± SD of triplicates of one experiment. Statistically significant difference was analysed using two-way ANOVA with Tukey's multiple comparisons test. **** $P < 0.0001$. Green or blue stars represent comparison between MFE.mCD3z and MFE.mCD3z.TA or MFE.mCD3z.DTA treatment respectively.

To demonstrate the binding capacity of secreted αPD-1 scFv and scFv-Fc and their ability to block the PD-1/PD-L1 interaction, the level of IFN-γ production was assessed post co-culture of MFE.mCD3z CAR-T cells and CEA-expressing MC38 cells in the presence of filtered supernatant from MFE.mCD3z.PA or MFE.mCD3z.DPA Plat-E cells. As shown in Figure 6.7, MFE.mCD3z CAR-T cells produced significantly higher levels of IFN-γ (13,549.8 ± 2,544.4 pg/ml) compared to mock T cells when co-cultured with CEA^+ MC38 cells ($P < 0.0001$). With the addition of MFE.mCD3z.PA or MFE.mCD3z.DPA supernatant which contained αPD-1 scFv and scFv-Fc respectively, IFN-γ production was further increased (33,400.7 ± 384.0 pg/ml, 42,444.3 ± 3,656.3 pg/ml respectively) ($P < 0.0001$). These results suggested that both secreted αPD-1 scFv and scFv-Fc can bind to PD-1 and inhibit the effects of PD-1 on T cell anergy, which subsequently leads to enhanced IFN-γ production of CAR-T cells in response to CEA-expressing MC38 cells.

It is of note that there was a significant difference between MFE.mCD3z.PA and MFE.mCD3z.DPA supernatant with more IFN-γ produced with addition of the MFE.mCD3z.DPA supernatant ($P < 0.0001$). However, given difference in transfection efficiency between MFE.mCD3z.PA or MFE.mCD3z.DPA Plat-E cells, the amount of scFv and scFv-Fc secreted was probably at various levels in the supernatant. It was difficult to determine whether αPD-1 scFv-Fc mediated better effects compared with monomer scFv.

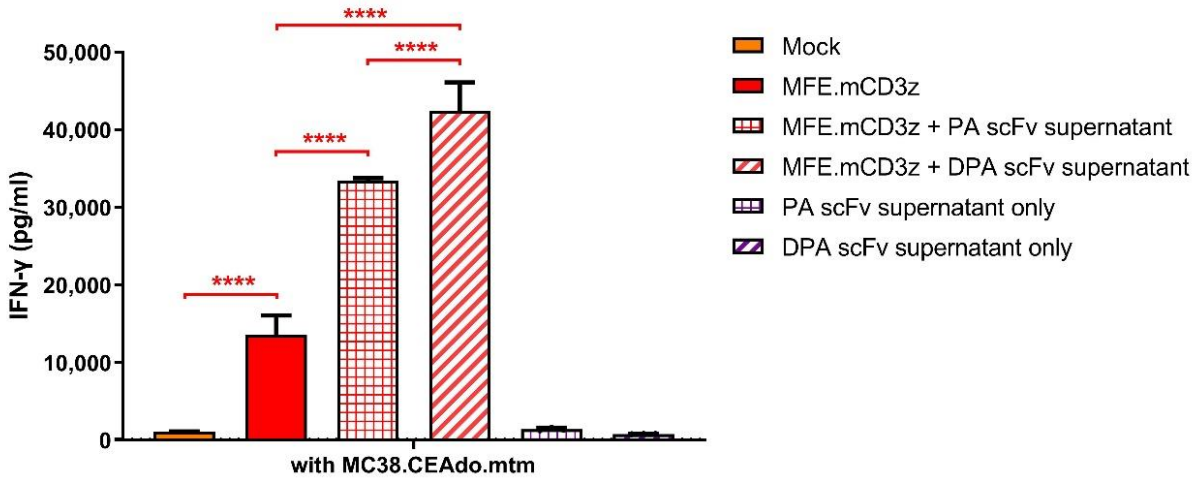

Figure 6.7 IFN-γ production of anti-CEA CAR-T cells treated with supernatant containing αPD-1 scFv and scFv-Fc

MFE.mCD3z CAR-T cells were co-cultured for 20 hours with 2 × 10^4 CEA^+ MC38 cells at E: T ratio of 1: 1 in the absence or presence of filtered supernatant from Plat-E cells transfected with either MFE.mCD3z.PA or MFE.mCD3z.DPA CAR constructs. The co-culture supernatant was collected and measured for IFN-γ production by ELISA. The level of IFN-γ in the culture supernatants from transfected Plat-E cells was also measured to control for IFN-γ in the supernatant. The data are plotted as mean ± SD of triplicates of one experiment. Statistically significant differences were analysed using one-way ANOVA with Tukey's multiple comparisons test. **** $P < 0.0001$. Red stars represent comparison between two treatments.

6.2.3 Generation of anti-CEA CAR-T cells secreting scFv

The effects of monomer scFv targeting TGF-β or PD-1 on anti-tumour efficacy of CAR-T cells were evaluated only due to time limitations. In addition, given that second-generation MFE.mCD28z CAR-T cells have shown better *in vitro* anti-tumour efficacy compared to first-generation CD3z CAR-T cells in section 3.2.5 and 3.2.6, the following studies only focused on MFE.mCD28z CAR-T cells secreting scFv.

CD3/CD28-activated mouse T cells were therefore transduced with MFE.mCD28z, MFE.mCD28z.TA and MFE.mCD28z.PA CAR constructs respectively. Transduction efficiency was determined by the expression of surface marker mCherry on CAR-T cells by flow cytometry. Whilst MFE23.mCD28z CAR-T cells had 35.2 ± 3.5 % mCherry$^+$ T cells, the incorporation of scFv expression cassette resulted in a slight decrease in transduction efficiency, which was 26.0 ± 9.4 % and 22.2 ± 6.0 % for MFE.mCD28z.TA and MFE.mCD28z.PA CAR-T cells respectively, with no significant difference between them (Figure 6.8 A).

The level of PD-1 expression on T cells post transduction was also measured. Compared with mock T cells where 17.1 ± 9.9 % of T cells were PD-1$^+$, an increase was seen in MFE.mCD28z, MFE.mCD28z.TA and MFE.mCD28z.PA CAR-T cells expressing PD-1 which were 42.2 ± 12.0 %, 33.1 ± 11.0 %, 36.9 ± 5.3 % PD-1$^+$ respectively, although this did not reach statistical significance (Figure 6.8 B). Additionally, MFE.mCD28z.PA CAR-T cells, which secreted αPD-1 scFv into the cell culture supernatant, showed similar levels of PD-1 expression to the other CAR-T cells. The antibody clones used for flow cytometry and for αPD-1 scFv were clone 29F.1A12 and clone J43 respectively. It is possible that two antibody clones have different binding sites which allows both the conjugated antibody and scFv to bind to the PD-1 molecule.

A.

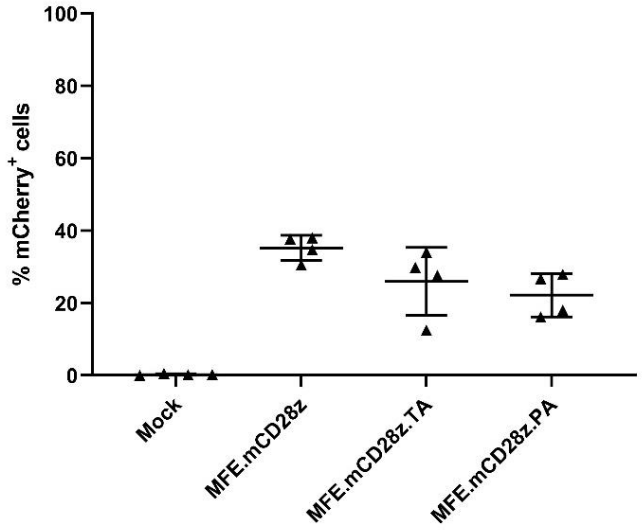

B.

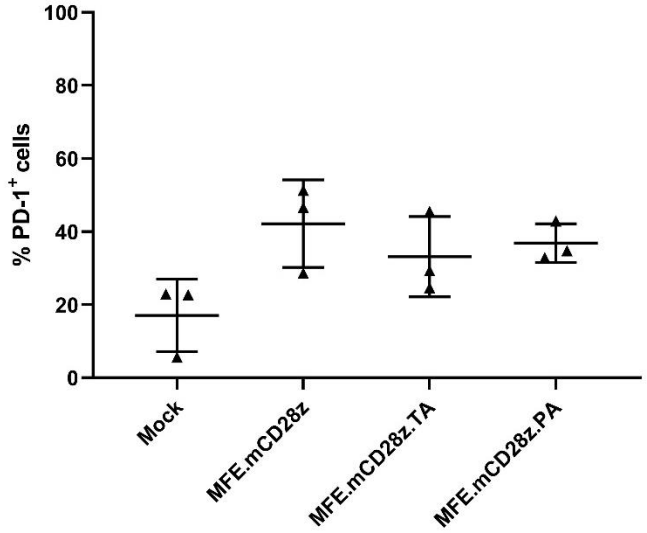

Figure 6.8 mCherry and PD-1 expression of transduced T cells

The detection of mCherry **(A)** and PD-1 **(B)** expression on transduced $CD4^+$ and $CD8^+$ T cells was performed by flow cytometry on day 4-5 post transduction. The data are plotted as mean ± SD of 3 - 4 independent transduction experiments performed. Statistically significant difference was analysed using one-way ANOVA with Tukey's multiple comparisons test.

6.2.4 Evaluation of *in vitro* function of anti-CEA CAR-T cells secreting scFv

The *in vitro* function of CEA-specific CAR-T cells with or without scFv secretion was determined by cytokine release and cytotoxicity post 20-hour co-culture with indicated target cells. Whilst the supernatant was collected post co-culture at E: T ratio of 1: 1 and measured for IFN-γ release by ELISA, the luciferase activity of target cells was examined for CAR-T cell cytotoxicity at various E: T ratios by performing luciferase assays.

As shown in Figure 6.9 A, MFE.mCD28z, MFE.mCD28z.TA and MFE.mCD28z.PA CAR-T cells produced IFN-γ at high levels compared to mock T cells when co-cultured with CEA-expressing MC38 cells. In line with IFN-γ production, CAR-T cells with or without scFv expression also exhibited significant cytotoxicity against luciferase-expressing CEA^+ target cells in comparison with mock T cells at various E: T ratios from 5: 1 to 0.125: 1 ($P < 0.0001$) (Figure 6.9 B). Notably, there was no significant difference in both IFN-γ production and cytotoxicity among MFE.mCD28z, MFE.mCD28z.TA and MFE.mCD28z.PA CAR-T cells. However, the non-concentrated supernatant containing αPD-1 scFv, which was collected post 2-day culture, could enhance IFN-γ production of MFE.mCD3z CAR-T cells in response to CEA^+ MC38 cells in section 6.2.2 (Figure 6.6). It is therefore hypothesised that a 20-hour co-culture period was not sufficient for scFv secretion and accumulation into the supernatant to improve the anti-tumour efficacy of CAR-T cells *in vitro*.

A.

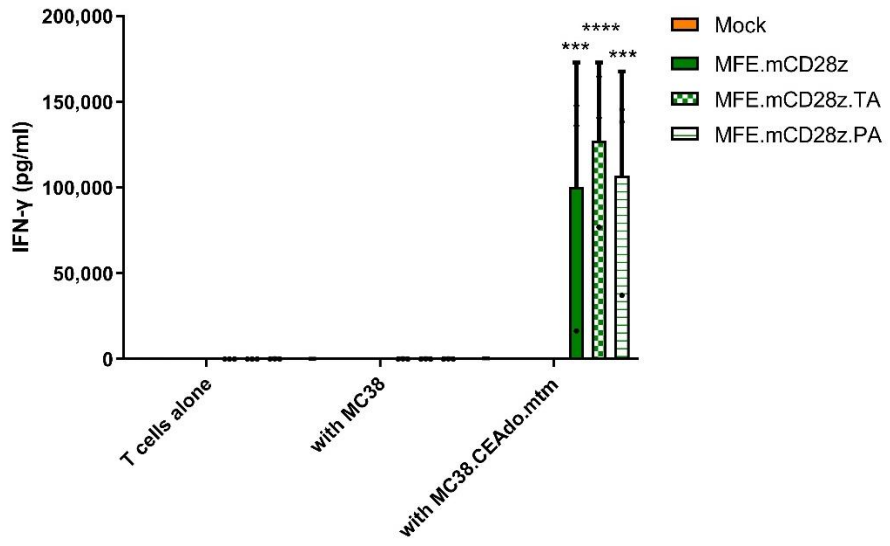

B.

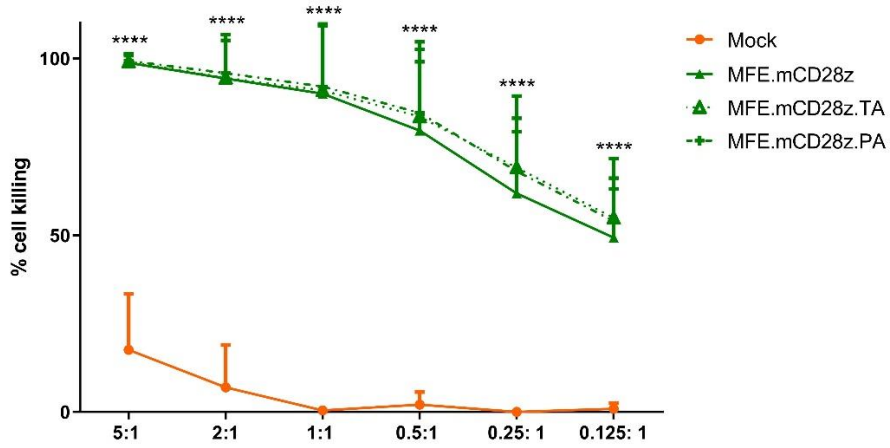

Figure 6.9 Cytokine secretion and cytotoxicity of anti-CEA CAR-T cells secreting scFv *in vitro*

(A) Transduced T cells were co-cultured for 20 hours with 2 × 10^4 CEA^+ MC38 cells and MC38 cells at E: T ratio of 1: 1. The supernatant collected post incubation was measured for IFN-γ production by ELISA. **(B)** Transduced T cells were co-cultured for 20 hours with 2 × 10^4 CEA^+ MC38 cells expressing luciferase and GFP at different E: T ratios from 5: 1 to 0.125: 1. Luminometry was performed to assess the cytotoxicity post co-culture. The data are plotted as mean ± SD of three independent experiments. Statistically significant difference was analysed using two-way ANOVA with Tukey's multiple comparisons test. **** $P < 0.0001$. Black stars represent comparison of each construct co-cultured with CEA^+ MC38 cells and parental MC38 cells (A) or comparison between mock and CAR constructs (B).

6.2.5 Evaluation of *in vivo* function of anti-CEA CAR-T cells secreting scFv

5Gy TBI for host lymphodepletion was utilised to facilitate the engraftment and expansion of CAR-T cells in previous chapters. However, lethal toxicities were observed in all pre-conditioned mice receiving IL-12-secreting CAR-T cells, and some receiving mock T cells or non-IL-12-secreting CAR-T cells in both C57BL/6 WT and CEAtg model. These results indicated that C57BL/6 mice were likely to be sensitive to CEA-specific CAR-T cells or large numbers of total T cells transferred following sublethal 5Gy TBI, showing the need for an alternative method for host lymphodepletion. Apart from radiotherapy pre-conditioning, non-myeloablative chemotherapy pre-conditioning has also been widely applied in preclinical and clinical studies of adoptive cell therapy [168, 273, 274]. Given that the combination of cyclophosphamide and fludarabine chemotherapy increased CAR-T cell expansion and persistence and consequently improved overall response rates in patients compared to the use of cyclophosphamide alone [275], this pre-conditioning approach was therefore utilised in tumour-established CEAtg mouse model in the following studies.

To achieve non-myeloablative lymphodepletion, tumour-bearing mice were treated with 100 mg/Kg cyclophosphamide for 1 day and 100 mg/Kg fludarabine for 2 days following the previous study reported [168]. To determine the lymphodepleting efficiency, blood cell counts were performed for peripheral blood samples collected on day 17, 24 and 32. As shown in Figure 6.10 A, the number of both white blood cells and lymphocytes in mice treated with cyclophosphamide and fludarabine were remarkably decreased compared with those treated with PBS on day 24, whilst they recovered to similar levels after 8 days. Whilst the administration of chemotherapy regimen seemed to have a slight effect on tumour growth (Figure 6.10 B), there was no significant difference on survival between two therapy groups analysed by log rank (Mantel-Cox) test ($P = 0.1098$) (Figure 6.10 C). These results suggested that the use of cyclophosphamide and fludarabine at 100 mg/Kg could be an efficient pre-conditioning without significantly affecting tumour burden for CAR-T cell treatment.

A.

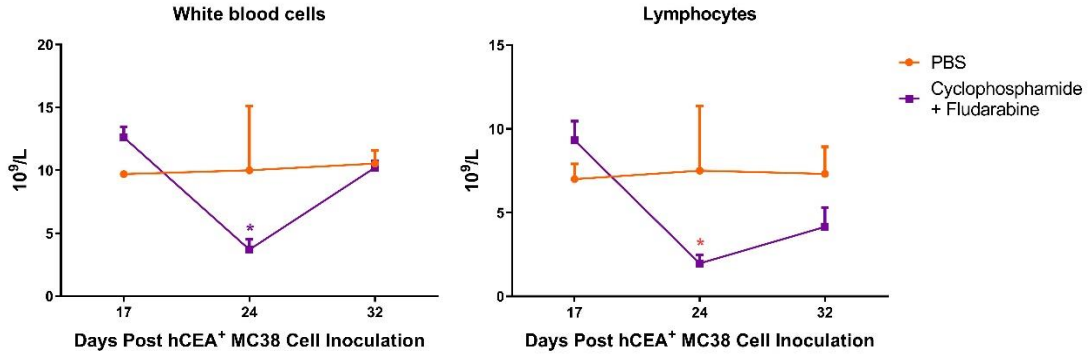

B.

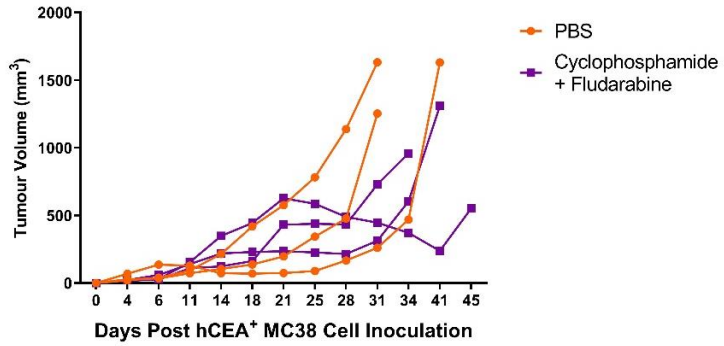

C.

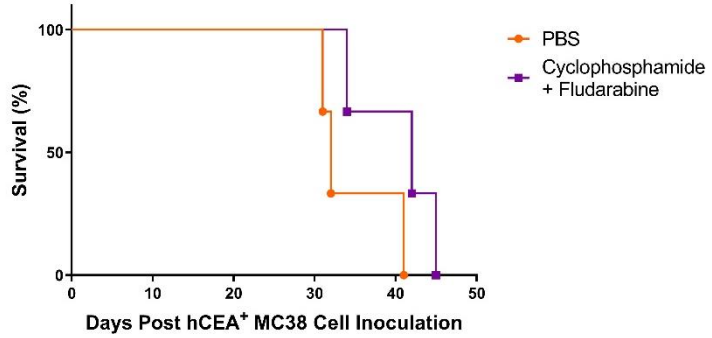

Figure 6.10 Evaluation of chemotherapy pre-conditioning in tumour-established mouse model

C57BL/6 CEAtg mice bearing subcutaneous CEA$^+$ MC38 tumour were treated with 100 mg/Kg fludarabine on day 19 and 20 and 100 mg/Kg cyclophosphamide on day 20 via intraperitoneal injection (n = 3). **(A)** The number of white blood cells and lymphocytes of individual mice before and after chemotherapy lymphodepletion was measured on day 17, 24 and 32 respectively. Statistically significant differences between two treatment groups on each indicated day were analysed using two-way ANOVA with Sidak's multiple comparisons test. $*$ $P < 0.05$. **(B)** Tumour volume of individual mice in each treatment group. **(C)** Survival of individual mice post treatment. Statistically significant differences were analysed using log rank (Mantel-Cox) test.

A schematic diagram of the experimental procedure giving CAR-T cell treatment with chemotherapy pre-conditioning was shown in Figure 6.11 A. Mice bearing 50 – 150 mm^3 tumours were treated with 1.7 x 10^7 total T cells containing 5 x 10^6 CAR-T cells by i.v. injection on day 2 post chemotherapy pre-conditioning. Additionally, aiming to inhibit both PD-1 and TGF-β signalling, the combination therapy of MFE.mCD28z.TA and MFE.mCD28z.PA CAR-T cells at a dose of 2.5 x 10^6 cell each was also assessed. To determine the efficiency of lymphodepletion by cyclophosphamide and fludarabine, peripheral blood samples were collected via tail vein bleeds on day 7, 15 and 22, and blood cell counts were performed. Mice were euthanized when tumours ulcerated or reached over 1,000 mm^3 or they displayed 20 % severe BWL, emaciation or pale extremities.

As before, a significant depletion of white blood cells and lymphocytes was seen in each T cell therapy group receiving chemotherapy on day 15 compared to pre-treatment levels measured on day 7 (Figure 6.11 B). With regards to the anti-tumour efficacy, each CAR-T cell therapy failed to eliminate subcutaneous CEA^+ tumour completely, although delayed tumour growth was observed in several mice receiving MFE.mCD28z.PA T cells with or without MFE.mCD28z.TA T cells (Figure 6.11 C). However, a delay in tumour growth was also seen in one mouse receiving mock T cells. More mice numbers are required to confirm whether this effect was due to non-specific T cell killing or a one off. No treatment-related toxicity occurred in all groups, suggesting that CEAtg mice were tolerant to CEA-specific CAR-T cells or large numbers of total T cells transferred following lymphodepleting pre-conditioning with cyclophosphamide and fludarabine. Whilst there was a significant survival benefit for mice receiving MFE.mCD28z.PA T cells with or without MFE.mCD28z.TA T cells over that receiving MFE.mCD28z T cells ($P = 0.048$ and $P = 0.025$ respectively), this statistical significance was not seen in comparison with that receiving mock T cells (Figure 6.11 D). Furthermore, given that the MFE.mCD28z.PA T cell therapy alone and the combination therapy of MFE.mCD28z.TA and MFE.mCD28z.PA T cells showed similar anti-tumour effects, it indicated that αPD-1 scFv was more likely to improve the anti-tumour efficacy of CAR-T cells compared to αTGF-β scFv. This was probably because αPD-1 scFv could function by binding to T cells directly, whilst αTGF-β scFv need to be delivered to tumour lesions to achieve its function.

A.

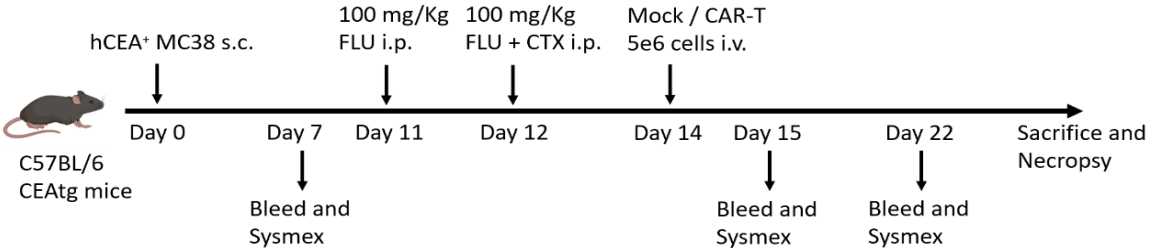
hCEA+ MC38 s.c.
100 mg/Kg FLU i.p.
100 mg/Kg FLU + CTX i.p.
Mock / CAR-T 5e6 cells i.v.
Day 0
Day 7
Day 11
Day 12
Day 14
Day 15
Day 22
Sacrifice and Necropsy
C57BL/6 CEAtg mice
Bleed and Sysmex
Bleed and Sysmex
Bleed and Sysmex

B.

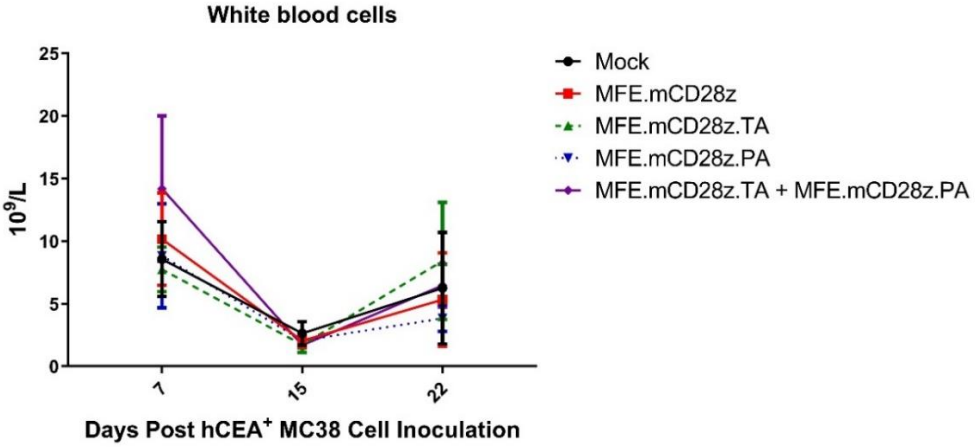
White blood cells
10⁹/L
Days Post hCEA+ MC38 Cell Inoculation
Mock
MFE.mCD28z
MFE.mCD28z.TA
MFE.mCD28z.PA
MFE.mCD28z.TA + MFE.mCD28z.PA

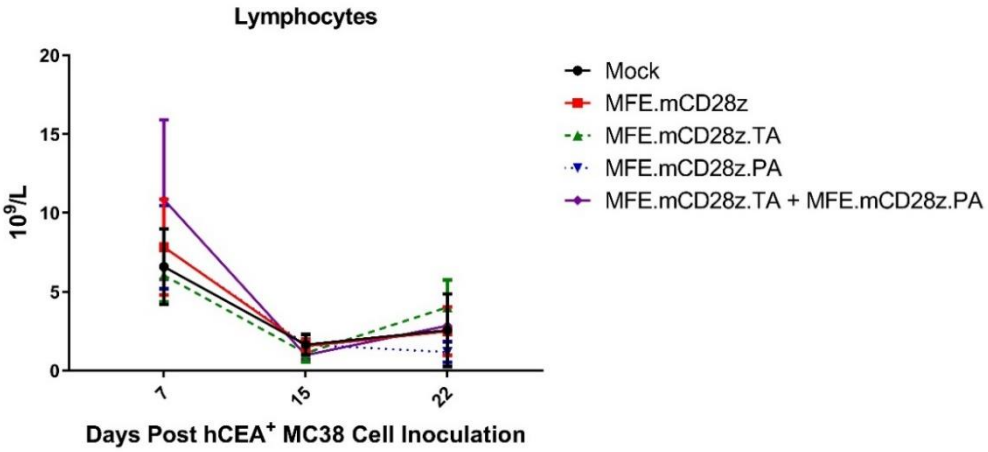
Lymphocytes
10⁹/L
Days Post hCEA+ MC38 Cell Inoculation
Mock
MFE.mCD28z
MFE.mCD28z.TA
MFE.mCD28z.PA
MFE.mCD28z.TA + MFE.mCD28z.PA

C.

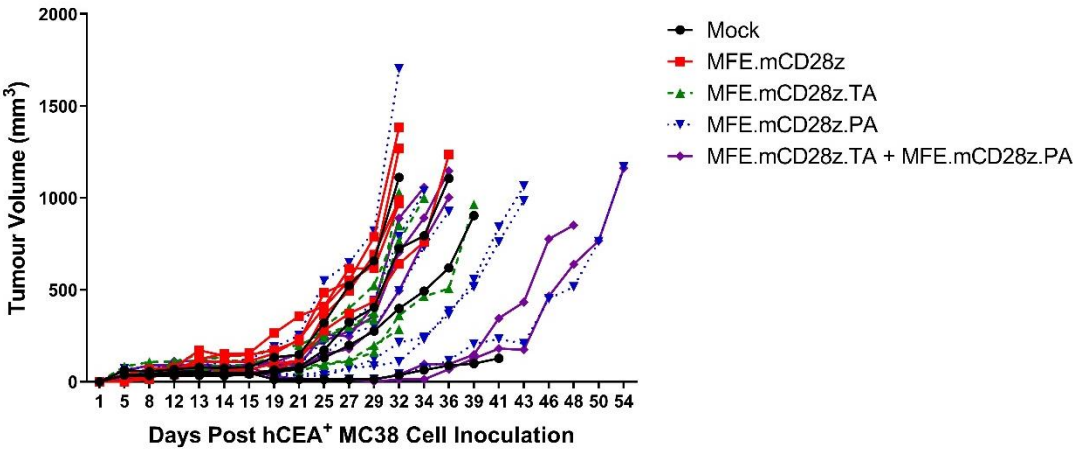
Tumour Volume (mm³)
Days Post hCEA+ MC38 Cell Inoculation
Mock
MFE.mCD28z
MFE.mCD28z.TA
MFE.mCD28z.PA
MFE.mCD28z.TA + MFE.mCD28z.PA

D.

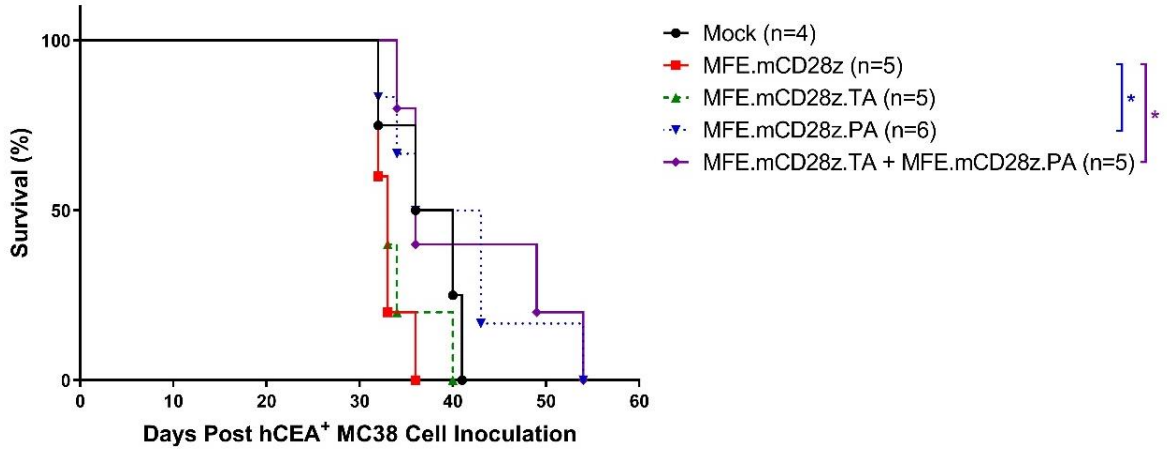

Figure 6.11 Evaluation of anti-tumour responses of scFv-secreting CEA-specific CAR-T cells in combination with host lymphodepletion

(A) Schematic diagram of the experimental procedure giving CAR-T cells in combination with chemotherapy pre-conditioning using cyclophosphamide (CTX) and fludarabine (FLU) *in vivo* (n = 4 - 6). **(B)** The number of circulating white blood cells and lymphocytes of individual mice before and after chemotherapy pre-conditioning was measured on day 7, 15 and 22. **(C)** Tumour volumes in individual mice in each treatment group. **(D)** Survival of individual mice post cell transfer treatment. Statistically significant differences were analysed using log rank (Mantel-Cox) test. $* P < 0.05$.

It has been reported that the presence of $CD8^+$ T cells in solid tumours impacts positively on anti-tumour responses and spontaneous tumour control [276]. Given that scFv-secreting CAR-T cells did not mediate significant therapeutic effects on tumour, it was of interest to evaluate the level of $CD8^+$ T cell infiltration in tumours during T cell treatment. To achieve this, tumour-bearing mice were treated with 5 x 10^6 Mock, MFE.mCD28z and MFE.mCD28z.PA T cells respectively on day 2 post chemotherapy pre-conditioning and tumour tissue was collected and fixed for IHC analysis on day 9 post T cell infusion. Spleens were also collected and used to assess the CEA-specific responses of immune cells *in vitro*.

As shown in Figure 6.12 A, $CD8^+$ T cells infiltrated into tumour sites at various levels among mice receiving CAR-T cell therapy. The number of infiltrated $CD8^+$ T cells was slightly increased in tumours treated with MFE.mCD28z and MFE.mCD28z.PA T cells (104.6 ± 88.5 and 125.1 ± 83.4 cells respectively), compared to those treated with mock T cells (74.3 ± 33.4 cells) (Figure 6.12 B). However, there was no statistically significant difference between T cell therapy groups, suggesting that the therapeutic effects of anti-CEA CAR-T cells were possibly limited by the level of T cell infiltration or CAR-T cell retention.

A.

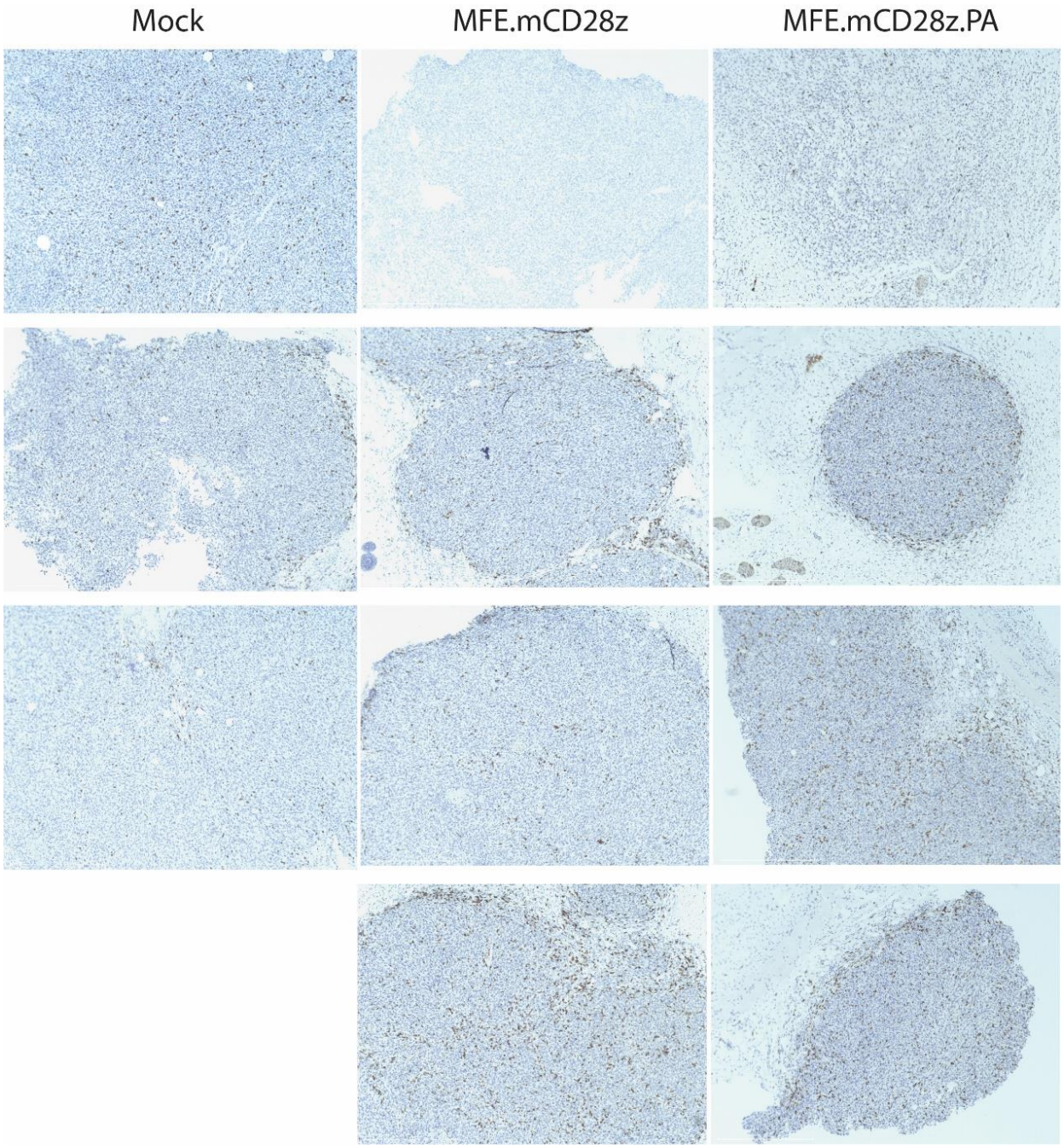

B.

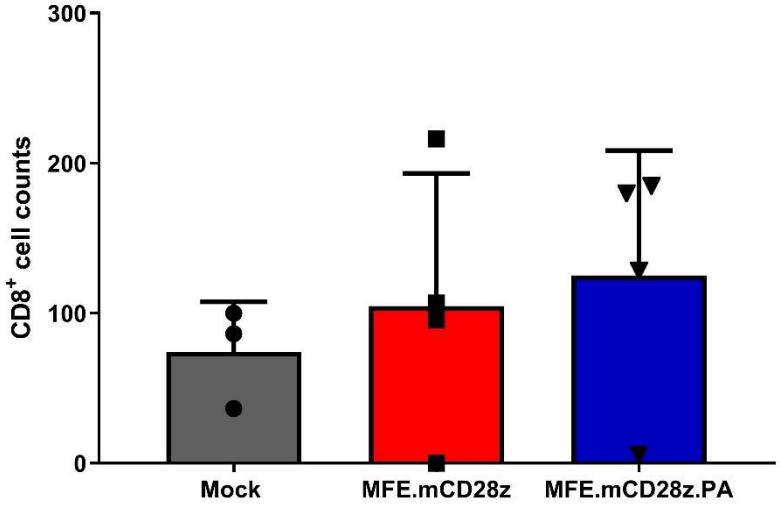

Figure 6.12 Infiltration of CD8$^+$ T cells in tumours post infusion

Tumour tissue of treated mice was collected for evaluation of CD8$^+$ T cell infiltration by IHC on day 9 post T cell infusion. **(A)** The sections of formalin-fixed and paraffin-embedded tumour tissues were stained with anti-mouse CD8α antibody. Magnification = 10X; Scale bar represents 500 μm. **(B)** CD8$^+$ T cell counting for each sample was performed three times on randomly selected regions of interest (ROI) (width x height: 500 x 500). The number of infiltrated CD8$^+$ T cells counted was averaged in each sample. The data are plotted as mean ± SD of 3 – 4 samples for each therapy group in one experiment. Statistically significant differences were analysed using one-way ANOVA with Tukey's multiple comparisons test.

The *in vitro* functional activity of immune cells from mice receiving T cell therapy was determined by IFN-γ production in response to CEA-expressing tumour cells. To achieve this, splenocytes were cultured with irradiated CEA^+ MC38 cells with the supplement of hIL-2 and mIL-7 for 5-day CEA-specific expansion. Activated splenocytes were re-cultured with irradiated CEA^+ MC38 cells at E: T ratio of 1: 1 for 20 hours. The supernatant was subsequently measured for IFN-γ release by ELISA.

It was seen that splenocytes in MFE.mCD28z and MFE.mCD28z.PA CAR-T cell therapy groups produced significant levels of IFN-γ (8,213.0 ± 1,538.2, 9,209.8 ± 3,638.4 pg/ml) in response to irradiated CEA^+ MC38 cells, compared to levels produced in splenocytes from mice receiving mock T cell therapy group (561.4 ± 445.1 pg/ml) ($P < 0.01$) (Figure 6.13). The presence of reactive T cells suggested that host immune responses towards CEA^+ target cells were induced post CAR-T cell treatment or CAR-T cells persisted in the spleen, although anti-CEA CAR-T cells failed to delay the growth of subcutaneous tumour or eradicate tumour. Similar levels of IFN-γ production between MFE.mCD28z and MFE.mCD28z.PA CAR-T cell therapy groups revealed that the additional secretion of αPD-1 scFv had no effects on improving the anti-tumour immunity.

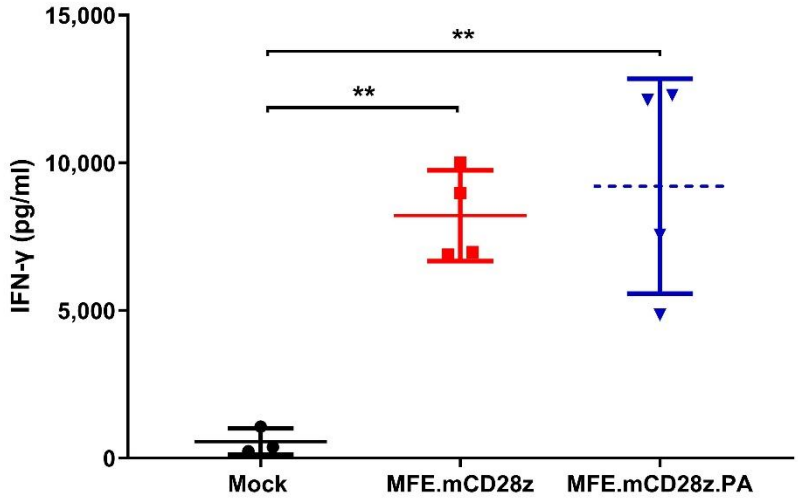

Figure 6.13 IFN-γ secretion by splenocytes in response to irradiated CEA$^+$ MC38 cells

Splenocytes were stimulated with irradiated CEA$^+$ MC38 cells with the supplement of hIL-2 and mIL-7 for 5-day CEA-specific expansion. Activated splenocytes were re-cultured with 5×10^5 irradiated CEA$^+$ MC38 cells at E: T ratio of 1: 1 for 20 hours. The supernatant collected post incubation was measured for IFN-γ production by ELISA. The data are plotted as mean ± SD of samples that could be collected in each therapy group (n=3 - 4). Statistically significant differences were analysed using one-way ANOVA with Tukey's multiple comparisons test. ** $P < 0.01$.

6.3 Discussion

The main aims of this chapter are to engineer anti-CEA CAR-T cells to secrete αTGF-β scFv or αPD-1 scFv and to evaluate their anti-tumour efficacy *in vitro* and *in vivo*. Compared to the combination therapy of CAR-T cells and systemic antibody treatment, delivery of scFv to tumour sites by CAR-T cells could minimise the potential toxicities associated with systemic administration of antibodies [266]. Whilst CAR-T cells have been designed to secrete αPD-1 scFv in several studies for preventing T cell exhaustion as described in section 6.1.1, the strategy of secreting αTGF-β scFv to inhibit TGF-β signalling has not been applied in CAR-T cell therapy so far. As mentioned in section 6.1.2, recent studies blocking TGF-β signalling in CAR-T cell therapy were to modify T cells to be TGF-β-insensitive or convert TGF-β into a potent T cell stimulant, which mainly aimed to boost CAR-T cell function [145, 146]. In this study, given the multi-functional effects of TGF-β in tumour, the use of αTGF-β scFv could potentially not only protect both T cells and other immune cells but also inhibit tumour progression and metastasis.

It has been demonstrated that mouse T cells were successfully engineered to express anti-CEA CAR constructs and constitutively secrete αTGF-β or αPD-1 scFv with functional binding capacity in this study. Notably, the level of PD-1 expression detected in MFE.mCD28z.PA CAR-T cells in culture was similar with other CAR-T cells without antigen stimulation (Figure 6.7 B), which was consistent with a study of anti-CD19 CAR-T cells secreting αPD-1 scFv [143]. In this study, since the antibody clone 29F.1A12 is used for flow cytometry, its binding site on PD-1 was thought to be different from the site of the clone J43 used for scFv, thus potentially could see similar levels of PD-1 expression even if the scFv is bound which blocks PD-1 binding to PD-L1. However, a study which also used different antibody clones for scFv and flow cytometry reported that the presence of αPD-1 scFv significantly reduced surface detection of PD-1 on CAR-T cells, suggesting direct binding of scFv [268]. These contrary observations were possibly due to various levels of scFv secreted and accumulated in the cell supernatant among studies.

Whilst scFv-secreting CAR-T cells exhibited antigen-specific cytotoxicity and produced abundant amounts of IFN-γ following CAR engagement with CEA^+ MC38 cells, no significant improvement in anti-tumour effects *in vitro* was seen compared to non-scFv-secreting CAR-T cells. In order to reveal the effects of αPD-1 scFv on CAR-T cells *in vitro*, the co-culture for 3-7 days should be used, as demonstrated by recent studies showing improved IFN-γ production and cell proliferation and lower levels of PD-1 expression of CAR-T cells secreting αPD-1 scFv after antigen-specific stimulation [143, 268]. Given that PSMA-specific CAR-T cells co-expressing dnTGF-βRII for TGF-β signalling blockade showed

enhanced proliferation ability over long-term repetitive antigen simulation [145], a similar strategy could be considered to assess the effects of αTGF-β scFv on CAR-T cells *in vitro*.

In this study, the anti-tumour function of scFv-secreting CAR-T cells was assessed in a subcutaneous CEA-expressing tumour model, which has not been used in previous studies of CAR-T cells in combination with blockade of PD-1 or TGF-β signalling. The results showed that scFv-secreting CAR-T cells could not efficiently eradicate the tumour, despite a prolonged survival in mice receiving MFE.mCD28z.PA T cells with or without MFE.mCD28z.TA T cells. Notably, the CEA-specific immune response determined by IFN-γ production was seen in splenocytes of CAR-T cells on day 9 post infusion, suggesting that CAR-T cells might persist in the early stage *in vivo*. Further investigation of the engraftment and expansion of CAR-T cells in peripheral blood and the spleen is necessary to demonstrate this. However, there was no enhanced $CD8^+$ T cell infiltration in tumour sites, leading to a hypothesis that the therapeutic effects of anti-CEA CAR-T cells were probably limited by the level of T cell infiltration. More information would have been provided if the infiltration level of CAR-T cells was evaluated in addition to total $CD8^+$ T cells.

Recent studies have reported that administration of CAR-T cells was performed via local/regional injection, showing improved anti-tumour activity compared to intravenous delivery in preclinical studies [136, 137] and extensive tumour cell death and other signs of anti-tumour inflammation such as macrophage recruitment in patients with metastatic breast cancer in a phase 0 clinical trial (NCT01837602) [138]. In order to circumvent the hurdle of T cell infiltration into tumour sites, intratumoral administration of CAR-T cells could be considered. Furthermore, given the important roles of chemokines in lymphocyte migration and homing, the intratumoral delivery of chemokines such as CCL5 expressed by a modified oncolytic adenoviral vector could be a strategy to improve CAR-T cell infiltration [277].

Apart from T cell infiltration, the amount of scFv secreted might be a factor that restrict the improvement on anti-tumour efficacy of CAR-T cells. Therefore, the quantity of scFv in the culture supernatant from scFv-secreting CAR-T cells should be determined in the future, whilst the same clone of the blocking antibody could be used as control if available.

In summary, the results outlined in this chapter demonstrated that αTGF-β or αPD-1 scFv and scFv-Fc with efficient binding and blocking ability could be successfully produced and secreted. Whilst significant functional activities *in vitro* were seen in scFv-secreting CAR-T cells, the effects of scfv on CAR-T cells or other immune cells could be further evaluated.

Anti-CEA CAR-T cells secreting scFv did not exhibit encouraging tumour eradication in a subcutaneous tumour model. For future studies, scFv quantification *in vitro* and CAR-T cell engraftment and infiltration *in vivo* should be investigated to better assess the anti-tumour efficacy of scFv-secreting CAR-T cells. It is also worth evaluating whether the αTGF-β or αPD-1 scFv-Fc could improve anti-tumour efficacy of CAR-T cells *in vitro* and *in vivo* and mediate better functions compared to monomer scFv.

7 Final Discussion

The key hypothesis underlying this project was that the effector function of CAR-T cells is strongly inhibited by the immunosuppressive microenvironment within solid tumours. The main aim of the work presented in this thesis was to explore new approaches in targeting cytokine networks or inhibitory immune checkpoints to endow anti-CEA CAR-T cells with the ability to resist TME immunosuppression. As such, research efforts have focused on developing immune modulatory CARs which can additionally secrete pro-inflammatory cytokines IL-12 or scFv blocking TGF-β or PD-1.

7.1 Anti-CEA CAR-T cells constitutively secreting IL-12

Murine T cells were effectively modified to co-express the anti-CEA CAR with varying signalling domains and constitutive IL-12. During *in vitro* culture, poor viability of IL-12-secreting CAR-T cells cultured at 1 x 10^6 cells/ml was observed, whilst viability could be improved by culturing at 0.3 x 10^6 cells/ml, most likely because more culture media was provided and the concentration of IL-12 was diluted in the culture medium. In addition, when cultured at 0.3 x 10^6 cells/ml, IL-12-expressing CAR-T cells expanded better than non-IL-12-expressing CAR-T cells on day 4 post transduction, suggesting that IL-12 could induce murine CAR-T cells to rapidly proliferate without antigen stimulation. Despite that, IL-12-secreting CAR-T cells still underwent apoptosis after 4 days in culture, probably caused by high levels of IFN-γ production induced by IL-12 [157]. Although culturing at a lower cell density could not maintain the survival of IL-12-secreting CAR-T cells in long-term culture, this approach was still acceptable to acquire enough cells for the following experiments.

Co-culture of anti-CEA CAR-T cells with CEA^+ tumour cell lines resulted in antigen-specific cytotoxicity and cytokine secretion *in vitro*. The inclusion of the murine CD28 co-stimulatory domain in the CAR construct significantly improved the functional activity of CAR-T cells. However, the addition of the murine 41BB domain did not enhance CAR-T cell potency, in accordance with this study using anti-mouse CD19 CAR-T cells [211]. This finding was in contrast to the anti-tumour efficacy of second-generation human CAR-T cells that include the 41BB domain [213]. Since the human 41BB domain can bind to TRAF 1-3 which are all required for 41BB co-stimulation signalling, it could be that the non- or compromised binding of TRAF3 by mouse 41BB domain, which partly resulted in suboptimal NF-κB signalling [211], contributed to the reduced efficacy.

The constitutive expression of IL-12 was able to enhance the anti-tumour function of CEA-specific CAR-T cells, as demonstrated by improved cytotoxicity and IFN-γ secretion in CD3z.mIL12 and CD28z.mIL12 CAR-T cells *in vitro*. In the presence of target antigen, 41BBz.mIL12 CAR-T cells also showed better cytotoxicity and cytokine production, compared to 41BBz CAR-T cells. However, there was no significant increase in IFN-γ production for 41BBz.mIL12 CAR-T cells when co-cultured with CEA^+ tumour cells in comparison with parental tumour cells. A possible explanation could be that 41BBz.mIL12 CAR-T cells were not stimulated as well as CD3z.mIL12 and CD28z.mIL12 CAR-T cells, because of the compromised co-stimulation signalling through the murine 41BB domain. A second possibility is that 41BB co-stimulation signalling mediated other mechanisms such as proliferation and persistence to enhance CAR-T cell function [212], which can be determined by CFSE assays. These findings also lead to a hypothesis that the cytotoxicity against CEA^+ tumour cells observed in 41BBz.mIL12 CAR-T cells was mediated through IFN-γ [217] which was induced by IL-12 but not through CAR engagement.

The immunocompetent WT C57BL/6 mouse strain was utilised to model subcutaneous CEA^+ MC38 tumour, as no endogenous immune responses against human CEA was observed when evaluated by IFN-γ production of splenocytes post the co-culture with CEA^+ MC38 cells. The *in vivo* anti-tumour function of CD28z.mIL12 CAR-T cells was evaluated, due to the better *in vitro* function compared to other CAR-T cells. A single dose of 2×10^6 CD28z.mIL12 CAR-T cells mediated complete regression of subcutaneous CEA^+ tumour in two of three mice even after tumours reached 400 mm^3. In addition, no apparent toxicity was observed in CD28z.mIL12 CAR-T cell therapy. This suggests that engineering anti-CEA CD28-CD3ζ CAR-T cells to constitutively secrete IL-12 could be a therapeutic strategy to improve anti-CEA CAR-T cell therapy for solid tumours *in vivo*, without causing IL-12-related toxicity. It also provides a rationale that higher doses of CD28z.mIL12 CAR-T cells is likely to mediate better therapeutic effects against subcutaneous CEA^+ tumour. This strategy is clinically relevant as it overcomes the need for lymphodepletion pre-conditioning and therefore allows for the application of CAR-T cell therapy to cancer patients intolerant to currently requisite toxic conditioning regimens [198].

For future studies, more mouse numbers are required to support this finding. In addition, it has been reported that murine anti-CD19 41BB-CD3ζ CAR-T cells with constitutive IL-12 expression alone could eradicate established systemic B cell lymphoma with long term survival in 22 % of lymphoreplete mice [156]. Therefore, it is also worthy to evaluate the *in vivo* anti-tumour function of 41BBz.mIL12 CAR-T cells.

In combination with lymphodepletion pre-conditioning via 5Gy TBI, lethal toxicity was observed in CD28z.mIL12 CAR-T cell therapy, with high levels of IL-12 detected in blood. This could be a consequence of rapid expansion of IL-12-secreting CD28z CAR-T cells in lymphodepleted hosts, although no mCherry marker gene could be detected in genomic DNA by qPCR in this study.

7.2 Anti-CEA CAR-T cells inducibly secreting IL-12

In an attempt to reduce the toxicity associated with CAR-T cells constitutively secreting IL-12 without compromising their anti-tumour efficacy in lymphodepleted hosts, CAR-T cells have been developed to inducibly produce IL-12 [153, 157, 208]. To achieve this, an NFAT-responsive promoter was utilised in this study. It is shown here that the release of inducible IL-12 could be triggered by activation of T cells through CAR engagement with target antigen, albeit at low levels. IL-12 expressed in an inducible manner could improve anti-tumour functions of CEA-specific CAR-T cells *in vitro*. However, a single dose of 2 x 10^6 CD28z.NFAT.mIL12 CAR-T cells alone did not show any therapeutic benefit for subcutaneous CEA^+ MC38 tumour in the CEAtg mouse model. The unsuccessful *in vivo* outcomes of inducible-IL-12-secreting CAR-T cells may be due to the dual effects of poor infiltration of CAR-T cells and insufficient levels of IL-12 production in tumour sites.

When combined with host lymphodepletion using 5Gy TBI, lethal toxicity was also observed in CD28z.NFAT.mIL12 CAR-T cell therapy, which appeared to be associated with IL-12. This suggests that the use of 5Gy TBI prior to inducible-IL-12-secreting CAR-T cell therapy was likely to be a factor that causes the IL-12-mediated toxicity, possibly by improving the engraftment and expansion of CAR-T cells [156] which led to a potential increase in IL-12 production. Notably, serum levels of IL-12 were not detectable. The inability to detect serum IL-12 in pre-conditioned mice treated with CD28z.NFAT.mIL12 CAR-T cells may be because the production of IL-12 was restricted to tumour sites. Despite that, this toxicity may be due to the secondary production of IFN-γ induced by IL-12, IL-6 and TNF-α which are known to be responsible for CRS in anti-CD19 CAR-T cell therapy [116].

To better understand the unsatisfactory efficacy and IL-12-related toxicity of CD28z.NFAT.mIL12 CAR-T cell therapy, more experimental data is needed. Evaluation of CEA expression on tumours, CAR-T cell infiltration and persistence and the level of IFN-γ and other cytokines in serum should be performed in future studies. Moreover, future work should focus on improving transduction efficiency of inducible-IL-12-secreting CAR-T cells. The use of lentiviral vectors which also can carry more transgenic payloads could be an

alternative strategy [250]. An increase in the level of CAR expression would make it possible to have higher number of CARs and NFAT-responsive promoters per cell and consequently increased levels of inducible IL-12. If transduction efficiency is improved, administration of higher cell doses could be a strategy to further determine whether inducible-IL-12-secreting CAR-T cells are efficacious in vivo. When TBI pre-conditioning is given, decreasing cell number is required to assess therapeutic effects and minimise IL-12-related toxicity.

In this study, CEAtg mice with tissue-specific CEA expression was utilised as an *in vivo* model to assess the on-target off-tumour toxicity of anti-CEA CAR-T cells. No apparent toxicity was induced by the therapy of IL-12-secreting CAR-T cells alone, or the combination therapy of CD28z CAR-T cells and TBI pre-conditioning. To further confirm this, histopathologic analysis of various tissues in CEAtg mice is required in future experiments.

7.3 Anti-CEA CAR-T cells constitutively secreting scFv

In this study, mouse T cells were successfully transduced to express anti-CEA CAR constructs and constitutively secrete αTGF-β or αPD-1 scFv with functional binding and blocking capacity. The *in vitro* and *in vivo* function of second-generation MFE.mCD28z CAR-T cells with or without scFv secretion were assessed. Whilst scFv-secreting CAR-T cells showed CEA-specific cytotoxicity and produced abundant amounts of IFN-γ following CAR engagement with CEA^+ MC38 cells *in vitro*, no significant difference was observed compared to non-scFv-secreting CAR-T cells. One hypothesis for this is that a 20-hour co-culture period was not sufficient for scFv secretion and accumulation into the supernatant to improve the anti-tumour efficacy of CAR-T cells *in vitro*. In addition, the effect of αTGF-β or αPD-1 scFv on the proliferation of anti-CEA CAR-T cells after antigen-specific stimulation *in vitro* could be investigated [268].

With regards to the *in vivo* function, anti-CEA CAR-T cells secreting scFv did not mediate tumour regression in CEAtg mice bearing subcutaneous CEA^+ MC38 tumours. Despite that, a delay in tumour growth was observed in several mice receiving MFE.mCD28z.PA CAR-T cells compared to those receiving MFE.mCD28z.TA CAR-T cells, suggesting that αPD-1 scFv was more likely than αTGF-β scFv to improve the anti-tumour efficacy of CAR-T cells. A possible explanation is that αPD-1 scFv could directly bind to T cells to achieve its function, whilst αTGF-β scFv need to be delivered to tumour lesions to block overexpressed TGF-β. It might also be due to the difference in secretion levels between αPD-1 scFv and

αTGF-β scFv. It is therefore necessary to determine the quantity of scFv in the culture supernatant from scFv-secreting CAR-T cells in the future.

It is of note that there was no significant difference in the infiltration of $CD8^+$ T cells in tumour sites between mock T cell therapy group and CAR-T cell therapy groups, although a slight increase in numbers was observed in CAR-T cell therapy groups. This leads to a hypothesis that the therapeutic effects of anti-CEA CAR-T cells were also possibly limited by the level of T cell infiltration or CAR-T cell retention.

For future studies, apart from scFv quantification, CAR-T cell engraftment and infiltration *in vivo* should be investigated to better understand the anti-tumour efficacy of scFv-secreting CAR-T cells. It is also worth evaluating whether the αTGF-β or αPD-1 scFv-Fc could facilitate the *in vitro* and *in vivo* function of CAR-T cells and mediate better effects compared to monomer scFv.

Overall, the results in this thesis suggest that immune modulation on anti-CEA CAR-T cells is a feasible immunotherapeutic strategy for solid tumours. The therapy of anti-CEA CAR-T cells constitutively secreting IL-12 displayed appears to be efficacious in tumour eradication *in vivo*, which needs to be further validated. More evaluations are also required to determine whether the inducible secretion of IL-12 or the constitutive secretion of αTGF-β or αPD-1 scFv results in improved anti-tumour responses of anti-CEA CAR-T cells.

In addition to overcoming the immunosuppressive TME, other approaches have been developed to improve CAR-T cell therapy for solid tumours in recent years, such as increasing the trafficking and infiltration of CAR-T cells and improving the function of CAR-T cells. Since solid tumours present cumulative defences for immune attack, the use of only one of these strategies may not make CAR-T cells work effectively. This thesis suggests that the efficacy of CAR-T cells secreting scFv was possibly limited by insufficient infiltration of T cells into tumour sites. Given that increased infiltration of $CD3^+$ T cells in a therapy model of CAR-T cells secreting inducible IL-12 has been reported [251], it is hypothesised that anti-CEA CAR-T cells secreting IL-12 may have a similar effect. The combination therapy of IL-12-secreting CAR-T cells and scFv-secreting CAR-T cells could be further explored as it may provide a possibility to circumvent the barriers within solid tumours and achieve successful tumour eradication.

References

1. Delves, P.J. and I.M. Roitt, *The immune system. First of two parts.* N Engl J Med, 2000. **343**(1): p. 37-49.
2. Male, D., et al., *Immunology, 8th Edi.* FRCPath, FRS Elsevier, 2012.
3. Neefjes, J., et al., *Towards a systems understanding of MHC class I and MHC class II antigen presentation.* Nat Rev Immunol, 2011. **11**(12): p. 823-36.
4. Heath, W.R. and F.R. Carbone, *Cross-presentation in viral immunity and self-tolerance.* Nat Rev Immunol, 2001. **1**(2): p. 126-34.
5. Acuto, O. and F. Michel, *CD28-mediated co-stimulation: a quantitative support for TCR signalling.* Nat Rev Immunol, 2003. **3**(12): p. 939-51.
6. Riley, J.L. and C.H. June, *The CD28 family: a T-cell rheostat for therapeutic control of T-cell activation.* Blood, 2005. **105**(1): p. 13-21.
7. Iwasaki, A. and R. Medzhitov, *Toll-like receptor control of the adaptive immune responses.* Nat Immunol, 2004. **5**(10): p. 987-95.
8. Blackburn, S.D., et al., *Coregulation of CD8+ T cell exhaustion by multiple inhibitory receptors during chronic viral infection.* Nat Immunol, 2009. **10**(1): p. 29-37.
9. Martínez-Lostao, L., A. Anel, and J. Pardo, *How Do Cytotoxic Lymphocytes Kill Cancer Cells?* Clin Cancer Res, 2015. **21**(22): p. 5047-56.
10. Sun, B., *T helper cell differentiation and their function*. Vol. 841. 2014: Springer.
11. Gray, J.C., P.W. Johnson, and M.J. Glennie, *Therapeutic potential of immunostimulatory monoclonal antibodies.* Clin Sci (Lond), 2006. **111**(2): p. 93-106.
12. Hanahan, D. and R.A. Weinberg, *The hallmarks of cancer.* Cell, 2000. **100**(1): p. 57-70.
13. Hanahan, D. and R.A. Weinberg, *Hallmarks of cancer: the next generation.* Cell, 2011. **144**(5): p. 646-74.
14. Bergers, G. and L.E. Benjamin, *Tumorigenesis and the angiogenic switch.* Nat Rev Cancer, 2003. **3**(6): p. 401-410.
15. Hynes, R.O. and A. Naba, *Overview of the matrisome--an inventory of extracellular matrix constituents and functions.* Cold Spring Harb Perspect Biol, 2012. **4**(1): p. a004903.
16. Bonnans, C., J. Chou, and Z. Werb, *Remodelling the extracellular matrix in development and disease.* Nat Rev Mol Cell Biol, 2014. **15**(12): p. 786-801.
17. Hanahan, D. and L.M. Coussens, *Accessories to the crime: functions of cells recruited to the tumor microenvironment.* Cancer Cell, 2012. **21**(3): p. 309-22.
18. Mueller, M.M. and N.E. Fusenig, *Friends or foes - bipolar effects of the tumour stroma in cancer.* Nat Rev Cancer, 2004. **4**(11): p. 839-49.
19. Qian, B.Z. and J.W. Pollard, *Macrophage diversity enhances tumor progression and metastasis.* Cell, 2010. **141**(1): p. 39-51.
20. Mueller, M.M., T. Werbowetski, and R.F. Del Maestro, *Soluble factors involved in glioma invasion.* Acta Neurochir (Wien), 2003. **145**(11): p. 999-1008.
21. Dunn, G.P., et al., *Cancer immunoediting: from immunosurveillance to tumor escape.* Nat Immunol, 2002. **3**(11): p. 991-8.
22. Mittal, D., et al., *New insights into cancer immunoediting and its three component phases--elimination, equilibrium and escape.* Curr Opin Immunol, 2014. **27**: p. 16-25.
23. Diamond, M.S., et al., *Type I interferon is selectively required by dendritic cells for immune rejection of tumors.* J Exp Med, 2011. **208**(10): p. 1989-2003.
24. Koebel, C.M., et al., *Adaptive immunity maintains occult cancer in an equilibrium state.* Nature, 2007. **450**(7171): p. 903-7.
25. Schreiber, R.D., L.J. Old, and M.J. Smyth, *Cancer immunoediting: integrating immunity's roles in cancer suppression and promotion.* Science, 2011. **331**(6024): p. 1565-70.

26. Muenst, S., et al., *The immune system and cancer evasion strategies: therapeutic concepts.* J Intern Med, 2016.
27. Zang, X. and J.P. Allison, *The B7 family and cancer therapy: costimulation and coinhibition.* Clin Cancer Res, 2007. **13**(18 Pt 1): p. 5271-9.
28. Wang, T., et al., *Regulation of the innate and adaptive immune responses by Stat-3 signaling in tumor cells.* Nat Med, 2004. **10**(1): p. 48-54.
29. Kataoka, T., et al., *FLIP prevents apoptosis induced by death receptors but not by perforin/granzyme B, chemotherapeutic drugs, and gamma irradiation.* J Immunol, 1998. **161**(8): p. 3936-42.
30. Hinz, S., et al., *Bcl-XL protects pancreatic adenocarcinoma cells against CD95- and TRAIL-receptor-mediated apoptosis.* Oncogene, 2000. **19**(48): p. 5477-86.
31. Shin, M.S., et al., *Mutations of tumor necrosis factor-related apoptosis-inducing ligand receptor 1 (TRAIL-R1) and receptor 2 (TRAIL-R2) genes in metastatic breast cancers.* Cancer Res, 2001. **61**(13): p. 4942-6.
32. Takahashi, H., et al., *FAS death domain deletions and cellular FADD-like interleukin 1beta converting enzyme inhibitory protein (long) overexpression: alternative mechanisms for deregulating the extrinsic apoptotic pathway in diffuse large B-cell lymphoma subtypes.* Clin Cancer Res, 2006. **12**(11 Pt 1): p. 3265-71.
33. Hamanishi, J., et al., *Programmed cell death 1 ligand 1 and tumor-infiltrating CD8+ T lymphocytes are prognostic factors of human ovarian cancer.* Proc Natl Acad Sci U S A, 2007. **104**(9): p. 3360-5.
34. Munn, D.H. and A.L. Mellor, *IDO and tolerance to tumors.* Trends Mol Med, 2004. **10**(1): p. 15-8.
35. Mellman, I., G. Coukos, and G. Dranoff, *Cancer immunotherapy comes of age.* Nature, 2011. **480**(7378): p. 480-9.
36. Ishida, T., et al., *Specific recruitment of CC chemokine receptor 4-positive regulatory T cells in Hodgkin lymphoma fosters immune privilege.* Cancer Res, 2006. **66**(11): p. 5716-22.
37. von Boehmer, H. and C. Daniel, *Therapeutic opportunities for manipulating T(Reg) cells in autoimmunity and cancer.* Nat Rev Drug Discov, 2013. **12**(1): p. 51-63.
38. Talmadge, J.E. and D.I. Gabrilovich, *History of myeloid-derived suppressor cells.* Nat Rev Cancer, 2013. **13**(10): p. 739-52.
39. Quail, D.F. and J.A. Joyce, *Microenvironmental regulation of tumor progression and metastasis.* Nat Med, 2013. **19**(11): p. 1423-37.
40. Gabrilovich, D.I. and S. Nagaraj, *Myeloid-derived suppressor cells as regulators of the immune system.* Nat Rev Immunol, 2009. **9**(3): p. 162-74.
41. Bouzin, C., et al., *Effects of vascular endothelial growth factor on the lymphocyte-endothelium interactions: identification of caveolin-1 and nitric oxide as control points of endothelial cell anergy.* J Immunol, 2007. **178**(3): p. 1505-11.
42. Buckanovich, R.J., et al., *Endothelin B receptor mediates the endothelial barrier to T cell homing to tumors and disables immune therapy.* Nat Med, 2008. **14**(1): p. 28-36.
43. Gkretsi, V., et al., *Remodeling Components of the Tumor Microenvironment to Enhance Cancer Therapy.* Front Oncol, 2015. **5**: p. 214.
44. Galon, J., W.H. Fridman, and F. Pagès, *The adaptive immunologic microenvironment in colorectal cancer: a novel perspective.* Cancer Res, 2007. **67**(5): p. 1883-6.
45. Clemente, C.G., et al., *Prognostic value of tumor infiltrating lymphocytes in the vertical growth phase of primary cutaneous melanoma.* Cancer, 1996. **77**(7): p. 1303-10.
46. Zhang, L., et al., *Intratumoral T cells, recurrence, and survival in epithelial ovarian cancer.* N Engl J Med, 2003. **348**(3): p. 203-13.
47. Mahmoud, S.M., et al., *Tumor-infiltrating CD8+ lymphocytes predict clinical outcome in breast cancer.* J Clin Oncol, 2011. **29**(15): p. 1949-55.
48. Mlecnik, B., et al., *Histopathologic-based prognostic factors of colorectal cancers are associated with the state of the local immune reaction.* J Clin Oncol, 2011. **29**(6): p. 610-8.

49. Badoual, C., et al., *Prognostic value of tumor-infiltrating CD4+ T-cell subpopulations in head and neck cancers.* Clin Cancer Res, 2006. **12**(2): p. 465-72.
50. Sharma, P., et al., *CD8 tumor-infiltrating lymphocytes are predictive of survival in muscle-invasive urothelial carcinoma.* Proc Natl Acad Sci U S A, 2007. **104**(10): p. 3967-72.
51. Nakakubo, Y., et al., *Clinical significance of immune cell infiltration within gallbladder cancer.* Br J Cancer, 2003. **89**(9): p. 1736-42.
52. Al-Shibli, K.I., et al., *Prognostic effect of epithelial and stromal lymphocyte infiltration in non-small cell lung cancer.* Clin Cancer Res, 2008. **14**(16): p. 5220-7.
53. Fridman, W.H., et al., *The immune contexture in human tumours: impact on clinical outcome.* Nat Rev Cancer, 2012. **12**(4): p. 298-306.
54. Pagès, F., et al., *In situ cytotoxic and memory T cells predict outcome in patients with early-stage colorectal cancer.* J Clin Oncol, 2009. **27**(35): p. 5944-51.
55. Pagès, F., et al., *International validation of the consensus Immunoscore for the classification of colon cancer: a prognostic and accuracy study.* Lancet, 2018. **391**(10135): p. 2128-2139.
56. Galon, J. and D. Bruni, *Approaches to treat immune hot, altered and cold tumours with combination immunotherapies.* Nat Rev Drug Discov, 2019. **18**(3): p. 197-218.
57. Hegde, P.S., V. Karanikas, and S. Evers, *The Where, the When, and the How of Immune Monitoring for Cancer Immunotherapies in the Era of Checkpoint Inhibition.* Clin Cancer Res, 2016. **22**(8): p. 1865-74.
58. Camus, M., et al., *Coordination of intratumoral immune reaction and human colorectal cancer recurrence.* Cancer Res, 2009. **69**(6): p. 2685-93.
59. Taube, J.M., *Unleashing the immune system: PD-1 and PD-Ls in the pre-treatment tumor microenvironment and correlation with response to PD-1/PD-L1 blockade.* Oncoimmunology, 2014. **3**(11): p. e963413.
60. Tumeh, P.C., et al., *PD-1 blockade induces responses by inhibiting adaptive immune resistance.* Nature, 2014. **515**(7528): p. 568-71.
61. Bonaventura, P., et al., *Cold Tumors: A Therapeutic Challenge for Immunotherapy.* Front Immunol, 2019. **10**: p. 168.
62. Lindsten, T., et al., *Characterization of CTLA-4 structure and expression on human T cells.* J Immunol, 1993. **151**(7): p. 3489-99.
63. Wing, K., et al., *CTLA-4 control over Foxp3+ regulatory T cell function.* Science, 2008. **322**(5899): p. 271-5.
64. Peggs, K.S., et al., *Blockade of CTLA-4 on both effector and regulatory T cell compartments contributes to the antitumor activity of anti-CTLA-4 antibodies.* J Exp Med, 2009. **206**(8): p. 1717-25.
65. Sharpe, A.H. and K.E. Pauken, *The diverse functions of the PD1 inhibitory pathway.* Nat Rev Immunol, 2018. **18**(3): p. 153-167.
66. Zou, W. and L. Chen, *Inhibitory B7-family molecules in the tumour microenvironment.* Nat Rev Immunol, 2008. **8**(6): p. 467-77.
67. Sfanos, K.S., et al., *Human prostate-infiltrating CD8+ T lymphocytes are oligoclonal and PD-1+.* Prostate, 2009. **69**(15): p. 1694-703.
68. Wu, K., et al., *Kupffer cell suppression of CD8+ T cells in human hepatocellular carcinoma is mediated by B7-H1/programmed death-1 interactions.* Cancer Res, 2009. **69**(20): p. 8067-75.
69. Matsuzaki, J., et al., *Tumor-infiltrating NY-ESO-1-specific CD8+ T cells are negatively regulated by LAG-3 and PD-1 in human ovarian cancer.* Proc Natl Acad Sci U S A, 2010. **107**(17): p. 7875-80.
70. Ahmadzadeh, M., et al., *Tumor antigen-specific CD8 T cells infiltrating the tumor express high levels of PD-1 and are functionally impaired.* Blood, 2009. **114**(8): p. 1537-44.

71. Alsaab, H.O., et al., *PD-1 and PD-L1 Checkpoint Signaling Inhibition for Cancer Immunotherapy: Mechanism, Combinations, and Clinical Outcome.* Front Pharmacol, 2017. **8**: p. 561.
72. Rosenberg, S.A., et al., *Durable complete responses in heavily pretreated patients with metastatic melanoma using T-cell transfer immunotherapy.* Clin Cancer Res, 2011. **17**(13): p. 4550-7.
73. Morgan, R.A., et al., *Cancer Regression in Patients After Transfer of Genetically Engineered Lymphocytes.* Science, 2006. **314**(5796): p. 126-129.
74. Garrido, F., et al., *Natural history of HLA expression during tumour development.* Immunol Today, 1993. **14**(10): p. 491-9.
75. Rapoport, A.P., et al., *NY-ESO-1-specific TCR-engineered T cells mediate sustained antigen-specific antitumor effects in myeloma.* Nat Med, 2015. **21**(8): p. 914-21.
76. Krebs, S., et al., *T cells redirected to interleukin-13Ralpha2 with interleukin-13 mutein--chimeric antigen receptors have anti-glioma activity but also recognize interleukin-13Ralpha1.* Cytotherapy, 2014. **16**(8): p. 1121-31.
77. Muniappan, A., et al., *Ligand-mediated cytolysis of tumor cells: use of heregulin-zeta chimeras to redirect cytotoxic T lymphocytes.* Cancer Gene Ther, 2000. **7**(1): p. 128-34.
78. Davies, D.M., et al., *Flexible targeting of ErbB dimers that drive tumorigenesis by using genetically engineered T cells.* Molecular Medicine, 2012. **18**(4): p. 565-576.
79. Whilding, L.M. and J. Maher, *CAR T-cell immunotherapy: The path from the by-road to the freeway?* Mol Oncol, 2015. **9**(10): p. 1994-2018.
80. Maude, S.L., et al., *CD19-targeted chimeric antigen receptor T-cell therapy for acute lymphoblastic leukemia.* Blood, 2015. **125**(26): p. 4017-23.
81. Hudecek, M., et al., *The nonsignaling extracellular spacer domain of chimeric antigen receptors is decisive for in vivo antitumor activity.* Cancer Immunol Res, 2015. **3**(2): p. 125-35.
82. Finney, H.M., A.N. Akbar, and A.D. Lawson, *Activation of resting human primary T cells with chimeric receptors: costimulation from CD28, inducible costimulator, CD134, and CD137 in series with signals from the TCR zeta chain.* J Immunol, 2004. **172**(1): p. 104-13.
83. Haynes, N.M., et al., *Redirecting mouse CTL against colon carcinoma: superior signaling efficacy of single-chain variable domain chimeras containing TCR-zeta vs Fc epsilon RI-gamma.* J Immunol, 2001. **166**(1): p. 182-7.
84. Carpenito, C., et al., *Control of large, established tumor xenografts with genetically retargeted human T cells containing CD28 and CD137 domains.* Proc Natl Acad Sci U S A, 2009. **106**(9): p. 3360-5.
85. Koehler, H., et al., *CD28 costimulation overcomes transforming growth factor-beta-mediated repression of proliferation of redirected human CD4+ and CD8+ T cells in an antitumor cell attack.* Cancer Res, 2007. **67**(5): p. 2265-73.
86. Kofler, D.M., et al., *CD28 costimulation Impairs the efficacy of a redirected t-cell antitumor attack in the presence of regulatory t cells which can be overcome by preventing Lck activation.* Mol Ther, 2011. **19**(4): p. 760-7.
87. Long, A.H., et al., *4-1BB costimulation ameliorates T cell exhaustion induced by tonic signaling of chimeric antigen receptors.* Nat Med, 2015. **21**(6): p. 581-90.
88. Zhao, Y., et al., *A herceptin-based chimeric antigen receptor with modified signaling domains leads to enhanced survival of transduced T lymphocytes and antitumor activity.* J Immunol, 2009. **183**(9): p. 5563-74.
89. Heimberger, A.B., et al., *Prognostic effect of epidermal growth factor receptor and EGFRvIII in glioblastoma multiforme patients.* Clin Cancer Res, 2005. **11**(4): p. 1462-6.
90. Gill, S., M.V. Maus, and D.L. Porter, *Chimeric antigen receptor T cell therapy: 25years in the making.* Blood Rev, 2016. **30**(3): p. 157-67.
91. Lipowska-Bhalla, G., et al., *Targeted immunotherapy of cancer with CAR T cells: achievements and challenges.* Cancer Immunol Immunother, 2012. **61**(7): p. 953-62.

92. Beauchemin, N., et al., *Isolation and characterization of full-length functional cDNA clones for human carcinoembryonic antigen.* Mol Cell Biol, 1987. **7**(9): p. 3221-30.
93. Schwab, M., *Encyclopedia of cancer*. 2008: Springer Science & Business Media.
94. Hodge, J.W., *Carcinoembryonic antigen as a target for cancer vaccines.* Cancer Immunol Immunother, 1996. **43**(3): p. 127-34.
95. Beauchemin, N. and A. Arabzadeh, *Carcinoembryonic antigen-related cell adhesion molecules (CEACAMs) in cancer progression and metastasis.* Cancer Metastasis Rev, 2013. **32**(3-4): p. 643-71.
96. Stern, N., et al., *Carcinoembryonic antigen (CEA) inhibits NK killing via interaction with CEA-related cell adhesion molecule 1.* J Immunol, 2005. **174**(11): p. 6692-701.
97. van Gisbergen, K.P., et al., *Dendritic cells recognize tumor-specific glycosylation of carcinoembryonic antigen on colorectal cancer cells through dendritic cell-specific intercellular adhesion molecule-3-grabbing nonintegrin.* Cancer Res, 2005. **65**(13): p. 5935-44.
98. Thomas, P., R.A. Forse, and O. Bajenova, *Carcinoembryonic antigen (CEA) and its receptor hnRNP M are mediators of metastasis and the inflammatory response in the liver.* Clin Exp Metastasis, 2011. **28**(8): p. 923-32.
99. Jessup, J.M., et al., *Carcinoembryonic antigen promotes tumor cell survival in liver through an IL-10-dependent pathway.* Clin Exp Metastasis, 2004. **21**(8): p. 709-17.
100. Samara, R.N., L.M. Laguinge, and J.M. Jessup, *Carcinoembryonic antigen inhibits anoikis in colorectal carcinoma cells by interfering with TRAIL-R2 (DR5) signaling.* Cancer Res, 2007. **67**(10): p. 4774-82.
101. Li, Y., et al., *Carcinoembryonic antigen interacts with TGF-{beta} receptor and inhibits TGF-{beta} signaling in colorectal cancers.* Cancer Res, 2010. **70**(20): p. 8159-68.
102. Davila, M.L., et al., *Efficacy and toxicity management of 19-28z CAR T cell therapy in B cell acute lymphoblastic leukemia.* Sci Transl Med, 2014. **6**(224): p. 224ra25.
103. Lee, D.W., et al., *T cells expressing CD19 chimeric antigen receptors for acute lymphoblastic leukaemia in children and young adults: a phase 1 dose-escalation trial.* The Lancet. **385**(9967): p. 517-528.
104. Maude, S.L., et al., *Chimeric antigen receptor T cells for sustained remissions in leukemia.* N Engl J Med, 2014. **371**(16): p. 1507-17.
105. Brentjens, R.J., et al., *CD19-targeted T cells rapidly induce molecular remissions in adults with chemotherapy-refractory acute lymphoblastic leukemia.* Sci Transl Med, 2013. **5**(177): p. 177ra38.
106. Porter, D.L., et al., *Chimeric antigen receptor T cells persist and induce sustained remissions in relapsed refractory chronic lymphocytic leukemia.* Sci Transl Med, 2015. **7**(303): p. 303ra139.
107. Porter, D.L., et al., *Randomized, phase II dose optimization study of chimeric antigen receptor modified T cells directed against CD19 (CTL019) in patients with relapsed, refractory CLL.* Blood, 2014. **124**(21): p. 1982-1982.
108. Kochenderfer, J.N., et al., *Chemotherapy-refractory diffuse large B-cell lymphoma and indolent B-cell malignancies can be effectively treated with autologous T cells expressing an anti-CD19 chimeric antigen receptor.* J Clin Oncol, 2015. **33**(6): p. 540-9.
109. Brown, J.R., D.L. Porter, and S.M. O'Brien, *Novel treatments for chronic lymphocytic leukemia and moving forward.* Am Soc Clin Oncol Educ Book, 2014: p. e317-25.
110. Schuster, S.J., et al., *Sustained remissions following chimeric antigen receptor modified T cells directed against CD19 (CTL019) in patients with relapsed or refractory CD19+ lymphomas*. 2015, Am Soc Hematology.
111. Maude, S.L., et al., *Tisagenlecleucel in Children and Young Adults with B-Cell Lymphoblastic Leukemia.* N Engl J Med, 2018. **378**(5): p. 439-448.
112. Neelapu, S.S., et al., *Axicabtagene Ciloleucel CAR T-Cell Therapy in Refractory Large B-Cell Lymphoma.* N Engl J Med, 2017. **377**(26): p. 2531-2544.

113. Kershaw, M.H., J.A. Westwood, and P.K. Darcy, *Gene-engineered T cells for cancer therapy.* Nat Rev Cancer, 2013. **13**(8): p. 525-41.
114. Kim, J.W. and J.P. Eder, *Prospects for targeting PD-1 and PD-L1 in various tumor types.* Oncology (Williston Park), 2014. **28 Suppl 3**: p. 15-28.
115. Flavell, R.A., et al., *The polarization of immune cells in the tumour environment by TGFbeta.* Nat Rev Immunol, 2010. **10**(8): p. 554-67.
116. Grupp, S.A., et al., *Chimeric antigen receptor-modified T cells for acute lymphoid leukemia.* N Engl J Med, 2013. **368**(16): p. 1509-18.
117. Morgan, R.A., et al., *Case report of a serious adverse event following the administration of T cells transduced with a chimeric antigen receptor recognizing ERBB2.* Mol Ther, 2010. **18**(4): p. 843-51.
118. Neelapu, S.S., et al., *Chimeric antigen receptor T-cell therapy - assessment and management of toxicities.* Nat Rev Clin Oncol, 2018. **15**(1): p. 47-62.
119. Howard, S.C., D.P. Jones, and C.H. Pui, *The tumor lysis syndrome.* N Engl J Med, 2011. **364**(19): p. 1844-54.
120. Lee, D.W., et al., *ASTCT Consensus Grading for Cytokine Release Syndrome and Neurologic Toxicity Associated with Immune Effector Cells.* Biol Blood Marrow Transplant, 2019. **25**(4): p. 625-638.
121. Gust, J., et al., *Endothelial Activation and Blood-Brain Barrier Disruption in Neurotoxicity after Adoptive Immunotherapy with CD19 CAR-T Cells.* Cancer Discov, 2017. **7**(12): p. 1404-1419.
122. Maher, J., *Immunotherapy of malignant disease using chimeric antigen receptor engrafted T cells.* ISRN Oncol, 2012. **2012**: p. 278093.
123. Tesniere, A., et al., *Immunogenic death of colon cancer cells treated with oxaliplatin.* Oncogene, 2010. **29**(4): p. 482-91.
124. Kroemer, G., et al., *Immunogenic cell death in cancer therapy.* Annu Rev Immunol, 2013. **31**: p. 51-72.
125. Hodge, J.W., et al., *Chemotherapy-induced immunogenic modulation of tumor cells enhances killing by cytotoxic T lymphocytes and is distinct from immunogenic cell death.* Int J Cancer, 2013. **133**(3): p. 624-36.
126. Lesterhuis, W.J., et al., *Platinum-based drugs disrupt STAT6-mediated suppression of immune responses against cancer in humans and mice.* J Clin Invest, 2011. **121**(8): p. 3100-8.
127. Lutsiak, M.E., et al., *Inhibition of CD4(+)25+ T regulatory cell function implicated in enhanced immune response by low-dose cyclophosphamide.* Blood, 2005. **105**(7): p. 2862-8.
128. Alizadeh, D., et al., *Doxorubicin eliminates myeloid-derived suppressor cells and enhances the efficacy of adoptive T-cell transfer in breast cancer.* Cancer Res, 2014. **74**(1): p. 104-18.
129. Wallen, H., et al., *Fludarabine modulates immune response and extends in vivo survival of adoptively transferred CD8 T cells in patients with metastatic melanoma.* PLoS One, 2009. **4**(3): p. e4749.
130. Proietti, E., et al., *Exploitation of the propulsive force of chemotherapy for improving the response to cancer immunotherapy.* Mol Oncol, 2012. **6**(1): p. 1-14.
131. Moon, E.K., et al., *Expression of a functional CCR2 receptor enhances tumor localization and tumor eradication by retargeted human T cells expressing a mesothelin-specific chimeric antibody receptor.* Clin Cancer Res, 2011. **17**(14): p. 4719-30.
132. Di Stasi, A., et al., *T lymphocytes coexpressing CCR4 and a chimeric antigen receptor targeting CD30 have improved homing and antitumor activity in a Hodgkin tumor model.* Blood, 2009. **113**(25): p. 6392-402.
133. Tokarew, N., et al., *Teaching an old dog new tricks: next-generation CAR T cells.* Br J Cancer, 2019. **120**(1): p. 26-37.
134. Parente-Pereira, A.C., et al., *Trafficking of CAR-engineered human T cells following regional or systemic adoptive transfer in SCID beige mice.* J Clin Immunol, 2011. **31**(4): p. 710-8.

135. Sridhar, P. and F. Petrocca, *Regional Delivery of Chimeric Antigen Receptor (CAR) T-Cells for Cancer Therapy.* Cancers (Basel), 2017. **9**(7).
136. Priceman, S.J., et al., *Regional Delivery of Chimeric Antigen Receptor-Engineered T Cells Effectively Targets HER2(+) Breast Cancer Metastasis to the Brain.* Clin Cancer Res, 2018. **24**(1): p. 95-105.
137. Katz, S.C., et al., *Regional CAR-T cell infusions for peritoneal carcinomatosis are superior to systemic delivery.* Cancer Gene Ther, 2016. **23**(5): p. 142-8.
138. Tchou, J., et al., *Safety and Efficacy of Intratumoral Injections of Chimeric Antigen Receptor (CAR) T Cells in Metastatic Breast Cancer.* Cancer Immunol Res, 2017. **5**(12): p. 1152-1161.
139. Rupp, L.J., et al., *CRISPR/Cas9-mediated PD-1 disruption enhances anti-tumor efficacy of human chimeric antigen receptor T cells.* Sci Rep, 2017. **7**(1): p. 737.
140. Tang, N., et al., *TGF-β inhibition via CRISPR promotes the long-term efficacy of CAR T cells against solid tumors.* JCI Insight, 2020. **5**(4).
141. Borkner, L., et al., *RNA interference targeting programmed death receptor-1 improves immune functions of tumor-specific T cells.* Cancer Immunol Immunother, 2010. **59**(8): p. 1173-83.
142. Ren, J., et al., *A versatile system for rapid multiplex genome-edited CAR T cell generation.* Oncotarget, 2017. **8**(10): p. 17002-17011.
143. Li, S., et al., *Enhanced Cancer Immunotherapy by Chimeric Antigen Receptor-Modified T Cells Engineered to Secrete Checkpoint Inhibitors.* Clin Cancer Res, 2017. **23**(22): p. 6982-6992.
144. Cherkassky, L., et al., *Human CAR T cells with cell-intrinsic PD-1 checkpoint blockade resist tumor-mediated inhibition.* J Clin Invest, 2016. **126**(8): p. 3130-44.
145. Kloss, C.C., et al., *Dominant-Negative TGF-β Receptor Enhances PSMA-Targeted Human CAR T Cell Proliferation And Augments Prostate Cancer Eradication.* Mol Ther, 2018. **26**(7): p. 1855-1866.
146. Chang, Z.L., et al., *Rewiring T-cell responses to soluble factors with chimeric antigen receptors.* Nat Chem Biol, 2018. **14**(3): p. 317-324.
147. Kobold, S., et al., *Impact of a New Fusion Receptor on PD-1-Mediated Immunosuppression in Adoptive T Cell Therapy.* J Natl Cancer Inst, 2015. **107**(8).
148. Shin, J.H., et al., *Positive conversion of negative signaling of CTLA4 potentiates antitumor efficacy of adoptive T-cell therapy in murine tumor models.* Blood, 2012. **119**(24): p. 5678-87.
149. Mohammed, S., et al., *Improving Chimeric Antigen Receptor-Modified T Cell Function by Reversing the Immunosuppressive Tumor Microenvironment of Pancreatic Cancer.* Mol Ther, 2017. **25**(1): p. 249-258.
150. Attia, P., et al., *Autoimmunity correlates with tumor regression in patients with metastatic melanoma treated with anti-cytotoxic T-lymphocyte antigen-4.* J Clin Oncol, 2005. **23**(25): p. 6043-53.
151. Topalian, S.L., et al., *Safety, activity, and immune correlates of anti-PD-1 antibody in cancer.* N Engl J Med, 2012. **366**(26): p. 2443-54.
152. Chmielewski, M. and H. Abken, *CAR T Cells Releasing IL-18 Convert to T-Bet(high) FoxO1(low) Effectors that Exhibit Augmented Activity against Advanced Solid Tumors.* Cell Rep, 2017. **21**(11): p. 3205-3219.
153. Chmielewski, M., et al., *IL-12 release by engineered T cells expressing chimeric antigen receptors can effectively Muster an antigen-independent macrophage response on tumor cells that have shut down tumor antigen expression.* Cancer Res, 2011. **71**(17): p. 5697-706.
154. Hoyos, V., et al., *Engineering CD19-specific T lymphocytes with interleukin-15 and a suicide gene to enhance their anti-lymphoma/leukemia effects and safety.* Leukemia, 2010. **24**(6): p. 1160-70.
155. Chmielewski, M., A.A. Hombach, and H. Abken, *Of CARs and TRUCKs: chimeric antigen receptor (CAR) T cells engineered with an inducible cytokine to modulate the tumor stroma.* Immunol Rev, 2014. **257**(1): p. 83-90.

156. Kueberuwa, G., et al., *CD19 CAR T Cells Expressing IL-12 Eradicate Lymphoma in Fully Lymphoreplete Mice through Induction of Host Immunity.* Mol Ther Oncolytics, 2018. **8**: p. 41-51.
157. Zhang, L., et al., *Improving adoptive T cell therapy by targeting and controlling IL-12 expression to the tumor environment.* Mol Ther, 2011. **19**(4): p. 751-9.
158. Grada, Z., et al., *TanCAR: A Novel Bispecific Chimeric Antigen Receptor for Cancer Immunotherapy.* Mol Ther Nucleic Acids, 2013. **2**: p. e105.
159. Srivastava, S. and S.R. Riddell, *Engineering CAR-T cells: Design concepts.* Trends Immunol, 2015. **36**(8): p. 494-502.
160. Fedorov, V.D., M. Themeli, and M. Sadelain, *PD-1- and CTLA-4-based inhibitory chimeric antigen receptors (iCARs) divert off-target immunotherapy responses.* Sci Transl Med, 2013. **5**(215): p. 215ra172.
161. Straathof, K.C., et al., *An inducible caspase 9 safety switch for T-cell therapy.* Blood, 2005. **105**(11): p. 4247-54.
162. Di Stasi, A., et al., *Inducible apoptosis as a safety switch for adoptive cell therapy.* N Engl J Med, 2011. **365**(18): p. 1673-83.
163. Jensen, M.C., et al., *Antitransgene rejection responses contribute to attenuated persistence of adoptively transferred CD20/CD19-specific chimeric antigen receptor redirected T cells in humans.* Biology of Blood and Marrow Transplantation, 2010. **16**(9): p. 1245-1256.
164. Tiberghien, P., et al., *Administration of herpes simplex-thymidine kinase-expressing donor T cells with a T-cell-depleted allogeneic marrow graft.* Blood, 2001. **97**(1): p. 63-72.
165. Budde, L.E., et al., *Combining a CD20 chimeric antigen receptor and an inducible caspase 9 suicide switch to improve the efficacy and safety of T cell adoptive immunotherapy for lymphoma.* PLoS One, 2013. **8**(12): p. e82742.
166. Chmielewski, M., et al., *T cells that target carcinoembryonic antigen eradicate orthotopic pancreatic carcinomas without inducing autoimmune colitis in mice.* Gastroenterology, 2012. **143**(4): p. 1095-107.e2.
167. Chmielewski, M., et al., *T cells redirected by a CD3ζ chimeric antigen receptor can establish self-antigen-specific tumour protection in the long term.* Gene Ther, 2013. **20**(2): p. 177-86.
168. Wang, L., et al., *Efficient tumor regression by adoptively transferred CEA-specific CAR-T cells associated with symptoms of mild cytokine release syndrome.* Oncoimmunology, 2016. **5**(9): p. e1211218.
169. Katz, S.C., et al., *Phase I Hepatic Immunotherapy for Metastases Study of Intra-Arterial Chimeric Antigen Receptor-Modified T-cell Therapy for CEA+ Liver Metastases.* Clin Cancer Res, 2015. **21**(14): p. 3149-59.
170. Thistlethwaite, F.C., et al., *The clinical efficacy of first-generation carcinoembryonic antigen (CEACAM5)-specific CAR T cells is limited by poor persistence and transient pre-conditioning-dependent respiratory toxicity.* Cancer Immunol Immunother, 2017. **66**(11): p. 1425-1436.
171. Zhang, C., et al., *Phase I Escalating-Dose Trial of CAR-T Therapy Targeting CEA(+) Metastatic Colorectal Cancers.* Mol Ther, 2017. **25**(5): p. 1248-1258.
172. Parkhurst, M.R., et al., *T cells targeting carcinoembryonic antigen can mediate regression of metastatic colorectal cancer but induce severe transient colitis.* Mol Ther, 2011. **19**(3): p. 620-6.
173. Ahnen, D.J., P.K. Nakane, and W.R. Brown, *Ultrastructural localization of carcinoembryonic antigen in normal intestine and colon cancer: abnormal distribution of CEA on the surfaces of colon cancer cells.* Cancer, 1982. **49**(10): p. 2077-90.
174. Holzinger, A. and H. Abken, *CAR T cells targeting solid tumors: carcinoembryonic antigen (CEA) proves to be a safe target.* Cancer Immunol Immunother, 2017. **66**(11): p. 1505-1507.
175. Grohmann, U., et al., *IL-12 acts directly on DC to promote nuclear localization of NF-kappaB and primes DC for IL-12 production.* Immunity, 1998. **9**(3): p. 315-23.

176. Airoldi, I., et al., *Expression and function of IL-12 and IL-18 receptors on human tonsillar B cells.* J Immunol, 2000. **165**(12): p. 6880-8.
177. Lasek, W. and R. Zagozdzon, *Interleukin 12: Antitumor Activity and Immunotherapeutic Potential in Oncology*. 2016: Springer.
178. Okamura, H., et al., *Interleukin-18: a novel cytokine that augments both innate and acquired immunity.* Adv Immunol, 1998. **70**: p. 281-312.
179. Chan, S.H., et al., *Induction of interferon gamma production by natural killer cell stimulatory factor: characterization of the responder cells and synergy with other inducers.* J Exp Med, 1991. **173**(4): p. 869-79.
180. Grohmann, U., et al., *Positive regulatory role of IL-12 in macrophages and modulation by IFN-gamma.* J Immunol, 2001. **167**(1): p. 221-7.
181. Trinchieri, G., et al., *Natural killer cell stimulatory factor (NKSF) or interleukin-12 is a key regulator of immune response and inflammation.* Prog Growth Factor Res, 1992. **4**(4): p. 355-68.
182. Zeh, H.J., 3rd, et al., *Interleukin-12 promotes the proliferation and cytolytic maturation of immune effectors: implications for the immunotherapy of cancer.* J Immunother Emphasis Tumor Immunol, 1993. **14**(2): p. 155-61.
183. Chowdhury, F.Z., et al., *IL-12 selectively programs effector pathways that are stably expressed in human CD8+ effector memory T cells in vivo.* Blood, 2011. **118**(14): p. 3890-900.
184. Parihar, R., et al., *IL-12 enhances the natural killer cell cytokine response to Ab-coated tumor cells.* J Clin Invest, 2002. **110**(7): p. 983-92.
185. Yoshimoto, T., et al., *LPS-stimulated SJL macrophages produce IL-12 and IL-18 that inhibit IgE production in vitro by induction of IFN-gamma production from CD3intIL-2R beta+ T cells.* J Immunol, 1998. **161**(3): p. 1483-92.
186. Grohmann, U., et al., *A tumor-associated and self antigen peptide presented by dendritic cells may induce T cell anergy in vivo, but IL-12 can prevent or revert the anergic state.* J Immunol, 1997. **158**(8): p. 3593-602.
187. Bianchi, R., et al., *Autocrine IL-12 is involved in dendritic cell modulation via CD40 ligation.* J Immunol, 1999. **163**(5): p. 2517-21.
188. Kanegane, C., et al., *Contribution of the CXC chemokines IP-10 and Mig to the antitumor effects of IL-12.* J Leukoc Biol, 1998. **64**(3): p. 384-92.
189. Eisenring, M., et al., *IL-12 initiates tumor rejection via lymphoid tissue-inducer cells bearing the natural cytotoxicity receptor NKp46.* Nat Immunol, 2010. **11**(11): p. 1030-8.
190. Airoldi, I., et al., *IL-12 can target human lung adenocarcinoma cells and normal bronchial epithelial cells surrounding tumor lesions.* PLoS One, 2009. **4**(7): p. e6119.
191. Ferretti, E., et al., *Direct inhibition of human acute myeloid leukemia cell growth by IL-12.* Immunol Lett, 2010. **133**(2): p. 99-105.
192. Leonard, J.P., et al., *Effects of single-dose interleukin-12 exposure on interleukin-12-associated toxicity and interferon-gamma production.* Blood, 1997. **90**(7): p. 2541-8.
193. Lacy, M.Q., et al., *Phase II study of interleukin-12 for treatment of plateau phase multiple myeloma (E1A96): a trial of the Eastern Cooperative Oncology Group.* Leuk Res, 2009. **33**(11): p. 1485-9.
194. Kerkar, S.P., et al., *Tumor-specific CD8+ T cells expressing interleukin-12 eradicate established cancers in lymphodepleted hosts.* Cancer Res, 2010. **70**(17): p. 6725-34.
195. Koneru, M., et al., *IL-12 secreting tumor-targeted chimeric antigen receptor T cells eradicate ovarian tumors in vivo.* Oncoimmunology, 2015. **4**(3): p. e994446.
196. Kerkar, S.P., et al., *IL-12 triggers a programmatic change in dysfunctional myeloid-derived cells within mouse tumors.* J Clin Invest, 2011. **121**(12): p. 4746-57.
197. Kerkar, S.P., et al., *Collapse of the tumor stroma is triggered by IL-12 induction of Fas.* Mol Ther, 2013. **21**(7): p. 1369-77.

198. Pegram, H.J., et al., *Tumor-targeted T cells modified to secrete IL-12 eradicate systemic tumors without need for prior conditioning.* Blood, 2012. **119**(18): p. 4133-41.
199. Engels, B., et al., *Retroviral vectors for high-level transgene expression in T lymphocytes.* Hum Gene Ther, 2003. **14**(12): p. 1155-68.
200. Verhaar, M.J., et al., *A single chain Fv derived from a filamentous phage library has distinct tumor targeting advantages over one derived from a hybridoma.* Int J Cancer, 1995. **61**(4): p. 497-501.
201. Klump, H., et al., *Retroviral vector-mediated expression of HoxB4 in hematopoietic cells using a novel coexpression strategy.* Gene Ther, 2001. **8**(10): p. 811-7.
202. Morita, S., T. Kojima, and T. Kitamura, *Plat-E: an efficient and stable system for transient packaging of retroviruses.* Gene Therapy, 2000. **7**(12): p. 1063-1066.
203. Yin, W., P. Xiang, and Q. Li, *Investigations of the effect of DNA size in transient transfection assay using dual luciferase system.* Anal Biochem, 2005. **346**(2): p. 289-94.
204. Fan, H., et al., *IL-12 plays a significant role in the apoptosis of human T cells in the absence of antigenic stimulation.* Cytokine, 2002. **19**(3): p. 126-37.
205. Su, W., et al., *The direct effect of IL-12 on tumor cells: IL-12 acts directly on tumor cells to activate NF-kappaB and enhance IFN-gamma-mediated STAT1 phosphorylation.* Biochem Biophys Res Commun, 2001. **280**(2): p. 503-12.
206. Zaidi, M.R., *The Interferon-Gamma Paradox in Cancer.* J Interferon Cytokine Res, 2019. **39**(1): p. 30-38.
207. Colosimo, A., et al., *Transfer and expression of foreign genes in mammalian cells.* Biotechniques, 2000. **29**(2): p. 314-8, 320-2, 324 passim.
208. Chinnasamy, D., et al., *Local delivery of interleukin-12 using T cells targeting VEGF receptor-2 eradicates multiple vascularized tumors in mice.* Clin Cancer Res, 2012. **18**(6): p. 1672-83.
209. Wagner, H.J., et al., *A strategy for treatment of Epstein-Barr virus-positive Hodgkin's disease by targeting interleukin 12 to the tumor environment using tumor antigen-specific T cells.* Cancer Gene Ther, 2004. **11**(2): p. 81-91.
210. Yeku, O.O., et al., *Armored CAR T cells enhance antitumor efficacy and overcome the tumor microenvironment.* Sci Rep, 2017. **7**(1): p. 10541.
211. Li, G., et al., *4-1BB enhancement of CAR T function requires NF-kappaB and TRAFs.* JCI Insight, 2018. **3**(18).
212. Milone, M.C., et al., *Chimeric receptors containing CD137 signal transduction domains mediate enhanced survival of T cells and increased antileukemic efficacy in vivo.* Mol Ther, 2009. **17**(8): p. 1453-64.
213. Zhong, X.S., et al., *Chimeric antigen receptors combining 4-1BB and CD28 signaling domains augment PI3kinase/AKT/Bcl-XL activation and CD8+ T cell-mediated tumor eradication.* Mol Ther, 2010. **18**(2): p. 413-20.
214. Zhou, Z., et al., *Characterization of human homologue of 4-1BB and its ligand.* Immunol Lett, 1995. **45**(1-2): p. 67-73.
215. Adusumilli, P.S., et al., *Abstract CT036: A phase I clinical trial of malignant pleural disease treated with regionally delivered autologous mesothelin-targeted CAR T cells: Safety and efficacy*. 2019, AACR.
216. Arch, R.H. and C.B. Thompson, *4-1BB and Ox40 are members of a tumor necrosis factor (TNF)-nerve growth factor receptor subfamily that bind TNF receptor-associated factors and activate nuclear factor kappaB.* Mol Cell Biol, 1998. **18**(1): p. 558-65.
217. Ni, L. and J. Lu, *Interferon gamma in cancer immunotherapy.* Cancer Med, 2018. **7**(9): p. 4509-4516.
218. Goldman, J.P., et al., *Enhanced human cell engraftment in mice deficient in RAG2 and the common cytokine receptor gamma chain.* Br J Haematol, 1998. **103**(2): p. 335-42.
219. Bosma, M.J. and A.M. Carroll, *The SCID mouse mutant: definition, characterization, and potential uses.* Annu Rev Immunol, 1991. **9**: p. 323-50.

220. Murayama, T. and N. Gotoh, *Patient-Derived Xenograft Models of Breast Cancer and Their Application.* Cells, 2019. **8**(6).
221. Zitvogel, L., et al., *Mouse models in oncoimmunology.* Nat Rev Cancer, 2016. **16**(12): p. 759-773.
222. Alcantar-Orozco, E.M., et al., *Potential limitations of the NSG humanized mouse as a model system to optimize engineered human T cell therapy for cancer.* Hum Gene Ther Methods, 2013. **24**(5): p. 310-20.
223. Gould, S.E., M.R. Junttila, and F.J. de Sauvage, *Translational value of mouse models in oncology drug development.* Nat Med, 2015. **21**(5): p. 431-9.
224. Chinnasamy, D., et al., *Gene therapy using genetically modified lymphocytes targeting VEGFR-2 inhibits the growth of vascularized syngenic tumors in mice.* J Clin Invest, 2010. **120**(11): p. 3953-68.
225. Li, S., et al., *Genetically engineered T cells expressing a HER2-specific chimeric receptor mediate antigen-specific tumor regression.* Cancer Gene Ther, 2008. **15**(6): p. 382-92.
226. Eades-Perner, A.M., et al., *Mice transgenic for the human carcinoembryonic antigen gene maintain its spatiotemporal expression pattern.* Cancer Res, 1994. **54**(15): p. 4169-76.
227. Zhou, L.J., et al., *Tissue-specific expression of the human CD19 gene in transgenic mice inhibits antigen-independent B-lymphocyte development.* Molecular and Cellular Biology, 1994. **14**(6): p. 3884-3894.
228. Piechocki, M.P., et al., *Human ErbB-2 (Her-2) transgenic mice: a model system for testing Her-2 based vaccines.* The Journal of Immunology, 2003. **171**(11): p. 5787-5794.
229. Mestas, J. and C.C. Hughes, *Of mice and not men: differences between mouse and human immunology.* J Immunol, 2004. **172**(5): p. 2731-8.
230. Newick, K., E. Moon, and S.M. Albelda, *Chimeric antigen receptor T-cell therapy for solid tumors.* Molecular Therapy-Oncolytics, 2016. **3**: p. 16006.
231. Siegler, E.L. and P. Wang, *Preclinical Models in Chimeric Antigen Receptor-Engineered T-Cell Therapy.* Hum Gene Ther, 2018. **29**(5): p. 534-546.
232. Chen, J. and D.E. Harrison, *Quantitative trait loci regulating relative lymphocyte proportions in mouse peripheral blood.* Blood, 2002. **99**(2): p. 561-6.
233. Mills, C.D. and K. Ley, *M1 and M2 macrophages: the chicken and the egg of immunity.* J Innate Immun, 2014. **6**(6): p. 716-26.
234. Foerster, F., et al., *Enhanced protection of C57 BL/6 vs Balb/c mice to melanoma liver metastasis is mediated by NK cells.* Oncoimmunology, 2018. **7**(4): p. e1409929.
235. Cheadle, E.J., et al., *Differential Role of Th1 and Th2 Cytokines in Autotoxicity Driven by CD19-Specific Second-Generation Chimeric Antigen Receptor T Cells in a Mouse Model.* The Journal of Immunology, 2014. **192**(8): p. 3654-3665.
236. Oh, T., et al., *Immunocompetent murine models for the study of glioblastoma immunotherapy.* J Transl Med, 2014. **12**: p. 107.
237. Bibby, M.C., *Orthotopic models of cancer for preclinical drug evaluation: advantages and disadvantages.* Eur J Cancer, 2004. **40**(6): p. 852-7.
238. Budhu, S., J. Wolchok, and T. Merghoub, *The importance of animal models in tumor immunity and immunotherapy.* Curr Opin Genet Dev, 2014. **24**: p. 46-51.
239. Cheadle, E.J., et al., *Eradication of established B-cell lymphoma by CD19-specific murine T cells is dependent on host lymphopenic environment and can be mediated by CD4+ and CD8+ T cells.* J Immunother, 2009. **32**(3): p. 207-18.
240. Carr-Brendel, V., et al., *Immunity to murine breast cancer cells modified to express MUC-1, a human breast cancer antigen, in transgenic mice tolerant to human MUC-1.* Cancer Res, 2000. **60**(9): p. 2435-43.
241. Penichet, M.L., et al., *In vivo properties of three human HER2/neu-expressing murine cell lines in immunocompetent mice.* Lab Anim Sci, 1999. **49**(2): p. 179-88.

242. Kulemzin, S.V., et al., *Design and analysis of stably integrated reporters for inducible transgene expression in human T cells and CAR NK-cell lines.* BMC Med Genomics, 2019. **12**(Suppl 2): p. 44.
243. Hogan, P.G., et al., *Transcriptional regulation by calcium, calcineurin, and NFAT.* Genes Dev, 2003. **17**(18): p. 2205-32.
244. Macian, F., *NFAT proteins: key regulators of T-cell development and function.* Nat Rev Immunol, 2005. **5**(6): p. 472-84.
245. Rao, A., C. Luo, and P.G. Hogan, *Transcription factors of the NFAT family: regulation and function.* Annu Rev Immunol, 1997. **15**: p. 707-47.
246. Hogan, P.G., R.S. Lewis, and A. Rao, *Molecular basis of calcium signaling in lymphocytes: STIM and ORAI.* Annu Rev Immunol, 2010. **28**: p. 491-533.
247. Macian, F., C. Garcia-Rodriguez, and A. Rao, *Gene expression elicited by NFAT in the presence or absence of cooperative recruitment of Fos and Jun.* Embo j, 2000. **19**(17): p. 4783-95.
248. Frey, M.R., et al., *Stimulation of protein kinase C-dependent and -independent signaling pathways by bistratene A in intestinal epithelial cells.* Biochem Pharmacol, 2001. **61**(9): p. 1093-100.
249. Dadsetan, S., V. Shishkin, and A.F. Fomina, *Intracellular Ca(2+) release triggers translocation of membrane marker FM1-43 from the extracellular leaflet of plasma membrane into endoplasmic reticulum in T lymphocytes.* J Biol Chem, 2005. **280**(16): p. 16377-82.
250. Zimmermann, K., et al., *Design and Characterization of an "All-in-One" Lentiviral Vector System Combining Constitutive Anti-GD2 CAR Expression and Inducible Cytokines.* Cancers (Basel), 2020. **12**(2).
251. Liu, Y., et al., *Armored Inducible Expression of IL-12 Enhances Antitumor Activity of Glypican-3-Targeted Chimeric Antigen Receptor-Engineered T Cells in Hepatocellular Carcinoma.* J Immunol, 2019. **203**(1): p. 198-207.
252. Atkins, M.B., et al., *Phase I evaluation of intravenous recombinant human interleukin 12 in patients with advanced malignancies.* Clin Cancer Res, 1997. **3**(3): p. 409-17.
253. Haicheur, N., et al., *Cytokines and soluble cytokine receptor induction after IL-12 administration in cancer patients.* Clin Exp Immunol, 2000. **119**(1): p. 28-37.
254. Wakefield, L.M. and A.B. Roberts, *TGF-beta signaling: positive and negative effects on tumorigenesis.* Curr Opin Genet Dev, 2002. **12**(1): p. 22-9.
255. Massague, J., *TGFbeta in Cancer.* Cell, 2008. **134**(2): p. 215-30.
256. Papageorgis, P. and T. Stylianopoulos, *Role of TGFbeta in regulation of the tumor microenvironment and drug delivery (review).* Int J Oncol, 2015. **46**(3): p. 933-43.
257. Gigante, M., L. Gesualdo, and E. Ranieri, *TGF-beta: a master switch in tumor immunity.* Curr Pharm Des, 2012. **18**(27): p. 4126-34.
258. Fridlender, Z.G., et al., *Polarization of tumor-associated neutrophil phenotype by TGF-beta: "N1" versus "N2" TAN.* Cancer Cell, 2009. **16**(3): p. 183-94.
259. Gong, D., et al., *TGFbeta signaling plays a critical role in promoting alternative macrophage activation.* BMC Immunol, 2012. **13**: p. 31.
260. Pickup, M., S. Novitskiy, and H.L. Moses, *The roles of TGFbeta in the tumour microenvironment.* Nat Rev Cancer, 2013. **13**(11): p. 788-99.
261. Katz, L.H., et al., *Targeting TGF-β signaling in cancer.* Expert Opin Ther Targets, 2013. **17**(7): p. 743-60.
262. Lucas, P.J., et al., *Disruption of T cell homeostasis in mice expressing a T cell-specific dominant negative transforming growth factor beta II receptor.* J Exp Med, 2000. **191**(7): p. 1187-96.
263. Hou, A.J., et al., *TGF-β-responsive CAR-T cells promote anti-tumor immune function.* Bioeng Transl Med, 2018. **3**(2): p. 75-86.
264. John, L.B., et al., *Anti-PD-1 antibody therapy potently enhances the eradication of established tumors by gene-modified T cells.* Clin Cancer Res, 2013. **19**(20): p. 5636-46.

265. Yin, Y., et al., *Checkpoint Blockade Reverses Anergy in IL-13Rα2 Humanized scFv-Based CAR T Cells to Treat Murine and Canine Gliomas.* Mol Ther Oncolytics, 2018. **11**: p. 20-38.
266. Naidoo, J., et al., *Toxicities of the anti-PD-1 and anti-PD-L1 immune checkpoint antibodies.* Ann Oncol, 2015. **26**(12): p. 2375-91.
267. Suarez, E.R., et al., *Chimeric antigen receptor T cells secreting anti-PD-L1 antibodies more effectively regress renal cell carcinoma in a humanized mouse model.* Oncotarget, 2016. **7**(23): p. 34341-55.
268. Rafiq, S., et al., *Targeted delivery of a PD-1-blocking scFv by CAR-T cells enhances anti-tumor efficacy in vivo.* Nat Biotechnol, 2018. **36**(9): p. 847-856.
269. Ledbetter, S.R., et al., *Antibodies to TGF-β*. 2010, Google Patents.
270. Agata, Y., et al., *Expression of the PD-1 antigen on the surface of stimulated mouse T and B lymphocytes.* International Immunology, 1996. **8**(5): p. 765-772.
271. Bujak, E., et al., *Reformatting of scFv antibodies into the scFv-Fc format and their downstream purification.* Methods Mol Biol, 2014. **1131**: p. 315-34.
272. Shirai, A., et al., *Global analysis of gel mobility of proteins and its use in target identification.* J Biol Chem, 2008. **283**(16): p. 10745-52.
273. Dudley, M.E., et al., *A phase I study of nonmyeloablative chemotherapy and adoptive transfer of autologous tumor antigen-specific T lymphocytes in patients with metastatic melanoma.* J Immunother, 2002. **25**(3): p. 243-51.
274. Brentjens, R.J., et al., *Safety and persistence of adoptively transferred autologous CD19-targeted T cells in patients with relapsed or chemotherapy refractory B-cell leukemias.* Blood, 2011. **118**(18): p. 4817-28.
275. Turtle, C.J., et al., *Immunotherapy of non-Hodgkin's lymphoma with a defined ratio of CD8+ and CD4+ CD19-specific chimeric antigen receptor-modified T cells.* Sci Transl Med, 2016. **8**(355): p. 355ra116.
276. Hadrup, S., M. Donia, and P. Thor Straten, *Effector CD4 and CD8 T cells and their role in the tumor microenvironment.* Cancer Microenviron, 2013. **6**(2): p. 123-33.
277. Nishio, N., et al., *Armed oncolytic virus enhances immune functions of chimeric antigen receptor-modified T cells in solid tumors.* Cancer Res, 2014. **74**(18): p. 5195-205.